



University of Huddersfield Repository

Wang, Jian

Sampling for the Measurement of Structured Surfaces

Original Citation

Wang, Jian (2012) Sampling for the Measurement of Structured Surfaces. Doctoral thesis, University of Huddersfield.

This version is available at <http://eprints.hud.ac.uk/id/eprint/17803/>

The University Repository is a digital collection of the research output of the University, available on Open Access. Copyright and Moral Rights for the items on this site are retained by the individual author and/or other copyright owners. Users may access full items free of charge; copies of full text items generally can be reproduced, displayed or performed and given to third parties in any format or medium for personal research or study, educational or not-for-profit purposes without prior permission or charge, provided:

- The authors, title and full bibliographic details is credited in any copy;
- A hyperlink and/or URL is included for the original metadata page; and
- The content is not changed in any way.

For more information, including our policy and submission procedure, please contact the Repository Team at: E.mailbox@hud.ac.uk.

<http://eprints.hud.ac.uk/>

SAMPLING FOR THE MEASUREMENT OF STRUCTURED SURFACES

JIAN WANG

A thesis submitted to the University of Huddersfield

in partial fulfilment of the requirements for

the degree of Doctor of Philosophy

The University of Huddersfield

April 2012

ABSTRACT

Structured surfaces are increasingly popular in manufacturing due to their ability to affect the function of a component, for example paintability and adhesiveness. Structured surfaces usually have complex geometrical structures on the micrometre to nanometre scale. These complex surface structures are challenging in terms of their measurement. For example, one widely recognised challenge comes from the increasingly high requirement of both measuring efficiency and measuring accuracy. Intelligent sampling is regarded as part of the solution to this challenge.

In this research, statistical sampling and signal sampling are investigated for the measurement of structured surfaces. Firstly, the widely used technique of uniform sampling is reviewed. Determination criteria for the sampling conditions of uniform sampling, i.e. the sampling intervals and lengths, are discussed. Four types of efficient (intelligent) sampling techniques, which were initially developed for the fields of statistics, computer graphics and coordinate metrology, are investigated. The intelligent techniques include: jittered uniform sampling, low-discrepancy sampling, model-based sampling and adaptive sampling. However, there are issues when applying these techniques to practical instruments; for example, they do not consider the measuring principles, such as the sensing mode or scanning method. Considering the measurement of surface topography, a sequential profiling adaptive sampling technique is proposed for raster scan-based stylus profilometers. Numerical evidence shows that the adaptive technique is promising for the measurement of linear patterns and tessellated structured surfaces.

To examine the performance of these intelligent sampling techniques, reconstruction techniques and error evaluation approaches are studied. A boundary segmentation algorithm has been developed to characterise the feature boundaries of surface features. With a sampling test toolbox, developed as part of the project, a sampling performance test is carried out in which the performance of seven selected sampling techniques is analysed. The experimental results show that adaptive sampling and model-based sampling methods have significant advantages over other methods. The proposed sequential profiling adaptive sampling has good performance in the measurement of linear patterned surfaces.

However, there are difficulties in fully enabling intelligence sampling for practical measurements. For example, the relationship between sampling and reconstruction has not been clearly understood. If the difficulties can be successfully addressed, intelligent sampling can be of promise in the next generation of measurement techniques.

Keywords: structured surfaces, metrology, sampling, uniform sampling, efficient sampling

ACKNOWLEDGEMENTS

I would firstly like to thank my first supervisor Prof Xiangqian Jane Jiang. Because of her, I have been involved in this research with sufficient support in terms of finance, equipments and emotions. This essential support gave a positive and remarkable boost to my later development.

I would also like to thank my supervisors Prof Liam A Blunt and Prof Richard K Leach (The National Physical Laboratory, UK) for their constant encouragement, guidance on the research directions, and critical comments on my research and writing.

I would also like to express my thanks to all of the following people for their advice and technical assistance during the last three years: Prof Paul J Scott, Dr Xiangchao Zhang, Dr Leigh Fleming, Dr Wenhan Zeng, Dr Feng Gao, Dr Shaojun Xiao, Mr Hussam Muhamedsalih, Dr Tukun Li and all the colleagues in the Centre for Precision Technologies.

Finally, I am grateful for the NPL for supporting this research work under the UK National Measurement System Programme for Engineering & Flow Measurement (2008-2011), the University of Huddersfield under the excellent research programme, and the European Research Council under its programme ERC-2008-AdG 228117-Surfund.

TABLE OF CONTENTS

ABSTRACT	2
ACKNOWLEDGEMENTS	3
TABLE OF CONTENTS	4
LIST OF FIGURES.....	8
LIST OF TABLES.....	12
PUBLICATION LIST.....	14
NOMENCLATURE	15
1. INTRODUCTION.....	17
1.1 Background.....	17
1.2 Aim and objectives	19
1.3 Outline of the thesis	20
1.4 Delimitations.....	21
1.5 Research highlights.....	21
2. STRUCTURED SURFACE AND ITS MEASUREMENT	23
2.1 Definitions of structured surfaces	23
2.1.1 Surface topography.....	23
2.1.2 Historical definitions	26
2.1.3 Definitions and classifications employed	28
2.1.4 Industrial applications.....	33
2.2 Measurement tasks.....	34
2.2.1 General measurement tasks	35
2.2.2 The intermediate task.....	42
2.3 Measurement challenges.....	43

2.4	Summary	48
3.	SAMPLING.....	50
3.1	Sampling in surface measurement.....	50
3.2	Global statistical sampling	54
3.2.1	Introduction	54
3.2.2	Determination of sampling units	55
3.2.3	Selection of sampling methods	56
3.2.4	Determination of sample size.....	59
3.3	Local signal sampling.....	62
3.3.1	Introduction	62
3.3.2	Emergence of intelligent sampling methods	65
3.4	Some signal sampling theories.....	66
3.4.1	Sampling in Paley-Wiener spaces	67
3.4.2	Sampling in shift-invariant spaces	69
3.4.3	Other sampling design ideas	79
3.5	Summary	80
4.	UNIFORM SAMPLING	82
4.1	Introduction	82
4.2	Selection of sampling spacing.....	83
4.2.1	Review of selection criteria for sampling interval	83
4.2.2	Ideal sampling and reconstruction.....	86
4.2.3	Spectral aliasing and practical solutions	89
4.3	Selection of sampling length	92
4.3.1	Spectral leakage.....	93
4.3.2	Frequency sampling	97
4.3.3	Sampling length determination	100
4.4	Summary and conclusions.....	107
5.	INTELLIGENT SAMPLING.....	109

5.1	Introduction.....	109
5.2	Jittered uniform sampling	111
5.2.1	Introduction to jittered uniform sampling.....	111
5.2.2	Section summary	114
5.3	Low-discrepancy sampling.....	114
5.3.1	Introduction to low-discrepancy sampling	114
5.3.2	Case studies in surface measurements.....	118
5.3.3	Section summary	122
5.4	Model-based sampling.....	123
5.4.1	Introduction to model-based sampling in surface metrology	123
5.4.2	Review of model-based methods in surface measurement.....	124
5.4.3	Triangle-patch and rectangle-patch adaptive subdivision sampling.....	127
5.4.4	Profile direct sampling.....	133
5.4.5	Profile DWT-based sampling	137
5.4.6	Section summary and discussion.....	142
5.5	Adaptive sampling	143
5.5.1	Introduction.....	143
5.5.2	Sequential profiling adaptive sampling	144
5.5.3	Section summary and conclusion	149
5.6	Summary and conclusions	149
6.	ERROR EVALUATIONS.....	152
6.1	Reconstruction	152
6.1.1	Introduction.....	152
6.1.2	Tensor product reconstruction using B-splines	155
6.1.3	Triangulation based reconstruction.....	165
6.1.4	An example illustration of the reconstruction methods.....	167
6.2	A sampling toolbox.....	169
6.3	Evaluation of sampling error	171
6.3.1	Root mean square height deviation.....	172

6.3.2	Feature-based characterisation	173
6.4	Numerical experiments	183
6.4.1	Experimental settings	183
6.4.2	Results and conclusions	185
6.5	Summary and conclusions.....	189
7.	CONCLUSIONS AND FUTURE WORK.....	192
7.1	The research conclusions	192
7.2	Future work	196
	REFERENCES	198

LIST OF FIGURES

Figure 1.1. The process loop relating to the creation of structured surfaces [93].	18
Figure 2.1. Different surface components and their relationships to S-filter, L-filter and F-operator.....	24
Figure 2.2. The eight surface classifications [136].....	27
Figure 2.3. The surface classification based on surface topography characteristics [77].	29
Figure 2.4. A 3M Trizact abrasive and the p4m tessellation diagram.	30
Figure 2.5. Surface topography of three tessellated surfaces.	30
Figure 2.6. Surface topography of two linear patterned surfaces.	31
Figure 2.7. Two rotationally symmetric patterned surfaces.	32
Figure 2.8. MEMS product surfaces with multi-patterns.	33
Figure 2.9. Usefulness of surface measurement.	35
Figure 2.10. General measurement tasks of structured surfaces.	42
Figure 2.11. General procedures for the measurement of surface topography.....	43
Figure 2.12. Typical measurement difficulties [94, 156].	44
Figure 3.1. Illustration of two-stage sampling for the evaluation of surface topography.	51
Figure 3.2. Schematic of sampling related issues in general surface measurement. ...	54
Figure 3.3. A sample design in the measurement of the surface roughness of a cylinder bore [123].	56
Figure 3.4. Illustration of simple random sampling, uniform sampling, stratified sampling and cluster sampling.	58
Figure 3.5. A DWT decomposition-based adaptive sampling of a spline-like signal.	64
Figure 3.6. The coherent spectral aliasing effect in computer graphics.	65

Figure 3.7. The ringing effect in frequency domain.	69
Figure 3.8. A partition of unity with a third degree B-spline basis (knots: 2, 5, 6, 9). 73	
Figure 3.9. The iterative reconstruction algorithm based on equation (3.28) [6].	74
Figure 3.10. Reconstruction of a shift-invariant signal using fast local algorithms.....	76
Figure 3.11. Reconstruction of a randomly noised shift-invariant signal..	78
Figure 4.1. Frequency interpretation of Shannon's sampling theorem.	88
Figure 4.2. Spectral aliasing caused by not small enough sampling spacing T	89
Figure 4.3. A periodic rectangle-wave surface and its power spectrum.	90
Figure 4.4. The power spectrum and the cumulative spectrum of a one-dimensional rectangle wave signal.	91
Figure 4.5. Interpretation of windowing for periodic signal in frequency domain.	95
Figure 4.6. Spectral leakage of the measurement of a sinusoidal surface.....	96
Figure 4.7. The effect of a Haan window.....	97
Figure 4.8. Frequency sampling in discrete Fourier analysis.....	100
Figure 4.9. Spectral leakage caused by non-integer period sampling.....	102
Figure 4.10. The effect of integral period sampling.....	103
Figure 4.11. Power spectrum of the noised sinusoidal profile expressed by equation (4.27) with the sampling length (a) 100 points and (b) 128 points.	104
Figure 4.12. Power spectrum of the noised sinusoidal surface expressed by equation (4.28) with sampling length (a) $50\ \mu\text{m} \times 50\ \mu\text{m}$ (b) $52\ \mu\text{m} \times 52\ \mu\text{m}$	105
Figure 4.13. Comparison of the DFT spectrums with the sampling length from 100 to 110.....	106
Figure 5.1. Schematic diagram of a new data format for surface measurement.	111
Figure 5.2. Comparison of a uniform sampling and a jittered uniform sampling.....	112
Figure 5.3. Illustration of approximation of the area of the square b	115

Figure 5.4. The 100 points sampling pattern of Hammersley and Halton sequences.	117
Figure 5.5. Validation of the efficiency of low-discrepancy sampling patterns on form-error estimation (flatness).	119
Figure 5.6. Comparison of uniform, Hammersley and Halton sampling for the measurement of an normal EDM surface	120
Figure 5.7. Comparison of uniform, Hammersley and Halton sampling for the measurement of a directional EDM surface	121
Figure 5.8. Comparison of uniform, Hammersley and Halton sampling for the measurement of a MEMS device.....	121
Figure 5.9. Comparison of uniform, Hammersley and Halton sampling for the measurement of a micro-lens array.....	122
Figure 5.10. Subdivision of triangle patch and rectangle patch.	128
Figure 5.11. Adaptive sampling patterns produced by the triangle patch adaptive sampling.....	128
Figure 5.12. Illustration of the error evaluation by single point estimation [130].....	130
Figure 5.13. A multi-patterned structured surface for sampling test.....	131
Figure 5.14. Comparison of adaptive sampling design of triangle patch algorithm and rectangle patch algorithm with different error estimation methods.....	132
Figure 5.15. Comparison of profile direct sampling and uniform sampling.	134
Figure 5.16. Comparison of adaptive sampling and uniform sampling	136
Figure 5.17. RMS reconstruction error and variations of adaptive sampling (blue) and uniform sampling (mauve) using different sampling sizes for practical samples	137
Figure 5.18. Two-stage wavelet decomposition tree and the DWT detail coefficients used for adaptive sampling setting.	138
Figure 5.19. An example illustration of the two-stage DWT details.....	138
Figure 5.20. A DWT-based sampling of a practical wave signal.	140

Figure 5.21. A DWT-based sampling of a practical profile of a micro-lens.....	141
Figure 5.22. A DWT-based sampling of a practical profile of a medal coin.	142
Figure 5.23. Two stages of the sequential profiling adaptive sampling.....	146
Figure 6.1. Approximation of a uniform sampling set.....	154
Figure 6.2. Three types of surface sample data with different point distributions.....	155
Figure 6.3. A third degree B-spline basis with the support $[-2, 2]$	159
Figure 6.4. Illustration examples of the performances of the tensor product reconstruction with B-splines for the grid data and the partial lattice data.....	164
Figure 6.5. Delaunay triangulation (red) and Voronoi tessellation-diagram (green) of a planar space based on a twenty-five scattered samples.....	165
Figure 6.6. The performance of the Delaunay triangulation-based reconstruction....	166
Figure 6.7. The module chart of the sampling toolbox.	170
Figure 6.8. The user interface of the sampling toolbox.	171
Figure 6.9. Illustration of a height residual map	173
Figure 6.10. A feature-based characterisation of a circle edged feature.	174
Figure 6.11. A ‘Maxwell’ feature characterisation of a human skin.....	175
Figure 6.12. Illustration of a boundary data.	179
Figure 6.13. Illustration of tangent analysis for a simple boundary.....	180
Figure 6.14. A noised segmentation.....	181
Figure 6.15. Type ACG crossed grating standard.....	182
Figure 6.16. A segmentation result of the type ACG measurement result in Figure 6.15.....	182

LIST OF TABLES

Table 2.1. Industrial applications and structured surfaces.....	34
Table 2.2. The three characterisation function of a scale limited surface.	37
Table 2.3. The thirty-one field parameters.	39
Table 2.4. The suggested nine feature parameters in ISO 25178 Part 2.....	40
Table 2.5. The common geometric dimensions of the general measurement tasks. ...	41
Table 2.6. Key lithography-related characteristics of semiconductor products [73]...	44
Table 2.7. Complexities of structured surfaces and examples of measurement difficulties or faults.....	45
Table 3.1. The sample means and variances in the cylinder liner measurement [123].	61
Table 3.2. <i>S5p</i> values of a random sample from the AC surface of Joint 1 [153] (OA grade 1).	61
Table 4.1. Selection of sampling spacing based on S-filter nesting index [69].....	92
Table 5.1. Comparison of existing three-dimensional non-uniform adaptive sampling techniques.	125
Table 5.2. The RMS error of uniform sampling and profile direct sampling for the typical periodic signals in Figure 5.15.....	135
Table 5.3. Performance comparison of uniform sampling and sequential profiling adaptive sampling.	148
Table 6.1. Performance of different reconstruction methods for a tessellation surface.	169
Table 6.2. Common feature attributes suggested by ISO 25178 Part 2 [68].	176
Table 6.3. Attribute statistics suggested by ISO 25178 Part 2 [68].	177
Table 6.4. Some commonly used dimensional parameters.....	178

Table 6.5. The three typical structured surface specimens and the experimental settings.....184

Table 6.6. Deviations of the evaluation parameters from the standard result for Sample 1, Sample 2 and Sample 3. (log-log plots)187

PUBLICATION LIST

- [1] Wang J, Jiang X, Gurdak E, Scott P J, Leach R K, Tomlins P 2011 Numerical characterisation of biomedical titanium surface texture using novel feature parameters *Wear* **271** 1059-65
- [2] Wang J, Jiang X, Blunt L A, Leach R K, Scott P J 2011 Efficiency of adaptive sampling in surface texture measurement for structured surfaces *J. Phys.: Conf. Ser.* **311** 012017. In: *13th International Conference on Metrology and Properties of Engineering Surfaces (Twickenham, April 12-15)*
- [3] Wang J, Jiang X, Blunt L A, Leach R K, Scott P J 2012 Intelligent sampling for the measurement of structured surfaces *Meas. Sci. Techol.* **23** 085006
- [4] Wang J, Jiang X, Blunt L A, Leach R K, Scott P J 2012 A boundary segmentation algorithm for extracting micro-scale dimensional parameters in the measurement of structured surfaces *Proceedings of the 12th International Conference of EUSPEN* **1** 113-6 (Stockholm, June 4-7)
- [5] Tian Y, Wang J, Peng Z, Jiang X 2011 Numerical analysis of cartilage surfaces for osteoarthritis diagnosis using field and feature parameters *Wear* **271** 2370-8
- [6] Tian Y, Wang J, Peng Z, Jiang X 2012 A new approach to numerical characterisation of wear particle surfaces in three-dimensions for wear study *Wear* **282-283** 59-68
- [7] Wang M, Peng Z, Wang J, Jiang X 2011 Wear characterisation of articular cartilage surfaces at a nano-scale using atomic force microscopy. In: *the International Conference on Bio Tribology 2011 (Imperial College, Sept. 18-21)*

NOMENCLATURE

- AC: Articular Cartilage.
AFM: Atomic Force Microscope.
ASIC: Application Specific Integrated Circuit.
cps: cycles per second.
CAD: Computer Aided Design.
CCD: Charge Coupled Device.
CSI: Coherence Scanning Interferometer.
CMM: Coordinate Measuring Machine.
CMOS: Complementary Metal Oxide Semiconductor.
DRAM: Dynamic Random Access Memory.
DFT: Discrete Fourier Transform.
DWT: Discrete Fourier Transform.
DTFT: Discrete Time Fourier Transform.
EDM: Electrical Discharge Machining.
EPS: Equal Probability Selection.
FFT: Fast Fourier Transform.
IC: Integrated Circuit.
ISO: International Organisation for Standardization.
LIGA: German acronym for Lithography, Electroplating, and Moulding.
MEMS: Microelectromechanical System.
MPU: Microprocessor Unit.
NURBS: Non-uniform rational B-spline.
OA: Osteoarthritis.
RBF: Radial Basis function.
RMSE: Root Mean Square Error.
 μ TAS: Micro Total Analysis System.
sinc: Normalised sinc function which has $\text{sinc}(x) = \frac{\sin(\pi x)}{\pi x}$.
 $S5p$: five point peak height.
 Sa : Arithmetical mean height.
 Sq : Root mean square height.
 Sz : Maximum height.
Std. Dev. or S_n : Standard deviation of a set of sample values.
 \mathbb{R}^d : The real number set in d dimensions.
 \bar{X} : Mean of a set of sample values.
 σ : Variance of a set of population values.
 L^p : A Lebesgue function space with p-norm.
 $B(-W, W)$: A band-limited space with the spectrum support on $(-W, W)$.
 \hat{f} : The Fourier transform of function f .

\overline{f} : The conjugate of f .

\hat{f} : Fourier transform of f with $\hat{f}(\xi) = \int_{\mathbb{R}^d} f(x) e^{-j2\pi \langle \xi, x \rangle} dx$.

β_3 : Third degree B-spline basis function.

$\chi [-1/2, 1/2]$: Characteristic function that has $\chi = 1$ for $[-1/2, 1/2]$ and $\chi = 0$ for others.

$V^2(\varphi)$: Shift-invariant space constructed by basis function φ and has 2-norm.

δ : The Dirac delta function.

$\#$: Number of elements of a set.

1. INTRODUCTION

1.1 Background

In engineering, the surfaces of an entity are usually manufactured to meet specific functions []. Structured surfaces are a typical type of engineered surface that are usually designed to provide specific functions such as adhesion, self-cleaning and broad spectrum absorption. These surfaces have received increasing attention from the end of the last century due to their useful functionalities [20, 46]. Some typical examples of structured surfaces include lab-on-a-chip devices, MEMS products, retro-reflection coatings, and micro-lens arrays [34, 43, 49, 99].

During the design-manufacture process of a structured surface there is a close interrelation between surface characterisation and surface functions. On the one hand, a surface is produced to meet specific functions (see Figure 1.1) by analysing the functional requirements and designating the design/manufacture specifications [93]. On the other hand, measurement of the surface properties (geometrical, mechanical, electronic, etc.) can be performed and used to give feedback information for functional comparison, optimisation of design or manufacturing parameters. In terms of the manufacture of structured surfaces, a successful measurement of surface geometry provides vital information that can be used to improve the surface qualities. However, metrology of structured surfaces can prove to be challenging due to their novel surface properties.

Metrological difficulties arise when characterising the properties of structured surfaces due to their geometric complexities. These complexities present a challenge to the measurement techniques available at the moment. Generally, these metrological difficulties can be divided into three categories which challenge the sensing techniques, mathematics and signal processing techniques.

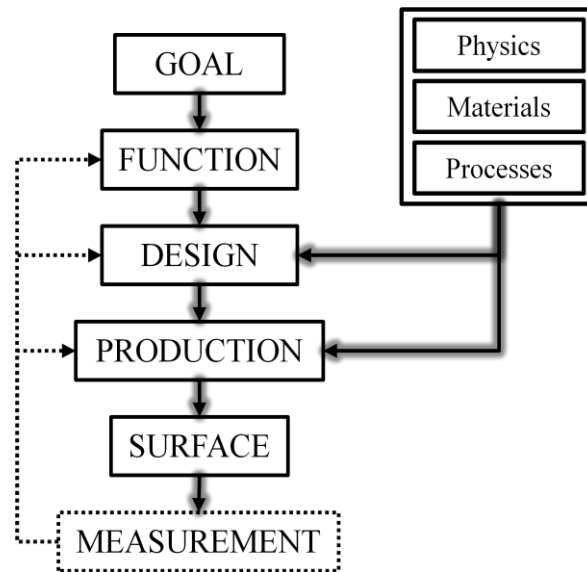


Figure 1.1. The process loop relating to the creation of structured surfaces [93].

1. Geometric complexities versus data acquisition approaches.

Structured surfaces are usually embedded with complex structures on the micrometre to nanometre scale, for example high aspect ratio, high slope, or high curvature features. General surface texture instruments with solid or optical tips have difficulties accessing these complex surface features.

2. Geometric complexities versus measurement efficiency and accuracy.

Structured surfaces usually have a large working surface area ranging from millimetres to metres. The contrast between the micro or nano-metre scale structures and the large dimensional span creates a problem of efficiency against measurement accuracy. For example, a stylus instrument may take hours to execute a single measurement.

3. Geometric complexities versus characterisation.

Complex structures require flexible and stable algorithms for feature recognition and functional characterisation. The general purpose characterisation techniques suggested in current ISO standards, for example ISO 25178 Part 2 [68], cannot work for all the cases.

More details and examples related to the metrological difficulties can be referred to Chapter 2.

Various techniques are being developed with the hope of resolving these difficulties. For example, a focus variation technique has recently been produced which has been very successful in the three-dimensional measurement of complex structures [33]. Feature-based characterisation techniques [68, 159] are under investigation and many algorithms have been developed. However, no systematic work has been carried out with the aim of solving the efficiency against accuracy problem which constitutes the original intention of this PhD work. Optimisation of sampling methods is one of the potential solutions to the problem of measurement efficiency, and as such is set as the focus of this research.

1.2 Aim and objectives

To be concise, the aim of this research is to develop innovative sampling methods to resolve the measurement difficulties relating to efficiency and accuracy which exist in current metrology techniques for structured surfaces. The sequential objectives are given as follows.

1. To survey the background information relating to the measurement of structured surfaces which includes the definitions of structured surfaces, the measurement challenges, and the state of the art in sampling techniques for general surface topography measurement including both uniform sampling and intelligent sampling.
2. To determine the sampling conditions for uniform sampling. Uniform sampling is currently the prevailing technique, so sampling related issues need to be revisited, but with new evidence and conclusions.
3. To develop potential intelligent sampling methods for the measurement of structured surfaces. To ensure a reliable examination of the proposed method, a quantitative evaluation of the performance of the method needs to follow.

1.3 Outline of the thesis

Based on the objectives above, this PhD research is carried out with the following chapter structure.

Chapter 1 introduces the background information for this PhD research, including the aim, objectives, thesis outline, research highlights and delimitations.

Chapter 2 reviews the background information related to the measurement of structured surfaces, such as the definitions of structured surfaces and the measurement tasks and related challenges.

Chapter 3 investigates the current sampling techniques used for surface topography measurement. A sampling framework for the measurement of structured surfaces is developed. Specifically, a global sampling procedure is suggested. The current situation regarding local sampling techniques is reviewed including different sampling theories.

Chapter 4 introduces uniform sampling for surface measurement, which is most commonly used at present. The issues relating to the selection of sampling spacing are revisited based on the work of former researchers. This chapter is not purely a review; some new results are concluded with evidence. In particular, the selection of sampling length is analysed in terms of frequency sampling, which has received little attention in the past. A conclusion on the selection of the sampling conditions for uniform sampling is given at the end.

Chapter 5 explores a series of potentially efficient sampling methods in statistics, computer graphics and coordinate metrology. These methods include jittered uniform sampling, low-discrepancy pattern sampling, model-based sampling and adaptive sampling. A sequential profiling adaptive sampling method is developed which is specifically designed for raster scan-based instruments. The numerical evidence shows that this method has clear advantages in terms of saving measuring time and improving measurement accuracies.

Chapter 6 runs a sampling error evaluation experiment in which the performance of diverse signal sampling methods and the proposed method are compared. At first, the reconstruction is introduced by presenting general reconstruction methods. A sampling toolbox is then developed which embeds the presented sampling and reconstruction methods. Error evaluation methods are introduced including a self-developed boundary characterisation algorithm. Finally, a sampling error evaluation experiment is carried out to obtain the experimental results and confirm the performance of the proposed method.

Chapter 7 consists of a conclusion showing the contributions of this PhD research and a description of the future work.

1.4 Delimitations

Optimisation of sampling methods is not the only solution to the problem of measurement efficiency against accuracy. For example, a combination of diverse sensing techniques (for example atomic force microscopy and interferometry) is also expected to provide measurements with a large scope and high resolution. However, in this research only sampling related issues are investigated. Issues related to instrumental design such as sensing techniques, scanning mechanisms and stitching techniques, are not considered.

In particular, sampling is investigated mainly from the point of view of signal processing. Statistical sampling is discussed briefly because it has already been highly developed and can be referred to in many textbooks.

1.5 Research highlights

The following contributions from this thesis are highlighted. If it is not specified clearly, the contributions refer to the measurement of structured surfaces.

1. A sampling framework is initially proposed for the measurement of structured surfaces. Many ideas of this framework are not new; however, the framework is summarised for the first time with reference to practical measurements.

2. The determination criteria of the sampling conditions of uniform sampling are revisited. New conclusions on the selection criteria of sampling conditions are obtained and the evidence is given.
3. An adaptive sampling technique is developed for raster scan-based instruments. This method shows promising performance for the measurement of specific types of structured surfaces.
4. A sampling test toolbox which embeds different sampling methods and selected reconstruction methods is developed. This toolbox can be used in later experiments to simplify the sampling error evaluation procedures.
5. A boundary characterisation algorithm is developed. The errors of the characterising dimensional parameters can be analysed. Hence, the performance of different sampling methods can be presented.
6. A numerical test is carried out to validate the performance of different sampling methods. The results confirm the expectations of the proposed sampling technique.

2. STRUCTURED SURFACE AND ITS MEASUREMENT

This chapter describes the background to the thesis. It presents the state of the art in the measurement of structured surfaces. The objective of this chapter is to provide a better understanding of structured surfaces and the measurement challenges. Hence, the scope of this research, i.e. sampling, can be determined as a solution to the challenges.

2.1 Definitions of structured surfaces

2.1.1 *Surface topography*

To clarify the definitions of structured surfaces, surface topography needs to be understood first. General terminology relating to surface topography measurement has differences among institutes and national or regional standards. For example, surface topography defined in US metrology systems [8, 160] is different from that described in UK systems [85, 87]; the NPL good practice guides [85, 87] have conflicting definitions for primary surface referring to ISO 25178 Part 2 [68].

Only with an unambiguous understanding of surface topography, can the measurement of structured surfaces be carried out accurately. In this section, some of the basic terminology relating to surface topography is clarified. The definitions employed try to be consistent with the international standard ISO 25178 series. Some terms that are defined by other materials, for example in [8, 86], are also considered if they are not clearly defined in ISO areal measurement specifications.

Surface: the boundary that separates an object from another object, substance or space.

Because the real surface (actual boundary) of a part and its nominal surface (intended boundary) are always different, the derived geometric surface deviations need to be inspected for the use of quality control, condition monitoring and so on. A real surface can be seen as a linear superposition of small scale components, S-F surface and form, which are given by the following definitions.

Form, or surface form, or real form, is defined as the widely spaced components of a real surface. It can be generally understood as a superposition of nominal form (shape of the nominal surface, for example, a cylinder liner has a cylindrical form) and errors of form (or form errors - the difference between form and nominal form). Errors of form are generally caused by such factors as errors in machine tool ways, guides or spindles, insecure clamping or incorrect alignment of the work-piece, or uneven wear [8]. Form can be removed using an **F-operator** (a high pass pre-filter) (see Figure 2.1).

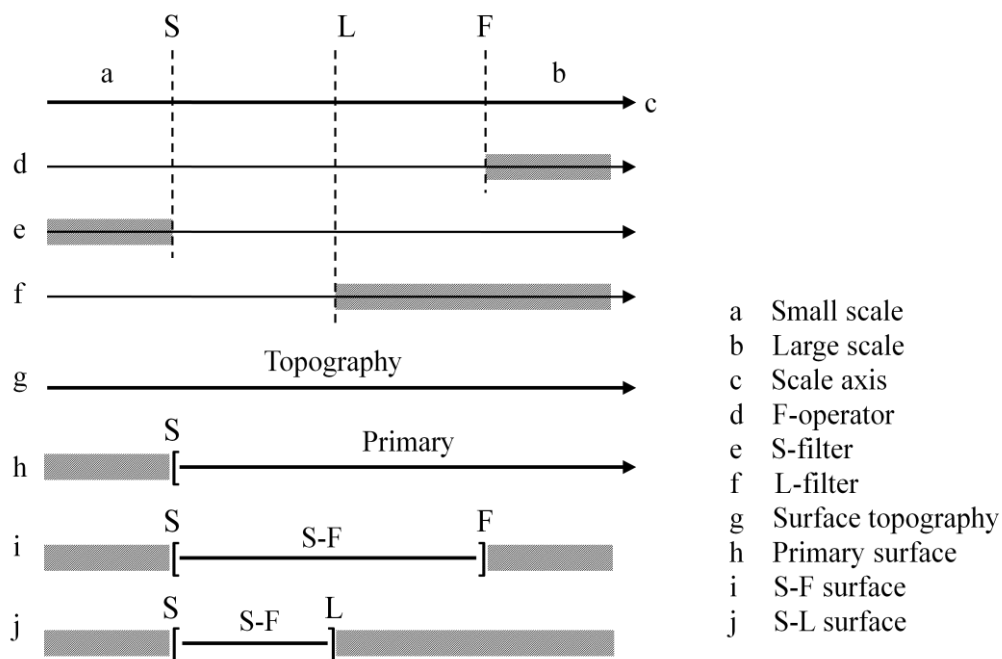


Figure 2.1. Different surface components and their relationships to S-filter, L-filter and F-operator.

Small scale components have not been rigorously defined. However, they are commonly recognised as the small wavelength components which are laterally shorter than roughness. Here **roughness** is described as the finer surface deviations which result from the inherent action of production process or material condition [8] (for example cutting tool marks, grit of grinding wheels). Because the small scale components usually cannot be steadily measured due to the effect of measurement noise or are less useful compared to larger components such as roughness and form,

an S-filter (low pass) is normally applied to remove them before analysis. This action results in a **primary surface** [68] (see Figure 2.1). For example, the size limitation of the stylus on a contact instrument induces the rejection of very short wavelengths and in practice this mechanical filtering effect is often used as a natural S-filter [86].

S-F Surface is the surface remaining when the form and the small scale components are removed from a real surface. It can also be understood as the surface derived from the primary surface when the form is removed. In practice, an L-filter (high pass) is normally applied to an S-F surface which results in an **S-L surface** (see Figure 2.1). The implication of this action is based on recognition of the existence of roughness (see above) and waviness (explained afterwards), and in most modern surfaces, for example a MEMS product surface, large scale components and finer scale components can be usually discriminated. Here **waviness** is the wider surface deviations which are caused by such factors as machine or workpiece deflections, vibration and chatter [8].

Surface topography is defined here as the overall surface structure (or wavelength components) of a real surface [86]. Surface topography presents the geometric properties of a real surface which differ from material characteristics or surface layer characteristics such as residual stresses, hardness, etc. In practice, small scale components are normally removed in a real measurement due to instrumental limits, on account of which, surface topography is commonly used as a substitute term for the primary surface [86].

Surface topography is distinct from surface texture [8, 66, 85], which consists of waviness and roughness only. The term surface texture is abandoned in this thesis because structured surfaces are recognised to have deterministic large scale features in micro- or nano-metre scales, such as micro-grooves etched on a lab-on-a-chip device [43]. These designed features usually consist of wide and narrow spectral information and cannot be simply filtered by mean line filters or envelope filters [75]. Besides, the form information of a structured surface might be functionally important, for example a Fresnel lens on a freeform car headlight cover. The term surface topography is preferred because the widely spaced components, i.e. the form, are

retained. Investigation of deterministic micro-scale geometry characteristics falls out of the scope of surface texture measurement.

2.1.2 Historical definitions

The definitions of structured surfaces are changed from when they were first proposed. The common first definition comes from the CIRP keynote paper presented in 1999 by Evans and Bryan [46]. They suggested a parallel surface classification of “engineered surface” and “structured surface” based on work by Stout [135] and Suh [140]. From a comprehensive view of the manufacturing characteristics, surface topography and surface functions, the definitions are given below.

Structured surfaces: surfaces with a deterministic pattern of usually high aspect ratio with geometric features designed to give a specific function.

Engineered surfaces: surfaces where the manufacturing process is optimised to generate variation in geometry and/or near surface material properties to give a specific function.

This classification resulted in a controversy from Stout and Blunt [136]. They pointed out the drawbacks of the Evans/Bryan classification and definitions. For example, the Evans/Bryan classifications seem to exclude the micro-electro-mechanical systems (MEMS) product surfaces from the consideration of surface metrology [168]. Stout and Blunt developed eight surface classifications and proposed them in a hierarchical structure (see Figure 2.2). In this structure, general surfaces are divided into two parallel categories: “engineered surfaces” and “non-engineered surfaces”, with structured surfaces belonging to the class of engineered surfaces. “Engineered surfaces” and “non-engineering surfaces” were redefined as follows:

Engineered surfaces: surfaces produced in specific ways that deliberately alter surface and subsurface layers to give a specific functional performance.

Non-engineered surfaces: surfaces produced as a direct consequence of the manufacturing process where little or no attempt is made to influence surface character.

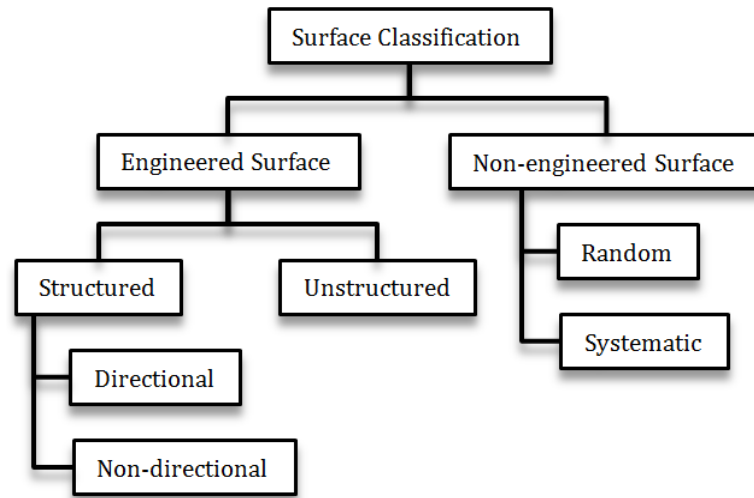


Figure 2.2. The eight surface classifications [136].

Conflicts emerge from the two views [94]. For example, machined surfaces, such as turned surfaces, are considered in the former case central to the production of structured surfaces, while in the latter case pertinent to non-engineered, and hence, unstructured surfaces. Besides, the Evans/Bryan classifications tend to ignore the variety of natural beings. For example, the micro-nipple array structure of a moth-eye is excluded from the Stout/Blunt's classifications. Although the classifications aim to reduce the ambiguity of surface description and to improve the understanding of surfaces in terms of their manufacturing processes and functions, these classifications are ambiguous and not really suited to cope with new manufacturing technologies and applications.

In the work of Jiang et al [76], various modern surface characterisation techniques are described for stochastic surfaces, structured surfaces and freeform surfaces. Here, **freeform surfaces** are those surfaces with complex forms which have no axes of rotation or translation symmetries. Freeform surfaces in engineering usually have designed shape that has larger scales compared to structured surfaces. Because of the difference in concern of surface geometry scales, sampling for freeform surfaces are excluded out of this thesis. However, some sampling techniques that are designed for surface topography measurement are also applicable to these larger scale surface geometries. Jiang's separate treatment of the different categories implies that a

feature-based understanding of surface topography has emerged. The concept of “engineered” and “non-engineered” surfaces are not preferred because they exhibit no apparent difference in the view of a metrologist. Designers and manufacturing engineers also do not always care about “engineered” surfaces because most surfaces which need to be inspected are engineered for a specific function. A classification based on “structured” or “stochastic” surface characteristics is regarded as more significant for engineers to choose proper manufacturing tools.

The definitions of “stochastic surfaces” and “structured surfaces” are given purely based on surface topography characteristics.

Stochastic surfaces: surfaces with dominant stochastic features.

Structured surfaces: surfaces with dominant deterministic features.

The term “dominant” is critical and sometimes controversial. For example, a turned surface can be allocated in both stochastic surfaces and structured surfaces because it is arbitrary for metrologists to identify the dominated features - stochastic roughness features or the structured waviness. A final decision is left to readers depending on specific applications.

Jiang et al [76] further divide structured surfaces into three types: linear patterns, tessellation patterns and rotationally symmetric patterns in 2007. It is obvious that based on this classification [76], MEMS surfaces which have complex geometries in micro/nano-metre scale are eliminated out from the range of structured surfaces. This has the same drawback as that of Evans/Bryan. In the following section, the structured surface classifications employed in this thesis are discussed.

2.1.3 Definitions and classifications employed

Considering the contributions of the predecessors and the critical issues above, a systematic surface classification of surface topography is given below (see Figure 2.3). The main classification criterion comes from a feature-based view of surface topography characteristics. Surface topographies with deterministic “multi-patterns”

are allocated as the fourth type of structured surfaces, which include the general MEMS surfaces. Relative terms are explained in this section.

Stochastic surface: a type of surface whose surface topography is dominated by stochastic features.

Among stochastic surfaces, the organisation of the stochastic features can be different. A stochastic surface is **isotropic** if its surface topographic features are organised uniformly in all directions. For example, the engineered surfaces produced using vertical electrical discharge machining (EDM), sandblasting method, etc., usually have isotropic surface topographies. A stochastic surface can also be **anisotropic** if its surface (topographic) features are organised directionally. For example, surfaces produced using turning usually have dominant feature directions, which are commonly termed as **lay**.

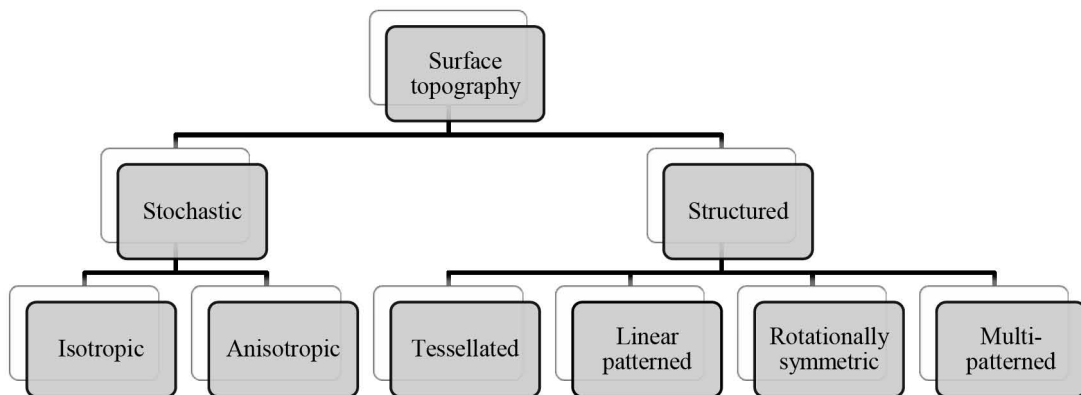


Figure 2.3. The surface classification based on surface topography characteristics [77].

Structured surface: a type of surface whose surface topography is dominated by deterministic features which are organised in a deterministic manner.

The deterministic organisation is recognised as an additional condition of a structured surface. If a surface topography is comprised of a random arrangement of a deterministic structure, it is still thought of as a stochastic surface. Structured surfaces can generally be divided into four sub-categories depending on different organisation

forms of the surface features. The four categories are tessellated, linear patterned, rotationally symmetric and multi-patterned surfaces.

Tessellated surface: a type of structured surface with a surface topography that is dominated by a repetitive pattern which comprises a collection of tiles that fills a plane with no overlaps and no gaps. This term comes from the tessellation (or tiling) techniques which are frequently used in architecture and decorative art [55]. For example, the seventeen wallpaper groups [55] are the tessellations with translational symmetries. Surface examples of tessellated surfaces include the majority of the structured surfaces such as golf balls, 3M structured abrasives [1], retroreflection coatings [99], and so on.

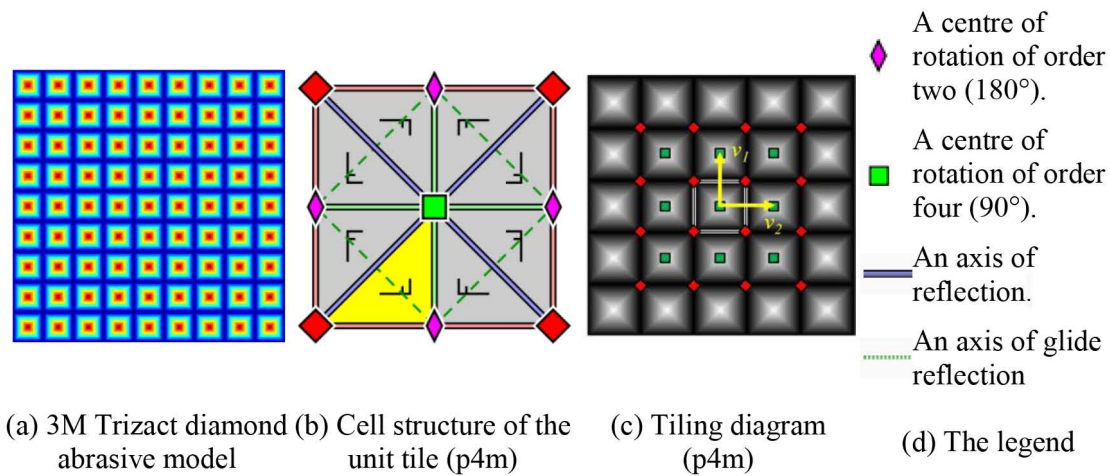


Figure 2.4. A 3M Trizact abrasive and the p4m tessellation diagram.

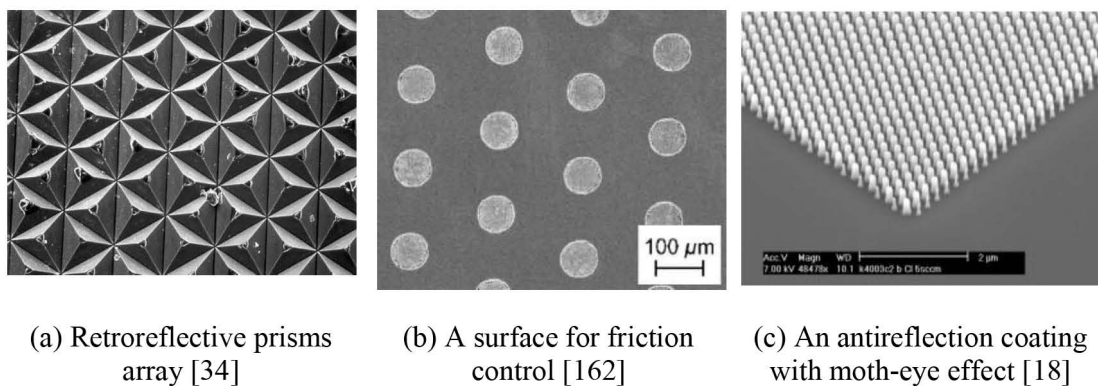
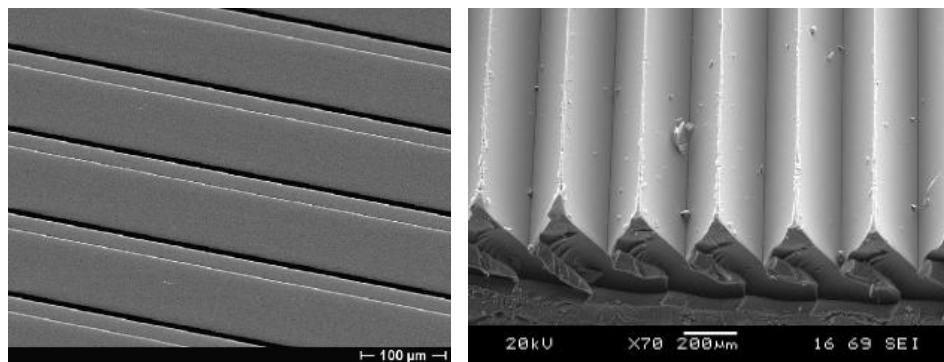


Figure 2.5. Surface topography of three tessellated surfaces.

Figure 2.4 presents an example of wallpaper group p4m used in 3M diamond abrasives [55]. The p4m wallpaper tessellation has two rotation centres of order four (90°), and reflections in four distinct directions (horizontal, vertical, and diagonals). The p4m type has additional glide reflections whose axes are not reflection axes; rotation centres of order two (180°) are centred at the intersection of the glide reflection axes. All rotation centres lie on reflection axes. The unit tile and the two translational vectors \mathbf{v}_1 and \mathbf{v}_2 (Figure 2.4c) are recognised as the central measures of tessellated surfaces [75].

Three other examples of tessellated surface are presented in Figure 2.5.

Linear patterned surface: a type of structured surface with its surface topography that is dominated by linear patterns. Here the linear pattern is a planar pattern which has translational symmetry on one dimension only. Some examples of this type surface, such as diffraction gratings and tribological textures [34, 78, 113] can also be categorised into tessellation wallpaper groups such as p1, pmm, pmg [55]. However, linear patterns are recognised separately from tessellations due to their distinct tile and tiling properties. For example, if the tiles of a linear pattern have infinite length in one direction \mathbf{d} , the tiling direction would be perpendicular to \mathbf{d} . See Figure 2.6 for two typical examples of linear patterns.



(a) A linear patterned surface for friction control [113]

(b) A prismatic film surface produced by Mircrosharp [28]

Figure 2.6. Surface topography of two linear patterned surfaces.

Rotationally symmetric surface: a type of structured surface with its surface topography that is dominated by a rotationally symmetric pattern, i.e. a surface function equal to its original after a rotation of a specific angle

$$z(r, \theta) = z(r, \theta + 2\pi / k), \quad k \in \mathbb{N} \cap [2, +\infty). \quad (2.1)$$

It is recognised that some tessellated surfaces may also be rotationally symmetric such as the wallpaper group p2 and p4m. Here only those rotationally symmetric patterns with no translational symmetry are concerned, such as Fresnel lenses, and the spiral groove patterns used in thrust bearings (see Figure 2.7).

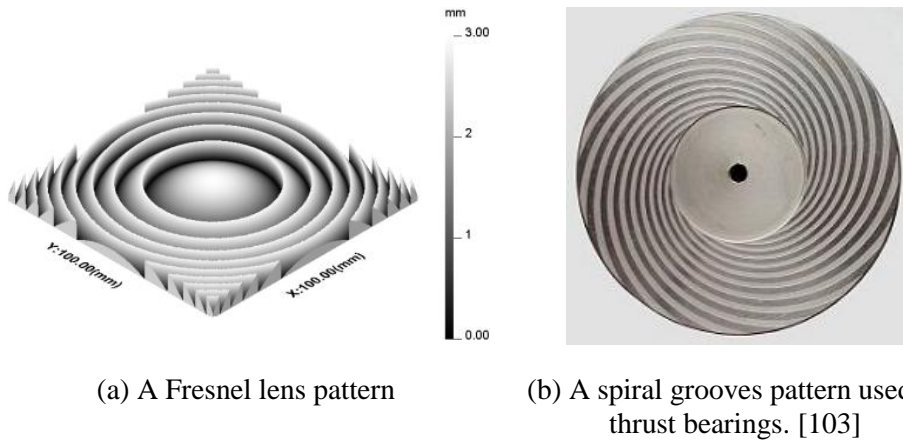


Figure 2.7. Two rotationally symmetric patterned surfaces.

Multi-patterned surface: a type of structured surface with its surface topography that is dominated by multiple patterns. Generally, a structured surface is recognised as multi-patterned if it is not a tessellation, linear or rotationally symmetric pattern. The majority of MEMS surfaces and lab-on-a-chip surfaces fall into this type (see Figure 2.8).

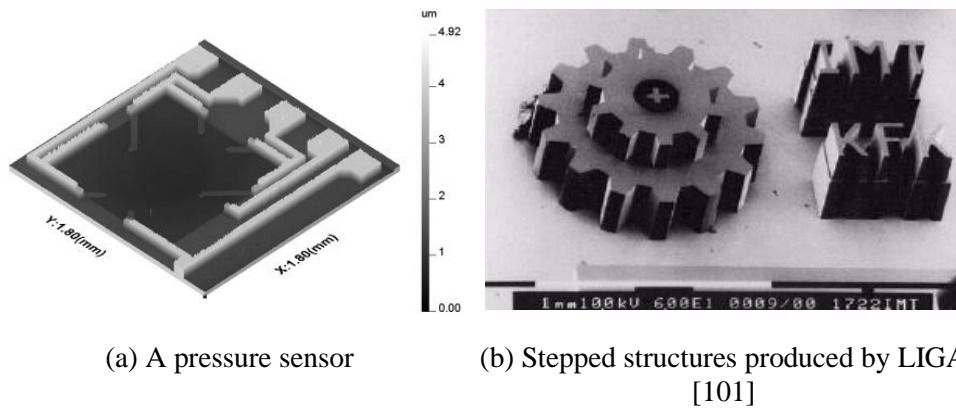


Figure 2.8. MEMS product surfaces with multi-patterns.

2.1.4 Industrial applications

With the development of precision engineering, micro-engineering and nanotechnology [7, 31, 35], a large field of structured surface applications has emerged. These applications cover the range of electronics, information technology, tribology, bio-medicine, optics, energy and so on. A list is given in this section to show the existing industrial applications with relative references.

Principles	Function details	Examples
Optics	Geometric optics	Fresnel lens [131, 143]
	Reflectivity	Retroreflection coatings [99, 141] anti-reflective coatings [18, 53]
	Diffractive optics and micro optics [34]	Diffractive gratings Lens arrays
Mechanics	Cutting tools	Micro tools [50, 78] Abrasive papers [51]
	Tribology [80, 113, 162]	High stiction surfaces Friction controlled surfaces Hard disk surfaces
	Hydrodynamics	Golf balls [146] Herringbone thrust bearings [103]
	Sensing	MEMS[49, 128]
	Surface energy	Adhesion[98] De-wetting and self-cleaning [11, 14]
	Metrology	Metrology artefacts [70]
	Others	Vacuum chunks [46]
Biomedicine	Medical implant [139]	Osseointegration Blood contact applications [48]
	Medical diagnostics [43, 139]	Lab-on-a-chip μ TAS
	Biomimetics [125, 161]	Photonics Hydrodynamics
Thermo-dynamics	[105, 132]	Spray cooling Boiling
Electronics		Information storage [59]
		ICs [121]

Table 2.1. Industrial applications and structured surfaces.

2.2 Measurement tasks

Measurement of surface topography aims to provide relative information to control the surface creation process or predict its performance (see Figure 2.9) [168]. For example, by understanding surface measurement data, i.e. functional characterisation,

feedback information can be obtained for engineering uses, for example control the surface production and manufacturing process, or control the wear conditions which the surface has suffered. Measurement of surface topography can also be used to predict the performance of an engineered surface, for example, testing the quality of a surface product and predicting the service life or its functional performances [168].

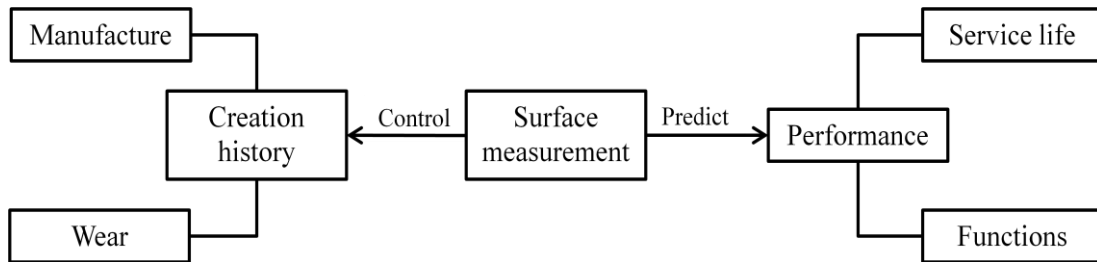


Figure 2.9. Usefulness of surface measurement.

There are various measurement tasks when considering the measurement of surface topography, particularly structured surfaces. Different engineering requirements determine unique measurement tasks. For example, in the fabrication of integrated circuits, critical dimension (CD) is a crucial measurement task which directly determines whether an IC product is desirable. In the fabrication of anti-reflective coatings, average nipple distance and height are the main measurement tasks. In the manufacture of MEMS, measurement of the draft angle of moulds may be a substantial task. Various measurement tasks in micro and nano engineering were reviewed by Hansen et al [59], which is the main reference for this section. On the measurement of structured surfaces, a summary of general measurement tasks is presented here.

2.2.1 General measurement tasks

The measurement tasks for structured surfaces are summarised based on the scale relevant properties of the general surface topography. The scale relevant properties include three surface components, i.e. form, stochastic components and deterministic components, which are generally considered separately. As has been introduced earlier, structured surfaces and stochastic surfaces have no clearly discriminated

boundary. The summarised measurement tasks also apply to stochastic surfaces, in which case, the stochastic features dominate.

General measurement tasks can be assigned to three general surface components: form, stochastic components and deterministic components. These surface components are scale-limited surface or primary surface. The three components are usually treated separately due to different characterisation approaches. Integrated measurement of the three surface components challenges the conventional surface topography measurement and dimensional metrology.

For example, measurement of the form error of the datum of a structured surface requires measuring a large area with limited samples and the sample size does not necessary to be dense. Measurement of the surface roughness of stochastic components requires uniform 2.5 dimensional dense sampling within each area of interest. Measurement of the dimensions of micro-scale structures requires three-dimensional measurement in micro/nano scale. Trying to fulfil the three measurement tasks in a single measurement is infeasible at the moment. An intermediate measurement task is accepted in general measurements.

Explanations of the three components are given as follows by considering the contributions from [59, 68, 168].

1. Form

Form is defined as the widely spaced components of a surface (see Section 2.1.1). It can often be judged using flatness, straightness, roundness, or cylindricity [64]. In surface topography measurement, an F-operator is usually implemented to remove form before characterisation of other surface components.

2. Stochastic components (see Figure 2.10a for an example)

Stochastic components or stochastically dominated components are generally measured based on a scale limited surface [68]. A scale limited surface is normally extracted using the proper spectral filters or spatial cutting tools to

remove uninteresting components, for example the form, or regional defects. With appropriate settings of S-filter, L-filter and F-operator, the S-F surface and the S-L surface of stochastic components can be obtained for later characterisation.

a. Three characterisation functions [68, 138]

Consider a scale limited surface which is presented by the areal data $\{z(x_i, y_j) : x_i = i \cdot \Delta_x; y_j = j \cdot \Delta_y; i = 1, 2, \dots, M; j = 1, \dots, N\}$, where Δ_x, Δ_y are the lateral distances of neighbouring sample points in the x and y directions, M and N are the column and row size of the data matrix z . Three surface functions can generally be deduced as in Table 2.2.

1. Auto-correlation function	$ACF(tx, ty) = \frac{1}{(M-i)(N-j)} \sum_{l=1}^{N-j} \sum_{k=1}^{M-i} z(x_k, y_l) z(x_{k+i}, y_{l+j}),$ <p>where $i = 0, 1, \dots, m < M; j = 0, 1, \dots, n < N; tx = i \cdot \Delta_x; ty = j \cdot \Delta_y$.</p>	(2.2)
2. Power spectral density function	$PSDF(\omega_p, \omega_q) = \frac{F(\omega_p, \omega_q) F^*(\omega_p, \omega_q)}{MN \Delta_x \Delta_y},$ <p>where $F(\omega_p, \omega_q)$ is the Fourier transform of the areal data $z(x_i, y_j)$ and $F^*(\omega_p, \omega_q)$ is the complex conjugate of $F(\omega_p, \omega_q)$. A Fourier transform of $z(x_i, y_j)$ can be computed as</p> $F(\omega_p, \omega_q) = \sum_{l=0}^{N-1} \sum_{k=0}^{M-1} z(x_{l+1}, y_{k+1}) e^{-j2\pi(\frac{p}{M}l + \frac{q}{N}k)}$ <p>where $p = 0, 1, \dots, M-1; q = 0, 1, \dots, N-1; \omega_p = \frac{p}{\Delta_x \cdot M}, \omega_q = \frac{q}{\Delta_y \cdot N}$.</p>	(2.3)
3. Areal material ratio function	The areal material ratio function $Smr(c)$ characterises a scale limited surface by presenting the material ratio as a function of surface height [67]. Specifically, it is the ratio of the area of the material at a specific height c to the evaluation area.	

Table 2.2. The three characterisation function of a scale limited surface.

b. Field parameters [68]

Height parameters			
1.	Sa	the arithmetic mean height	$Sa = \frac{1}{A} \iint_A z(x, y) dx dy$
2.	Sq	the root mean square height	$Sq = \sqrt{\frac{1}{A} \iint_A z^2(x, y) dx dy}$
3.	Sp	the maximum peak height	
4.	Sv	the maximum valley height	
5.	Sz	the maximum peak to valley height	
6.	Ssk	the skewness	$Ssk = \frac{1}{Sq^3} \left[\frac{1}{A} \iint_A z^3(x, y) dx dy \right]$
7.	Sku	the kurtosis	$Sku = \frac{1}{Sq^4} \left[\frac{1}{A} \iint_A z^4(x, y) dx dy \right]$
Spacing parameters (default $s = 0.2$ [69])			
8.	Sal	the autocorrelation length, i.e. the horizontal distance of the ACF which has the fastest decay to a specified value s .	$Sal = \min_{tx, ty \in R} \sqrt{tx^2 + ty^2}$ where $R = \{(tx, ty) : f_{ACF}(tx, ty) \leq s\}$
9.	Str	the texture aspect ratio	$Str = \frac{\min_{tx, ty \in R} \sqrt{tx^2 + ty^2}}{\max_{tx, ty \in Q} \sqrt{tx^2 + ty^2}}$ where $R = \{(tx, ty) : ACF(tx, ty) \leq s\}$ $Q = \{(tx, ty) : ACF(tx, ty) \geq s \& **\}$
Hybrid parameters			
10.	Sdq	the root mean square gradient	$Sdq = \sqrt{\frac{1}{A} \iint_A \left[\left(\frac{\partial z(x, y)}{\partial x} \right)^2 + \left(\frac{\partial z(x, y)}{\partial y} \right)^2 \right] dx dy}$
11.	Sdr	the developed interfacial area ratio	$Sdr = \frac{1}{A} \iint_A \left[\sqrt{1 + \left(\frac{\partial z(x, y)}{\partial x} \right)^2 + \left(\frac{\partial z(x, y)}{\partial y} \right)^2} - 1 \right] dx dy$
Functional parameters [69]			
12.	$Smr(c)$	the areal material ratio at a	

		specified height c	
(Continued)			
13.	$S_{mc}(mr)$	the inverse areal material ratio, i.e. the height at a given material ratio mr	
14.	Sk -family	areal parameters for stratified functional surfaces which contain eight variables $Sk, Spk, Svk, Smr1, Smr2, Svq, Spq$ and Smq [67]	
15.	$V_v(mr)$	the void volume at a given material ratio mr	
16.	V_{vv}	the dale void volume at p material ratio	$V_{vv} = V_v(p)$, with default $p = 80\%$
17.	V_{vc}	the core void volume between p and q material ratio	$V_{vc} = V_v(p) - V_v(q)$, with default $p = 10\%$, $q = 80\%$.
18.	$V_m(mr)$	the material volume at a given material ratio mr	
19.	V_{mp}	the peak material volume at p material ratio	$V_{mp} = V_m(p)$, with default $p = 10\%$.
20.	V_{mc}	the core material volume between p and q material ratio	$V_{mc} = V_m(q) - V_m(p)$, with default $p = 10\%$, $q = 80\%$.
21.	S_{xp}	the peak extreme height. i.e. the height difference between material ratio p and q .	$S_{xp} = S_{mc}(p) - S_{mc}(q)$ with default $p = 97.5\%$, $q = 50\%$.
Fractal parameters			
22.	S_{fvc}	the volume fractal complexity	
23.	S_{afc}	the areal fractal complexity	
Miscellaneous parameters			
24.	Std	the texture direction	

Table 2.3. The thirty-one field parameters. Note: the functions V_v and V_m describe the volume of the voids and materials per unit area which are derived from the inverse areal

$$\text{material function } S_{mc}: V_m(p) = \frac{K}{100\%} \int_0^p S_{mc}(q) - S_{mc}(p) dq, \text{ and}$$

$$V_v(p) = \frac{K}{100\%} \int_p^{100\%} [S_{mc}(p) - S_{mc}(q)] dq, \text{ where } K \text{ is a constant to convert to millilitres}$$

per metres squared.

A scale limited surface can be characterised based on a statistic of the continuous surface data (cloud of points) which results in the field parameters. Field parameters can be divided in to five groups in terms of their describing capabilities. Here these parameters are presented with a brief explanation because they are not relevant to the main theme of this thesis (see Table 2.3). In conventional surface texture measurement, the field parameters are usually the most common measurement tasks.

c. Feature parameters

In the novel feature-based [15] characterisation system [68], a real surface is seen as a composition of various geometric features. By applying statistics to a subset of the predefined topographic features, feature parameters can be calculated. The feature parameters characterise a common geometric property of a set of surface features. In the current ISO standard [68], nine feature parameters are initially given (see Table 2.4).

1.	<i>Spd</i>	the density of peaks
2.	<i>Spc</i>	the arithmetic peak curvature
3.	<i>S10z</i>	the ten point height
4.	<i>S5p</i>	the five point peak height
5.	<i>S5v</i>	the five point valley height
6.	<i>Sda</i>	the closed dale area
7.	<i>Sha</i>	the closed hill area
8.	<i>Sdv</i>	the closed dale volume
9.	<i>Shv</i>	the closed hill volume

Table 2.4. The suggested nine feature parameters in ISO 25178 Part 2.

3. Deterministic components (See Figure 2.10b, c and d for examples)

Deterministic components are comprised of pre-designed surface topography. The deterministic components of a structured surface can be

linear patterned, tessellated, rotationally symmetric or multi-patterned. Characterisation techniques for the different features vary a lot. For example, many feature recognition and characterisation methods have been developed for different surface structures, for example steps, tessellations and edges[75, 159]. Generally, the measurement tasks of these deterministic features can be divided into two categories [59]: geometric dimensions and geometric errors.

a. Geometric dimensions [59]

1.	<i>Distance</i>	as defined between two surfaces oriented in the same direction. Example: distance between two lines of a line grating
2.	<i>Width</i>	as defined by the distance between two opposing surfaces. Example: width of a channel
3.	<i>Height</i>	as defined by the distance between two surfaces of same orientation but placed in a vertical direction. Example: depth of a micro-fluidic channel
4.	<i>Thickness</i>	of layers
5.	<i>Aspect ratio</i>	as defined by the depth of a structure divided by its width
6.	<i>Slope</i>	‘steepness’ of a line, the ratio of vertical rise to horizontal distance and expressed as a percentage or as degrees of angle
7.	<i>Angle</i>	as defined by the amount of relative rotation of two rays by their common endpoint. It falls into side angle, helix angle, etc.
8.	<i>Curvature radius</i>	of an edge
9.	<i>Area</i>	as defined by the quantity of two-dimensional size of specific parts or features of a surface
10.	<i>Volume</i>	the three-dimensional space size of specific parts of features occupies within a surface

Table 2.5. The common geometric dimensions of the general measurement tasks.

b. Geometric errors

The real geometry of the deterministic features of a structured surface always deviates from the intended geometries. The shape, orientation and position deviations of the micro-scale geometries are usually of concern. To a metrologist there is no difference

between characterisation of the shape deviations of a micro-feature and form evaluation. The general geometric errors include straightness, flatness, circularity, cylindricity, parallelism, perpendicularity, angularity, concentricity, coaxiality, and so on [64].

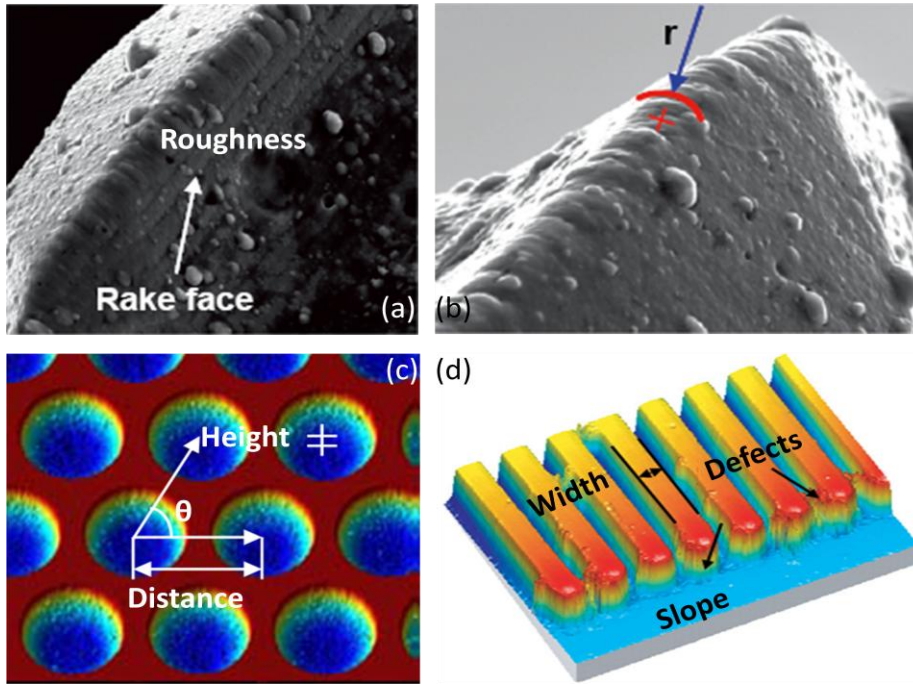


Figure 2.10. General measurement tasks of structured surfaces (a) (b) in micro-tools [15], (c) micro-optics and (d) ‘Lab-on-a-chip’.

2.2.2 The intermediate task

Due to the miniaturisation of novel structured surfaces, the general measurement tasks proposed above cannot be accomplished through conventional dimensional metrology. Besides, with commercial surface profilometry instruments, the characterisation parameters of functional relevance for a specific surface are not usually provided. On account of these, to metrologists, an intermediate measurement task is to collect discrete topography data of a surface. From the topography data, the general measurement tasks above can be extracted indirectly.

Statistics and signal process techniques [26, 74, 75, 126, 174] have been widely used to characterise the intermediate topography data. For example, a surface with tessellated topography can be segmented into a series of regions with separate unit features. The geometric parameters related to each single feature or between neighbouring features can be calculated. Practical solutions for dimensional or functional characterisation of surface topography data have been proposed, for example in [17, 75, 159, 165].

A widely recognised procedure for the measurement of surface topography is illustrated in Figure 2.11. The measurement tasks in this procedure becomes the surface topography measurement and the characterisation [86]. A stable measurement of the surface topography by providing a digital presentation of the surface geometric information (usually a cloud of points expressed by a data matrix) has been recognised as the direct measurement task in surface measurement. However, many challenges have arisen at present in the first procedure, i.e. surface topography measurement.

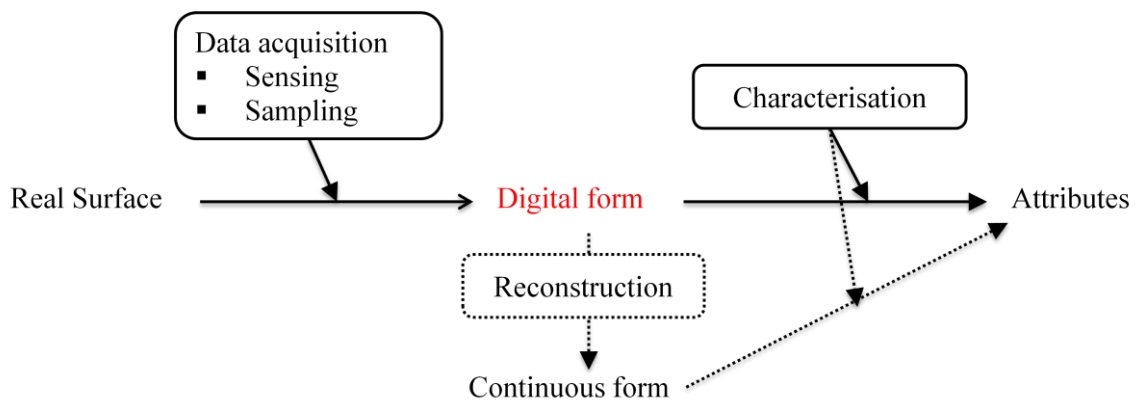


Figure 2.11. General procedures for the measurement of a patch of surface topography.

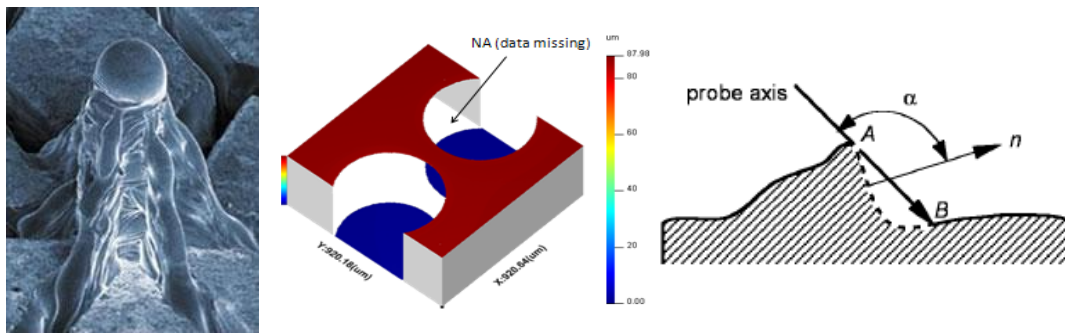
2.3 Measurement challenges

Measurement of structured surfaces by providing a cloud of data of the topographic height information suffers from a range of technical difficulties. For example, the measurement difficulties brought about by miniaturisation are becoming critical, for

example, in semiconductor industries (see Table 2.6). Current CMM tips are too large to penetrate into small structures. Besides, many novel surface topographies have complex geometries (see Figure 2.12a) or tend to be higher in aspect ratio or slope in terms of local features. Hence, some measurement problems or faults result such as missing data (see Figure 2.12b) and optical defects of optical measurements (see Figure 3.7), and inability to analyse re-entrant features (see Figure 2.12c). In addition, material properties also increase measurement difficulties, for example the transparency of glass surfaces. A list of the geometric complexities and commonly induced measurement difficulties or problems is presented in Table 2.7.

Year of production	2005	2010	2015	2020
DRAM stagger-contacted Metal 1 (M1) $\frac{1}{2}$ Pitch (nm)	80	45	25	14
MPU/ASIC stagger-contacted Metal 1 (M1) $\frac{1}{2}$ Pitch (nm)	90	45	25	14
Flash Uncontacted Poly Si $\frac{1}{2}$ Pitch (nm)	76	36	20	11
MPU Printed Gate Length (nm)	54	30	17	9
MPU Physical Gate Length (nm)	32	18	10	5.6

Table 2.6. Key lithography-related characteristics of semiconductor products [73].



(a) Complex patterns by electron beam texturing (b) NA in optical measurements (c) Re-entrances unreachable

Figure 2.12. Typical measurement difficulties [94, 156].

In terms of the material, dimensional and local geometric complexities (Table 2.7), the challenges of measurement in sensing, sampling and characterisation have been recognised. Much work has been carried out to find solution for these problems [76,

86, 164, 168]. Specifically, three categories of challenges are described in the following context.

Complexities	Details	Measurement difficulty/fault examples
Material	<ol style="list-style-type: none"> 1. Elastic or plastic deformation 2. Low reflectivity 3. Special condition requirements 	<ul style="list-style-type: none"> • Deformation caused by stylus and AFM [107] instruments • Requirements of dark room, aqueous solution, vacuum, etc.
Dimensions	<ol style="list-style-type: none"> 1. Miniaturisation For example, micro or nano scale structures, very fine roughness. 2. Large dimensional span For example, large surface size with very small structures, or large dimension span on different directions. 	<ul style="list-style-type: none"> • Critical dimensions in IC industry are foreseen to decrease dramatically during the next decade [73] (Table 2.6) which exceeds the measurement resolution of most of the current instruments • Micro scale groove width with millimetre scale groove length of an optical grating
Local geometric complexities	<ol style="list-style-type: none"> 1. High aspect ratio For example, Optical/mechanical tips unreachable 2. High slope For example, Objective aperture limitation, limitation of the Included angle of a mechanical tip 3. Three-dimensional nature with re-entrances For example, Multi-valuedness of a surface texture 4. Complex patterns For example, Demand for advanced characterisation techniques 	<ul style="list-style-type: none"> • High aspect ratio of a moth-eye like anti-reflective coating [18] • The included angle [137] of a tip determines the maximum slope that is measurable $\tan \alpha_{max} = 90^\circ - \theta / 2$ • Data missing can be caused by slope limitation of objective apertures. Usually a slope limit is 32° [46] • In Figure 2.12c, feature is not detected when the angle α between the probe axis and the local normal is larger than 90° (ideally)

Table 2.7. Complexities of structured surfaces and examples of measurement difficulties or faults.

1. Challenges for sensing techniques

Structured surfaces are embedded with miniaturised structures (usually in micro-scale or nano-scale), or high aspect ratio, high slope and re-entrant features. General

instruments have difficulty in sensing these complex features. Most current instruments cannot always reveal the true surface geometries and incorrect measurement results usually take place, such as missing data or optical artefacts in optical measurement, immeasurability of high aspect ratio or re-entrant features, physical resolution limitation of tips, and so on.

These local measurement difficulties challenge current surface geometry sensing techniques. Progress has been made recently in terms of development of advanced sensing techniques. For example, a focus variation technique has been developed [33] which is able to measure those high slope features using different scatter. Multi-sensor techniques are also in development nowadays using data fusion. Hence, the limitations of a sensor can be compensated by other sensors [56]. These novel techniques are not covered in this PhD work.

2. Challenges for sampling techniques

In conventional surface topography measurement, the conflict between measurement efficiency and accuracy is usually ignored because it is always acceptable. However, the emergence of structured surfaces intensifies this conflict. Many structured surfaces have a large working area ranging from millimetres to metres but embedded with micro- or nano-scale structures, such as 3M diamond abrasives, Fresnel lenses, retroreflective prism arrays, etc (see Section 2.1 for illustrations). Some structured surfaces tend to have large dimensional spans in different lateral directions. For example, some Microsharp prismatic film [28] has a separation distance between neighbouring lenses of approximately 100 μm , but has an effective length of approximately 100 mm in the orthogonal lateral direction. This large dimensional span makes the problem of measurement efficiency against accuracy critical. For example, a stylus instrument may take hours to perform a single measurement to cover the whole working area to ensure the sampling resolution in all the directions and positions.

Intelligent sampling designs are a potential solution to this difficulty. By employing intelligent sampling methods, for example, Hammersley or adaptive sampling patterns [172], stylus or optical instruments are able to flexibly detect the important positions

within a surface topography. The geometric information of these positions has a critical influence on the reconstruction accuracy when the sampled data are employed to reconstruct a continuous surface. In this way, the sampling efficiency can be improved and the sampling accuracy can be retained. Some developments in efficient sampling have been made in engineering measurement, such as the flatness, or free-form measurement [44, 172] using CMMs. However, no work has been carried out in terms of surface topography measurement, in the knowledge of the author.

In this research, an investigation of intelligent sampling techniques in surface topography measurement is carried out. Potential sampling methods to guarantee both the efficiency and accuracy are explored. As a research output, a sequential profiling adaptive sampling method is proposed. In the later chapters, the issues relating to intelligent sampling methods are given.

3. Challenges for functional characterisation

Some complex structures embedded in a structured surface require flexible and stable algorithms for functional characterisation. Current statistics-based characterisation techniques [16, 68, 134] have been well used in relation to stochastic surfaces. However, the statistics-based techniques do not work efficiently for the characterisation of some predefined surface features, for example hills and dales that exist in an imperfectly manufactured planar surface. The recently standardised feature characterisation technique [126, 142] is designed to be work for structured surfaces. Many achievements have been made based on this technique, for example in the characterisation of titanium artificial human teeth surfaces [166], sheep and human articular cartilage surfaces [154], and the recognition of the cutting edges of a grinding wheel [126]. Some practical cases [159, 174] indicate that far more flexible characterisation techniques are necessary. For example, the standardised feature characterisation in ISO 25178 Part 2 [68] does not consider the evaluation of the dimensional parameters of a deterministic surface component.

Outstanding work has been carried out in terms of this challenge based on feature recognition techniques, such as the PhD thesis by Verma [159]. Characterisation techniques are out of the scope of the thesis. But as an evaluation tool which can be

used to judge the performance of different sampling methods, feature-based techniques are partially considered as a research topic in this thesis. A boundary segmentation algorithm has been developed, which is successfully used in the performance validation of the proposed adaptive sampling.

Overall, this research is conducted by focusing on the challenges in sampling.

2.4 Summary

In this foreword chapter, the state of the art of surface topography measurement structured surfaces is reviewed. The following viewpoints are summarised on the basis of the review of this chapter.

1. There are some utilisation conflicts in the definitions of structured surfaces. Evans/Bryan's definition seems to exclude the classification of MEMS; Stout/Blunt's definition is engineering-oriented and lacks the considerations of the variety of natural existences. The adopted definition and surface classifications is based on a feature-based view of surface topography geometries. There have a rational avoidance of most of the potential disputes and tends to be simple and stable for surface classification.
2. Four basic categories of structured surfaces are classified based on the shape of the layout of the surface topography features. They include linear patterns, tessellations, rotational symmetric patterns and multi-patterns. The variety of the geometric properties may necessitate different measurement and characterisation methods.
3. Structured surfaces have shown promising performance in engineering and a wide range of applications have been developed.
4. In terms of the measurement of structured surfaces, the general measurement tasks and the measurement components are summarised. The measurement components include the form, stochastic components and deterministic components. The measurement tasks of the three components include a variety of surface characterisation functions, parameters and dimensional parameters and errors. The

integrated measurement of these tasks is challenging for conventional surface topography measurement.

5. The surface dimensional span, local geometric complexities and possible material complexities constitute three categories of challenges in terms of sensing, sampling and characterisation. The challenges for sampling fall into the scope of this thesis.

3. SAMPLING

This chapter starts with a review of the state of the art of sampling techniques for surface topography measurement. This chapter does not go deep into the development of new sampling methods. It summarises the sampling framework for practical surface topography measurement. The ideas of this chapter, for example global and local sampling, are not new. However, they are argued for the first time within a complete sampling framework. Also, conventional and novel sampling theories are revisited. As an introductory chapter on sampling, explanations of the related terminologies are included to avoid ambiguity.

3.1 Sampling in surface measurement

Sampling is regarded as a selection of some parts from a population. Given a sensing technique, for example a stylus measurement, sampling areas and sample densities determine the measurement efficiency and accuracy. An optimised design of the sample positions can improve the measurement efficiency or enhance the accuracy [114]. Exploration or development of intelligent sampling methods for the measurement of structured surfaces is the ultimate objective of this research.

However, definitions of sampling are not uniform across different fields such as statistics or signal processing. **Sampling in signal processing** refers to taking discrete sample values from a continuous signal [114] such that the continuous signal can be recovered or approximated by the discrete samples. For example, a photograph of a real scene is taken as a composition of discretized pixels by a digital camera before storage. **Sampling in statistics** consists of selecting some part of a population to observe so that the characteristics of the whole population can be estimated [82, 151]. For example, to estimate the population of a region, samples of streets or communities are chosen before a systematic estimation.

It is apparent that the two disciplines have different emphases. Sampling in signal processing focuses on sampling fidelity when the discrete samples are employed to reconstruct a continuous signal that is similar to the original. For example, the band-

limited signal sampling theory [129] which has been widely used in engineering concentrates on how to perfectly recover a band-limited signal by determining a proper sampling spacing. Sampling in statistics focuses on the estimation of the statistical characteristics of a population. For example, a characteristic of a population is measured using a statistic such as the sample mean, variance, standard deviation, maximum, minimum, kurtosis and skewness [24].

Sampling related terms usually differ between statistics and signal processing. An unambiguous use of these terms needs to be carefully considered. An imprudent use certainly causes a misunderstanding. To be on the safe side, the following content gives an unambiguous explanation of sampling related terms which will be used in general surface topography measurement in later chapters.

In surface metrology, a two-stage sampling strategy has typically been constructed for practical measurement, where the two different sampling related techniques are in sequence, for example in the work of Rosen [123]. Taking measurement of the surface roughness Sq of a composite surface as an example (see Figure 3.1), the two-stage sampling strategy is carried out as follows.

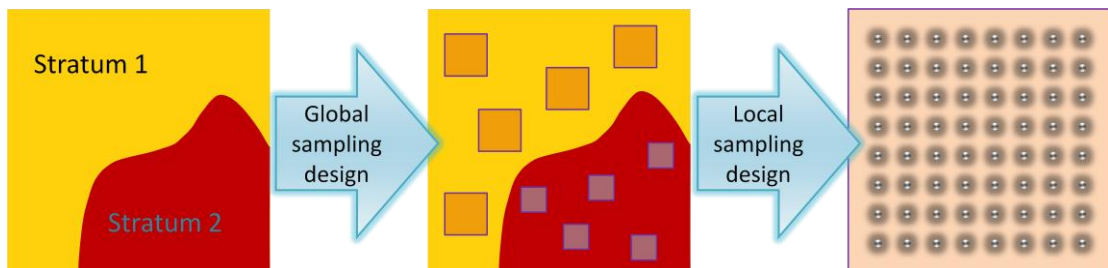


Figure 3.1. Illustration of two-stage sampling for the evaluation of surface topography. Global stage: simple random selection of sampling units within a stratum. Local sampling: uniform signal sampling within each sampling unit.

1. Global stage. In the global statistical sampling stage, a series of **sampling units** (also referred to as **sample units** – one of the individual parts into which the population is divided [65, 151]) is selected from different population strata (different strata may have different properties and need to be measured

separately). Statistical tools are used in this stage to understand the whole surface by evaluating the characteristics of the selected sampling units.

2. Local stage. A local signal sampling with a specific method (for example uniform or simple random selection) is carried out within each sample unit. The signal **samples** (a set of values of a signal at selected positions) are collected with specific sampling density to give a representation of the local geometries of the selected sampling unit. This stage can be executed easily using surface topography measuring instruments, such as coherence scanning interferometers (CSI).

The former stage concentrates on a rational estimation of the characteristics of the whole surface; while the latter focuses on approximation of local surface geometries with discrete samples. The term sample is not preferred in the global sampling stage because a surface is essentially a continuous signal population; a sample may give the impression of a signal value or values. To be unambiguous, the terms of sampling unit(s) and sample(s) are used separately for the global and local stages in this thesis.

By adjusting the sampling positions or sample sizes in both stages, the measurement accuracy and efficiency can be controlled. The procedure by which the sample units (in the global sampling stage) or samples (in the local signal sampling) are selected from the population is called the **sampling design**. For example in the two-stage sampling of surface measurement in Figure 3.1, global statistical sampling and local signal sampling have different sampling designs, i.e. the former employs a simple random sampling; the latter uses a uniform sampling. In other words, a sampling design assigns the sampling method and sampling conditions in a specific sampling process. Here **sampling methods** refers to a method or pattern by which the sample or sample units are selected. For example, uniform or random selection of sample units can be regarded as a sampling method. **Sampling conditions** refers to the control parameters of a sampling method, such as the density of samples, spatial distances between neighbouring sample units or samples, and so on. A hierarchical structure of the sampling procedures used in surface metrology is presented in Figure 3.2.

Since sampling works for selection of some part from a population in both these stages above, **sampling errors** are normally induced by this process. In statistical sampling, sampling errors refer to the estimation errors of the sample properties from the corresponding population properties, for example a bias produced by estimation using an unrepresentative selection of the sampling units. In signal sampling, sampling errors refer to any deviations of the approximation signal from the original continuous signal. In practice, many non-sampling errors also exist which are consequences of the mechanical and electronic accuracy or repeatability of measurement devices, such as the measurement uncertainties of a single sample value. The sampling errors and practical non-sampling errors are sometimes regarded as logic errors and physical errors [172].

Research [90, 134] on sampling in surface measurement has been carried out in the past. ISO 25178 Part 3 [69] has published suggestions on selecting sampling conditions for areal surface measurement. However, only uniform sampling in surface topography measurement has been investigated. During the sixty years since the publishing of Shannon's sampling theory [129], a lot of innovative work on adaptive sampling, low-discrepancy sampling, wavelet, approximation theory and function analysis, has been conducted. A systematic investigation of modern intelligent or efficient sampling methods needs to be carried out.

In this research, global statistical sampling and local signal sampling are systematically investigated based on the hierarchical schematic in Figure 3.2. The proposed sampling framework consists of the sampling related issues during a practical surface topography measurement. Many ideas in this framework are not new. However, the framework is proposed for the first time in the reference to the considerations involved with practical measurements.

In later sections, statistical sampling methods for the global stage are introduced. A general procedure on selection of the sampling conditions of the global sampling stage is given. For the local stage, the drawbacks of the present uniform sampling are analysed. The intelligent sampling techniques, which have the potential for the improvement of surface measurement, are investigated. Typical techniques including

jittered uniform sampling, low-discrepancy pattern sampling, model-based sampling and adaptive sampling are tested. With proper reconstruction algorithms, the performances of different methods can be compared. A framework of sampling for the measurement of structured surfaces is produced.

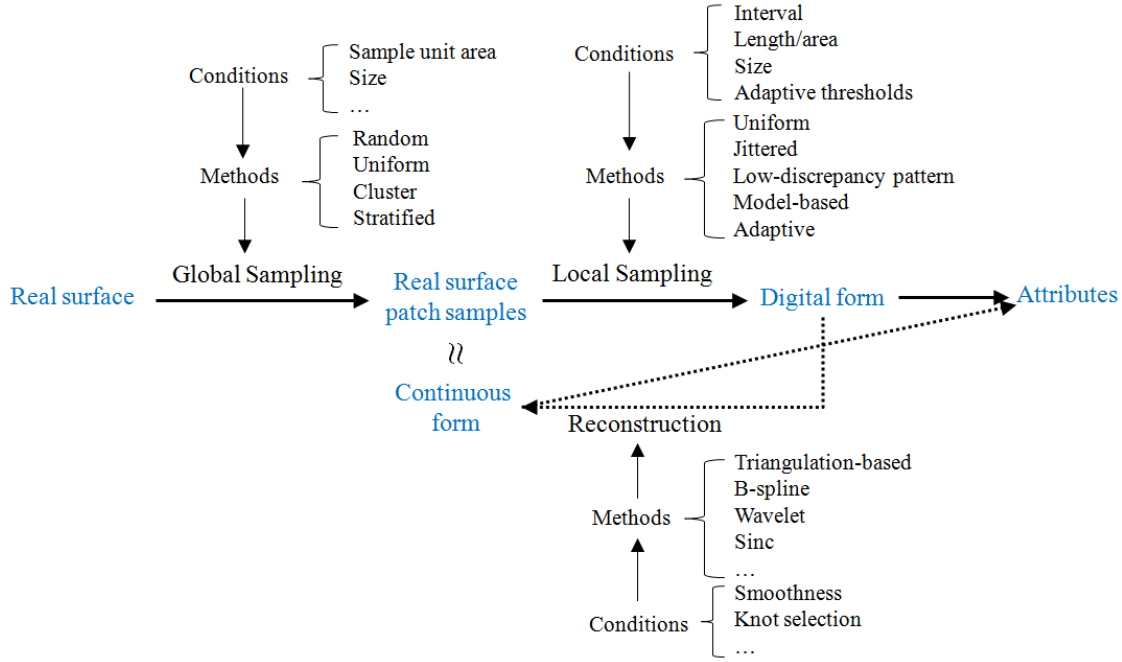


Figure 3.2. Schematic of sampling related issues in general surface measurement.

3.2 Global statistical sampling

3.2.1 Introduction

In general measurement of surface topography, global sampling is usually regarded as the first stage of a complete sampling design. Global sampling is concerned with selection of proper surface segments (i.e. sampling units) for observation. The theory of sampling in statistics [82, 151] is employed at this stage. Hence, the properties of interest of the population can be rationally estimated. For example, several tens of surface patches ($3 \text{ mm} \times 3 \text{ mm}$) are randomly selected from a cylinder liner surface. Then each surface patch can be conveniently inspected using interferometers.

The properties of interest can be a statistic (for example sample mean, variance, standard deviation, maximum, minimum, kurtosis and skewness) of the surface topography characteristic such as dimensional parameters or field parameters (see Section 2.2). In some advanced cases, regression analysis and time series analysis methods [24, 25], such as Fourier transform and auto/cross correlation, are used.

Statistical sampling has been widely introduced into modern higher education. There are many textbooks in statistics regarding to the selection of samples from a finite population, for example in [82, 151]. Related topics include the determination of sampling units, determination of sample methods and sample size. It is not necessary to go into detail regarding the statistical theories in this thesis; rather a general procedure used for global sampling is given as a general reference. This procedure has not been consistently adopted for general surface topography measurement because no global sampling guide has been produced in the past. This proposed procedure reflects a complete consideration of sampling in practice. In the following context, the procedure summarised here as a general reference.

3.2.2 Determination of sampling units

The division of sampling units is a general procedure in surface measurement. In practice, a real surface of a substance is a continuous population. It is necessary to divide a surface into discrete sampling units (for explanations of the terms, please refer to Section 3.1) which can then be selected in some part for observation. For example, Rosen uniformly divides a cylinder liner surface into grid units for the measurement of surface roughness [123]. Tian uniformly cuts an articular cartilage into small pieces and selects some part for wear analysis [153].

Normally, a metrologist can be free to choose alternative sizes and shapes of units, and such choices may affect the evaluation accuracy. To guarantee high evaluation accuracy, the application environments of the samples to be measured always need to be considered. In surface metrology, as the observed surface topography is usually on the micrometre scale, it is not necessary to choose large sampling lengths over 8 mm [168]. Nowadays, international or national standards, and modern surface topography measurement instruments, have restrained the sample length or area into a series of

common values, such as 0.25 μm , 0.5 mm, 0.8 mm, 1 mm, 2 mm, 2.5 mm and so on [69]. If simple sampling methods, for example simple random sampling, are used, the size of the sample unit can be set as the same as the sampling length which is suggested by standards or instruments. For example in [123], the size of a sampling unit is set as equal to the measurement area of the microscope MicroXAM² HD100, i.e. 0.81 mm \times 0.61 mm (see the sampling units A1, B4, C2, E1 and E3 in Figure 3.3).

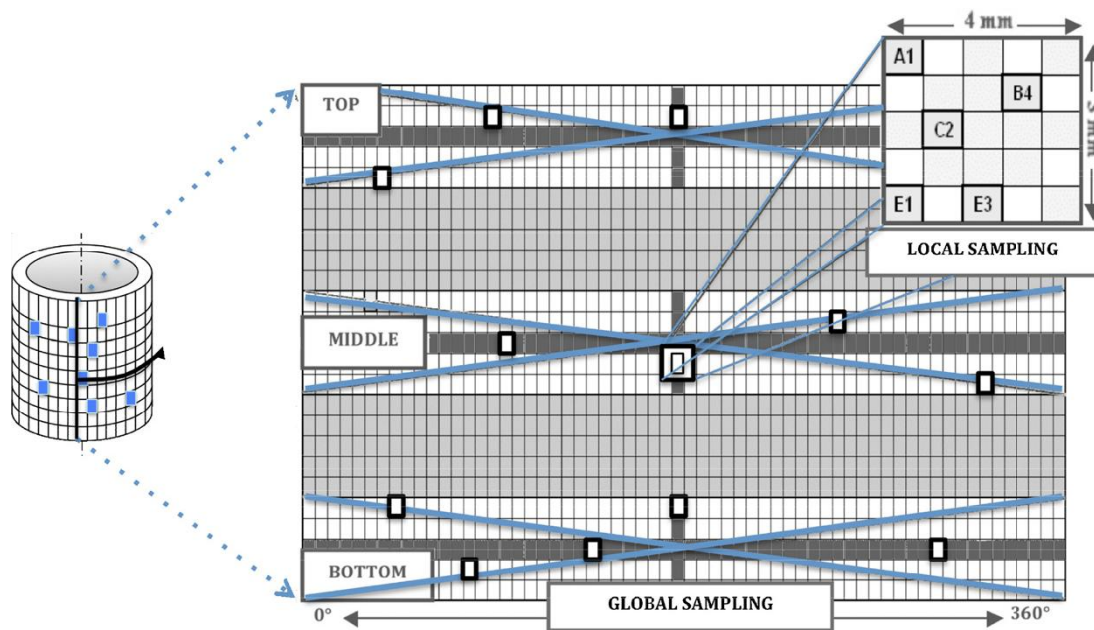


Figure 3.3. A sample design in the measurement of the surface roughness of a cylinder bore [123].

3.2.3 Selection of sampling methods

Proper sampling methods need to be determined for the selection of sampling units from a population. Four types of statistical sampling methods are generally used in a statistical surveys [82]. These methods are simple random sampling, uniform sampling, stratified sampling and cluster sampling (see Figure 3.4).

Simple random sampling (SRS) is a sampling such that each individual is randomly selected from a population. It is an ‘equal probability of selection’ (EPS) sampling

design in which every element in a population has the same probability of being selected.

Uniform sampling, as also called systematic sampling or regular sampling, is a sampling design in which the samples are selected from an ordered sampling frame at a regular interval. The method provides an alternative for random sampling, which is also an EPS as long as the starting sampling position is randomly determined. Uniform sampling and simple random sampling are perhaps the most widely know selection procedures at present.

In some complex cases, the two methods described above are used solely or jointly with stratification or with cluster sampling. For a population with a huge amount of sample units, measurement efficiency is improved considerably when properly packing neighbouring sample units into clusters. When a population has different sub-populations and they vary considerably, samples need to be independently selected from each stratum. Finally, a weighted statistic can be estimated.

Cluster sampling, sometimes regarded as two-stage sampling, is a special case of multi-stage sampling. In the first stage, some primary units, which contain a bundle of secondary units (i.e. the sampling units), are selected; in the second stage, sampling units within each primary unit are selected, which are used to give an estimation of each primary unit, and finally of the whole population. Cluster sampling is common in surface measurement, for example in [123], all 5×5 sampling units are bundled into a cluster, which are randomly selected from each stratum at first.

In **stratified sampling**, the population is partitioned into regions or strata, and a sample is selected by some design within each stratum. For example in Figure 3.4, Strata 1, 2 and 3 are partitioned because of their different properties on average. Samples from each stratum are representative of the each stratum. Because the samples are selected from each stratum independently, characteristics of the whole population can be obtained by a weighted statistic of the characteristic of each stratum. The variances of a characteristic for individual strata can be added together to obtain the variances of characteristics of the whole population. A prior knowledge of the population is necessary before stratification. A practical stratification in surface

measurement by grouping the whole surface into homogeneous sub-regions can be related to previous work [122].

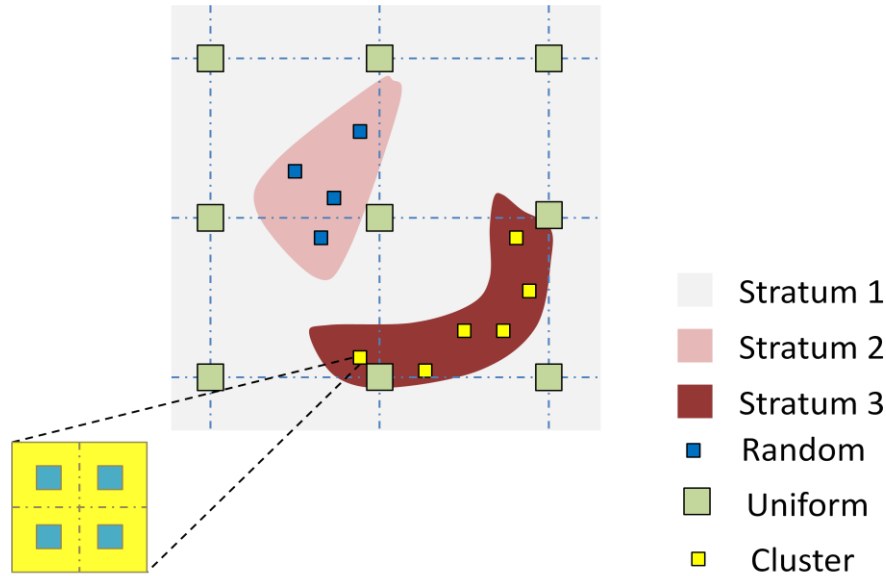


Figure 3.4. Illustration of simple random sampling, uniform sampling, stratified sampling and cluster sampling.

In addition to the four sampling methods described above, there are other intelligent methods such as adaptive sampling and model-based sampling [151, 152]. Adaptive sampling selects sampling units for observation may depend on observed values of interest. The model-based methods select sampling units depending on a prior knowledge of the probability distribution model of the population. For example, the existence of correlations between different sampling units, depending on the distance between the sites, has implications for the choice of sampling design. The main purpose of these intelligent methods is to achieve gains in accuracy or efficiency.

Determination of an appropriate sampling method should consider specific measurement tasks, the characteristics of the population and the measurement cost. In most simple cases (i.e. the population is not too large, the distribution of the properties of interest among the population is simple random), simple random sampling or uniform sampling is preferred. If the population is large, cluster sampling would be

able to reduce the sampling cost. If the population has regional differences in terms of the properties of interest, a stratification process is carried out first.

Selection of sampling methods has been discussed in many classic books such as in [82, 151]. But there has been very limited work on selection of proper sampling methods has been carried out in surface metrology. An example can be found in Rosen's work [123] in the surface roughness measurement of cylinder liners. It is demonstrated that “star” shaped global sampling provides an optimised way to offer a stable result compared to simple random sampling.

3.2.4 *Determination of sample size*

Determination of sample size is directly connected with sampling errors. A small sample size usually produces a large sampling error, i.e. the characteristics of interest of the sample tend to have a big bias from that of the population. In order that the error is eliminated under a threshold at a specific probability (for example 95 %), a sample size with enough sample units needs to be determined.

As estimation of the population mean is the most general case in surface measurement (for example estimating the average roughness values of a milled surface, estimating the average cutting edges per unit area of a grinding wheel, etc.), a model to determine sample size is given here in terms of estimation of the population mean.

Assuming the characteristic mean c of a sample $X : \{x_1, x_2, \dots, x_n\}$ with the sample size n is an unbiased and normally distributed estimator of the characteristic mean of the population μ , with the variance σ^2 , i.e. $\bar{X} \sim N(\mu, \frac{1}{n}\sigma^2)$, the probability that \bar{X} falls within confidence interval $(\mu - 2\sigma/\sqrt{n}, \mu + 2\sigma/\sqrt{n})$ is 95 % [151]. If an error bound is required to be limited at $\pm e$ of μ , i.e. \bar{X} should be limited within $(\mu - e, \mu + e)$, the equation

$$e = 2\sigma / \sqrt{n} \quad (3.1)$$

needs to be solved. Therefore, the sample size n should be

$$n = \frac{4\sigma^2}{e^2} \quad (3.2)$$

to guarantee the mean estimation error within $\pm e$ at 95 % confidence level.

In the same way, if the estimation error needs to be ensured within $\pm e$ at 99.7 % of the probability. The sample size n should satisfy

$$n = \frac{9\sigma^2}{e^2}. \quad (3.3)$$

For example, in Rosen's work of the surface roughness measurement of the top, middle, and bottom regions of a cylinder liner surface (see Figure 3.3), the sample means and standard deviations are obtained (see Table 3.1) by initially using a sample size of twenty-five at each region, which is thought to be sufficient for a stable observation based on earlier experience. To estimate the population variance σ^2 using the unbiased estimator $\hat{\sigma}^2 = \frac{n}{n-1} S_n^2$ [102], where S_n is the sample standard deviation

$S_n = \frac{1}{n} \sum_{i=1}^n (x_i - \bar{X})$, the sample size for each region of this cylinder liner can be determined to guarantee the sample mean within $\mu \pm 0.05 \mu\text{m}$ at 99.7 % confidence level:

$$n_{Top} = \frac{9\sigma^2}{e^2} = \frac{9(n/n-1)S_n^2}{e^2} = \frac{9 \times 25 / 24 \times 0.04^2}{0.05^2} = 6 \quad (3.4)$$

$$n_{Middle} = \frac{9 \times 25 / 24 \times 0.06^2}{0.05^2} \approx 14 \quad (3.5)$$

$$n_{Bottom} = \frac{9 \times 25 / 24 \times 0.06^2}{0.05^2} \approx 14 \quad (3.6)$$

equation (3.3) can be applied to general measurement to guarantee of a stable and confident estimation of the population characteristics. One more example can be seen in the determination of the sample size for the estimation of the mean $S5p$ [68] of the worn articular cartilage (AC) surface topography. In Tian's work [153], nine sample surface pitches are initially collected based on earlier experience to guarantee the

estimation stabilities from the AC surface of Joint 1, which has grade 1 osteoarthritis (OA) (see Table 3.2). Under the 99.7 % confidence level, to ensure the estimated mean value of $S5p$ within the ± 10 % bias of the population mean (i.e. $e = 2.15 \mu\text{m}$), the required sample size has the minimum value:

$$n = \frac{9\sigma^2}{e^2} = \frac{9 \times 5.6^2}{2.15^2} \approx 61. \quad (3.7)$$

ISO 25178	Height parameter	Arithmetic mean height		Sa (unfiltered, 4 th degree polynomial form removal)		μm
Region						
Top		Middle		Bottom		
Mean	Std. Dev.	Mean	Std. Dev.	Mean	Std. Dev.	
(25 measurements)	(25 measurements)	(25 measurements)	(25 measurements)	(25 measurements)	(25 measurements)	
0.34	0.04	0.47	0.06	0.48	0.06	

Table 3.1. The sample means and variances in the cylinder liner measurement [123].

But, if the level of assurance is not high, for example setting the confidence level at 68 %, the minimum requirement for the sample size can be

$$n = \frac{\sigma^2}{e^2} = \frac{5.6^2}{2.15^2} \approx 7. \quad (3.8)$$

Based on the result in equation (3.8), the sample size nine that was used in [153] ensures the mean $S5p$ of the sample is within $\pm 2.15 \mu\text{m}$ error of the population mean value at the 68 % confidence level.

Joint 1	No. 1	No. 2	No. 3	No. 4	No. 5	No. 6	No. 7	No. 8	No. 9	Mean	S_n	$\hat{\sigma}$
S5p (μm)	24.8	22.3	14.2	23.1	19.9	16.6	30.1	24.8	17.4	21.5	4.9	5.6

Table 3.2. $S5p$ values of a random sample from the AC surface of Joint 1 [153] (OA grade 1).

Note: S_n is the standard deviation of the nine sample values; $\hat{\sigma}$ is the estimated standard

deviation of the population by using $\hat{\sigma} = \sqrt{\frac{n}{n-1}} S_n$ where n is the tested sample size.

3.3 Local signal sampling

3.3.1 Introduction

As introduced in Section 3.1, sampling in signal process is a discretisation process to represent a continuous signal using discrete samples (points). The sampling process should ensure that the original continuous signal can be reconstructed or approximately reconstructed from the sampling data. The sampling in signal processing has different focus from sampling in statistics. Signal sampling concentrates on the fidelity when a series of discrete samples are reconstructed to a continuous signal. In other words, the sampling in signal processing aims to find a sampling design (design of the sample methods and conditions, i.e. distribution of the sample positions) which can present the original continuous signal using a discrete form with no or little distortion if specific reconstruction is carried out. For example, a band-limited signal $f(x)$ on $L^2(\mathbb{R}^d) \cap B(-W, W)$, i.e. $f(x)$ is an energy limited function, i.e.

$$\|f(x)\| = \left(\int_{\mathbb{R}^d} f(x) \overline{f(x)} dx \right)^{1/2} < +\infty \quad (3.9)$$

with x belonging to \mathbb{R}^d , and its Fourier transform

$$\hat{f}(\xi) = \int_{\mathbb{R}^d} f(x) e^{-j2\pi \langle \xi, x \rangle} dx \quad (3.10)$$

has $\hat{f} = 0$ if $\xi \notin (-W, W)^d$, can be presented by a sample set with a series of uniformly distributed samples

$$S = \left\{ f(kT) : k \in \mathbb{Z}, T \leq \frac{1}{2W} \right\} \quad (3.11)$$

with the reconstruction equation

$$f(x) = \sum_{k \in \mathbb{Z}} f(kT) \text{sinc}(x/T - k) \quad (3.12)$$

where $\text{sinc}(x) = \frac{\sin(\pi x)}{\pi x}$. The expression (3.12) is also known as the cardinal series expansion [129, 170]. Another practical example that can be referred to is a discrete wavelet transform (DWT) decomposition-based sampling which guarantees the original signal can be approximated by an adaptively designed samples [111] (see Figure 3.5).

Unlike the statistical sampling design at the global stage which is free of design by the sampling operators, local sampling design in surface measurement is usually been designated in the manufacture of measuring instruments. For instance, most coherence scanning interferometers (CSI) use a regular grid CCD camera to record surface topography geometric information; stylus profilometers use a regular raster sampling design to obtain the surface height data. Also, the current instruments usually have single or multiple fixed sampling conditions which cannot be selected by users arbitrarily. For example,

1. **Sampling (or sample) spacing**, also called sampling interval, refers to the distance between neighbouring samples. In areal measurement, sampling spacing is usually denoted by two components in x - and y -direction respectively. Sampling spacing is usually fixed for most CSIs depending on the objective employed; but it can be flexibly selected in most stylus instruments.
2. **Sampling (or sample) length**, or sampling area in two-dimensional cases, refers to the length or area which is inspected by current sampling design. In optical measurements, sampling length is also usually fixed when an objective is selected. But some instruments provide several optional length/areas, for example an optical zoom. For stylus instruments, this parameter can usually be selected freely.
3. **Sampling (or sample) size**, refers to the size of samples used in a sampling design. Sample size is automatically determined if the former two parameters, i.e. the sample spacing and sample length, are given. In most interferometers,

sample size is fixed, for example, the image resolution 1024×1024 , 736×480 pixels used on some CSIs.

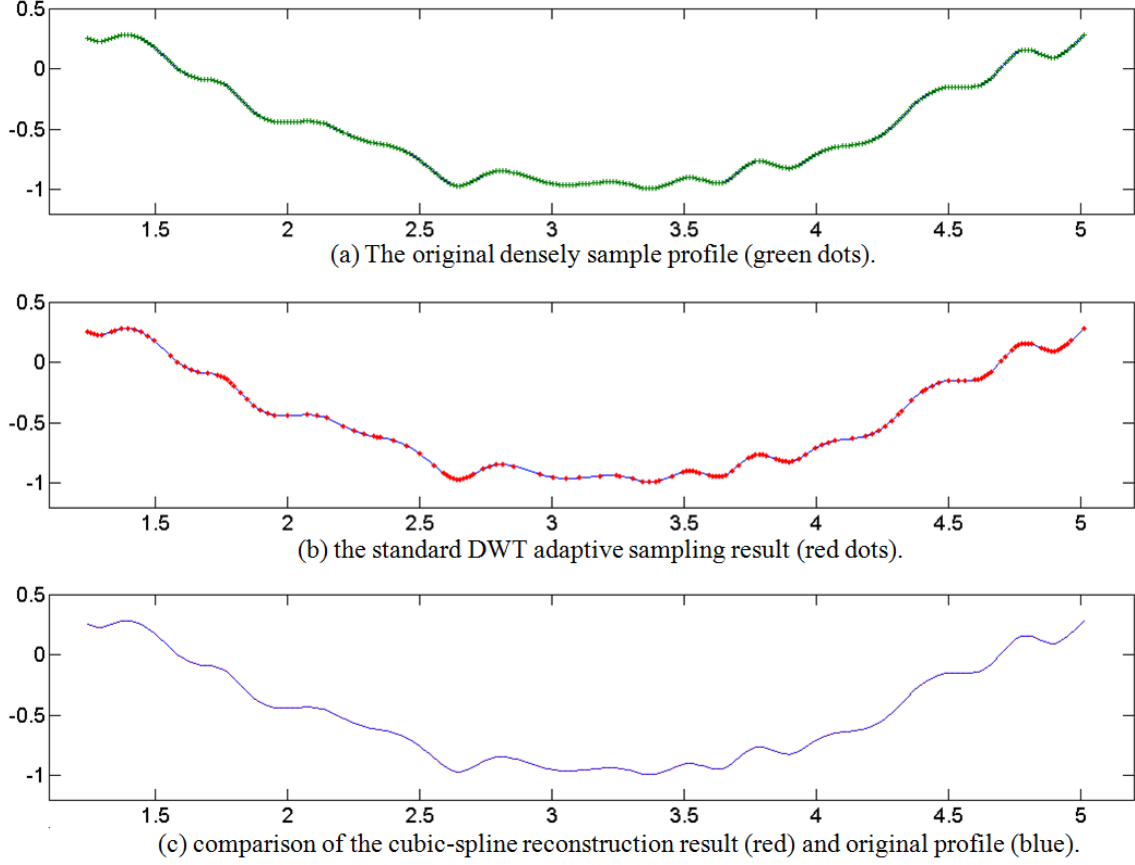


Figure 3.5. A DWT decomposition-based adaptive sampling of a spline-like signal.

The three conditions cannot be adjusted in a real time if a measurement starts. All of these limitations induce some efficiency problems such as limited measurement accuracy or efficiency. Focusing on current uniform sampling, many researchers have developed smart methods to optimize the sampling conditions for surface measurement, for example selection of proper sampling spacing and length. However, the emergence of structured surfaces [46, 76] leads researchers to consider intelligent methods which break through the conservatively inflexible uniform pattern.

3.3.2 Emergence of intelligent sampling methods

Classical uniform sampling designs are widely used in nearly all the current commercial surface measuring instruments [134]. In computer graphics however, uniform sampling is always regarded as tending to induce spectral aliasing or spectral leakage. For example in Figure 3.6a, constant uniform sampling produces a spectral aliasing distortion. The jaggy artefacts at the edges of checks in the foreground are obviously observed. Also the artefacts in the distance show that the check functions go through many cycles between samples. Hence the information between neighbouring samples is lost in a constant rate, and the original high frequency details are incorrectly expressed as lower frequency artefacts, i.e. aliasing. A jittered uniform sampling of the same sample size converts the regular aliasing into random noise, which is seen as less objectionable [114].

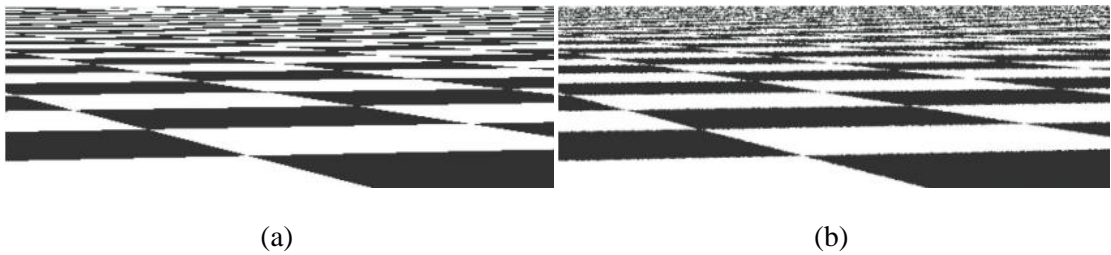


Figure 3.6. The coherent spectral aliasing effect in computer graphics. (a) Uniform sampling produces coherent aliasing; (b) Jittered uniform sampling transforms the aliasing into noise [114].

In terms of the measurement of structured surfaces, uniform sampling has induced some problems that are more awkward, for example, the sharp contradiction between measurement accuracy and efficiency. As discussed in Section 2.3, many structured surfaces have a large working area ranging from millimetres to metres but are embedded with micro- or nano-scale structures. A stylus instrument may take hours to perform a single measurement covering the whole working area of a structured surface. Some special surfaces tend to have large dimensional spans in different lateral directions. For example, a vee-groove structure on a blazed grating usually has a micrometre scale in one direction but a millimetre scale in the perpendicular direction. The following is discussed [164] for the measurement of structured surfaces.

1. Evaluation of micro-scale dimensions and form error parameters are usually of more importance than the more standard surface texture parameters.
2. CMMs are usually not able to probe or resolve such micro-scale surface structures. Extraction of the dimensional or form error parameters from the surface texture data is the general measurement requirement.
3. Most surface structures require both large measuring range and small resolution as is common for sharp curvature changes to be observed in practical applications and features may have high aspect ratios.

The above requirements mean that efficient sampling methods need to be generated.

Some intelligent sampling techniques have been proposed in the past which aim to enhance sampling accuracy (i.e. avoid spectral aliasing, leakage) or efficiency (i.e. saving the sampling time, storage space, cost, etc.) oriented from computer graphics and coordinate metrology. Examples include jittered uniform sampling, low-discrepancy pattern sampling, model-based sampling, adaptive sampling, and so on [9, 44, 83, 114, 130, 152, 172]. Model-based methods design a sampling pattern adaptively based on a given model of the surface, for example the CAD model or a rough measurement of the surface beforehand. Adaptive methods design the sampling positions in sequences based on earlier sampling values. In this research, an adaptive sampling technique is developed aiming to improve the measurement efficiency of current stylus instruments. Diverse intelligent sampling techniques are analysed in terms of their measurement performance.

3.4 Some signal sampling theories

A review of current signal sampling theory is given in this section to provide the theoretical foundations of the current sampling techniques. Some of the theories are rarely considered in surface topography measurement but are regarded as very important. Only with the aid of a robust sampling theory, can the design of intelligent sampling methods and evaluation of the performance of diverse sampling methods become feasible.

Diverse sampling theories have been proposed during the past few decades. The most well-known theories are the Shannon sampling theory [129, 170] and the sampling theory in shift-invariant space [6, 157]. These theories tend to find a perfect sampling with a specific sample density which can recover the original signal with little or no error. Theoretical success has been widely obtained, for example in band-limited function space [129, 170], wavelet space [92, 163, 167, 180], spline spaces [4, 5, 54], etc. However, practical signals are usually unknown before measurement, and most of them may not be band-limited [133] or in specific function spaces. Other solutions derived from statistics or approximation theories have been widely proposed for practical measurements. For example, low-discrepancy sampling patterns are designed from a statistical viewpoint [83, 114]. Many model-based sampling methods and adaptive sampling methods are designed to reduce the reconstruction error directly without consideration of the function spaces of the surface signal [9, 130, 144]. A brief introduction to these theories is given here and the connection between the theories and current practical sampling solutions is given.

3.4.1 Sampling in Paley-Wiener spaces

A **Paley-Wiener space** P_W is a subspace of $L^2(\mathbb{R}^d)$ which contains all the band-limited functions in $B(-W, W)^d$, i.e. $P_W = L^2(\mathbb{R}^d) \cap B(-W, W)^d$ [163]. Sampling theory in a Paley-Wiener space is the classical theory that was first formulated by Shannon in 1949 [129]. This theory has other different forms, for example the form in Whittaker's work [170]. Shannon stated that: "If a function $f(t)$ contains no frequencies higher than W cps (cycles per second), it is completely determined by giving its ordinates at a series of points spaced $1/2W$ seconds apart." An extended expression of this theorem was given in Section 3.3.1. For convenience, substitute the band-width W using $1/2$, i.e. a band-limited function $f(x)$ in the space $P_{1/2} = L^2(\mathbb{R}^d) \cap B(-1/2, 1/2)^d$. Hence, a uniform sampling set

$$S = \{f(k), k \in \mathbb{Z}\} \quad (3.13)$$

ensures an exact reconstruction using the reconstruction equation

$$f(x) = \sum_{k \in \mathbb{Z}} f(k) \text{sinc}(x - k). \quad (3.14)$$

It can be seen that the function $\text{sinc}(\cdot - k)$ has the property

$$\langle \text{sinc}(\cdot - k), \text{sinc}(\cdot - l) \rangle = \int_{\mathbb{R}^d} \text{sinc}(\cdot - k) \overline{\text{sinc}(\cdot - l)} dx = \delta(k - l), \quad (3.15)$$

where $\delta(k - l) = \begin{cases} 1, & \text{if } l = k; \\ 0, & \text{if } l \neq k. \end{cases}$. This result indicates that the function set $\{\text{sinc}(\cdot - k), k \in \mathbb{Z}\}$ forms a series of orthogonal bases in $P_{1/2}$.

However, Shannon's theorem is idealised because (1) practical signals are never band-limited [133], (2) practical sampling may not be exactly regular due to missing data, disturbance of sampling positions or special sampling designs [12], and (3) the basis function $\text{sinc}(\cdot - k)$ is difficult use in numerical computation because of its infinite support [108]. The traditional three-step sampling techniques, i.e. pre-filtering (a low-pass filtering is applied to the original signal to force it to be band-limited), sampling and post-filtering (i.e. reconstruction), guarantees the input function $f(x)$ is band-limited before sampling. In surface metrology, the stylus tips employed (or equivalent for optical methods) produce a pre-filtering of the real surface signal, which has been demonstrated to be traceable and stable. However, the infinite support of the sinc function is difficult to overcome; a simple spatial truncation of the sinc function would produce a ringing [108, 119] effect in the frequency domain (see Figure 3.7).

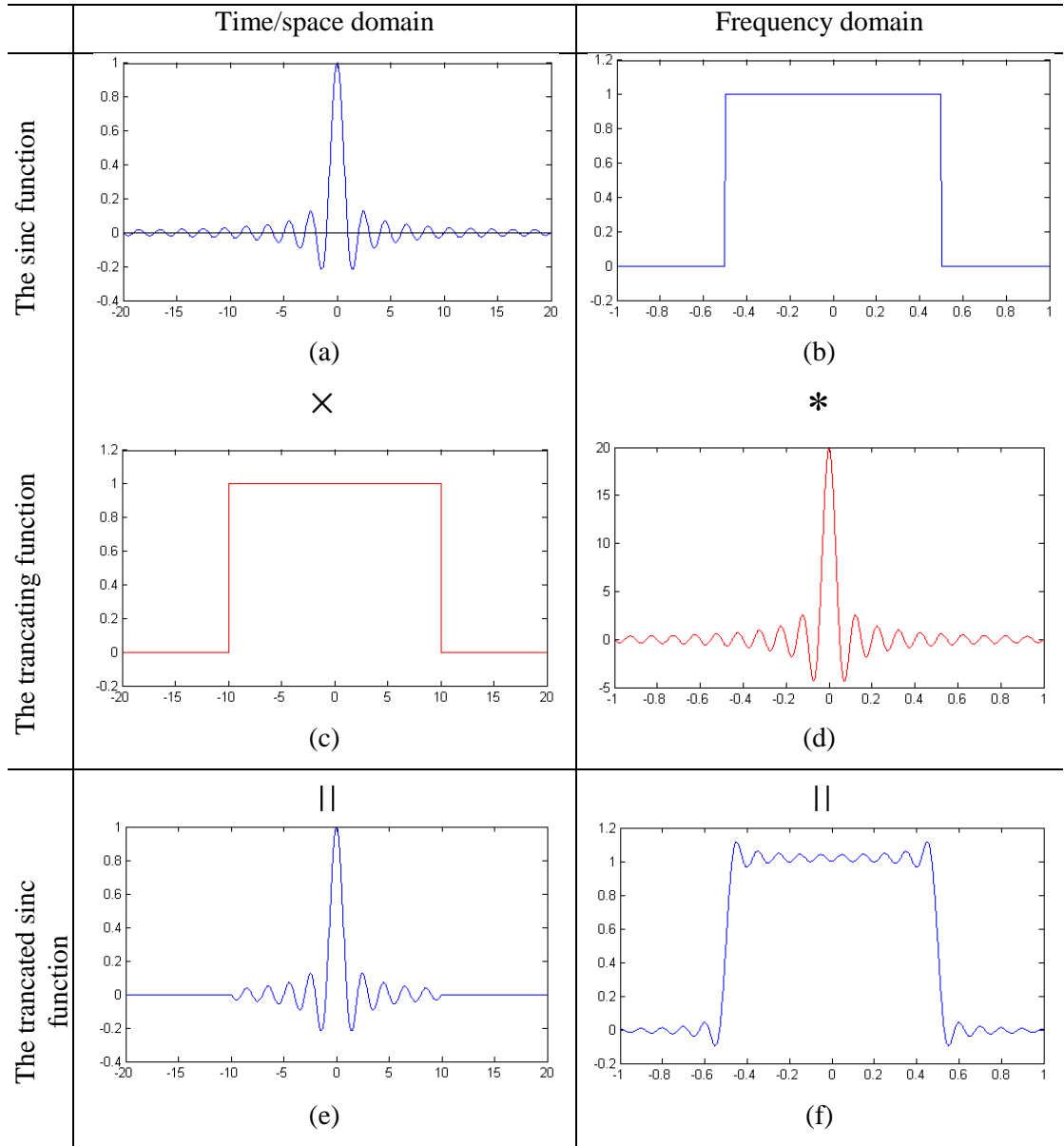


Figure 3.7. The ringing effect in frequency domain.

3.4.2 Sampling in shift-invariant spaces

In the past sixty years after Shannon's sampling theorem, researchers have tried to extend the theory to avoid the practical limitations. Many proposed methods focus on sampling of a signal within different function spaces, such as wavelet subspaces [92, 163, 167, 180], spline-like subspaces [4, 5], and so on. It can be noticed that the sinc function plays a very important role in the reconstruction in equation (3.14). In other words, the reconstruction operator from the integer position sampling set $f(k)$

$$Rf(k) = \sum_{k \in \mathbb{Z}} f(k) \varphi(x-k) \quad (3.16)$$

with the generator $\varphi(\cdot-k) = \text{sinc}(\cdot-k)$ approximates the original function $f(x)$ in the space $P_{1/2}$. If substitute the generator $\text{sinc}(\cdot-k)$ with other general functions, for example a “mother wavelet” function [163]

$$\psi(x) = \text{sinc}(x - \frac{1}{2}) - \text{sinc}[2(x - \frac{1}{2})] \quad (3.17)$$

or the third degree (fourth order) B-spline function

$$\beta_3(x) = \chi[-\frac{1}{2}, \frac{1}{2}] * \chi[-\frac{1}{2}, \frac{1}{2}] * \chi[-\frac{1}{2}, \frac{1}{2}] * \chi[-\frac{1}{2}, \frac{1}{2}], \quad (3.18)$$

where $\chi[-\frac{1}{2}, \frac{1}{2}]$ is the characteristic functionⁱ, the reconstruction operator $Rf(k)$ can approximate the original function in a wavelet or spline-like subspace of L^2 .

A sampling theory in shift-invariant spaces has been proposed [6, 12, 54]. The novel theory is a great improvement on the traditional Shannon sampling theorem, which can be applied to non-uniform sampling situations and the applicable functions are no longer a band-limited function in P_W . The theoretical completeness of this theory has been demonstrated from a mathematical viewpoint. However, the numerical operation in practice still has many difficulties [6]. Extensive knowledge of function analysis, frame theory, wavelet theory and signal processing is necessary to fully understand the shift-invariance space sampling theory, which is difficult for general engineers. Here, a brief introduction to this theory is given for users in engineering measurement. The core theorems involved are contained and the proofs are omitted.

Given a generator $\varphi(x)$, a shift-invariant space [3, 6] is defined as

ⁱ $\chi[-\frac{1}{2}, \frac{1}{2}]$ has $\chi = 1$ if $x \in [-\frac{1}{2}, \frac{1}{2}]$, and $\chi = 0$ if $x \notin [-\frac{1}{2}, \frac{1}{2}]$. A two-dimensional general expression of the characteristic function for example $\chi[-W, W]^2$, has the decomposition $\chi[-W, W]^2 = \chi[-W_1, W_1] \chi[-W_2, W_2]$.

$$V_\nu^p(\varphi) = \left\{ \sum_{k \in \mathbb{Z}^d} c_k \varphi(\cdot - k) : c \in l_\nu^p \right\}, \quad (3.19)$$

where φ is a generator function which can be a wavelet, spline basis or other functions, ν is a non-negative weighting function, p defines a p -norm which force $c \in l_\nu^p$, i.e.

$$\|c\|_{l_\nu^p} = \|c\nu\|_{l^p} = \sum_{k \in \mathbb{Z}^d} |c_k|^p \nu(k)^p < +\infty. \quad (3.20)$$

This generated function space is regarded as translationally invariant, i.e. if $f \in V_\nu^p$, then $f(\cdot - y) \in V_\nu^p$. It is apparent that the shift invariant space covers far more signals in practice compared to P_W .

The sampling theory in shift invariant space [6] states sequentially that:

- 1) If $\varphi \in W_0(L_\nu^1)$ (many basis functions belong to this space, for example a B-spline basis over order 2^{ii} [4, 92, 163]), i.e. φ is continuous function (order zero) in a Wiener amalgam space $W(L_\nu^1)$ for which

$$W(L_\nu^p) = \left\{ f : \sum_{k \in \mathbb{Z}^d} \text{ess sup} \{ |f(x+k)|^p \nu(k)^p ; x \in [0,1]^d \} < \infty \right\}, \quad (3.21)$$

$V^2(\varphi)$, i.e. V_ν^p with $\nu=1$ and $p=2$, is a **reproducing kernel Hilbert space** (RKHS) [176], and the kernel functions can be obtained by

$$K_x(y) = \sum_{k \in \mathbb{Z}^d} \overline{\varphi(x-k)} \tilde{\varphi}(y-k), \quad (3.22)$$

ⁱⁱ A B-spline basis with N order has the form $\beta_N = \chi[-1/2, 1/2] * \chi[-1/2, 1/2] \dots * \chi[-1/2, 1/2]$ (N-1 times fold convolution).

such that $f(x) = \langle f, K_x \rangle$, where $\tilde{\varphi}$ is a unique dual generator of φ which satisfies

$$\langle \tilde{\varphi}(\cdot), \varphi(\cdot - k) \rangle = \delta(k) \text{ iii.} \quad (3.23)$$

- 2) Given a separated^{iv} sampling set $X = \{x_j, j \in J\}$ of $f \in V^2(\varphi)$ where J is a countable indexing set, the reproducing kernel function sequence $\{K_{x_j}, x_j \in X\}$ constructs a **frame** [41] for $V^2(\varphi)$ (i.e. $\{K_{x_j}, x_j \in X\}$ is a **Riesz basis** of $V^2(\varphi)$) if and only if X is a **stable sampling set**, i.e.

$$f(x) = \sum_{j \in J} \langle f, K_{x_j} \rangle \tilde{K}_{x_j}(x) = \sum_{j \in J} f(x_j) \tilde{K}_{x_j}(x), \quad (3.24)$$

where $\{\tilde{K}_{x_j}, x_j \in X\}$ is dual frame of $\{K_{x_j}, x_j \in X\}$, according to the frame theory [41].

In other words, a f in $V^2(\varphi)$ can be exactly recovered from a stable sampling set $X = \{x_j, j \in J\}$ if and only if $\{K_{x_j}, x_j \in X\}$ is a Riesz basis. However, the dual frame $\{\tilde{K}_{x_j}, x_j \in X\}$ is very difficult to find in practice, iterative algorithms are suggested.

- 3) Let $\varphi \in W_0(L_v^1)$, P be a bounded projection from L_v^p to V_v^p , for example,

$$P: f \rightarrow \sum_{k \in \mathbb{Z}^d} \langle f, \tilde{\varphi}(\cdot - k) \rangle \varphi(\cdot - k), \quad (3.25)$$

and let Q_X be a quasi-interpolant based on a sample set $X = \{x_j, j \in J\}$ which has

ⁱⁱⁱ $\delta(k)$ is a Dirac delta function which has $\delta(0) = 1$ and $\delta(k) = 0$ for $k \neq 0$.

^{iv} "Separated" here means for $\forall i \in \mathbb{Z}$, $x_i \neq x_{i+1}$.

$$Q_X f = \sum_{j \in J} f(x_j) \beta_j, \quad (3.26)$$

where $\{\beta_j\}_{j \in J}$ is a **partition of unity** (i.e. $0 \leq \beta_j \leq 1$ for $j \in J$; $\text{supp } \beta_j \subset B_\gamma(x_j)$ ^v and $\sum_{j \in J} \beta_j = 1$, for example a B-spline basis [32] in Figure 3.8), then there exists a stable sample set $X = \{x_j, j \in J\}$ with sample density $\gamma > 0$ which satisfies the equality

$$\bigcup_{j \in J} B_\gamma(x_j) = \mathbb{R}^d, \quad (3.27)$$

such that any $f \in V_v^p$ can be recovered from the sample by the iterative algorithm

$$\begin{cases} f_1 = PQ_X f \\ f_{n+1} = PQ_X(f - f_n) + f_n \end{cases} \quad (\text{see Figure 3.9}). \quad (3.28)$$

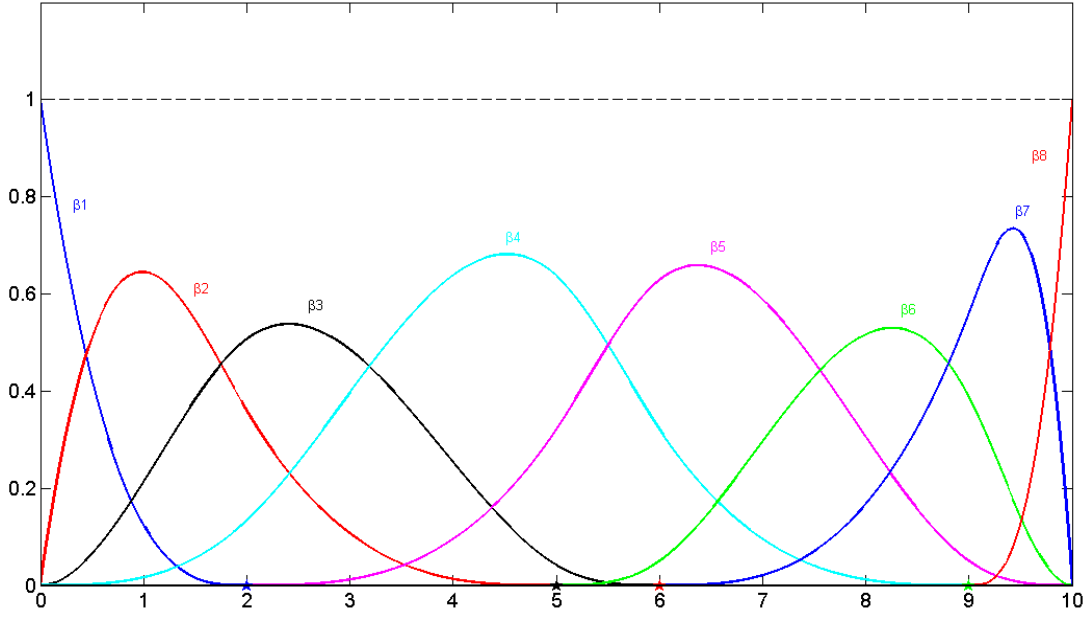


Figure 3.8. A partition of unity with a third degree B-spline basis (knots: 2, 5, 6, 9).

^v $B_\gamma(x_j)$ is a continuous bound set $B_\gamma(x_j) = [x_j - \gamma, x_j + \gamma]$.

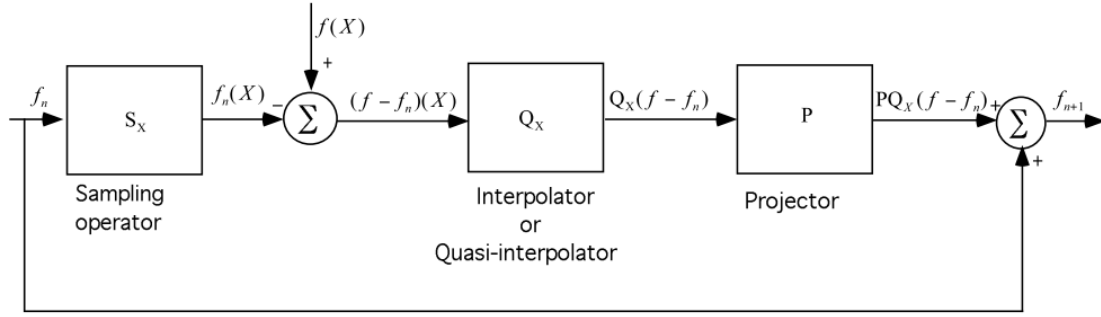


Figure 3.9. The iterative reconstruction algorithm based on equation (3.28) [6].

Shift-invariant space sampling theories have been demonstrated to be a great success [4-6, 92, 167]. However, the dual generator $\tilde{\varphi}$ is difficult to calculate in practice. On account of this, fast local algorithms have been proposed [54]. To recover a shift-invariant signal, researchers could simply try to solve the (infinite) system of linear equations

$$\sum_{j \in J} c_k \varphi(x_j - k) = f(x_j) \quad (3.29)$$

for the coefficients $\{c_k\}$. To be practical, with a finite sample set $X = \{x_1, x_2, \dots, x_N\}$ of a finite length signal $f = \sum_{k=1, \dots, K} c_k \varphi(\cdot - k)$, construct the following matrix

$$U = \begin{bmatrix} u_{x_1,1} & \cdots & u_{x_1,K} \\ \vdots & u_{x_n,k} & \vdots \\ u_{x_N,1} & \cdots & u_{x_N,K} \end{bmatrix}, \text{ where } u_{x_j,k} = \varphi(x_j - k), \quad (3.30)$$

and $c = [c_1, c_2, \dots, c_K]^T$. Thus the linear system to be solved in equation (3.29) can be written in the form

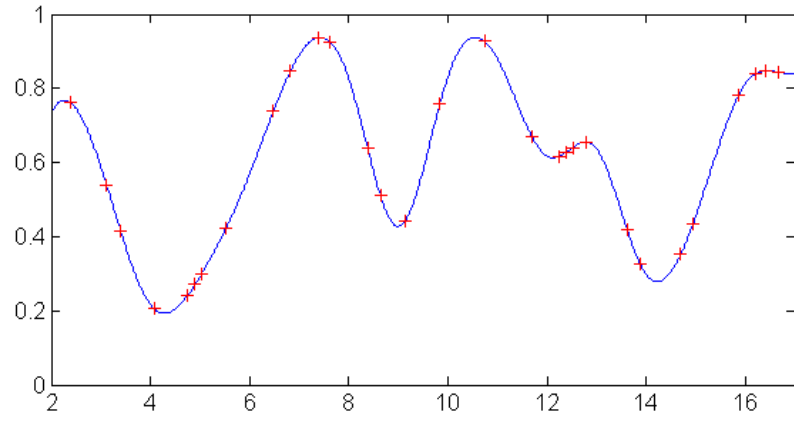
$$Uc = f|_X. \quad (3.31)$$

where $f|_X$ is the sample values which have $f|_X = [f(x_1), f(x_2), \dots, f(x_N)]^T$. This linear system can be solved easily [52].

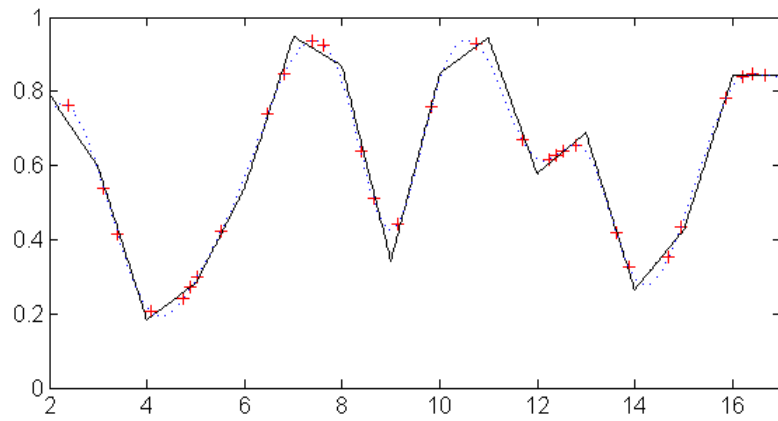
A numerical example can be found in Figure 3.10 in which the reconstruction error is calculated as

$$Error = \frac{\|f_{rec}|_X - f|_X\|^2}{\|f|_X\|^2}. \quad (3.32)$$

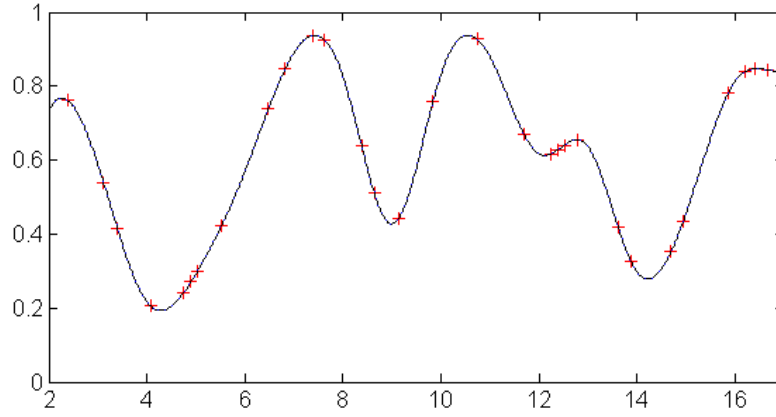
If Gaussian random noise with 0.1 as the standard deviation is added to the sampling process of the signal in Figure 3.10a, the fast local algorithm also works stably and provides an approximation of the noisy samples in $V^2(\varphi)$ (see Figure 3.11).



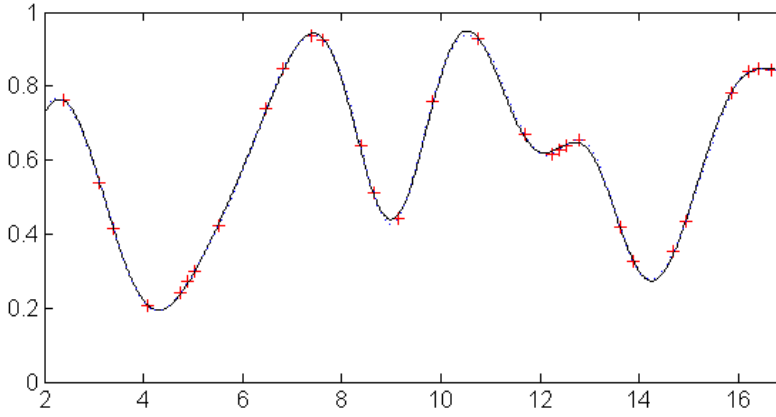
(a) Original signal and samples



(b) reconstruct using the second order B-spline, error = 7.1×10^{-4}

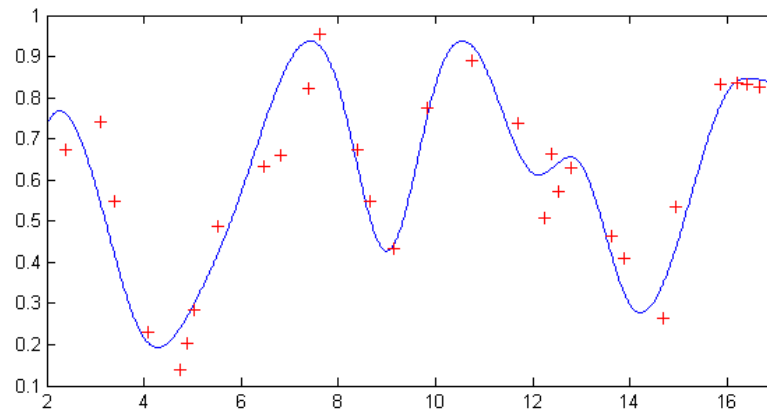


(c) Reconstruct using the fourth order B-spline, error = 1.7×10^{-30} .

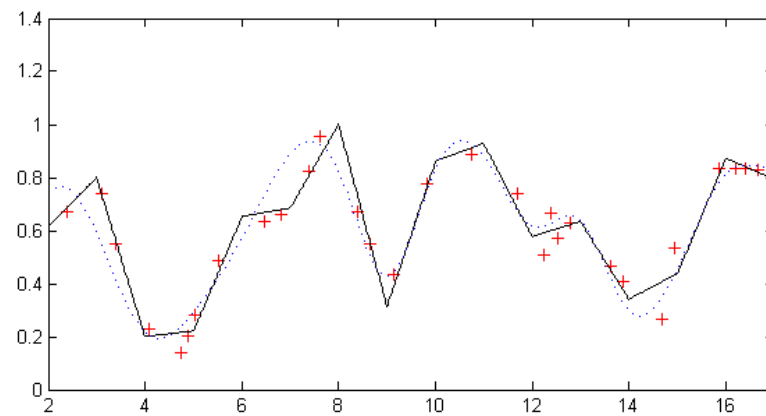


(d) Reconstruct using the sixth order B-spline, error = 5.9×10^{-5} .

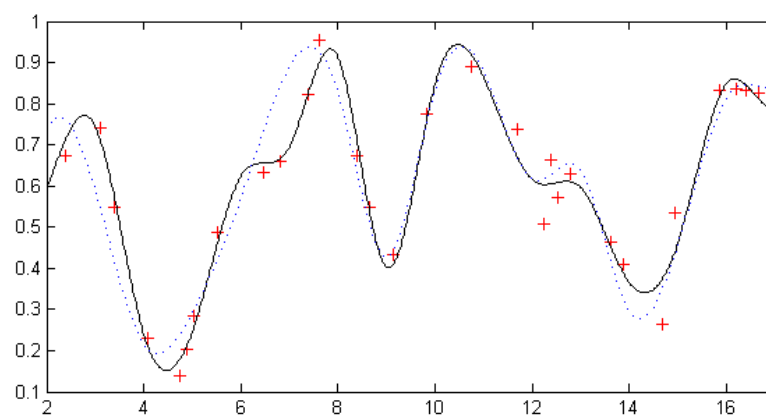
Figure 3.10. Reconstruction of a shift-invariant signal using fast local algorithms. (a) shows the original signal which is generated by the third degree B-spline β_3 (blue curve) and a non-uniform sample set with density $\gamma = 0.5$ (red dots); (b), (c) and (d) show the reconstructed continuous signal using the first, third and fifth degree B-spline respectively (the black curve is the reconstructed signal, the blue dashed curve is the original signal).



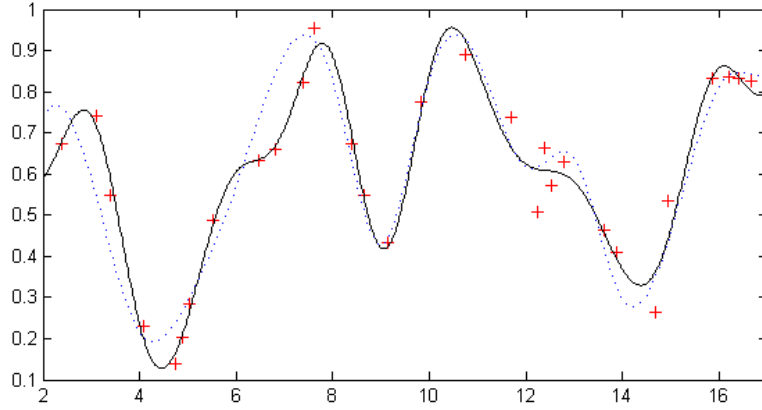
(a) Original signal and noisy samples.



(b) Reconstruct using the second order B-spline, error = 12.2 %.



(c) Reconstruct using the fourth order B-spline, error = 11.2 %



(d) Reconstruct using the sixth order B-spline, error = 12.4 %

Figure 3.11. Reconstruction of a randomly noised shift-invariant signal. (a) shows the original shift invariant signal which is generated by the third degree order B-spline β_3 (blue curve) and a noisy sample set with density $\gamma = 0.5$ (red dots); (b), (c) and (d) show the reconstructed continuous signal using the first, third and fifth degree respectively (black curve is the reconstructed signal, blue dashed curve is the original signal).

In summary, sampling theorems in shift-invariant space extend the Shannon sampling theory. The shift-invariant space sampling theorem states that a shift-invariant signal can be exactly recovered from a stable sampling set with properly defined sampling density γ . Such a sampling set allows a limited disturbance based on a uniform sampling set. However, in the measurement of structured surfaces, many signals have different frequency components regionally or have a sparse distribution of the features of interest, which indicates that the structured surface signals may not be efficiently approximated in a shift-invariant space in terms of the computation cost. Rather, it may be valuable to consider such a space for structured surfaces such that

$$V^2(\varphi) = \left\{ \sum_{k \in \mathbb{Z}} c_k \varphi(\cdot - x_k), c \in l_\nu^p \right\}. \quad (3.33)$$

where $\{x_k\}$ is a separated increasing sequence, i.e. $x_k < x_{k+1}$ for $\forall k \in \mathbb{Z}$.

3.4.3 *Other sampling design ideas*

In the measurement of structured surfaces, the Shannon theory and shift-invariant space theorems can guarantee an approximation of the original signal in Paley-Wiener spaces or shift-invariant spaces. However, these theorems do not consider the sparse property of the surface features of structured surfaces. This indicates that the Shannon's theorem and shift-invariant space theorems may not be able to completely solve the efficiency issue for the measurement of structured surfaces.

A new theory referred to as compressed sensing or compressive sensing [21, 39, 95] which detects a signal by sampling at a reduced rate has emerged recently. A successful application example of this theory is the single pixel camera developed by the Rice University [40]. This technique transforms a scene image into a series of single pixel light intensities using a spatial light modulator (encoding). With different encoding and single-pixel sensor detections in thousands of times (or more), a mega-pixel image can be recovered at a specific accuracy. The more times of modulation and detection usually means better accuracy. However, the technical transfer of compressed sensing from image processing into the length measurement is still questionable and the reconstruction accuracy needs to be validated.

In practice, metrologists understand that it is often impossible to give an exact sampling and reconstruction for practical signals. Rather they try to give sampling solutions that aim to reduce the sampling error to within an acceptable range. Many attempts have been carried out to achieve this objective.

In geometrical measurement with CMMs or surface topography measuring instruments, researchers tend to enhance the measuring efficiency using adaptive or model-based sampling. Adaptive sampling uses iterative search methods on an error space which determines new sampling positions based on earlier sample results, [9, 42] while model-based sampling uses a given population model (for example a CAD model or a probability distribution function of a given surface) [44, 130]. For example, with an initial sampling set, substitute geometry can be approximated. By comparing the substitute geometry with the original geometry, the positions with the highest deviations can be found and new samples are added into these regions to minimise the

evaluation error in the next iterative loop. Diverse adaptive sampling and model-based sampling designs have been developed based on approximations during the last twenty years [9, 42, 44, 45, 84, 88, 111, 114, 130, 164, 172].

Statistics have also been employed in surface measurement. Since optimised sampling patterns, for example Hammersley pattern or Halton-Zaremba pattern, [83, 114] can improve the evaluation accuracy of the population mean or total values, these statistical methods have been widely used in the measurement of flatness or surface roughness [81, 88, 172].

3.5 Summary

The topics of this chapter include many introductory issues such as the sampling framework of surface topography measurement, procedures of global sampling, challenges for local sampling, and available sampling theories. In short, the follow issues are summarised

1. The practical sampling framework in surface topography measurement consists of global statistical sampling and local signal sampling. The former focuses on a statistical estimation of a characteristic of the whole surface population. The latter focuses on a recoverable discrete presentation of a continuous surface geometry. In this thesis, the framework is summarised for the first time with reference to the considerations of future practical measurements.
2. Because no global sampling guide has been provided in the past, a general global sampling design procedure for surface topography measurement is suggested. The suggested global sampling procedure includes division of the sampling unit, determination of sampling methods and sample size. This procedure reflects a complete consideration of sampling in practice. It is expected that this general procedure can be experimentally validated in the future.
3. At the local signal sampling stage, uniform sampling based on Shannon's sampling theorem is the prevailing technique at present. However, this method is not flexible in practice and it lacks efficiency. Many intelligent sampling methods have been developed from statistics, computer graphics and coordinate metrology.

In surface topography measurement, potential intelligent sampling (local) needs to be explored which constitutes the main work of this thesis.

4. Shannon's sampling theorem guarantees an exact reconstruction from a uniform sampling set in the Paley-Wiener spaces. The shift-invariant space sampling theorem guarantees an exact reconstruction from a non-uniform sampling set in a shift-invariant space, such as the spline-like subspace, or wavelet subspaces. However, for a signal which has sparse feature distribution, for example most structured surfaces, these theorems have little evident efficiency. Practical developments of adaptive sampling and model-based sampling methods have been proposed based on approximations or statistics. None of these have been developed for surface topography measurement.

Based on this background information, the prevailing uniform sampling and potential intelligent sampling will be investigated in the following chapters. As the main scope of this research, "local signal sampling" will simply be referred to as "sampling" in the following context if not otherwise specified.

4. UNIFORM SAMPLING

4.1 Introduction

At present, uniform sampling is the prevailing sampling method in surface measurement, both in surface topography measurement using a profilometer or form measurement using a scanning CMM. Due to instrumentation limitations, almost all the present surface topography measuring instruments adopt uniform sampling. Uniform sampling, that has been the core research area in the past surface topography measurement, forms the motivation for this chapter.

In signal processing, **uniform sampling**, as also called systematic sampling or regular sampling, is a sampling design in which sampling positions have a constant spacing. That means the samples of uniform sampling are taken on a uniform grid. Although Shannon stated in his fundamental work on information theory [129] that “if a function $f(x)$ contains no frequencies higher than W (cycles per second), it is completely determined by giving its ordinates at a series of points spaced $T = 1/2W$ seconds apart”, the presented theory is too idealised to use in practice (see section 3.4). Real world signals are never exactly band-limited [133]. Typically in structured surface measurement, for example, a periodic step surface has a discrete spectrum which is infinitely supported.

Therefore, the selection of proper sampling conditions, i.e. sampling spacing (also called interval), sampling length (or sampling area in two-dimensions) and number of sampling points which aims to provide an approximation of the original signal, has been a hot spot in previous research. Specifically, if the instrumental availability is not considered, the following issues are the most important to be considered for sampling.

1. Enough data points must be collected within a specific area which causes as little spectral aliasing as possible.
2. Sampling area should be broadened as much as possible to make the evaluation results statistically stable.

The two issues above are theoretically true; however, the requested conditions are not necessary and usually impossible to satisfy in practice. Adoption of the above requested condition is likely to result in a large amount of data. Such a measurement entails both excessive storage and computing time.

Therefore, the optimal selection of sampling conditions has become the hot topic of uniform sampling. Many researchers have contributed to this research (see Section 4.2 for a review). All of these studies derive from determination of the basic criterion for choosing proper sampling conditions. Two approaches have been presented: **parameter variation**, and **spectrum analysis**. The former detects the variation of the specific evaluation parameters. An optimal sampling condition can be given to guarantee the parameters vary within an acceptable range. In the latter approach, the sampling conditions employed should guarantee the interested spectral components are almost covered. A systematic review of these selection approaches follows.

4.2 Selection of sampling spacing

4.2.1 *Review of selection criteria for sampling interval*

Surface texture parameters are usually the final indicators in surface evaluation. The stability of the parameter evaluation has to be guaranteed if sampling conditions cannot be determined by a more powerful tool. Tsukada and Sasajima [155] developed a method for determination of optimum sampling intervals. Their method assumes that the surface height follows a random distribution. Based on a comparison of the parameters' variation of the digitised profile and its original continuous profile, an optimal interval can be determined.

Yim and Kim [177] used the surface texture parameter Ra as the detecting indicator. Some authors later stated the drawback of Yims' method is an assumption that the Ra is distributed normally (Gaussian distribution). Actually in Yim's work, the Ra of a digitized surface had been proved to comply with a normal distribution under the central limit theorem. Therefore, the main problem cannot be addressed on this issue. An evident drawback is that the spatial or hybrid parameters are ignored in this work and they are more sensitive to the sampling conditions than the amplitude parameter

Ra. Thomas has also demonstrated the differences produced by using different parameter for the variation inspection [150].

The parameter variation approach uses a parameter originating from the original surface as the reference. But the “standard” parameter originating from the original continuous surface is always unknown. A “pseudo standard” parameter characterised from a high-density sample result is usually used as a replacement. Further, one parameter within a safe range does not guarantee all the other parameters in the same safe range. Hence, the “parameter variation” criterion is not preferred in practice due to the potential estimation dangers.

As another development, Fourier analysis is introduced in this topic. The first practical surface sampling criteria was developed by Lin, Dong and Mainsah. The selection of the sampling conditions is completely based on the distribution of the frequency components in the spectrum, rather than the final computed parameters. Lin et al [91] firstly introduced the radial power spectrum in determination of sampling conditions. In this work [91] and Lin’s PhD thesis [90], the aliasing effect [117] was taken into consideration. Here, the criterion for determining the proper frequency bandwidth for 3-D topography measurement is set, i.e. the **Nyquist folding frequency**, or half of the sampling rate is set at the position where the cumulative spectral power reaches 95 % of the total power. However, a problem is encountered similar to the “parameter variation” criterion that any initial measurement cannot obtain the whole power spectrum. This indicates that the accurate 95 % position is usually unknown.

Mainsah [97] and Dong et al [38] improved Lin’s work. Mainsah [97] developed an optimum method by using high-density profile scanning instead of an initial areal measurement. Hence, the pre-processing time can be reduced significantly. This idea was also used by Pawlus [109] for cylinder bores. Continuing Mainsah’s work, Dong developed a “**80 % - 1/8**” selection criterion [38] for sampling interval. It is found that the frequency at 80 % of a complete cumulative spectrum power is closest to 1/8 of the Nyquist folding frequency, for most of machined surfaces. Based on this finding, it is possible to check whether the sampling interval is small enough. With

this method, several pre-tests need to be carried out to determine an optimal sampling spacing before a full measurement.

A point showing the rationality of the bottom-to-top approach has been demonstrated in [90]. It was demonstrated that the variation of the amplitude parameters, for example Sq , Sku , etc., is small enough based on Lin's spectral method. The spectral method has the same practical implementation difficulty as the parameter variation approach, i.e. the reference parameter or the reference power spectrum is usually unknown. However, more and more researchers believe in the rationality of Lin's method because this criterion reflects the scale relevant property of the surface features.

Some practical issues need to be taken into consideration. For example, the minimum sampling interval should be equal to half, or the same size as the tip radius which is used in a stylus instrument. Wu [173] stated that due to mechanical filtration, the spectral density function is not reliable when the sampling interval is smaller than a critical value. Pawlus recognised that the minimum sampling interval depends on the radius of the tip, the correlation length of the inspected surface and the Rq parameter value [110].

An empirical philosophy is that the determination of sampling intervals should depend on the aim of investigation [169]. Therefore, if the components of interest are the surface waviness, Dong's method [38] cannot simply be used because it focuses on measurement of surface roughness.

In the past ten years, the development of this field has been slow. In 2005, a correlation length-based method was proposed by Nguyen [104]. The novel viewpoint derives from the use of scale space, rather than frequency space. Nguyen's work is a practical improvement for industry because the calculation of correlation length costs less on computation compared to spectrum analysis. It has been shown that this method is in agreement with the spectrum approach by understanding that the high frequency limit at the reciprocal of the correlation length ($1/Sa_l$) covers approximately 90 % of the energy of the power spectrum. Pawlus [110] analysed the influence of the number of sampling points on the parameters' variation once again in 2006. The

parameters used in this work contain hybrid parameters such as the peak/valley radius, and the investigated objects are classified into deterministic and random types. A proposal for selection of sampling intervals was developed based on the fitting of the radial spectral analysis. Basically, Pawlus's method [110] and Dong's method [38] are derived from analysis of the radial spectrum. Both methods suggested a relationship between the developed critical frequencies ($f_{i,j}$ in Dong's work, f_k in Pawlus' work) and the Nyquist folding frequency.

However, structured surfaces usually have sharp edges which indicate that such surfaces have very long frequency support compared to conventional harmonic surfaces. Therefore, Dong's "80 % - 1/8" criterion [38] will not apply to these surfaces. The following section will show the reasons. A compromise selection criterion is concluded at the end.

4.2.2 *Ideal sampling and reconstruction*

Shannon's sampling theorem states [129]:

If a function $f(x)$ contains no frequencies higher than W cps (cycles per second), it is completely determined by giving its ordinates at a series of points spaced $T = 1/2W$ seconds apart. The reconstruction formula (Cardinal series expansion) that complements the sampling theorem was given in equation (3.12).

The sampling theorem can be easily understood in frequency domain which is illustrated in Figure 4.1. To extend the theorem on two dimensions, consider a continuous band-limited surface signal $f(x) \in L^2(\mathbb{R}^2) \cap B(-W, W)^2$ which has the Fourier transform $\hat{f}(\omega)$ as shown in Figure 4.1a, according to equation (3.10). If the signal is sampled using an ideal sampling device, i.e. multiplied with a unit impulse sequence

$$\Delta_T(x) = \sum_{k \in \mathbb{Z}^2} \delta(x - kT), \text{ where } x, T \in \mathbb{R}^2, \text{ and } k \in \mathbb{Z}^2, \text{vi} \quad (4.1)$$

which has the corresponding Fourier transform

$$\widehat{\Delta_T}(\xi) = \frac{1}{T} \sum_{m \in \mathbb{Z}^2} \delta(\xi - m/T), \text{vii} \quad (4.2)$$

the obtained discrete signal is

$$f_\delta(x) = \sum_{k \in \mathbb{Z}^2} f(x) \delta(x - kT) = f(kT), (k \in \mathbb{Z}^2, \text{ and } x, T \in \mathbb{R}^2). \quad (4.3)$$

The ideally sampled signal has the spectrum which is a periodisation of the Fourier transform $\frac{1}{T} \hat{f}(\xi)$ with the period $1/T$ as in Figure 4.1b:

$$\hat{f}_\delta(\xi) = \hat{f}(\xi) * \frac{1}{T} \sum_{m \in \mathbb{Z}^2} \delta(\xi - m/T) = \frac{1}{T} \sum_{m \in \mathbb{Z}^2} \hat{f}(\xi - m/T). \quad (4.4)$$

Consequently, if an ideal two-dimensional low-pass filter $\{\varphi(x), x \in \mathbb{R}^2\}$ (sometimes also called box function) which has the Fourier transform

$$\hat{\varphi} = T \mathcal{X}[-\frac{1}{2T}, \frac{1}{2T}]. \quad (4.5)$$

as shown in Figure 4.1c, is convolved with the sampled signal $f_\delta(x)$, the reconstructed signal can be obtained

^{vi} Note that the two-dimensional Dirac delta function has the decomposed form $\delta(x_1, x_2) = \delta(x_1)\delta(x_2)$, and the two-dimensional Dirac comb function can be decomposed into $\sum_{k \in \mathbb{Z}^2} \delta(x - kT) = \sum_{k_1 \in \mathbb{Z}} \sum_{k_2 \in \mathbb{Z}} \delta(x_1 - k_1 T_1, x_2 - k_2 T_2)$, where $x = [x_1, x_2]$, $T = [T_1, T_2]$, $k = [k_1, k_2]$.

^{vii} Note that this expression is a two-dimensional case, i.e. $\frac{1}{T} \sum_{m \in \mathbb{Z}^2} \delta(\omega - m/T) = \frac{1}{T_1 T_2} \sum_{m \in \mathbb{Z}} \delta(\omega_1 - m_1/T_1, \omega_2 - m_2/T_2)$ where $x = [x_1, x_2]$, $T = [T_1, T_2]$, $k = [k_1, k_2]$, which applies to other similar expressions in this section, for example equation (4.4), (4.5), and so on.

$$f_{rec} = f_{\delta} * \varphi = \sum_{k \in \mathbb{Z}^2} f(kT) \varphi(k - \cdot). \quad (4.6)$$

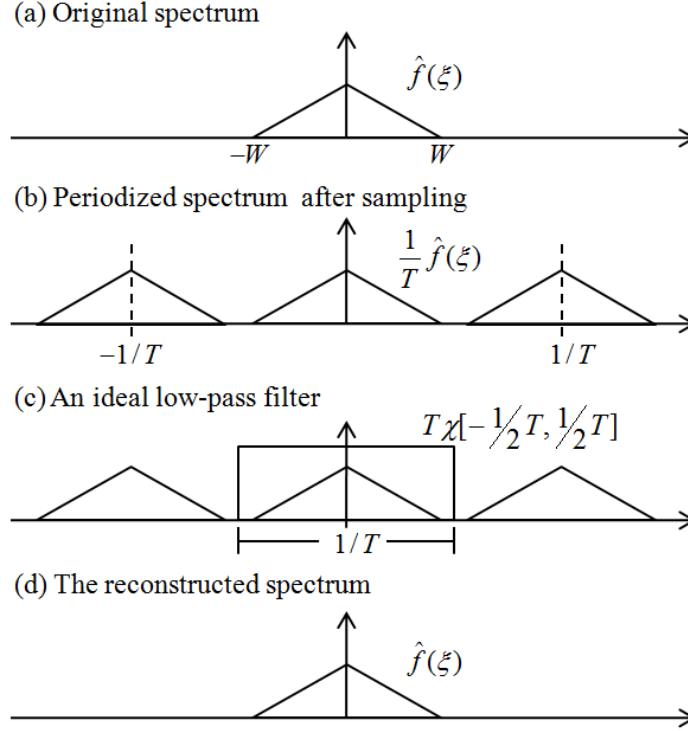


Figure 4.1. Frequency interpretation of Shannon's sampling theorem. (a) Fourier transform of original signal; (b) periodisation of the Fourier transform caused by unit impulse sequence sampling with the sampling spacing T ; (c) reconstruction of the continuous signal using an ideal low-pass filtering based on equation (3.10). (d) the reconstructed signal has the same spectrum as the original.

This reconstructed signal is identical to the original signal because in the frequency domain, the convolution process in equation (4.6) gives that

$$\hat{f}_{rec}(\xi) = \hat{f}_{\delta}(\xi) \cdot \hat{\varphi}(\xi) = \left[\sum_{m \in \mathbb{Z}^2} \hat{f}(\xi - m/T) \right] \cdot \chi\left[-\frac{1}{2T}, \frac{1}{2T}\right] = \hat{f}(\xi). \quad (4.7)$$

Since the ideal low-pass filter has the function in the spatial domain

$$\varphi(x) = \int_{\mathbb{R}^2} \hat{\varphi}(\xi) e^{j2\pi \langle x, \xi \rangle} d\xi = T \int_{(-\frac{1}{2T}, \frac{1}{2T})^2} e^{j2\pi \langle x, \xi \rangle} d\xi = \text{sinc}(x/T),^{\text{viii}} \quad (4.8)$$

the sampling-reconstruction in areal surface measurement can be expressed as

$$f_{\text{rec}}(x) = \sum_{k \in \mathbb{Z}^2} f(kT) \text{sinc}(x/T - k) = f(x), \quad (4.9)$$

where $x, T \in \mathbb{R}^2, k \in \mathbb{Z}^2$, $f(kT)$ is a two-dimensional sampling sequence with the sampling spacing T .

4.2.3 Spectral aliasing and practical solutions

However, if the sampling spacing $T > 1/2W$, the high frequency components in the spectrum will be folded into the lower parts which causes aliasing – “**spectral aliasing**” (see Figure 4.2). In this case, even though an ideal low-pass filter is employed, the original signal cannot be recovered exactly. Also in practice, an ideal sampling device and reconstruction mechanism are never available. Furthermore, as discussed in [133], real world signals are rarely band-limited. Therefore, spectral aliasing is unavoidable. Optimisation of sampling spacing to minimize the influence caused by aliasing becomes the compromise consideration for the selection of sampling conditions.

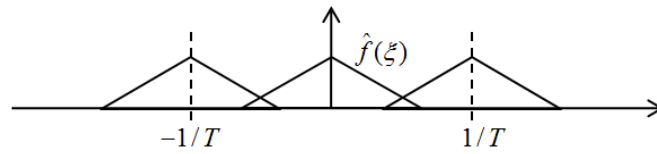


Figure 4.2. Spectral aliasing caused by not small enough sampling spacing T .

In 1993, it was suggested by Lin [90] that an optimal sampling interval can be determined at the 95 % position of the cumulative spectrum power. However, the complete cumulative spectrum of a given surface is always unknown. In 1995, an

^{viii} The two-dimensional expression of the sinc function has $\text{sinc}(x/T) = \text{sinc}(x_1/T_1) \text{sinc}(x_2/T_2)$ where $x = [x_1, x_2]$, $T = [T_1, T_2]$.

improvement was suggested by Dong and Mainsah [38]. It was pointed out in that work, the 80 % position in the cumulative power spectrum should fall within 1/8 to 1/3 of the Nyquist folding frequency for isotropic surfaces. This criterion coincides with Pawlus' work in 2005 [110], in which it was pointed that from investigations of simulated and real surfaces that the 80 % position of the cumulative spectrum should be smaller than 1/3 of the Nyquist folding frequency for random surfaces, but 1/5 for others (deterministic and mixed surfaces). However, practical compromises do not work for many structured surfaces because they require too many sampling points. For example, a rectangle-wave surface as shown in Figure 4.3 has a wavelength of typical rectangle structure with 20 μm . When using a sampling spacing of $T = 0.125 \mu\text{m}$ (i.e. 160 points per step structure), it can be observed that the 80 % position of the cumulative spectrum is still greater than $0.8 \mu\text{m}^{-1}$, i.e. 1/5 of the Nyquist folding frequency (see Figure 4.4b). This indicates that a sampling spacing of $0.125 \mu\text{m}$, which is 1/160 of the typical period $20 \mu\text{m}$, is still far away from the required spectral condition proposed by Lin.

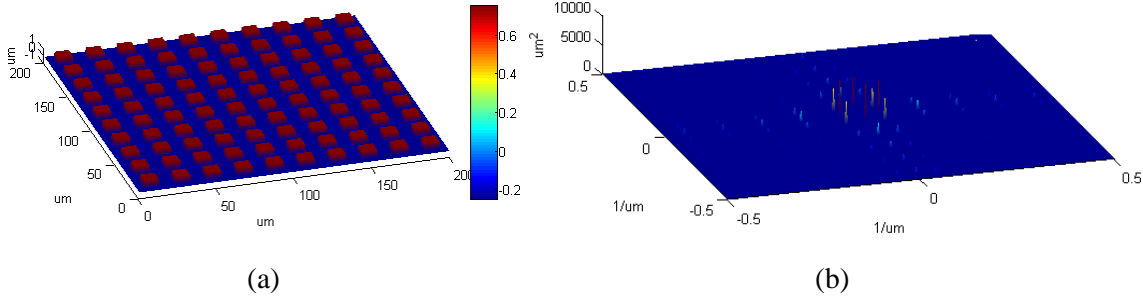


Figure 4.3. A periodic rectangle-wave surface and its power spectrum. (a) A simulated two-dimensional rectangle-wave surface with the typical wavelength 20 μm , (b) Partial illustration of the spectrum. (sampling conditions: spacing $1 \mu\text{m} \times 1 \mu\text{m}$, area: $200 \mu\text{m} \times 200 \mu\text{m}$.)

An alternative approach to find a proper sampling spacing involves parameter variation. The authors of [116] proposed that the maximum sampling interval requirement for sinusoidal surfaces be 1/6 of the main wavelength. For more general periodic surfaces, which usually have an infinitely supported spectrum such as the rectangle-wave surface and v-groove surface, other authors consider sixteen [91] or twenty [110, 175] discrete data points within a typical period as satisfactory. The

typical period here denotes the wavelength of the frequency component of most interest. In particular, in Pawlus's work [110], analysis of parameter variations on different sampling points within a sample period was carried out and it was pointed out that a sampling interval equal to 1/20 of the main wavelength (wavelength of the main surface structure) assures small parameter changes. However, this recommendation is rarely used because the 1/20 criterion ignores too much geometric detail within a main wave length of a practical surface.

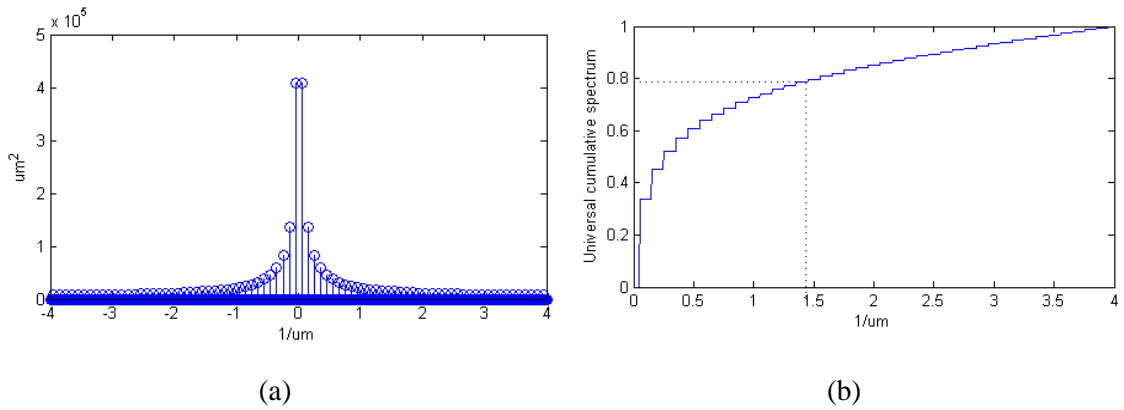


Figure 4.4. The power spectrum and the cumulative spectrum of a one-dimensional rectangle wave signal. (a) Power spectrum of the discrete samples of a rectangle-wave profile in Figure 4.3a; (b) the corresponding universal cumulative spectrum.

All of the past research shows that it is difficult to find a widely acceptable criterion to select sampling spacing for the measurement of structured surfaces. More practical issues including instrumental limitations and experience, for example the tip size and stage movement precision, have been considered instead. For example, ISO 25178 Part 3 [69] guides people to set an S-filter nesting index which limits the minimum wavelength component of interest for a practical measurement. The allowed maximum sampling spacing is suggested as approximately 1/5 of the S-filter nesting index. From a practical viewpoint, the ISO selection solutions are hence recommended in this research (see Table 4.1).

S-filter nesting index [μm]	Maximum sampling spacing [μm]	Maximum ball radius [μm]
...*	...*	...*
0.6	0.12	0.5
0.8	0.15	0.5
1.5	0.3	1.0
2.5	0.5	2.0
3	0.6	2.5
6	1.2	5
8	1.5	5
15	3	10
25	5	20
30	6	25
60	12	50
80	15	50
150	30	100
250	50	200
300	60	250
...*	...*	...*
* indicates that the series continue.		

Table 4.1. Selection of sampling spacing based on S-filter nesting index
[69]

4.3 Selection of sampling length

Selection of sampling length for surface measurement has been rarely investigated in past research. The reason is that a surface geometry is usually characterised in the spatial domain in which case only spectral aliasing effects cause sampling error. On the selection of sampling length, the new international standard ISO 25178 Part 3 [69] suggests that the F-operator/L-operator nesting index (thus implying the sampling length) is typically set at ten times the wavelength of the coarsest structure of interest. However, if researchers want to investigate the spectrum of a surface signal accurately, selection of proper sampling for structured surfaces has to be carefully considered. Recently, spectral analysis has been recognised to be of more importance, for example

the defined two-dimensional power spectral calculation in ISO 25178 Part 2 [68], and the angular spectrum used for isotropy analysis [178].

It is fortunate that the selection of sampling length looks to be more flexible because the sampling length can be adjusted later by proper data manipulation. However, selection of sampling length/area needs attention regarding frequency sampling and spectral leakage. Here a study of the influence of different sampling lengths is given.

4.3.1 Spectral leakage

Another effect which has been seldom mentioned by past researchers in surface metrology is “spectral leakage”. It is induced by choosing a finite sampling length l for a surface signal $f(x) \in L^2(\mathbb{R}^2)$. This procedure acts like sampling a surface using a rectangle window $\{w(x)=1, x \in (-l/2, l/2)^2\}$. Thus the windowed signal has the form

$$f_w(x) = f(x) \cdot w(x). \quad (4.10)$$

Since $w(x)$ has the Fourier transform

$$\hat{w}(\xi) = \int_{(-l/2, l/2)^2} e^{-j2\pi \langle x, \xi \rangle} dx = l \operatorname{sinc}(l\xi),^{\text{ix}} \quad (4.11)$$

in the frequency domain, such a windowing process results in a convolution of the spectrum of the original surface and the spectrum of the rectangle window function, i.e.

$$\hat{f}_w(\xi) = \hat{f}(\xi) * \hat{w}(\xi) = l \int_{\mathbb{R}^2} \hat{f}(\tau) \operatorname{sinc}(l\xi - \tau) d\tau. \quad (4.12)$$

^{ix} Note that the two-dimensional Fourier transform $l \operatorname{sinc}(l\xi) = l_1 l_2 \operatorname{sinc}(l_1 \xi_1) \operatorname{sinc}(l_2 \xi_2)$ for $l, \xi \in \mathbb{R}^2$, $l = [l_1, l_2]$, $\xi = [\xi_1, \xi_2]$.

Considering a structured surface $\bar{f}(x) \in L^2(\mathbb{R}^2)$ with periodic surface structures with a period $T \in \mathbb{R}^2$ (i.e. $\bar{f}(x) = \bar{f}(x + kT)$ for $\forall k \in \mathbb{Z}^2$), it has a discrete spectrum only at the positions $\{\xi_k = k / T, k \in \mathbb{Z}^2\}$

$$\hat{\bar{f}}(\xi) = \sum_{k \in \mathbb{Z}^2} F_k \cdot \delta(\xi - k / T) = \hat{\bar{f}}(k / T). \quad (4.13)$$

where F_k are the Fourier coefficients of the periodic signal $\bar{f}(x)$

$$F_k = \frac{1}{T} \int_{T^2} \bar{f}(x) e^{-j2\pi \frac{\langle x, k \rangle}{T}} dx, \quad (4.14)$$

i.e.

$$F_{k_1, k_2} = \frac{1}{T_1 T_2} \int_{-T_1/2}^{T_1/2} \int_{-T_2/2}^{T_2/2} \bar{f}(x_1, x_2) e^{-j2\pi \left(\frac{x_1 k_1}{T_1} + \frac{x_2 k_2}{T_2} \right)} dx_1 dx_2. \quad (4.15)$$

Thus equation (4.12) can be written as

$$\hat{\bar{f}}_w(\xi) = l \sum_{k \in \mathbb{Z}^2} \hat{\bar{f}}\left(\frac{k}{T}\right) \text{sinc}\left(l\xi - \frac{k}{T}\right), \quad (4.16)$$

which indicates that the spectrum of a windowed periodic signal becomes continuous because of the convolution with a sinc function, which is also continuous. This convolution process is illustrated in Figure 4.5. It can be observed that after windowing, the original frequency spectrum is distorted. If the original signal is periodic (most structured surfaces are of this type), the distortion effect appears as if some energy has "leaked" out of the original signal spectrum at other frequency regions. This distortion is called **spectral leakage**. If leakage is present in a spectrum, much of the information, for example periodicity of the original signal, may be hidden.

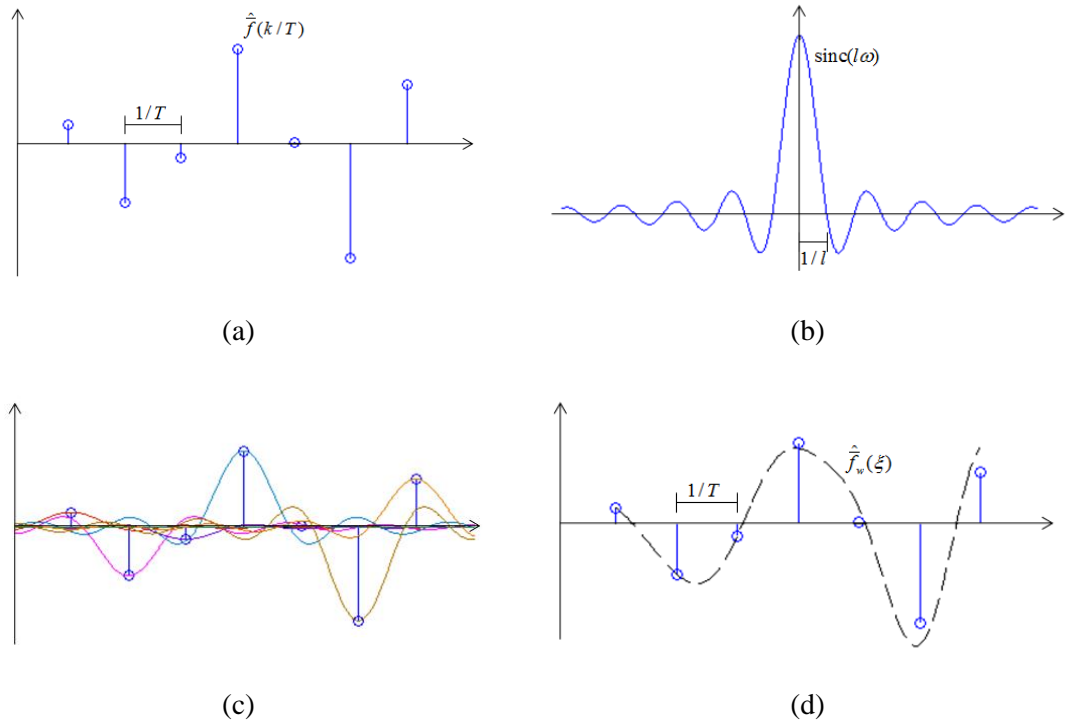


Figure 4.5. Interpretation of windowing for periodic signal in frequency domain. (a) Partial frequency spectrum of the original periodic signal; (b) the Fourier transform of the unit rectangle window function with the support $(-l/2, l/2)$; (c) the convolution illustration and (d) the convolution result.

Specifically, take a sinusoidal surface which has a single impulse in the frequency domain $\xi = 1/T$ as an example.

$$\begin{aligned}
 f(x, y) &= \cos\left(\frac{2\pi}{T_x} x\right) \cos\left(\frac{2\pi}{T_y} y\right) \\
 &= \frac{1}{4} \left[e^{-j2\pi\left(\frac{x}{T_x} - \frac{y}{T_y}\right)} + e^{-j2\pi\left(-\frac{x}{T_x} + \frac{y}{T_y}\right)} + e^{-j2\pi\left(\frac{x}{T_x} + \frac{y}{T_y}\right)} + e^{-j2\pi\left(-\frac{x}{T_x} - \frac{y}{T_y}\right)} \right], \\
 &= \frac{1}{4} (f_1 + f_2 + f_3 + f_4)
 \end{aligned} \tag{4.17}$$

in which $x, y \in \mathbb{R}$. By providing $T_x = T_y = 5 \mu\text{m}$ part of the surface is shown in Figure 4.6a. The periodic surface has a Fourier transform (see Figure 4.6b)

$$\begin{aligned}
\hat{f}(\xi_1, \xi_2) &= \frac{1}{4} \iint_{-\infty, +\infty} (f_1 + f_2 + f_3 + f_4) e^{-j2\pi(\xi_1 x + \xi_2 y)} dx dy \\
&= \frac{1}{4} \sum_{k_1=-1,1} \sum_{k_2=-1,1} \delta\left(\xi_1 - \frac{k_1}{T_x}, \xi_2 - \frac{k_2}{T_y}\right)
\end{aligned} \tag{4.18}$$

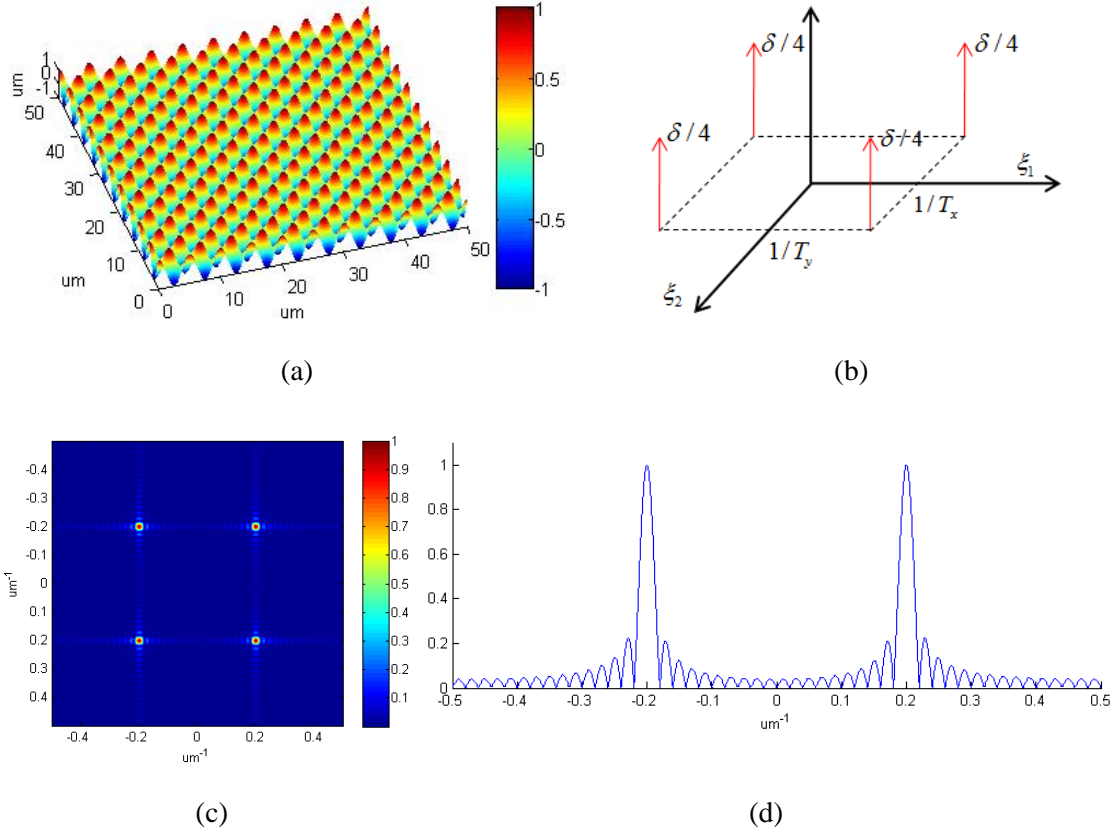


Figure 4.6. Spectral leakage of the measurement of a sinusoidal surface. (a) A simulated sinusoidal surface which has the periods $T_x = T_y = 5 \mu\text{m}$ and (b) its frequency spectrum; (c) the leaked frequency spectrum after windowing using a rectangle-window with the length $l_x = l_y = 50 \mu\text{m}$; (d) a cross-section view of the leaked spectrum (normalised) where the main lobe and side lobes are clearly identified.

Windowing this surface signal using a rectangular window with support $(-l/2, l/2)^2$ causes the frequency spectrum to leak. Figure 4.6c and Figure 4.6d show the frequency “lobes” induced by spectral leakage from the original four impulses in Figure 4.6b. Note that the leaked frequency part $\{\mu \in (-1/l_x, 1/l_x), \omega \in (-1/l_y, 1/l_y)\}$ is called the “main lobe” while others are “side lobes”. The length $1/l$, $l \in \mathbb{R}^2$ is

called “lobe width”. The lobe width is determined by the windowing support, i.e. the sampling length l . Generally, the longer the sampling length l , the smaller the spectral leakage.

Since practical analysis cannot process an infinite signal, a method generally used to alleviate spectral leakage is to employ a dedicated window function. For instance, Hann window, Hamming window, Kaiser window and other non-rectangular windows are usually used in current signal processing techniques to prevent the abrupt truncation in time or space [106]. Figure 4.7a presents the Hann window $w_{Hann}(x)$:

$$w_{Hann}(x_1, x_2) = \begin{cases} 0.5[1 + \cos(2\pi x_1 / l_1) \cos(2\pi x_2 / l_2)], & x \in (-l/2, l/2) \\ 0, & \text{otherwise} \end{cases} \quad (4.19)$$

Replacing the rectangular window in the test described in Figure 4.6 with a Hann window of the same length, the spectral leakage is evidently alleviated. A review of the windowing techniques is given in [60]. However, non-rectangular windowing processes can only alleviate spectral leakage, especially the side lobes; the main lobe leakage is hardly affected.

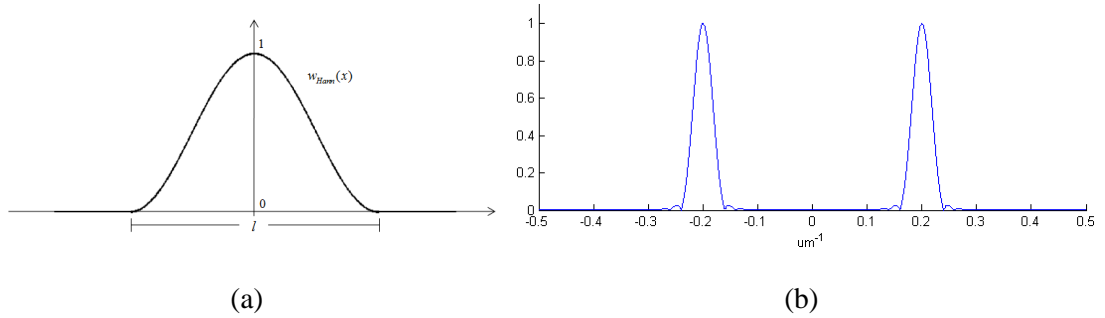


Figure 4.7. The effect of a Haan window. (a) The Hann window with the window length l ; (b) the improved frequency spectrum of the sinusoidal signal described Figure 4.6a when the Hann window is employed.

4.3.2 Frequency sampling

Sampling discretisation causes periodisation of the frequency spectrum. If sampling spacing is not small enough, spectral aliasing is produced. Finite length sampling, i.e.

windowing, causes spectral leakage. Avoiding aliasing can be achieved by reducing the sampling spacing to $1/2W$, if the original signal is band-limited, i.e. $f(x) \in B(-W, W)$. However, in the latter case, spectral leakage always exists; although non-rectangular windowing can be used to alleviate leakage. Avoiding spectral leakage can be a troublesome.

In practice, the continuous Fourier transform (CFT) or the discrete-time Fourier transform (DTFT) [61] are not available. The discrete Fourier transform (DFT) and its computing-oriented optimizing version – the fast Fourier transform (FFT) – are always used. Differing from CFT and DTFT, DFT is a transform which is discrete both in the time domain and frequency domain because data for computer processing is always discretised and with a finite length. Specifically, a finite sampling length l induces a sampling in the frequency domain with the sampling spacing $1/l$, i.e. $\hat{f} = \{\hat{f}(k/l), k \in \mathbb{Z}\}$. If the spectral leakage can be controlled within each open frequency band $\{B(\frac{k}{l}, \frac{k+1}{l}), k \in \mathbb{Z}\}$, the frequency samples at $\{\hat{f}(k/l), k \in \mathbb{Z}\}$ would stay as the original. A detailed explanation is given in the following.

For simplicity, one-dimensional analysis of DFT is explained here. An input sequence with the finite length $\{x(n), n = 0, 1, \dots, N-1\}$, there exists the following discrete Fourier transform pair:

$$\hat{x}(k) = \sum_{n=0}^{N-1} x(n) e^{-j \frac{2\pi}{N} nk}, k = 0, 1, \dots, N-1; \quad (4.20)$$

$$x(n) = \frac{1}{N} \sum_{k=0}^{N-1} \hat{x}(k) e^{j \frac{2\pi}{N} nk}, n = 0, 1, \dots, N-1. \quad (4.21)$$

A windowed discrete sequence has a leaked frequency spectrum (for example Figure 4.6d). An N point DFT of a sequence is equivalent to using a uniformly-spaced N point **frequency sampling** set $K = \{0, \frac{1}{N}, \frac{2}{N}, \dots, \frac{N-1}{N}\}$ to observe one period^x of its

^x A discretized signal has a periodic frequency spectrum (see Figure 4.1b).

frequency spectrum. In practical spectral analysis, it has to be noted that a discrete Fourier transform recognizes any input sequence with finite length N as a periodic signal with the period N .

If increase the number of frequency-sampling points from N to M in the DFT computation, i.e.

$$\hat{x}(k) = \sum_{n=0}^{N-1} x(n) e^{-j \frac{2\pi}{M} nk}, M > N, k = 0, 1, \dots, M-1, \quad (4.22)$$

the same frequency information can be observed at other positions (frequency sample positions). Here M controls the frequency sampling resolution. An M point DFT acts like observing a spectrum through a picket-fence. If the spacing of the fence is altered, the information observed changes subsequently. As people know, the interfered pattern of two patterns can be referred to the Moire patterns [47]. The Moire pattern effect produced in frequency-sampling is called the **picket-fence effect** in signal processing. The picket-fence effect has a significant impact on the analysis of the spectrums of signals. The frequency-sampling induced by a finite sampling length in the time/spatial domain needs to be considered carefully in Fourier analysis. For example, in Figure 4.8 in which the sinusoidal signal described in Figure 4.6a is analysed. The spectral leakage brought about by a finite sampling length (50 μm) is shown by the DTFT analysis. While in the DFT analysis, using fifty sampling points and fifty-one sampling points creates completely different power spectra.

An increase in frequency-sampling resolution M can apparently obtain more frequency information. However, this is not equivalent to an improvement of the real **spectral resolution**, because a simple increase of M does not add real information to the analysed signal. Once the sampling length of a signal is determined, its frequency spectrum is determined with a specific spectral resolution. An increase of the number of frequency-sampling point amount M is equivalent to supplementing $M - N$ zeros after the original sequence $\{x(n), n = 0, 1, \dots, N-1\}$ in a DFT computation. This indicates that the original periodic signal with period N is revised into a new periodic signal which has period M . When $M \rightarrow +\infty$, the DFT is tantamount to calculating a DTFT of a windowed discrete signal. To avoid spectral leakage in DFT or FFT, the

frequency sampling resolution M should be kept the same as the time sampling resolution N , i.e.

$$\hat{x}(k) = \sum_{n=0}^{N-1} x(n) e^{-j2\pi nk/M}, M = N, k = 0, 1, \dots, N-1. \quad (4.23)$$

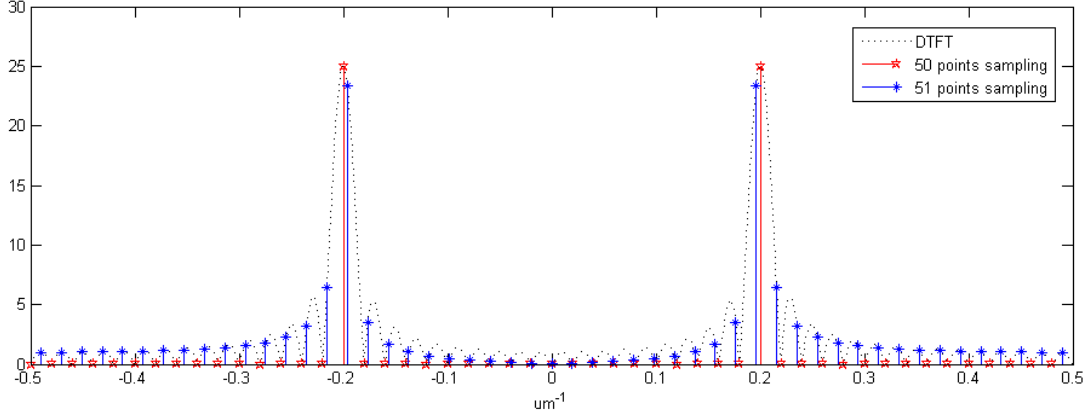


Figure 4.8. Frequency sampling in discrete Fourier analysis. The induced picket-fence effect is clearly visible: frequency sampling using fifty points has nearly complete different result with that using fifty-one points.

4.3.3 Sampling length determination

It is known that periodic signals have a DFT expressed by equation (4.13) and most structured surfaces fall into this type of signal. Equation (4.23) gives a necessary condition to avoid spectral leakage in DFT/FFT computation; but this is an insufficient condition. Improper selection of the sampling length would produce a leaked spectrum which cannot be correctly sampled with any frequency sampling resolution. An illustrative example can be seen in Figure 4.9.

With a proper sampling length, the sampled spectrum can be the same as the original (see Figure 4.10 for example). As described by equation (4.13), a periodic surface $\bar{f}(x) \in L^2(\mathbb{R}^2)$ with period $T \in \mathbb{R}^2$ has a discrete spectrum only at the positions $\{\xi_k = k/T, k \in \mathbb{Z}^2\}$. Meanwhile, sampling using a rectangular window with length l ,

has a sinc like spectrum with zero values at $\{\xi_k = k/L, k \in \mathbb{Z}^2\}$. Therefore, it is possible that the original discrete frequency spectrum can be retained if

$$l = ZT, Z \in \mathbb{Z}^+, \quad (4.24)$$

where Z is usually taken as $Z \geq 10$ with reference to the stability of statistics [69].

However, leakage cannot essentially be avoided in this way. The only benefit is that such an integer period sampling produces a frequency sampling result only at the un-leaked frequency positions (see Figure 4.10 for a schematic).

The sampling technique which asks that sampling length is an integral multiple of the signal period is called **integral period sampling**. A coherent sampling technique has been proposed to eliminate spectral leakage [19, 30], which is originated from the integral period sampling. The coherent sampling states that

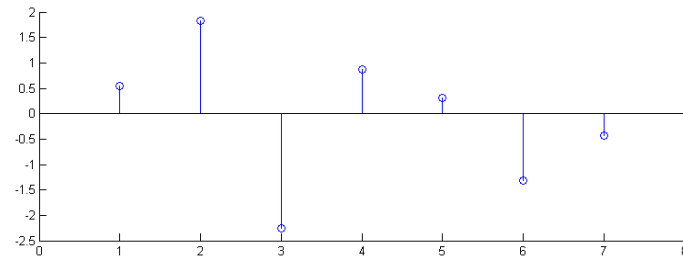
$$\frac{f_{signal}}{f_{sampling}} = \frac{M}{N}. \quad (4.25)$$

where f_{signal} and $f_{sampling}$ are the input signal frequency and sampling frequency, M is the number of sampled cycles and N is the number of total sampling points ($M, N \in \mathbb{Z}^+$). The equation (4.25) indicates that the sampling length is an integral multiple of the signal period, i.e.

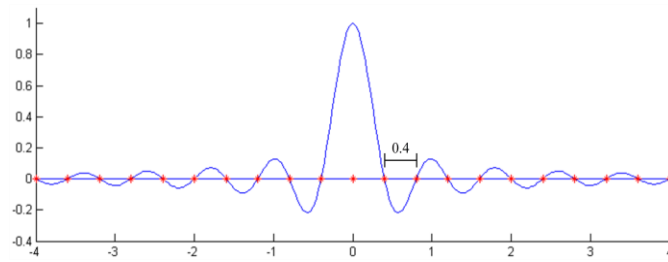
$$l = N \cdot T_{sampling} = M \cdot T_{signal}. \quad (4.26)$$

In this case, there is no spectral leakage when a rectangular window is used [19].

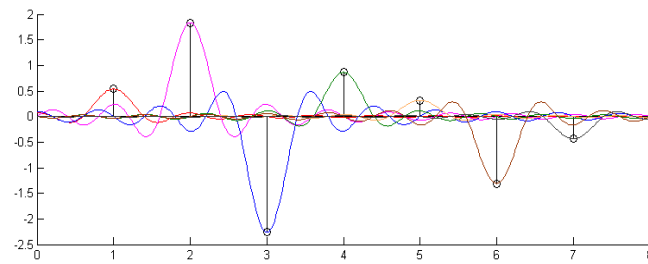
The effect of retaining the original discrete frequency spectrum is presented in Figure 4.10. In comparison with Figure 4.9, where the sampling length is a non-integral multiple of the period of original signal, the integral period sampling shows an excellent performance regarding the avoidance of spectral leakage.



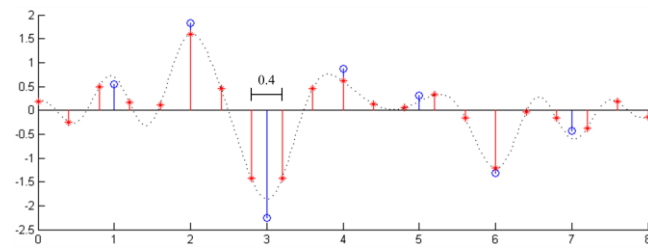
(a)



(b)

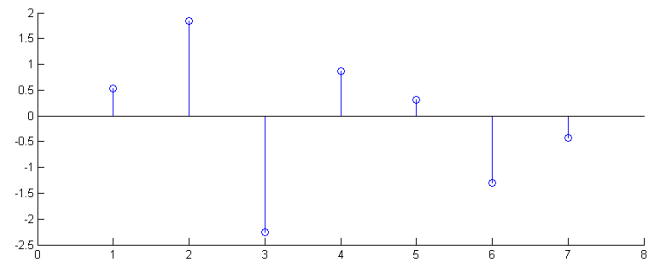


(c)

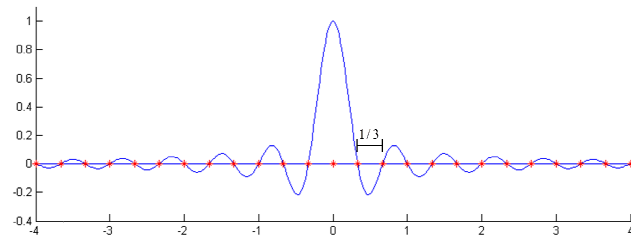


(d)

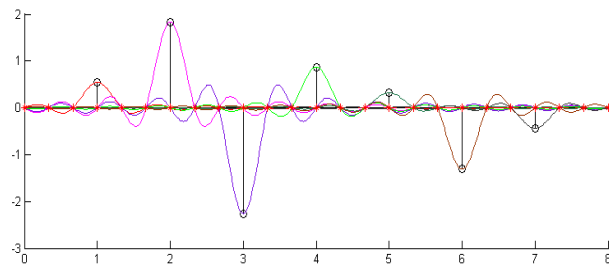
Figure 4.9. Spectral leakage caused by non-integer period sampling (a) Partial discrete frequency spectrum of a periodic signal; (b) the spectrum of a sampling window with 2.5 times period length; (c) thus the spectrum is leaked because of the sampling truncation based on equation (4.16); (d) The frequency sampling result (red dots) based on DFT/FFT computation using equation (4.23).



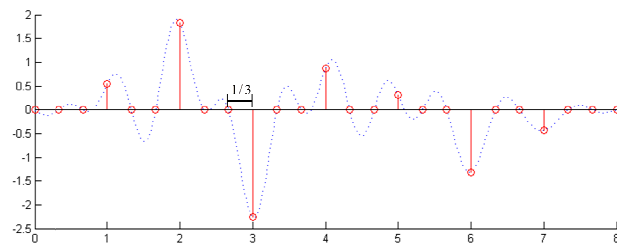
(a)



(b)



(c)



(d)

Figure 4.10. The effect of integral period sampling. (a) Partial discrete frequency spectrum of a periodic signal; (b) The spectrum of a sampling window with three times period length; (c) The spectrum is leaked because of the sampling truncation based on equation (4.16); (d) Comparison of the leaked spectrum (blue curve) and the frequency sampling result (red dots) based on FFT/DFT computation using equation (4.23).

Integral period sampling also shows excellent performance in noisy signal analysis. Taking a noisy sinusoidal profile as an example:

$$x(n) = \cos(2\pi n/10) + r(n), \quad (4.27)$$

in which $r(n)$ is a normally distributed random noise $r \sim N(1, 0.125)$. Adopting sampling length $l_1 = 100$ and $l_2 = 128$, the corresponding power spectrum is presented in Figure 4.11. Another example of analyzing a noisy sinusoidal surface is shown in Figure 4.12. The surface is simulated as

$$f(x, y) = \cos(2\pi x/5) \cos(2\pi y/5) + r(x, y), \quad (4.28)$$

where $r \sim N(1, 0.125)$. Sampling areas of $50 \mu\text{m} \times 50 \mu\text{m}$ and $52 \mu\text{m} \times 52 \mu\text{m}$ are calculated. It is observed that the sampling length, which is an integral multiple of the period of the original surface, presents an accurate spectrum, without spectral leakage.

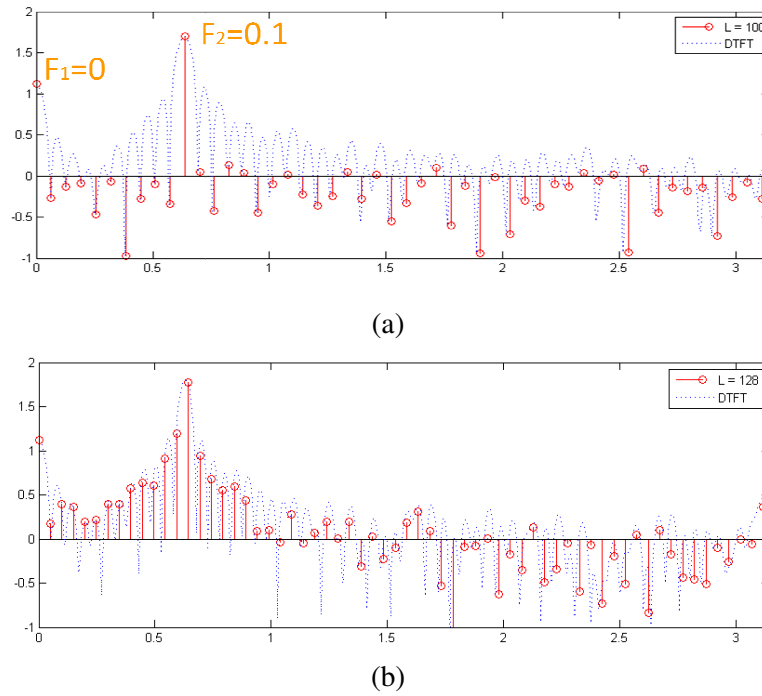
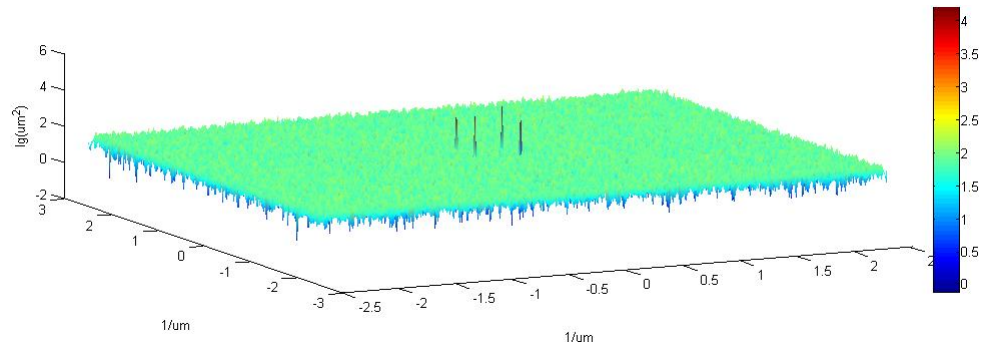
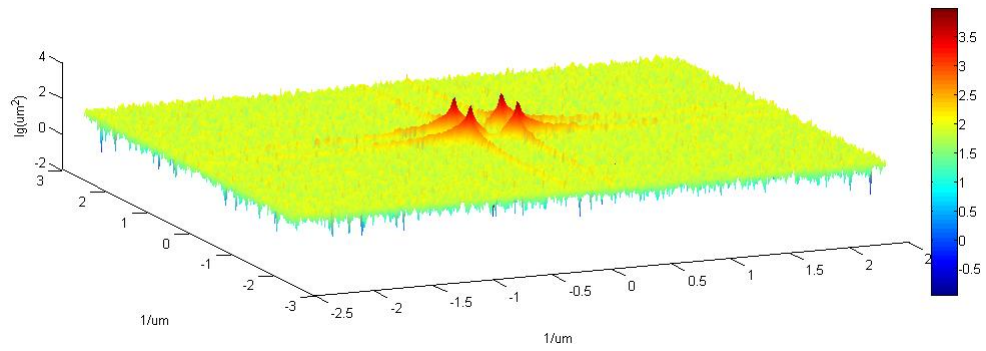


Figure 4.11. Power spectrum of the noised sinusoidal profile expressed by equation (4.27) with the sampling length (a) 100 points and (b) 128 points.



(a)



(b)

Figure 4.12. Power spectrum of the noised sinusoidal surface expressed by equation (4.28) with sampling length (a) $50 \mu\text{m} \times 50 \mu\text{m}$ (b) $52 \mu\text{m} \times 52 \mu\text{m}$.

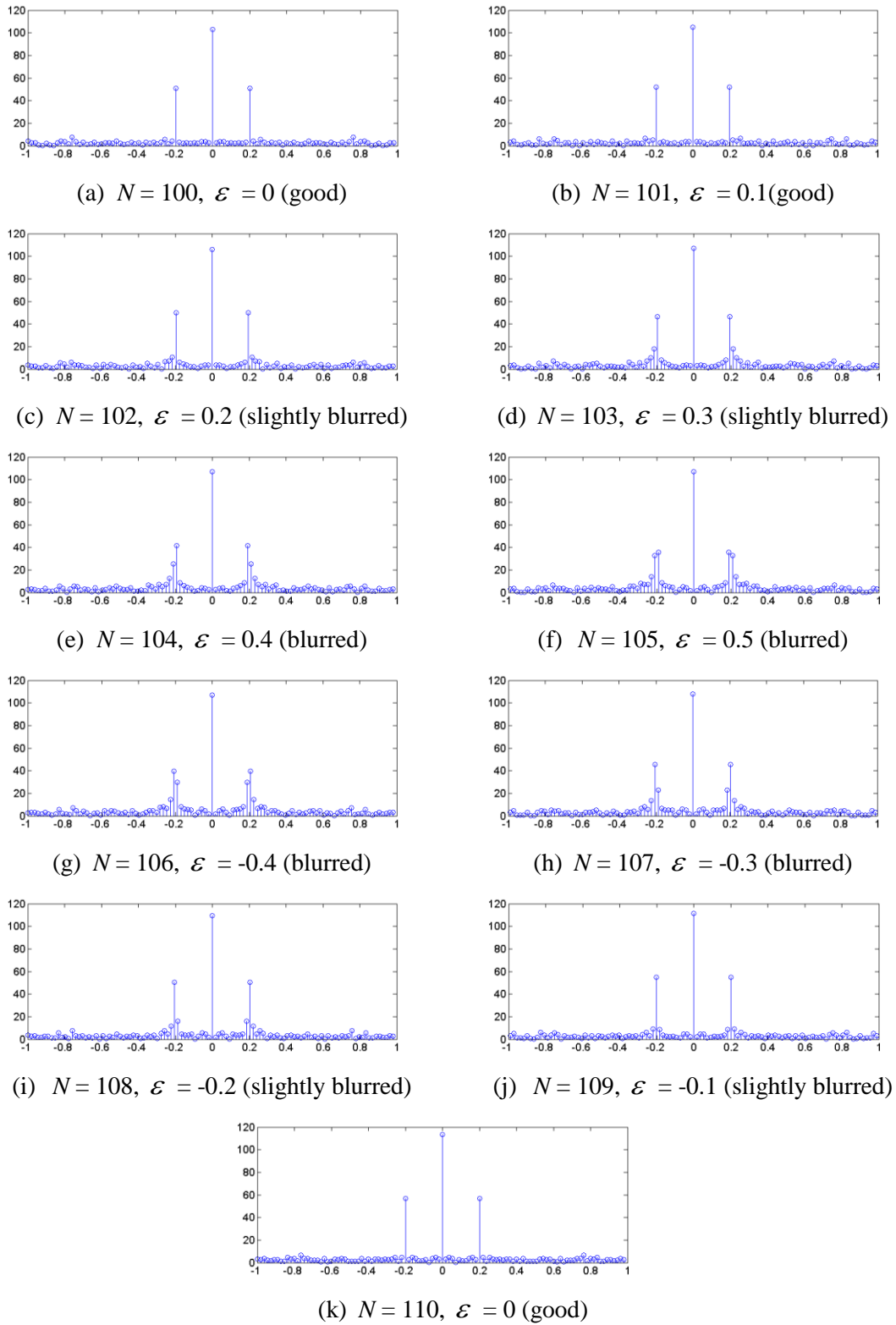


Figure 4.13. Comparison of the DFT spectra with the sampling length from 100 to 110, i.e. M from ten to eleven, for the signal expressed by equation (4.27).

In practice, an exact integer-period sampling is usually difficult to manipulate, i.e. M in equation (4.24) is usually not an exact integer, because the period of a real signal is usually unknown or has a discrepancy from an expected value due to manufacturing error. However, the spectral leakage can still be minimised by controlling Z close to an integer. For example, if test the DFT computation of the signal (4.27) using sampling lengths from 100 ($Z = 10$) to 110 ($Z = 11$), the spectrums can sequentially be obtained in Figure 4.13. It can be observed that the spectra gradually become distorted as Z becomes further away from its nearest integer. Therefore, the following conclusion for the determination of sampling length/area for practical measurement can be obtained

$$l = (Z \pm \varepsilon)T, Z \in \mathbb{Z}^+, \quad (4.29)$$

where Z is usually taken as ten or more, ε has not been decided at the moment but the evidence in Figure 4.13 indicates that $\varepsilon \in [0, 0.2)$ is acceptable. More research on this topic should validate this conclusion.

4.4 Summary and conclusions

Determination criteria of sampling conditions for uniform sampling for the measurement of structured surfaces have been revisited in this chapter. Some new evidence and conclusions are given and summarised. Specifically,

1. For the measurement of structured surfaces, the determination criteria for the sampling spacing (or interval) developed by past researchers are generally not applicable. For example, regarding the spectral analysis for determination of sampling spacing, it is shown that former researchers' methods, for example Dong's "80 % - 1/8" criterion, do not apply to structured surfaces. Also, the "parameter variation" criterion, which asks for a perfect measurement for comparison, is not available in practice.
2. Instrumental limitations and experience become the selection considerations to determine the sampling spacing. This study recommends the international standard ISO 25178 Part 3 [69] as the practical determination of sampling spacing.

The international standard states that the maximum allowed sampling spacing should be set as $1/5$ of the S-filter nesting index (i.e. the wavelength of the smallest features of interest). A series of common values are recommended for convenience. Under this condition, the features of interest can be recovered at a considerable accuracy level. Also in this way, the sampling spacing can be easily determined in a practical situation.

3. Determination of sampling length/area has received little attention in the past. The reason is that sampling length determines the frequency sampling resolution which is rarely considered in practice. Though selection of sampling length can be properly adjusted in the post data manipulations, for example clipping, for researchers who are interested in spectral analysis, determination of sampling length/area needs to be carefully considered.
4. The current international standard ISO 25178 Part 3 [69] suggests that the F-operator/L-operator nesting index (thus implying the sampling length) is typically set at ten times the wavelength of the coarsest structure of interest from a statistical viewpoint. This criterion is not sufficient for the measurement of structured surfaces from the view of frequency sampling.
5. The study of integral period sampling in this chapter indicates that the sampling length should be an integer (or close to an integer) multiple of the feature period of a structured surface, i.e. following equation (4.29). Hence, spectral leakage can be effectively avoided.

5. INTELLIGENT SAMPLING

5.1 Introduction

It was stated in Chapter 2 that the emergence of structured surfaces [46, 76] has forced surface metrologists to consider the drawbacks of uniform sampling. The main drawbacks include coherent spectral aliasing [114] (see Figure 3.6) and a lack of efficiency in terms of measuring time and data storage [164]. Structured surfaces usually consist of repeated geometrical structures over wide areas or are in the form of large step like features as encountered on MEMS or micro-fluidic devices. These novel kinds of surfaces usually require both large sampling areas and small sampling intervals (or spacing) to guarantee both measuring efficiency and accuracy simultaneously. The requirement described here is for intelligent sampling methods that are able to address the drawbacks of uniform sampling.

Intelligent sampling in the fields of computer graphics and coordinate metrology has been discussed elsewhere [9, 42, 44, 45, 84, 88, 111, 114, 130, 164, 172]. Some techniques have been developed to overcome the coherent spectral aliasing problem such as jittered uniform sampling [114] (see Figure 3.6). Some methods are used to reduce the statistical error of form estimation, such as low-discrepancy pattern sampling [84]. Other intelligent sampling methods have flexible sampling designs adapting to the surface geometric changes based on a surface geometry model or earlier samples, i.e. model-based sampling and adaptive sampling methods. Thus the sample size and sampling duration can be reduced efficiently. However, to date, none of the intelligent sampling methods have been used in surface metrology. On account of this situation, an adaptive sampling method is proposed in this chapter. It is developed for raster scan-based stylus profilometers. This development provides a technically transferable approach for the development of surface topography instruments.

Four different types of intelligent sampling methods have been categorised: jittered uniform sampling, low-discrepancy pattern sampling, model-based sampling and adaptive sampling. These methods vary in terms of the original ideas and purposes. In

general, no single sampling method has ideal performance or is flexible enough to be applied to all surface types [46]. It is anticipated that an intelligent sampling toolbox will form the core part of the next generation of the measurement modules in surface measuring instruments. Before the advantages of intelligent sampling can be fully exploited two specific issues need to be addressed.

1. Reconstruction

In surface metrology, measurement results are usually presented in the form of a cloud of regularly spaced points. This regular lattice data can be easily manipulated for mathematical computation or transforms, such as convolution or DFT [137]. With the traditional triangulation-based rendering techniques, or other reconstruction techniques such as bilinear interpolation, the results are generally expressed as a continuous surface for visual inspection, for example in OpenGL and MATLAB [120, 148].

Most intelligent sampling methods result in a non-regular lattice of distributed (or scattered) sample points. In this case, advanced reconstruction methods need to be considered, such as tensor product B-spline reconstruction, triangulation, and radial basic function (RBF) reconstruction [179]. In this way, the point cloud can be reconstructed into a continuous surface for visual inspection in a stable manner; regular latticed data can then be extracted from the constructed continuous surface for fast numerical manipulation.

2. New data formats

Current sampling data are usually saved as a coded matrix (for example, the reference data format SDF defined in ISO/FDIS 25178 Part 71 [71]) which corresponds to the height information of regular latticed sample points. This format cannot represent non-regularly spaced latticed data, in which case the whole three-dimensional information of each sampled data point needs to be saved. Intelligent sampling requires a new data format that supports saving of the non-regular latticed data. Also in the “trailer” part of this new data format (see Figure 5.1), the specifications in terms of the reconstruction should be

assigned aiming to reduce the reconstruction uncertainties. Figure 5.1 gives an outline schematic of a new data format.

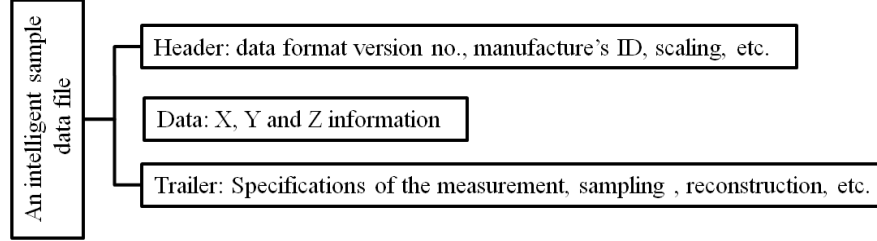


Figure 5.1. Schematic diagram of a new data format for surface measurement.

Relating to the realisation of efficient measurement, some intelligent scanning techniques and instruments have been developed. For example, Wieczorowski developed a spiral scanning-based surface texture measurement instruments [171], which avoids the time-consuming reciprocating movement of a raster scan. Machleidt et al [96] developed a large scale AFM measuring machine based on a nanopositioning and nanomeasuring machine (NPM) stage. Also, the recent success in manufacturing a 128-cantilever array [118] enables fast surface measurement on the nano-scale. With the development of intelligent sampling designs and scanning techniques, efficient measurements are on their way to current instruments. But these advanced devices and techniques will not be covered in this thesis; only the theoretical research relating to sampling is discussed.

In the following context, four types of intelligent sampling will be introduced regarding the principles and possible applications. This chapter can be seen as a systematic review but some new techniques and results are also added. For the reconstruction methods and performance evaluation of the sampling methods, please refer to Chapter 6.

5.2 Jittered uniform sampling

5.2.1 Introduction to jittered uniform sampling

It is well known that a signal with an infinite-frequency spectrum cannot be reconstructed completely by a uniform sampling sequence because of spectral aliasing.

It is possible to reduce the aliasing impact by varying the spacing between samples in a non-uniform way [114]. A variation of uniform sampling has been introduced to convert aliased frequency components into noise (see Figure 3.6), which is called jittered uniform sampling. This sampling technique is a combination of uniform stratifying and random allocation. Let $X_U = \{x_j : j \in J^d\}$ be a uniform sampling set where J^d is a countable index set in d -dimensions, i.e. for $\forall j, j-1 \in J$, $x_j - x_{j-1} = T$ where T is the sampling period $T \in \mathbb{R}^{+d}$. Then let Y be a random jittering disturbance sequence which has

$$Y = \left\{ y_j : y_j \in \left(-\frac{d}{2}, \frac{d}{2}\right), d \leq T, j \in J^d \right\}. \quad (5.1)$$

A jittered uniform sampling set can be generated by

$$X_{\text{Jittered}} = X_U + Y. \quad (5.2)$$

See Figure 5.2 for an example illustration of the comparison of a uniform sampling and jittered uniform sampling pattern, in which case the disturbance amplitude d equals to T .

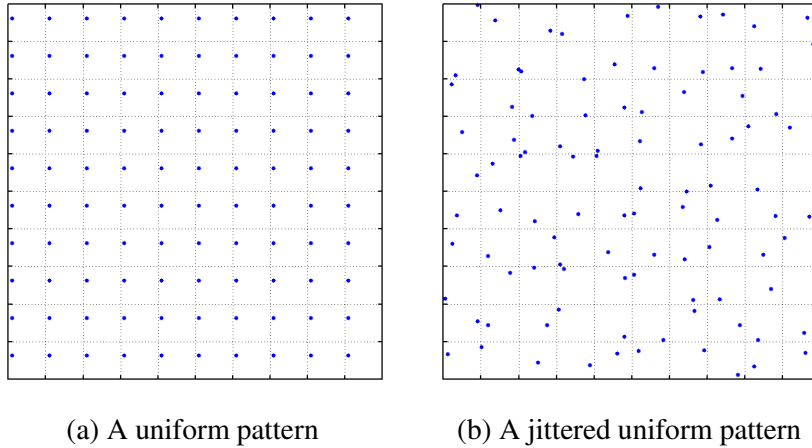


Figure 5.2. Comparison of a uniform sampling and a jittered uniform sampling.

In the frequency domain, the copies of the sampled signal spectrum are randomly shifted as well, so that when reconstruction is performed, the result has a random error

rather than a coherent aliasing. More information about this method can be found in [114].

However, in measurement, the randomisation of the sampling points within each uniformly stratified region may result in a difficulty for physical realisation in instrument design. A possible application is CSIs. Aided by a large size CCD/CMOS detector, a randomly selected pixel pattern can be activated for a measurement which saves the computation time. Jittered sampling works well but has received little attention from metrologists. Kim and Raman [81] first employed this method in flatness measurement with a CMM probing system in 2000. It was found that jittered uniform sampling presented the highest accuracy compared to uniform sampling and low-discrepancy sampling (Hammersley and Halton-Zaremba sequence sampling), when given the same sample size. If a large size CCD/CMOS detector can be employed in surface topography measurement, jittered uniform sampling is a promising solution in terms of efficiency.

Another advantage of this method comes from the complete sampling theory support in shift-invariant spaces (see section 0). For example, Kadec's theory [6] states that if there is a sampling set $X = \{x_k \in \mathbb{R} : |x_k - k| \leq L < 1/4\}$ for all $k \in \mathbb{Z}$, then the set $\{e^{j2\pi x_k \xi}, k \in \mathbb{Z}\}$ is a Riesz basis [41] of $L^2(-1/2, 1/2)$, i.e. for any $f \in L^2 \cap B(-1/2, 1/2)$, the signal in a shift-invariant space can be exactly recovered from the samples $f|_X = \{f(x_k), k \in \mathbb{Z}\}$ if the sample set satisfies $X = \{x_k \in \mathbb{R} : |x_k - k| \leq L < 1/4\}$. Also Liu's theory [92] states that in the Franklin wavelet subspace V_0 , if a sample set satisfies $X = \{x_k : |x_k - k| \leq L < 1/2, k \in \mathbb{Z}\}$, then there exists a set $\{Q_k(x) \in V_0\}$ such that $f(x) = \sum_{k \in \mathbb{Z}} f(x_k) Q_k(x)$, which ensures an exact reconstruction of f from its samples $f|_X$. With theory support, a jittered uniform sampling pattern with proper set d in equation (5.1) can guarantee an exact recovery for a shift-invariant space signal.

5.2.2 Section summary

Jittered uniform sampling has been proved to provide a high accuracy result compared to uniform sampling and low-discrepancy sampling methods for flatness measurement. Also, jittered uniform sampling has a robust support from the non-uniform sampling theory in shift-invariant spaces. It is promising that this technique can be integrated in current measurement instruments, for example a large size CCD/CMOS CSI. Further validation of the efficiency of jittered uniform sampling is given in Chapter 6. However, the capability of jittered uniform sampling to the measurement of surface topography and feature related parameters is still unknown.

5.3 Low-discrepancy sampling

5.3.1 Introduction to low-discrepancy sampling

As stated in Section 1.1, the measurement of structured surfaces usually demands for both a large sampling length (or area) and small sampling spacing (or interval) in a single measurement. Efficient sampling has been recognised as important. A statistics-based solution – low-discrepancy sampling, is a novel sampling technique that optimises the sampling positions to improve statistical stability and efficiency. Low-discrepancy sampling predicates that fewer sampling points can induce a higher reconstruction accuracy.

It is well known that a measurement with N points creates an estimation discrepancy from the true value which cannot be infinitely small. To evaluate the discrepancy of a set of sampling points, a basic idea is to evaluate the volume of a box b which belongs to $B = \{[0, u]^n : u \in [0, 1]^n\}$ by throwing points $X_P = \{x_i \in [0, 1]^n : i \in 1, 2, \dots, N\}$ in a specific form P , such as uniform, into the domain $[0, 1]^n$, and calculate the ratio of the number of points inside b and the total amount, i.e. $\#(X_P \cap b) / N$. It is apparent that $\#(X_P \cap b) / N$ becomes an approximation of the volume of the box b given by the sample points X_P , i.e.

$$E(\#(X_P \cap b) / N) = V(b), \quad (5.3)$$

where $V(b)$ is the volume of region b . An illustration of this approximation idea is shown in Figure 5.3. Thus the discrepancy of the finite sampling X_P to approximate the area of region b can be defined as:

$$D_N(B, X_P) = \sup_{b \in B} \left| \frac{\#(X_P \cap b)}{N} - V(b) \right|. \quad (5.4)$$

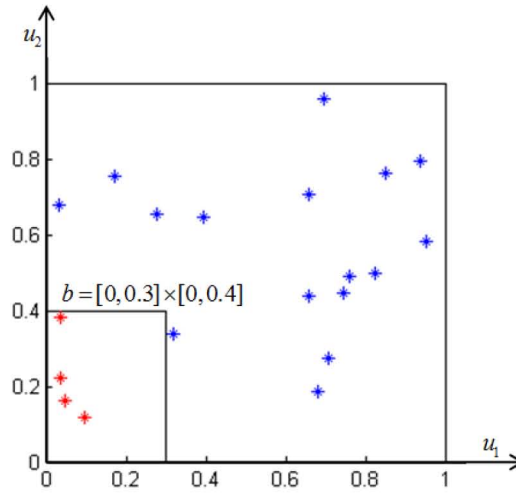


Figure 5.3. Illustration of approximation of the area of the square b .

The distribution pattern of sample points P determines the magnitude of the discrepancy D . It is possible to design an intelligent sampling sequence or pattern to minimize the evaluation discrepancy. For example, let X_P be a uniform sampling set in one-dimension, i.e. $X_P = (i/N, i=1, 2, \dots, N)$, and b be a box $b=[0, 1/N]$ which has the volume $V(b) = 1/N$. Then $D_N = 1/N$ can be obtained because $\#(X_P \cap b) = 0$.

However, if X_P has $X_P = (\frac{i-1/2}{N}, i=1, 2, \dots, N)$, then $D_N = 1/2N$. Many scientists have contributed to this statistical model. For example, It has been pointed out by Roth [124, 172] that the discrepancy of N -point sampling has a minimum bound

$$D_N \geq O((\log N)^{(d-1)/2} / N). \quad (5.5)$$

Considering a one-dimensional case, one of the simplest low-discrepancy sequences is the van der Corput sequence [158], which is given by the radical inverse function $\Phi_b(i)$ in base $b = 2$, i.e.

$$X = \{x_j : x_j = \Phi_2(j) = 0.d_1d_2\dots d_m, j \in J\}, \quad (5.6)$$

where d_i satisfies $\sum_{i=1}^{\infty} d_i b^{i-1} = j, b = 2$ in base 2. For instance, the first ten points in the

sequence are $\left\{\frac{1}{2}, \frac{1}{4}, \frac{3}{4}, \frac{1}{8}, \frac{5}{8}, \frac{3}{8}, \frac{7}{8}, \frac{1}{16}, \frac{15}{16}, \frac{5}{16}\right\}$. The first ten points of the van der Corput

sequence in base 3 are $\left\{\frac{1}{3}, \frac{2}{3}, \frac{1}{9}, \frac{4}{9}, \frac{7}{9}, \frac{2}{9}, \frac{5}{9}, \frac{8}{9}, \frac{1}{27}, \frac{10}{27}\right\}$. The intelligent sequence has the discrepancy

$$D_N(P) = O(\log N / N). \quad (5.7)$$

Based on the van der Corput sequence, two well-known low-discrepancy sequences that are defined in an arbitrary number of dimensions are the Halton [57] and Hammersley [58] sequences. The two patterns are separately defined as follows:

$$X_{\text{Hammersley}} = \{x_j : x_j = [j / N, \Phi_{b_1}(j), \Phi_{b_2}(j), \dots, \Phi_{b_{d-1}}(j)], j \in J\}, \quad (5.8)$$

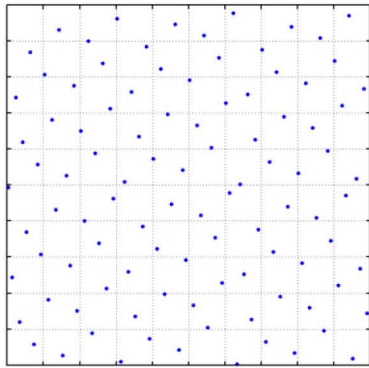
$$X_{\text{Halton}} = \{x_j : x_j = [\Phi_{b_1}(j), \Phi_{b_2}(j), \dots, \Phi_{b_d}(j)], j \in J\}, \quad (5.9)$$

where b_i are the relative primes. Usually b_i can be set as first $d-1$ or d primes in \mathbb{Z}^+ , such as 2, 3, 5, 7 and so on. If $d = 2$, the first 100 points of the Hammersley and Halton sequences are shown in Figure 5.4.

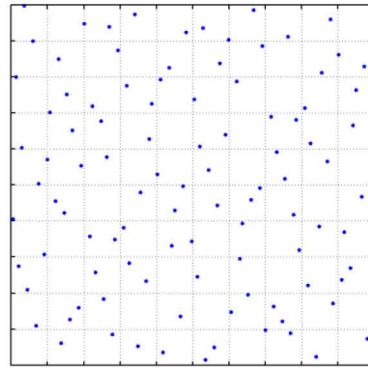
In addition to the two classical sequences, there are several other variations such as the Sobol sequence, Hammersley-Zaremba, Halton-Zaremba and [t,s] sequences. A computational investigation of the diverse techniques is given in [83].

In surface metrology, low-discrepancy sampling was first introduced in [172] where the Hammersley sequence and Halton-Zaremba sequence are used to calculate the surface roughness and flatness of planar surfaces. Later in [88], the root mean square

error (RMSE) of the average deviation was estimated for different simulated surfaces. All these results show that a low-discrepancy sampling sequence is more effective than random or uniform sampling, in terms of the improvement of measurement accuracy or saving of sample size. In 2000, Kim [81] analysed the accuracy and efficiency of low-discrepancy sampling in flatness measurement by CMM experiments. For practical measurement, it can be found that the improvement in accuracy is not so clear when compared with uniform sampling. This point is explicitly described in the following section.



(c) A Hammersley pattern



(d) A Halton pattern

Figure 5.4. The 100 points sampling pattern of Hammersley and Halton sequences.

Low-discrepancy sampling patterns are expected to minimize the evaluation error of the population means or totals, for example the arithmetic mean of the surface height S_a , as S_a is a quadrature of absolute positive surface height function [68]. Though earlier experiments have shown flatness measurement can be benefited from the intelligent sampling methods [81, 88, 172], no experiment validates the performance of these methods in surface topography measurement. Also it is questionable whether low-discrepancy sampling methods can be applied to evaluation of feature related characteristics or other non-quadrature based parameter evaluations, like S_z (maximum height), local feature dimensions [159], feature parameters and the ISO-defined functional parameters such as the bearing curve related parameters [68].

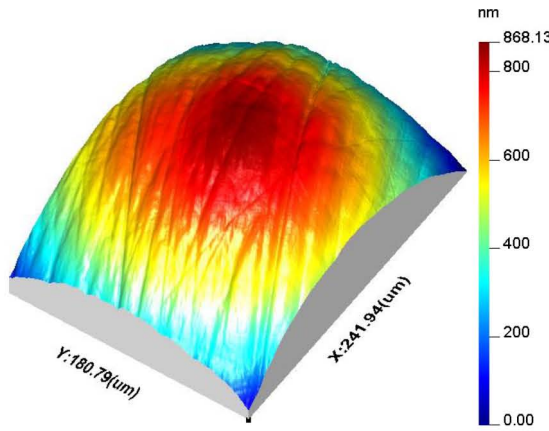
Similar to jittered uniform sampling, low-discrepancy sampling methods can provide an exact recovery of the original surfaces on shift-invariant spaces so long as the

sample density is high enough, i.e. two samples required in minimum for any unit length (e.g. between neighbouring integer knots) in a shift-invariant space.

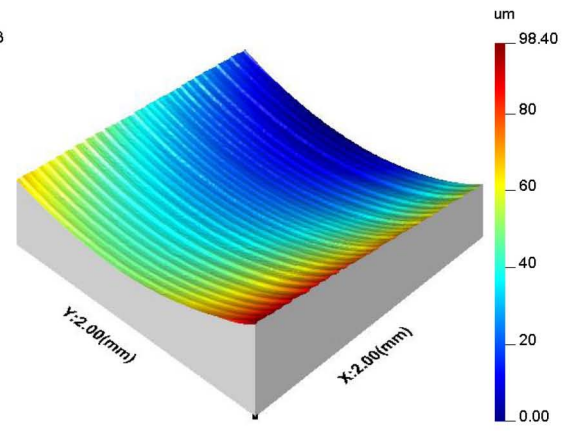
There is another issue that may need a serious concern but usually neglected in the past. In the former researchers' demonstrations [57], the efficiency of using an optimised sequence can be proved (e.g. a two-dimensional pattern) only when estimating the volume of the same dimension function (e.g. a two-dimensional curve) [57]. Earlier applications [81, 88, 172] demonstrate the efficiency of two-dimensional optimised patterns for the evaluation of the volume of higher dimension functions (e.g. a three-dimensional surface), the rationality is mysterious and lack proof. The following case studies show that on the measurement of surface topography attributes, the low-discrepancy patterns do not have clear priority in efficiency.

5.3.2 Case studies in surface measurements

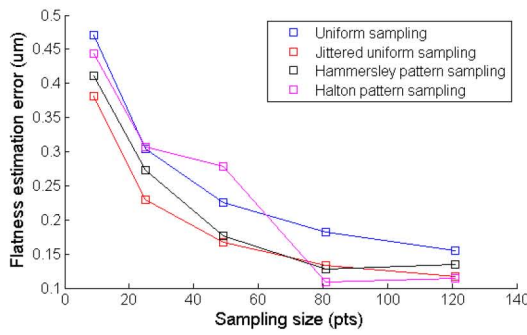
Earlier simulations and experiments have show advantages of low-discrepancy sampling patterns in the measurement of flatness [81, 88, 172]. This merit was once again confirmed is the following case, where fifty times of simulation sampling are carried out with a random start point to estimate the flatness of form (large lateral scale components) dominated surfaces. Figure 5.9 shows the discrepancy rate of the estimated flatness from the 'standard' high sample density result for a sphere worn artificial hip and a cylinder inner surface. These results (in Figure 5.9c and d) indicate that for the form dominated surface, low-discrepancy patterns show prominent advantages on estimation of their flatness.



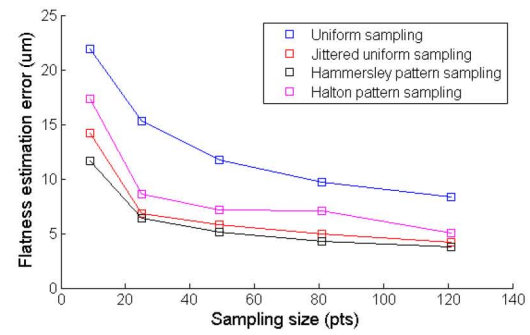
(a) Sphere shape worn artificial hip.



(b) Turned cylinder inner surface.



(c) Discrepancy rate of flatness for sphere surface.



(d) Discrepancy rate of flatness for cylinder surface.

Figure 5.5. Validation of the efficiency of low-discrepancy sampling patterns on form-error estimation (flatness).

In terms of the measurement of surface topography, sampling using Hammersley patterns, Halton patterns and uniform methods for four typical random and structured surfaces^{xi} (see Figure 5.6 to Figure 5.9) has been carried out. To generate stable statistics, for each tested surface, simulations were executed one hundred times by randomly allocating the starting points of each sampling pattern (uniform, Hammersley and Halton sequence). After sampling, triangulation reconstruction (see Chapter 6 for the reconstruction algorithms) by linear interpolation within each

^{xi} The sampling test is numerically simulated by given an areal surface measurement data. For example, given a real surface, a densely sampled measurement result is obtained as the standard data. Sampling is simulated based on the standard data and reconstruction is followed.

triangle patch was implemented. Comparing with the original sampling data, the surface topography parameters Sq , Sz (here Sz is the flatness calculated by ordinary least squares method because the original data have been levelled) and root mean square deviations (height residuals) are calculated. Though Sq and Sz are known for inefficiency for the characterisation of structured surfaces [75, 76], they provide a view to the performance of different sampling methods. The results are presented in Figure 5.6 to Figure 5.9.

The results shown for the measurement of surface topography are not as the expectation described by Woo et al [172]. In these results, the Hammersley and Halton patterns do not give a significant improvement compared to uniform sampling. In the root mean square deviation graphs of the four tests shown in from Figure 5.6 to Figure 5.9, uniform sampling seems to exhibit better reconstruction accuracy. However, an interesting finding is that in all these tests, low-discrepancy sampling patterns exhibit better repeatability compared to the uniform method. Sampling stability is important in engineering measurement. If a series of methods have the same accuracy, the one with high stability or repeatability is preferred.

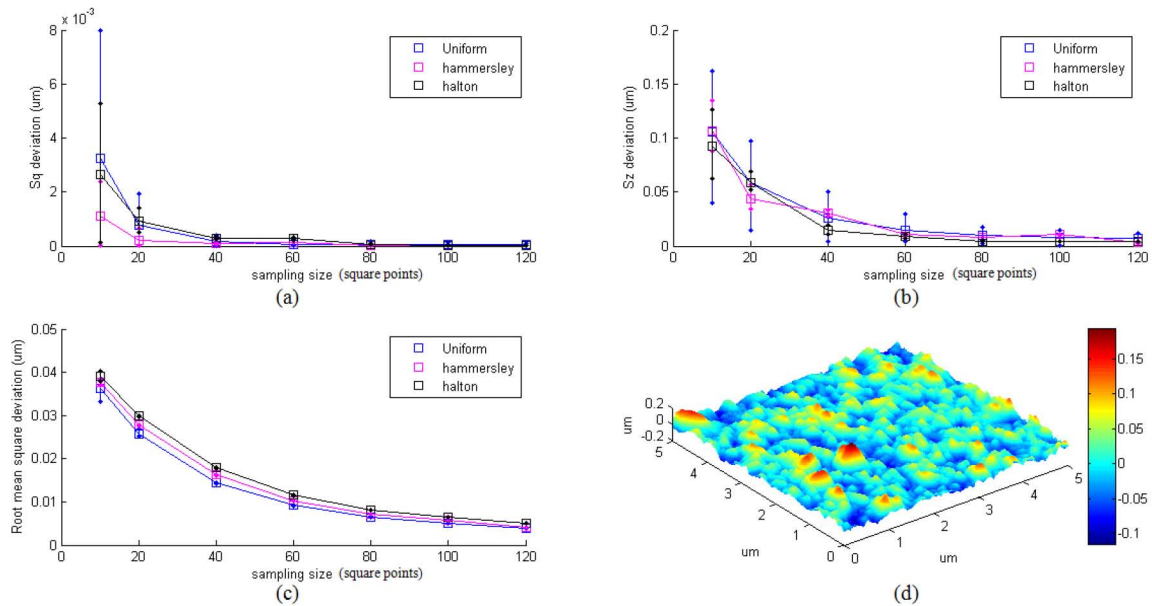


Figure 5.6. Comparison of uniform, Hammersley and Halton sampling for the measurement of an normal EDM surface, by estimating (a) Sq , (b) Sz and (c) root mean square deviation from

(d) the original data (512×512 points).

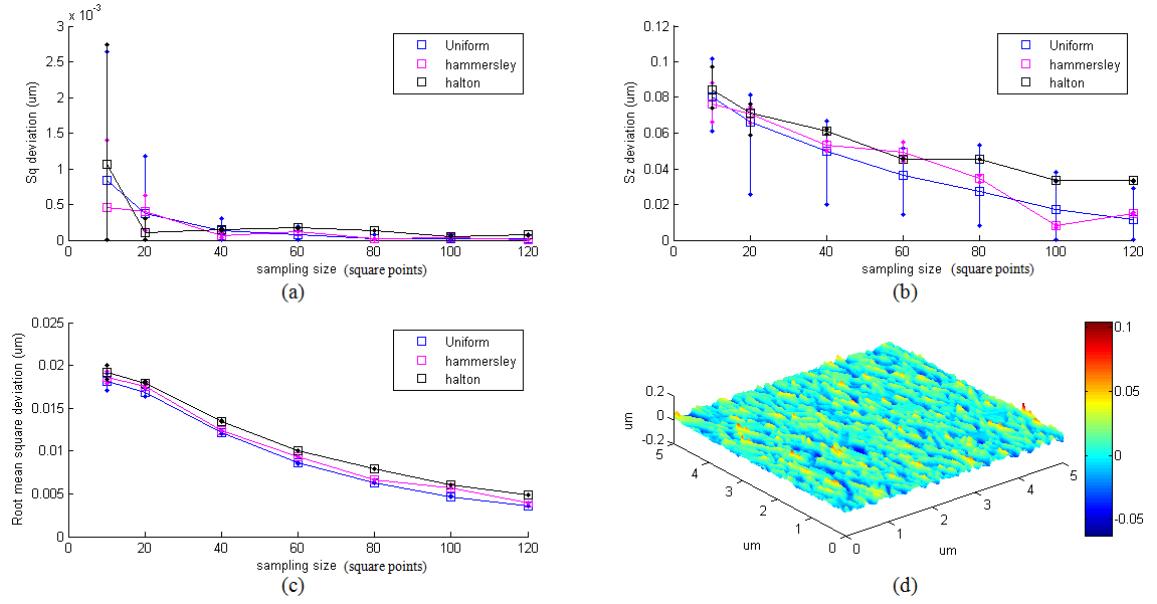


Figure 5.7. Comparison of uniform, Hammersley and Halton sampling for the measurement of a directional EDM surface, by estimating (a) Sq , (b) Sz and (c) root mean square deviation from (d) the original random data (512×512 points).

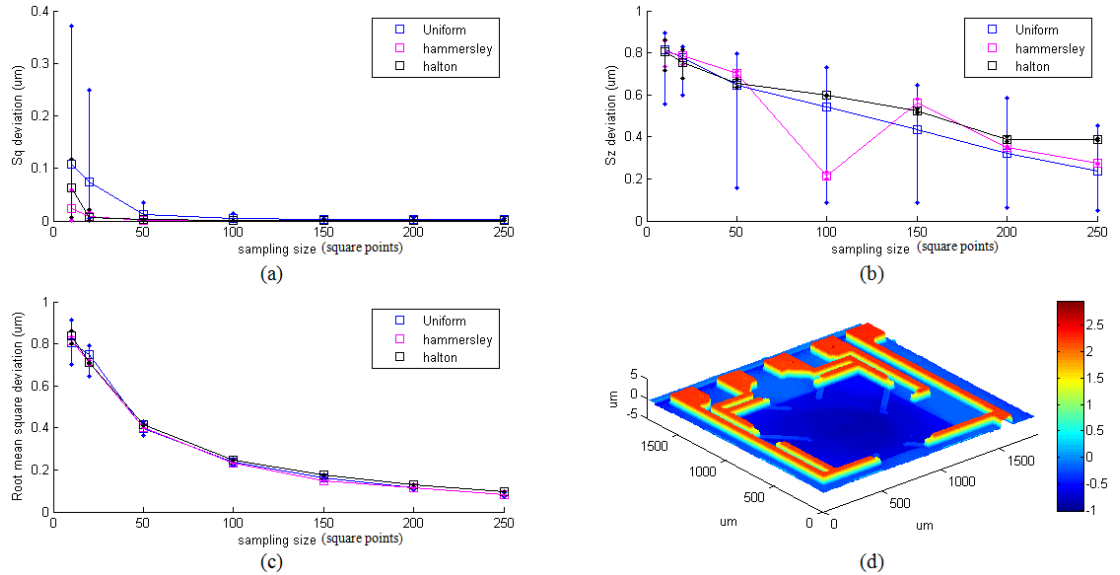


Figure 5.8. Comparison of uniform, Hammersley and Halton sampling for the measurement of a MEMS device, by estimating (a) Sq , (b) Sz and (c) root mean square deviation from (d) the

original structured data (1024×1024 points).

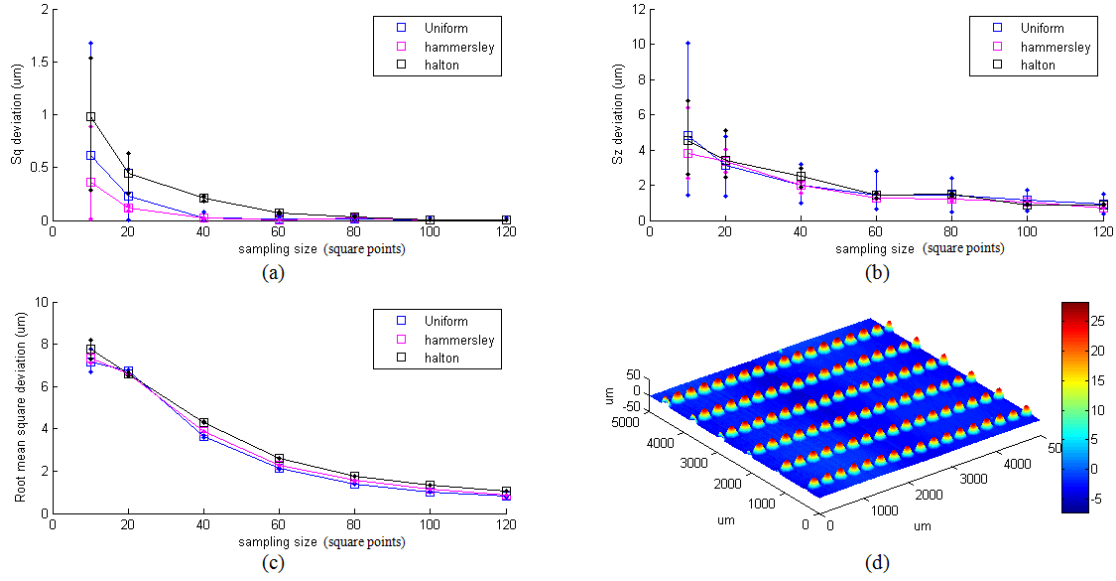


Figure 5.9. Comparison of uniform, Hammersley and Halton sampling for the measurement of a micro-lens array, by estimating (a) S_q , (b) S_z and (c) root mean square deviation from (d) the original structured data (800×800 points).

Though the former researchers predicted potential efficiency in surface topography measurement and evidence has been given regarding to flatness measurement, the test results above indicates the infeasibility of low-discrepancy patterns in surface topography measurement. The reason for this is not clear and understanding of Roth and Hammersley's demonstration process [57] is necessary which is currently excluded from this thesis.

5.3.3 Section summary

The principle of low-discrepancy sampling has been demonstrated to be efficient based on statistics. These non-uniform sampling methods can provide an exact recovery of the original surface signals in shift-invariant spaces if the sample density is high enough, i.e. two samples required in minimum for any unit length (e.g. between neighbouring integer knots) in a shift-invariant space.

Present evidence in this study does not show a stable intelligence over uniform sampling in terms of surface topography measurement, for example S_z or S_a . However, low discrepancy sampling patterns present a high stability for geometric measurement compared to uniform methods. Though former researchers have found prominent advantages of using low-discrepancy patterns in flatness measurement, the evidence shown in this thesis do not suggest low-discrepancy pattern sampling as an efficient sampling method regarding to the measurement of surface topography.

5.4 Model-based sampling

5.4.1 Introduction to model-based sampling in surface metrology

Uniform sampling, low-discrepancy sampling and related variations are sampling methods which are matched with a fixed sampling pattern. This means that for any signal, the sampling positions are determined identically if the sampling size has been given. These sampling methods do not consider the distribution of signal properties within a population. If a surface model is known in advance, optimised sample positions can be adaptively designed to enhance the measurement efficiency and accuracy. Another solution, which has received considerable attention and is more efficient compared to the methods described earlier, is regarded as model-based sampling.

In statistics, a model relating to the distribution of a population property is normally employed, which ensures the sampling accuracy. A model relating to the distribution of the properties of interest is usually used in ratio and regression estimation [151]. For example, by assuming the property values of each sampling unit are independent and identically distributed, a simple random sampling provides an unbiased estimation of the population. In surface measurement, surface models have been used by many researchers to improve sampling efficiency. Model-based sampling designs sample positions based on a nominal signal model (for example a CAD surface model, or a preliminary measurement with a simple sample design) by analysing its local surface properties such as mean curvature. Therefore, regions which contain complex features are adaptively allocated with dense samples while regions with plain features are allocated with sparse samples.

Most of the earlier work on intelligent sampling for surface measurement is based on given models [27, 44, 45, 111, 130]. These sampling methods are sometimes regarded as a type of adaptive sampling because their samples are adapted to a given surface model or a preliminary measurement. These methods have been shown to be advantageous in terms of saving sample size or improving sampling accuracy for most general cases. However, CAD model-based solutions do not consider unexpected defects that are generally present in practical manufactured products and the pre-positioning error in clamping a surface product may induce a significant bias in the sampling positions. These deficiencies restrict the popularity of the method for practical measurement.

5.4.2 Review of model-based methods in surface measurement

Many researchers have contributed to model-based sampling designs and many sampling pattern generation algorithms have been developed. Cho and Kim [27] developed an adaptive sampling method based on mean curvature analysis and various probe path generation algorithms were tested. Killmaier et al [79] presented a solution for measurement of a workpiece which detects the standard geometric features such as straight lines, circles, columns, cones or peaks by using a genetic algorithm, and then the distribution of sampling points are allocated by establishing a knowledge-based system. Elkott introduced several CAD-based sampling methods for freeform surface metrology; this included four kinds of automatic sampling [44], curvature change-based sampling and iso-parametric sampling [45]. Shih et al [130] developed three kinds of adaptive sampling methods for coordinate metrology, including direct sampling, indirect sampling and local adjustment sampling. Discrete wavelet decomposition-based adaptive sampling techniques have also been proposed [111]. More published work is listed in Table 5.1 in chronological order.

Year	Authors	Contributions	Characteristics	Applications
1991	Terzopoulos et al [147]	Adaptive mesh sampling based on a ‘node-spring system’ on an initial regular mesh where regions with high gradient are sampled densely	Iterative, bilinear interpolation	Computer graphics
1995	Tanaka [144]	Iteratively triangularises surface hierarchically into triangle patches according to local surface properties such as orientation, curvature and colour (or height)	Iterative, triangularisation	Computer graphics
1995	Li 1995 [89]	A simple iterative mesh generation based on surface curvedness where regions with high curvedness are sampled densely	Iterative, curvedness, bilinear interpolation	Computer graphics, CAD
1995	Cho et al [27]	Ranks a series of sub-regions by mean curvatures, and then allocates new sampling points in selected regions iteratively.	Iterative, surface curvature ranking	CMM measurement
2002	Elkott et al [44]	Proposes four adaptive sampling methods for NURBS models based on patch size or Gaussian curvedness, etc.	NURBS models, patch properties ranking, non-iterative	CMM measurement
2003	Killmaier et al [79]	Detects standard geometrical primitives using genetic algorithm, and aims to give an optimal number and distribution of sampling points	Genetic algorithm, knowledge-based system	CMM measurement
2005	Elkott et al [45]	Proposes three adaptive sampling methods based on iso-parametric lines of NURBS models: automatic sampling, curvature-change based sampling, and iso-planar sampling	NURBS models, non-iterative and iterative	CMM measurement
2006	Petkovski [111]	A discrete wavelet transform (DWT)-based adaptive sampling algorithm which is essentially equivalent to curvature analysis.	DWT analysis, patch properties ranking, non-iterative	Signal processing
2008	Shih et al [130]	Proposes three adaptive sampling methods: direct sampling (quadtree hierarchical division), indirect (two-dimensional binary tree hierarchical division) sampling and local adjustment.	iterative, root mean square error evaluation, local adjustment	CMM measurement, CAD

Table 5.1. Comparison of existing three-dimensional non-uniform adaptive sampling techniques.

Some conclusions can be summarised based on past developments.

1. Most model-based sampling methods adopt an iterative algorithm which indicates that a final sampling result is sensitive to the initial conditions of the algorithm, for example the initial sample position [42]. This method can adapt the sampling design to a pre-defined accuracy but is time-consuming.
2. The concept of hierarchical stratifying of a surface population prevails in much of the work [27, 111, 144]. With a hierarchical stratification, a surface can be subsequently divided into strata which have different surface complexities, for example local mean curvature or approximation deviation. For high strata, dense sampling points are allocated; while for low strata, they are sparse. An advantage of hierarchical stratification is that the sampling points are locally regular and, therefore, it is feasible for them to be transferred to surface measuring instruments, such as interferometers and general stylus instruments.
3. Model-based sampling methods have difficulties of practical measurement due to their lack of consideration of irregular surface topography or defects of a practical workpiece. It is difficult to control positioning error when matching the sample design to a surface product.
4. For many model-based sampling methods, a rough preliminary measurement can be used as a substitute of the surface model. In this way, the model-based method can be used in most practical measurements for which a CAD model of a surface is unavailable.
5. If a preliminary measurement is given with a dense sample setting, model-based sampling methods provide an adaptive compression of the samples at a specific accuracy. Such compressions are useful in data storage.

Overall, model-based methods can be of potential use in surface measurement. If the CAD model is substituted with a preliminary measurement, an intelligent efficient measurement device can be generated. A large scan range (25 mm × 25 mm) AFM has been developed recently by Machleidt et al [96] which stitches a series a camera

pictures into a large initial surface model before regional AFM measurement starts. Through pattern analysis, the regions of interest are found and then measured.

As a representative, two two-dimensional methods and two one-dimensional methods are given in the following.

5.4.3 *Triangle-patch and rectangle-patch adaptive subdivision sampling*

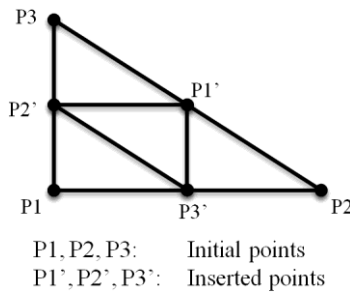
5.4.3.1 The sampling algorithms

Triangle patch and rectangle patch adaptive subdivision-based sampling are two CAD model-based methods. They require a CAD model or a preliminary measurement (with a simple sample design, for example uniform sampling) for determination of the adaptive samples. The two methods have been introduced as “direct sampling” [130]; hereby a brief introduction is given and a minor modification to the error evaluation criteria is made. The algorithms are as follows.

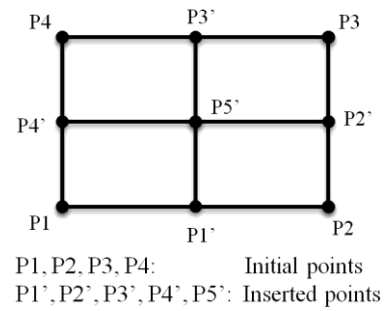
1. Triangle patch adaptive subdivision sampling.
 - 1) Select a rectangle region on a surface as the sampling object.
 - 2) Select four initial points on the extreme corners of the rectangle region and group the four corner points into two triangles.
 - 3) Subdivide each triangle into four triangles by inserting three points on the centre of the edges of the triangle, as in Figure 5.10a.
 - 4) Evaluate the reconstruction error^{xii} of each triangle.
 - 5) If the error is greater than a preset threshold, then repeat steps 3 and 4. Otherwise, stop.
2. Rectangle patch adaptive subdivision sampling.

^{xii} The reconstruction error in step (4) of the two methods is the maximum deviation between the original surface patch and the reconstructed surface patch using linear interpolation (for triangle surface patch) or bilinear interpolation (for rectangle surface patch).

- 1) Select a rectangle region on a surface as the sampling object.
- 2) Select four initial points on the extreme corners of rectangle region.
- 3) Subdivide the projected area into four rectangles by inserting five points as shown in Figure 5.10b.
- 4) Evaluate the reconstruction error^{xiii} of each rectangle.
- 5) If the error is greater than a preset threshold, then repeat steps 3 and 4. Otherwise, stop.



(a) Triangle patch subdivision



(b) Rectangle patch subdivision

Figure 5.10. Subdivision of triangle patch and rectangle patch.

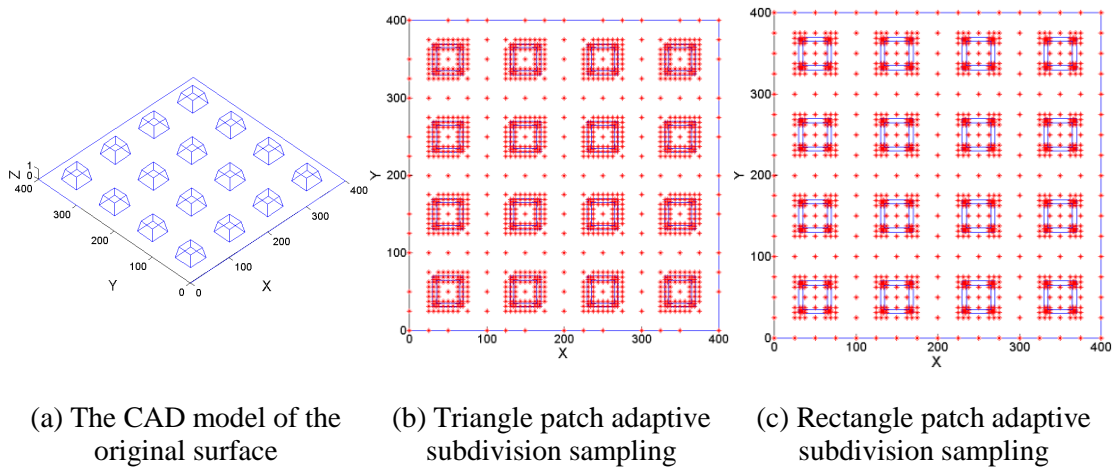


Figure 5.11. Adaptive sampling patterns produced by the triangle patch adaptive sampling (approximately 1500 sample points).

Representative sample patterns generated by the two methods are illustrated in Figure 5.11 in which the ideal surface tested in Figure 5.11a is sampled respectively using each method above with a sample size of approximately 1500 points. It is found that triangle patch and rectangle patch adaptive division samplings generate regular designed sample patterns on the edge features. Specifically, the former has dense samples regularly on the feature edges; while the latter yields more dense samples at the feature lateral corners in this tessellation surface case.

5.4.3.2 The iterative error evaluation criteria

A critical issue relating to the accuracies of these two methods comes from the iterative reconstruction error evaluation in Step (4) above. Using different error evaluation approaches, the resulting sampling designs vary a great deal. Shih proposed a single point error evaluation approach [130] when describing these algorithms. However, it has been found that the single point error evaluation approach may not be stable and accurate. Two other error evaluation approaches: multiple random point evaluation and extreme error evaluation are tested with comparison of the single point error evaluation, in terms of the accuracy of sample designs and computation cost. Specifically, the three error evaluation criteria are described as follows.

Single point estimation: For a rectangular or triangular patch with the corner points projected onto the object surface P1, P2, P3 and P4 (for a triangular patch with P1, P2 and P3, P4 can be set as the gravity centre), the equation of the plane passing through the three points P1, P2, and P3 can be derived. The estimation point, P4', can be generated by intersection of the projection line passing through P4 and the derived plane (see Figure 5.12). The height difference between the estimated point P4' and the surface point P4 can thus be obtained [130].

Multiple random point estimation: This method is an improvement of the single point estimation approach. A series of extra referencing points [P5, P6, ... , Pn-4] of the original surface, which are within the tested triangle or rectangle patch, are randomly selected (or based on the low-discrepancy sequences, $n = 10$ in the next test) [83, 172]. By fitting a plane based on three of the patch corner points, the

corresponding projection points $[P_4', P_5', \dots, P_{n-4}']$ can thus be generated. Then the maximum height difference between the fitting points $[P_4', P_5', \dots, P_{n-4}']$ and the corresponding surface points $[P_4, P_5, \dots, P_{n-4}]$ can be obtained.

Extreme error estimation: The whole region of points within the surface patch of interest is evaluated. By constructing a fitting plane from three of the corner points $[P_1, P_2, P_3]$, the error map of the whole region can thus be computed. The extreme error value is obtained for error estimation. This approach considers the height error of all the points within an evaluation patch, thus can be seen as the most rigorous criterion but may be time consuming.

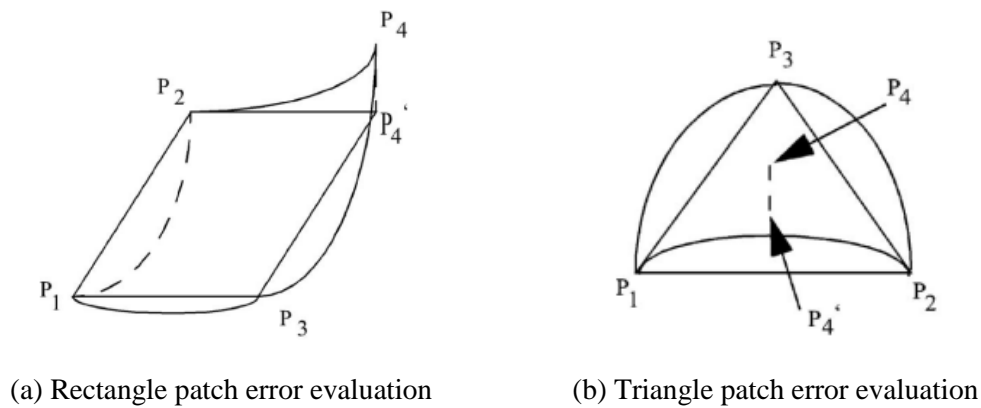


Figure 5.12. Illustration of the error evaluation by single point estimation [130].

Figure 5.13 shows a multi-patterned structured surface for the sampling test. Figure 5.14 shows the resulting sampling patterns if the detecting threshold is set as 5 % of the extreme surface height S_z . These results indicate that single point estimation is efficient in terms of computation but induces the worst sampling design. The multiple random point estimation has a similar performance compared to the extreme error estimation. The rectangle patch method produces more sample points compared to the triangle-patch method. Considering that single point estimation is not stable, and multiple random point estimation and extreme error estimation have little difference, extreme error estimation is preferred in the later tests. If not mentioned otherwise, extreme error estimation is the default error estimation method used in this thesis.

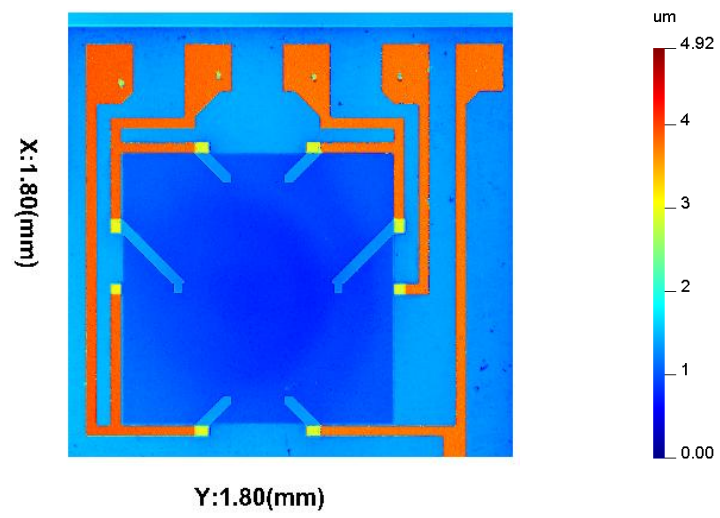


Figure 5.13. A multi-patterned structured surface for sampling test.

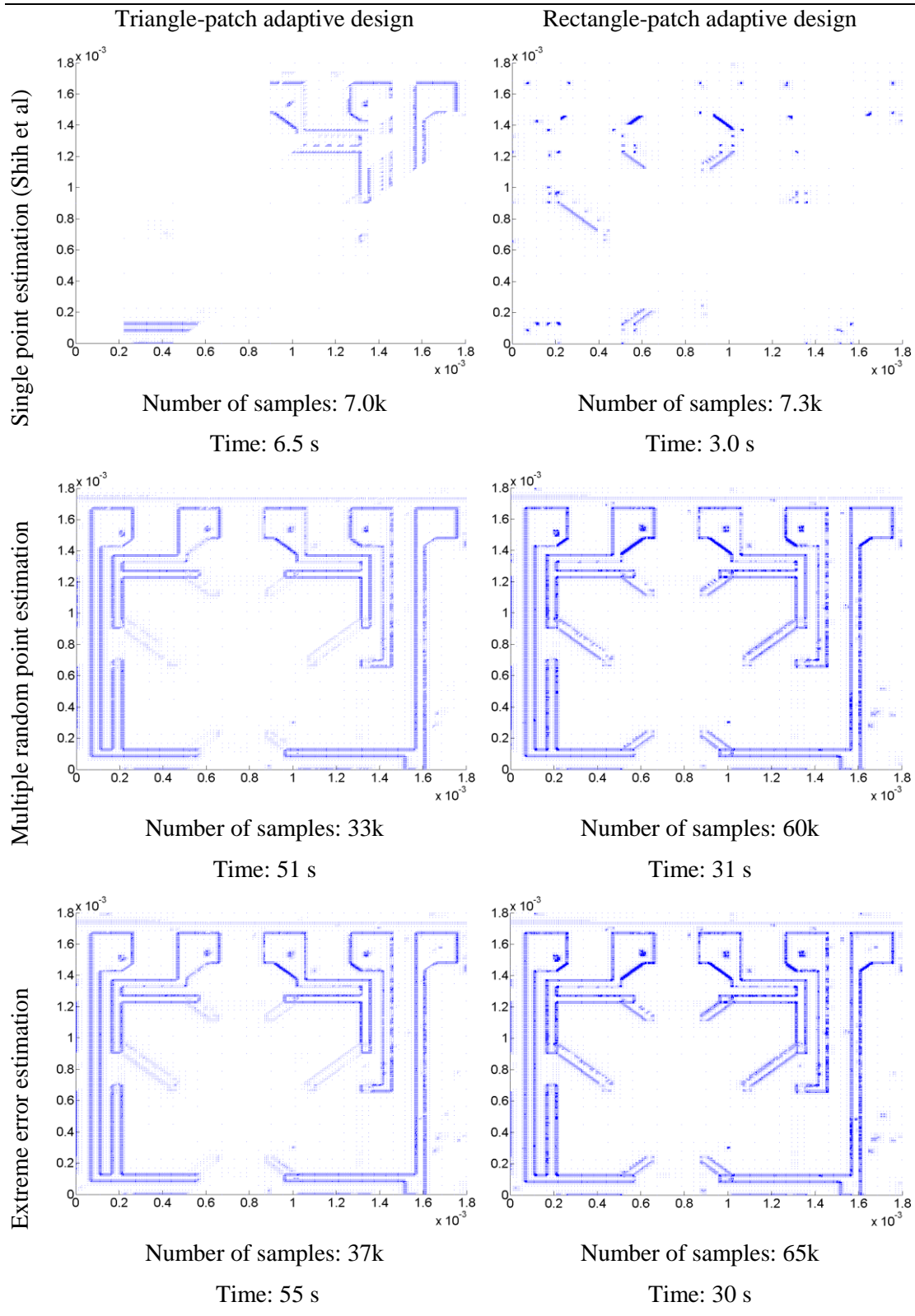


Figure 5.14. Comparison of adaptive sampling design of triangle patch algorithm and rectangle patch algorithm with different error estimation methods (threshold = 5 %).

5.4.4 *Profile direct sampling*

5.4.4.1 The sampling algorithm

Many model-based sampling methods are developed based on profile models, i.e. one-dimensional signal models. With proper extension, these methods can be applied to two-dimensional surface measurement (see an example in Section 5.5.2). Here, two typical cases are introduced in Section 5.4.4 and Section 5.4.5. They are: profile direct sampling and profile discrete wavelet transform (DWT)-based sampling.

Shih et al [130] used an efficient one-dimensional adaptive sampling design algorithm, which is referred to as profile direct sampling here. The profile direct sampling method gives a sample design based on a profile model.

1. For a given profile, divide the curve at inflection points, if any, into several segments that are solely concave or convex.
2. For each segment, evaluate the approximation error of the interval containing the two endpoints on the profile curve.
3. If the error is greater than a threshold that is a fraction of the initial error from step 2, an extra sampling point is inserted on the profile curve at the midpoint of the interval; Otherwise, stop;
4. For each subinterval formed by insertion of a new point, repeat steps 3 and 4 until the approximation error of each interval is smaller than a threshold value.

Tests were carried out by applying the algorithm on several typical simulation signals, (see Figure 5.15). It is shown that adaptive sampling allocates dense sampling points at key locations which have high curvatures. After reconstruction with linear interpolation, the root mean square error (RMSE) of the deviation from the original profile is computed using the Newton-Cotes formula in rectangle rule ($N = 400$) (Table 5.2). It can be seen that, except for the sinusoidal wave, the profile direct

sampling presents significantly lower RMS errors. In particular for the triangle wave signal, the construction error is reduced by an order of magnitude.

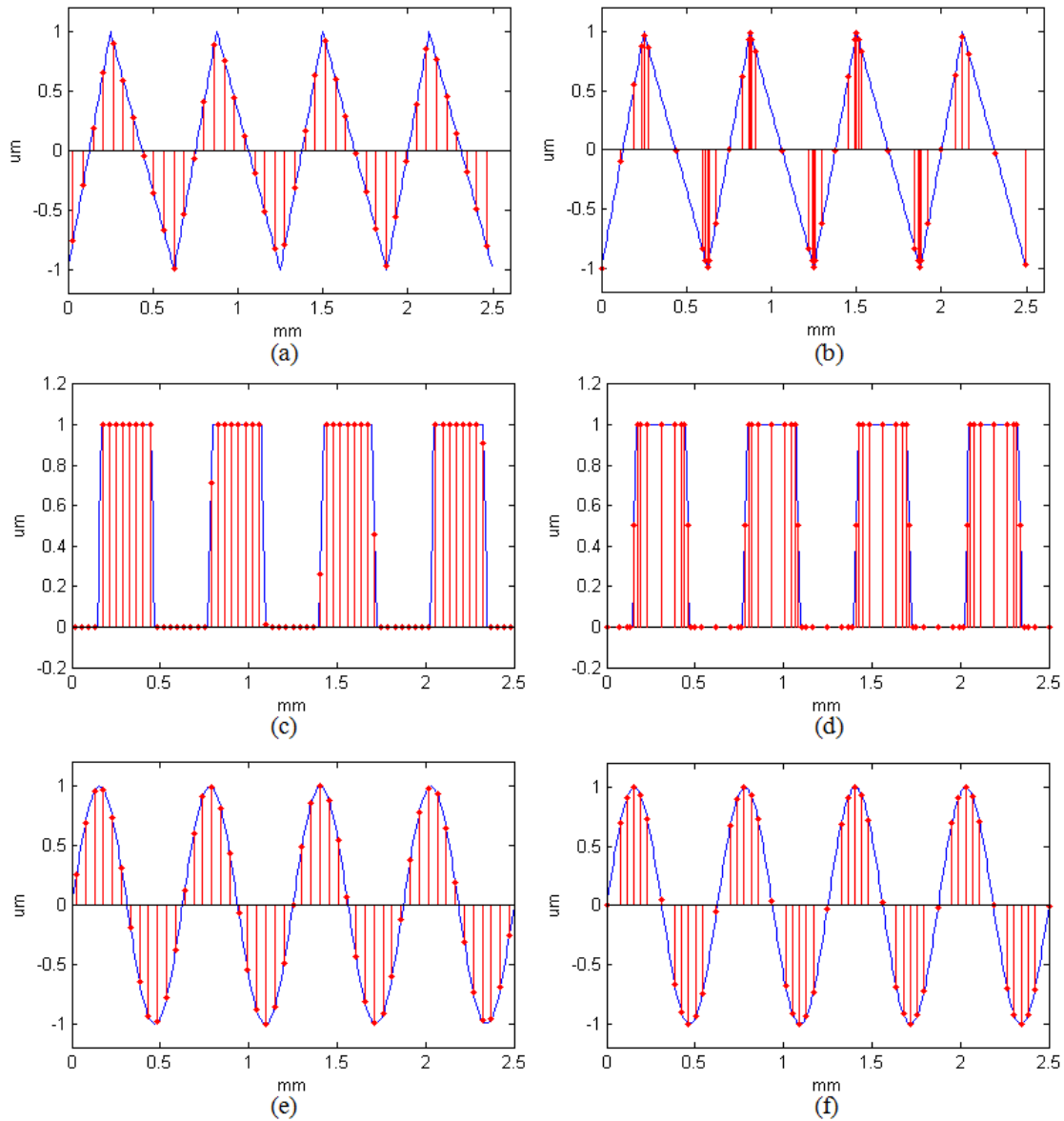


Figure 5.15. Comparison of profile direct sampling and uniform sampling. (a) Forty-two points uniform sampling and (b) profile direct sampling for triangle-wave signal; (c) sixty-five points uniform sampling and (d) profile direct sampling for square wave signal; (e) forty-nine points uniform sampling and (f) profile direct sampling for sinusoidal signal.

Signal type	Triangle wave (42 points)	Square wave (65 points)	Sinusoidal signal (49 points)
RMSE of uniform sampling	$3.6 \times 10^{-3} \mu\text{m}^2$	$9.5 \times 10^{-3} \mu\text{m}^2$	$2.1 \times 10^{-3} \mu\text{m}^2$
RMSE of adaptive sampling	$3.2 \times 10^{-4} \mu\text{m}^2$	$5.2 \times 10^{-3} \mu\text{m}^2$	$2.2 \times 10^{-3} \mu\text{m}^2$

Table 5.2. The RMS error of uniform sampling and profile direct sampling for the typical periodic signals in Figure 5.15.

5.4.4.2 Case studies in surface measurements

Model-based sampling technique can be used in practice if the model is given by a preliminary measurement. A performance test of this direct sampling is presented as follows compared to uniform sampling in terms of the sampling efficiency, accuracy and stability. Four typical structured surfaces containing bumps, triangle waves, saw-tooth and undulation curves are measured using a stylus instrument using $0.25 \mu\text{m}$ as the sampling spacing. Considering repositioning uncertainty, a random starting point for each sampling simulation is set. Then, the target data are sampled by numerical simulation using differing sample settings. After one hundred simulations of each test, the reconstruction error and its variations are computed. The distribution of the sampling points is shown in Figure 5.16, and the reconstruction accuracy and repeatability is presented in Figure 5.17. The results in Figure 5.17 indicate that profile direct sampling has lower reconstruction errors and uncertainties compared to uniform sampling with the same size. The RMS error of profile direct sampling is usually half of the error of uniform sampling.

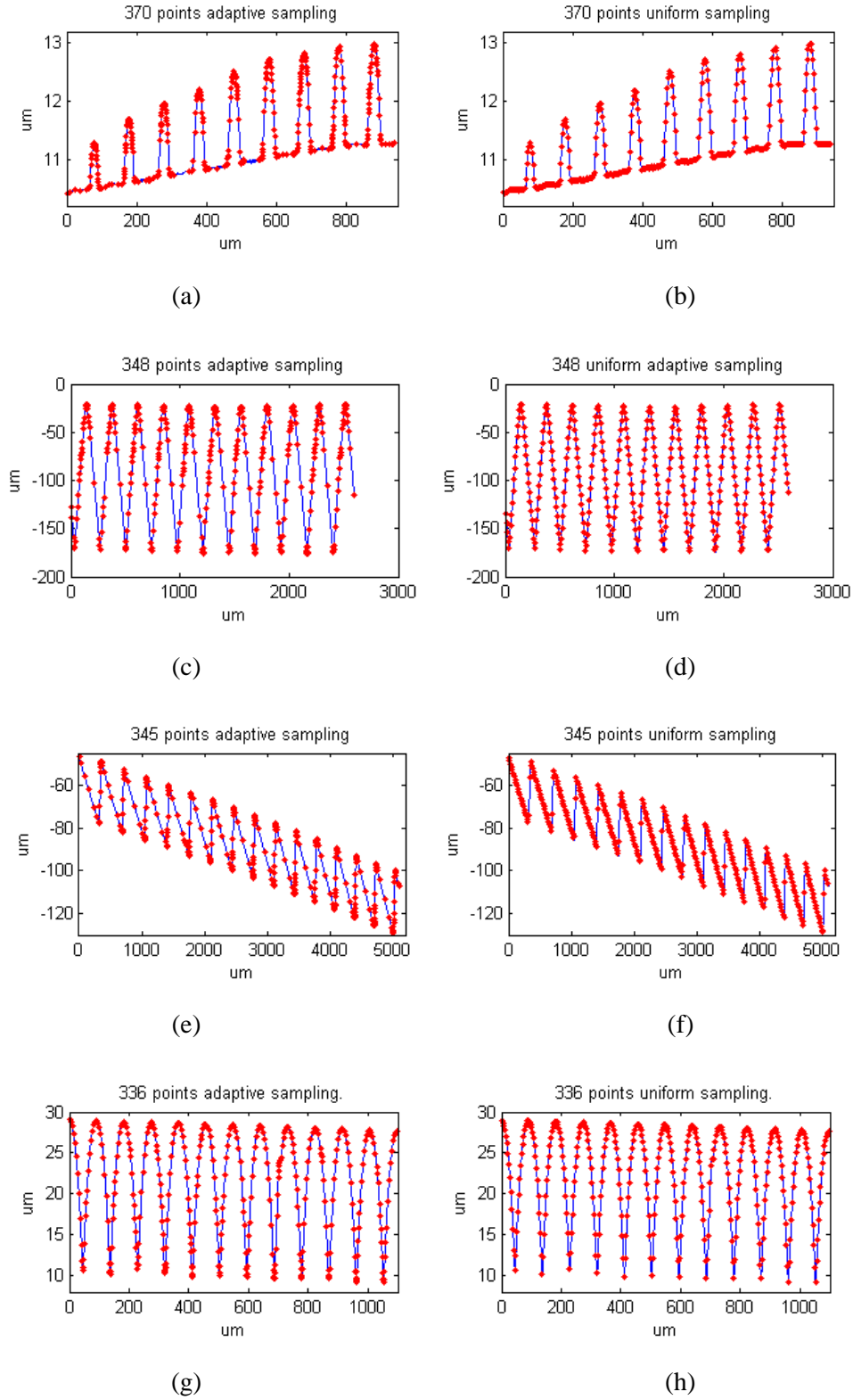


Figure 5.16. Comparison of adaptive sampling and uniform sampling for (a, b) bumps, (c, d) triangle wave, (e, f) saw-tooth and (g, h) undulation curve.

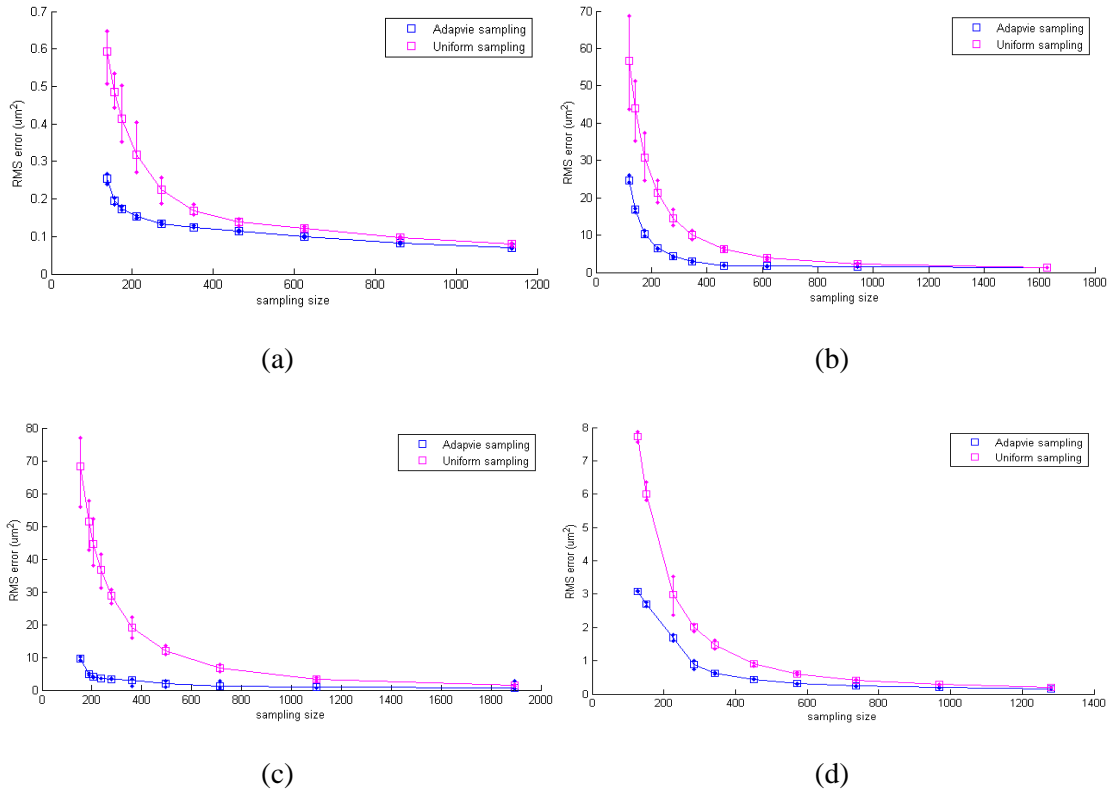


Figure 5.17. RMS reconstruction error and variations of adaptive sampling (blue) and uniform sampling (mauve) using different sampling sizes for practical samples (a) bumps (b) triangle wave (c) saw-tooth wave and (d) undulation wave.

5.4.5 Profile DWT-based sampling

5.4.5.1 The algorithm

Another profile model-based sampling method has been developed by Petkovski et al [111]. This method adopts a DWT to obtain the curvature information of a signal. Then a hierarchical adaptive sampling design is generated by allocating different sample densities to different regions with different curvatures.

Details generated through a two-stage DWT decomposition used as the reference for adaptive sampling setting. As shown in Figure 5.18, the second stage details d_{d2k} are obtained for use as the reference. If the Haar wavelet is employed, the absolute value of d_{d2k} presents the change of the original profile, which has a direct relationship with

the profile curvedness (see Figure 5.19). For example, If the original profile has a constant change (zero curvature), its corresponding second DWT details d_{d2k} have the zero values. If the original profile has a sudden change (large curvature), its corresponding second DWT details d_{d2k} has a large value. Figure 5.19 shows an example of second DWT detail coefficients and its original profile.

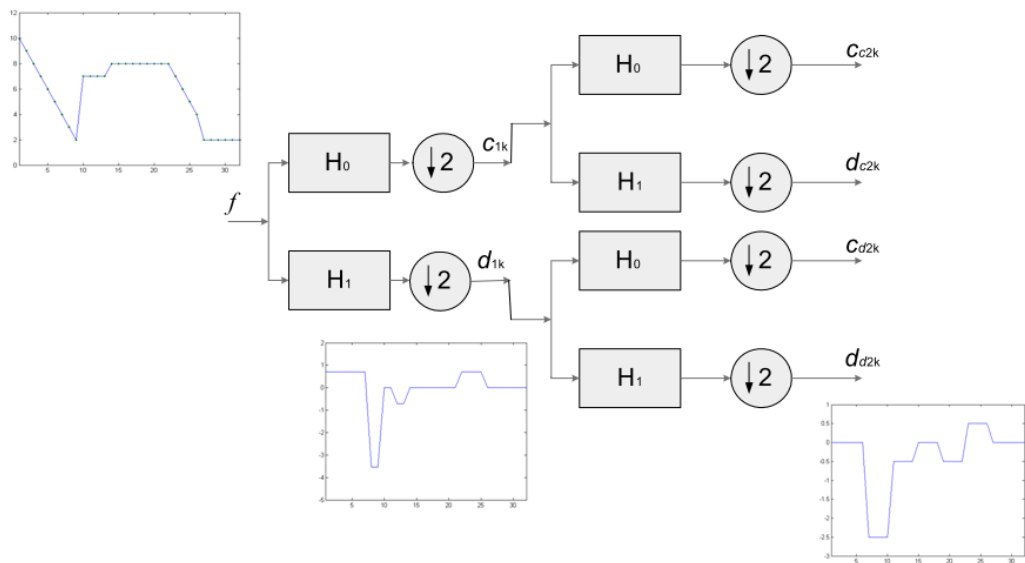
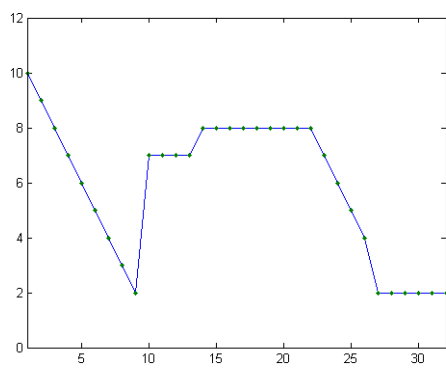
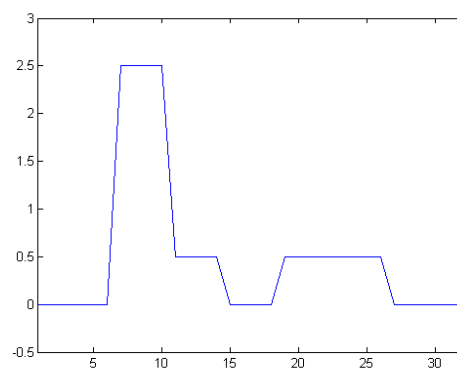


Figure 5.18. Two-stage wavelet decomposition tree and the DWT detail coefficients used for adaptive sampling setting.



(a)



(b)

Figure 5.19. An example illustration of the two-stage DWT details (absolute values) (b) and

its original profile (a).

Allocating dense sampling settings near the high DWT coefficient regions and sparse sampling settings near the low DWT coefficient regions, a wavelet decomposition-based adaptive sampling is anticipated. By using different settings of spacing levels and precisions, the adaptive sampling can produce different results. Petkovski [111, 112] allocates different sampling rates within each region according to the second DWT details d_{d2k} . Then, Chaikin's reconstruction algorithm [23] is used to generate a continuous signal.

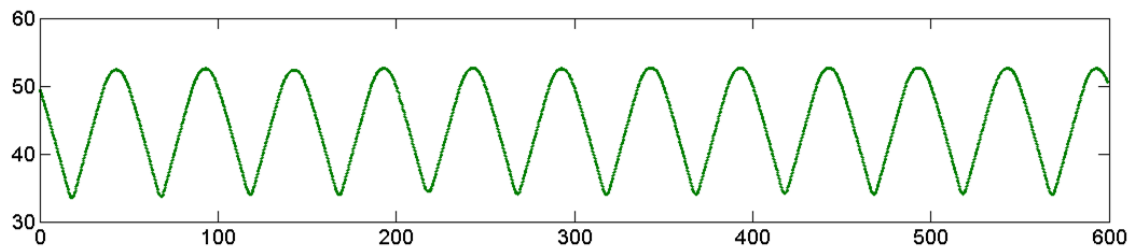
DWT-based sampling maps the second-stage detail coefficients to the regional sampling rate which is a simple and efficient method. The method used in this experiment is a linear mapping, which indicates that

$$R \propto d_{d2k} . \quad (5.10)$$

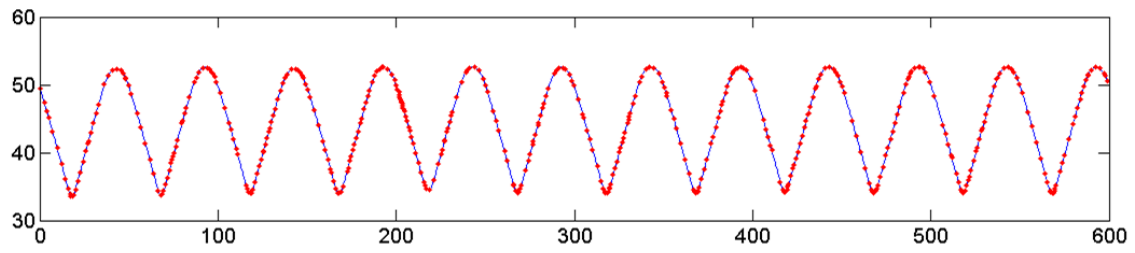
where R is the sampling rate which defines the amount of sample points within a unit space or time length.

5.4.5.2 Some cases

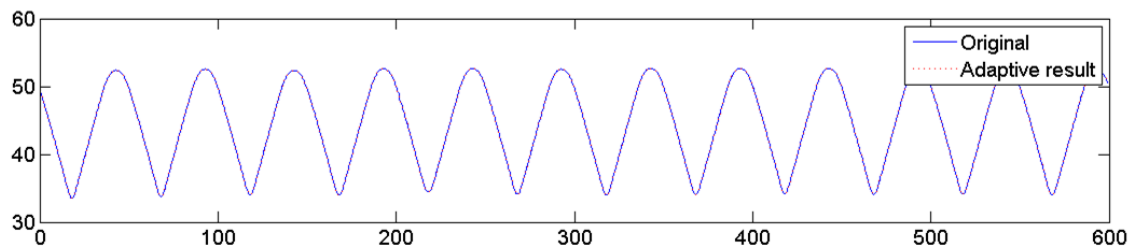
Applying the DWT-based sampling algorithm to some surface signals, the adaptive performance of the sampling method can be presented (See Figure 5.20, Figure 5.21 and Figure 5.22 for details). With different precision settings, this method can produce different adaptive sampling designs. The reconstruction error has not been accurately analysed due to limited time. However, the performance of the model-based sampling can be observed, which provides good flexibility to the surface models.



(a) The original densely sample profile.



(b) The standard DWT adaptive sampling result.



(c) Comparison of the cubic-spline reconstruction result and original profile.

Figure 5.20. A DWT-based sampling of a practical wave signal.

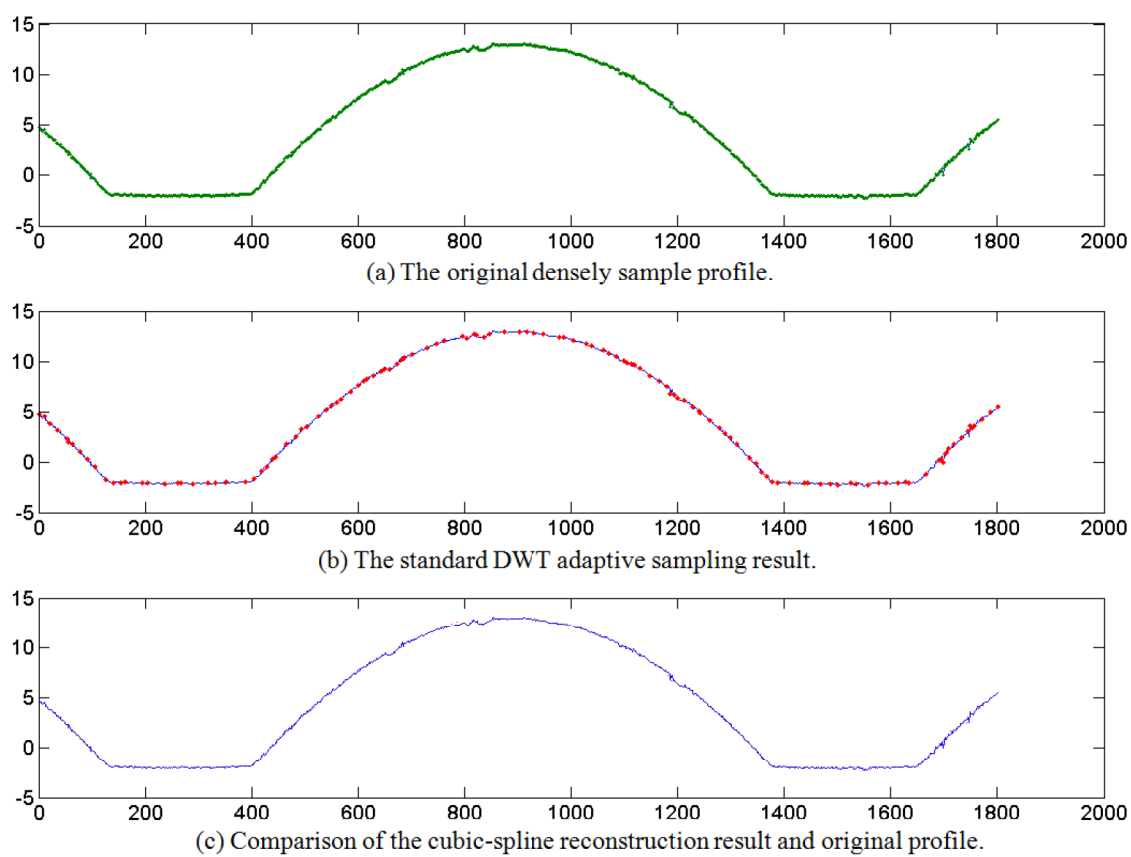


Figure 5.21. A DWT-based sampling of a practical profile of a micro-lens.

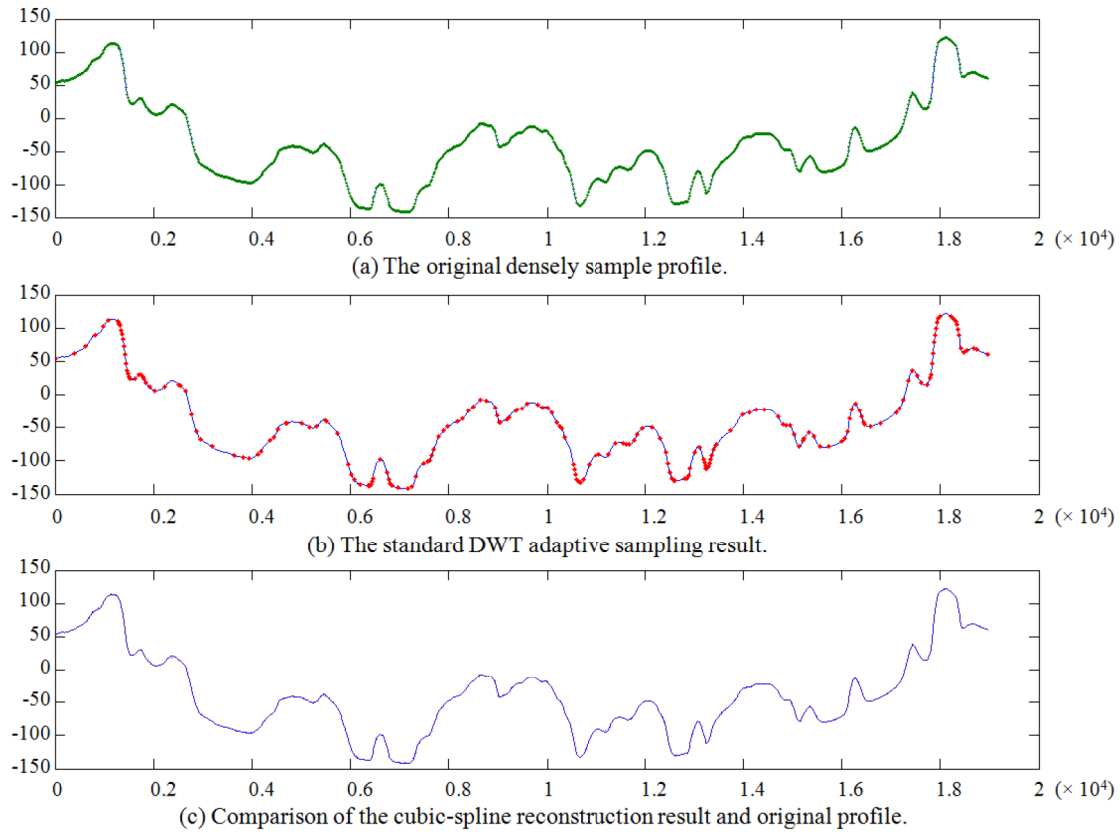


Figure 5.22. A DWT-based sampling of a practical profile of a medal coin.

5.4.6 Section summary and discussion

Model-based sampling is a popular sampling method in current geometric metrology. It aims to produce an optimised sampling pattern by examining the reconstruction error using a specific surface/profile reconstruction method. A lot of variations of these methods have been developed in the past. Many of them show prominent advantages in the measurement of structured surfaces. However, a pure CAD model-based sampling may require a high-precision positioning of the surface product. Existing defects or geometric error between the CAD model and the surface product may be difficult to measure using these sampling methods. If replacing the CAD model with a preliminary measurement, the induced two technical problems above

can be overcome. However, the measuring time is prolonged. Therefore, an intelligent use of these model-based sampling methods needs to be investigated in the future.

The iterative error evaluation criteria directly influence the production of the sampling pattern and thus the sampling accuracy. Diverse iterative error evaluation criteria have been proposed in the past. However, the robustness of these methods has not been uniformly examined. The relationship between sampling accuracy and error evaluation has not been uniformly summarised and resolved. A breakthrough is expected based on a robust solution to this problem, i.e. establishment of the relationship between the iterative error evaluation method and the sampling accuracies.

The number of sampling points usually cannot be exactly designated in advance for model-based sampling. By designating the number of iteration cycles or the error tolerance thresholds, sampling patterns can be designed to meet the predefined conditions. These predefined threshold conditions are equivalent to the adaptive thresholds shown in Figure 3.2. Specifically, the adaptive threshold can be a tolerant value of the random single point height error, the extreme height error, the error volume, or the predefined highest sampling rate in the DWT-based method. The disadvantage of the model-based sampling methods is that the users cannot intuitively designate the sampling number, which might cause discomfort for metrologists. However, the proposed sampling conditions provide novel approaches to understanding the sampling. Users can directly designate the tolerance sampling error which meets the fundamental requirement of geometric measurement.

5.5 Adaptive sampling

5.5.1 Introduction

Adaptive sampling is a novel sampling design that can redirect sampling effort during a survey in response to the observed values [152]. In Pharr's words [114], "if we can identify the regions of the signal with frequencies higher than the Nyquist limit, we can take additional samples in those regions without needing to incur the computational expense of increasing the sampling frequency everywhere." This is the

basic viewpoint from which adaptive sampling originates. This adaptability has no essential difference from those model-based sampling methods; however, adaptive sampling uses different approaches which design sample positions based on earlier sample values, rather than a given signal model.

Non-model-based adaptive sampling methods have the ability to adjust their sampling points in real time. For example, Edgeworth and Wilhem [42] proposed a real-time adaptive sampling method based on the earlier sampling results of surface position and normal measurement. Hu et al [62] proposed an adaptive scanning strategy that automatically adjusts its sample step length according to surface slope variations using extrapolation. Unlike model-based sampling, these solutions avoid inherent positioning errors and are able to effectively pick up the necessary information to identify potential defects. However, the real-time sampling designs of non-model-based methods may not be as optimised as in the case of the model-based method. Also, the results are generally sensitive to the initial conditions, such as the initial sample position. However, they can easily generate good sampling results without accurate pre-positioning.

At present, adaptive sampling methods have been developed for CMM measurement systems. These methods can also be applied to surface topography measurements using stylus instruments. However, differences in scanning mechanisms between stylus instruments and CMM need to be considered. For example, stylus instruments use fast raster-scan technique and cannot accurately scan in y -direction. In the following context, a novel adaptive sampling method is developed which can be simply applied to general stylus instruments. A performance validation of this method is given in Chapter 6.

5.5.2 *Sequential profiling adaptive sampling*

5.5.2.1 The method

Considering stylus profilometers that have a mechanism allowing for raster-scanning of samples, an adaptive sampling method known as sequential profiling adaptive sampling has been developed in this thesis. It employs profile direct sampling (profile

DWT-based sampling also works) for two-dimensional measurement, thus areal adaptive sampling can be achieved. This proposed method has been tested on some typical structured surfaces by numerical simulation. The results have shown promising performance in terms of reduction of the sampling duration and minimisation of the sampling error.

Since model-based profile direct sampling provides a data compression solution for profile data storage, a rational use of this method for areal measurement provides an adaptive sampling, which can improve measurement efficiency or accuracy. The sequential adaptive profiling algorithm works in two stages. It requires an initial profile direct sampling with a high density sample size setting (instrument allowing) such that key samples can be selected. A fine adaptive sampling is then implemented in x -direction at each key scanning position. A step-by-step description of this algorithm is presented in the following.

1. Randomly (or uniformly) select N (usually ten) profiles parallel to the main measuring axis (x -axis in Figure 5.23)^{xiii}.
2. Implement profile direct sampling for each profile. The key positions can be found.
3. Re-sort all the pruned key samples in accordance with their positions along the measurement axis (y -axis in Figure 5.23).
4. Downsample the key samples list produced in Step 3 by the factor N to prune out samples that are too dense.

^{xiii} Step 1 aims to find the key scanning positions in y -direction, rather a preview. A random selection of scanning routes can avoid inherent missing of periodic features that usually happen in a uniform selection, and hence random selection is recommended. Uniform selection can also be suggested if metrologists know beforehand that the specimen is dominated by non-periodic features. Selection of number N of initial scan route is an experience-based action. People know from statistics, a bigger N guarantees a smaller evaluation uncertainty, but may be time-consuming simultaneously. The suggested $N = 10$ is an experience-based value which can guarantee a smaller sampling error (compared with jittered uniform or uniform sampling).

5. For the downsampled key sample positions, implement profile direct sampling for each profile on the main axis direction.

An improvement in measurement efficiency has been presented by the adaptive sampling result shown as the red sample points in Figure 5.23c. Dense sampling intervals are arranged near the edges of the square step structures; while the low curved regions have a sparse allocation of samples. This method is thought to be useful for efficient measurement of linear and rectangularly tessellated structures for raster scanning profilometers. Using this method, the measuring size and duration can be effectively reduced and simultaneously reconstruction error, such as the residual root mean square (RMS) error and the error of the dimensional parameter evaluation, can be minimised (see the section below).

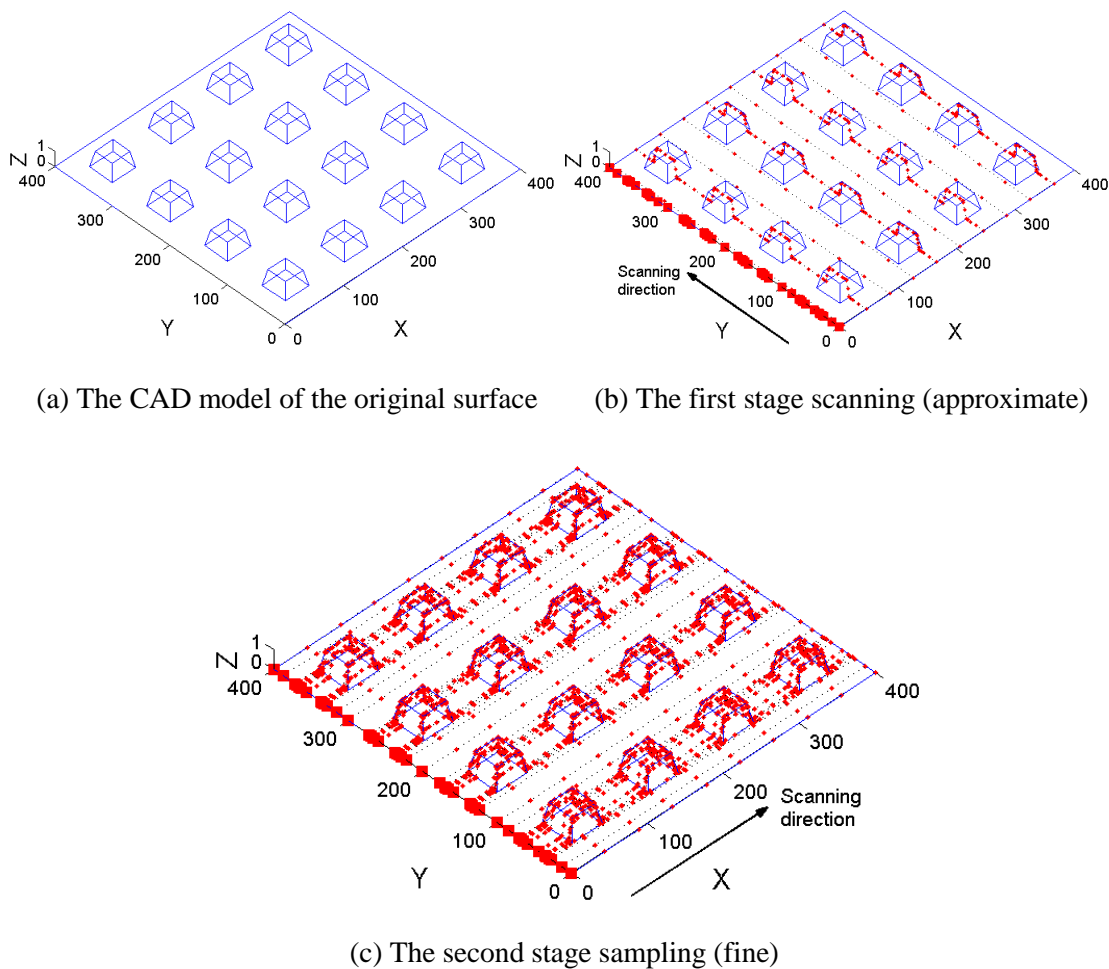


Figure 5.23. Two stages of the sequential profiling adaptive sampling. (a) The original

structured surface. (b) First stage: implementation of ten profile adaptive compression sampling in the y-direction (dashed lines); and based on the pruned key sample positions (red dots), the downsampled key scanning positions are selected (red squares). (c) Second stage: implementation of the profile adaptive compression sampling in the x-direction at each selected position.

5.5.2.2 Some case studies

Two typical structured surfaces (vee-groove-like array structures and micro lens array structures) and a MEMS device surface are used as the testing samples. The three surface samples are presented in Table 5.3 with an initial measurement using an extra dense sample setting. Following this, the sequential profiling adaptive sampling and uniform sampling are simulated. Three typical adaptive sample designs have been illustrated. With the tensor product second order B-spline reconstruction (see Chapter 6), the root mean square (RMS) height errors (RMSE) compared to the original surfaces are analysed. Simultaneously, the number of measuring profiles that are directly related to the measuring duration was computed. One hundred simulations were carried out with differing sample sizes so that repeatability could be quantified. By observing the results in Table 5.3, a remarkable performance improvement can be found.

1. The proposed adaptive sampling usually produces 20 % to 50 % lower RMS residual error than uniform sampling when using the same sample size.
2. When using the same sample size, the adaptive sampling usually uses 20 % to 50 % less measuring time (proportional to the number of scanning profiles) than uniform sampling for the measurement of linear patterns and rectangular tessellations; while for general MEMS surfaces, no obvious difference can be observed.
3. At the same accuracy level, the adaptive sampling usually needs 40 % to 60 % less sample size than uniform sampling. This indicates that the adaptive sampling is able to achieve a 50 % to 80 % improvement in reduction of measuring duration while keeping the same accuracy level as uniform methods.

- The two methods have nearly the same repeatability level while maintaining accuracy. However, in terms of measurement duration estimation, the adaptive method generally presents a slightly reduced repeatability.

By applying this method to the case of raster scanning stylus profilometers, the sample size and measurement duration can be reduced effectively or the sampling accuracy can be improved significantly.

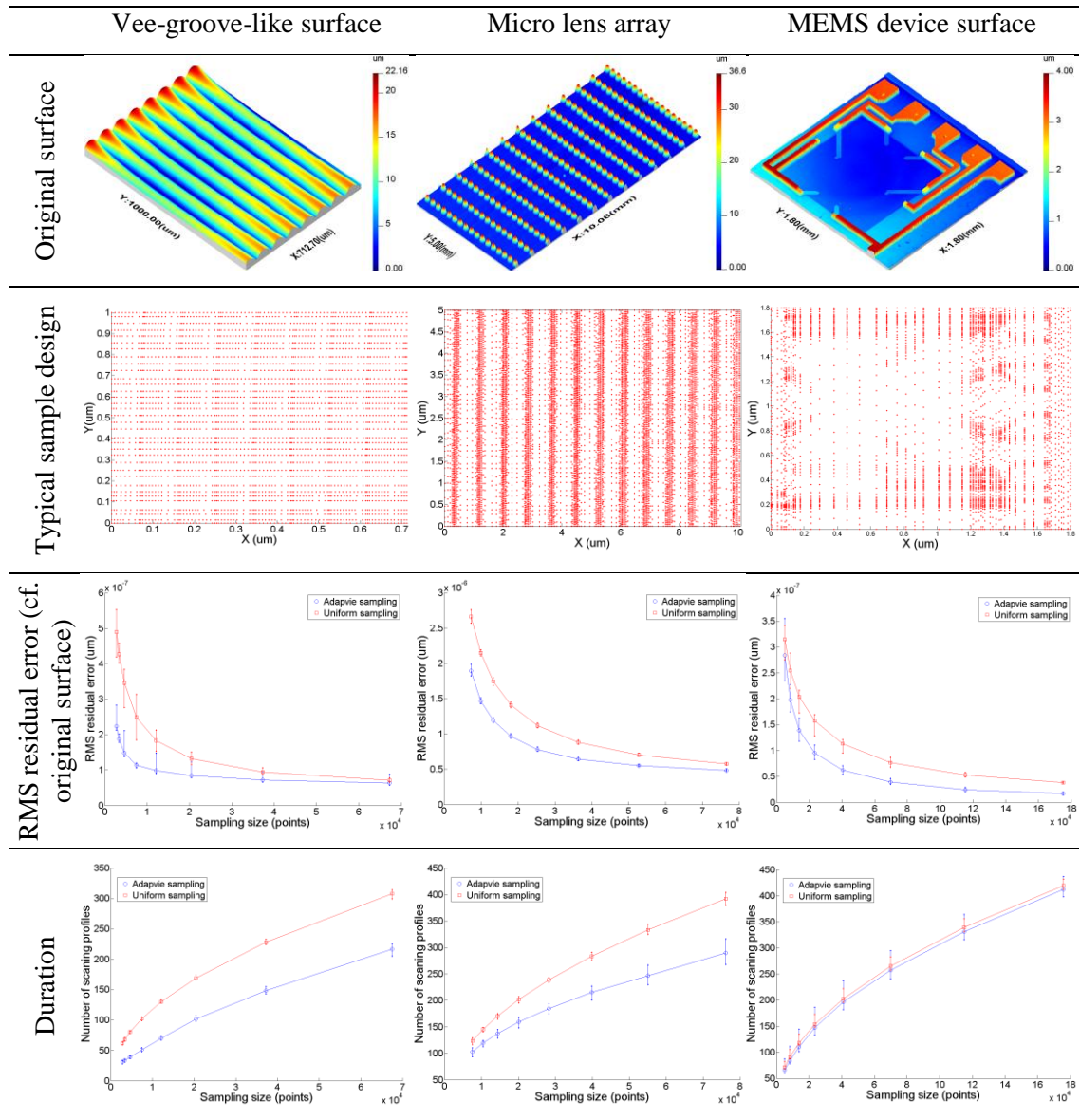


Table 5.3. Performance comparison of uniform sampling and sequential profiling adaptive sampling.

5.5.3 *Section summary and conclusion*

Adaptive sampling and model-based sampling originate from the same idea. However, adaptive sampling concentrates on real-time adaptability, rather than based on a model analysis. This merit makes it promising for the measurement of surfaces which have numerous deviations from an ideal model, for example manufacturing flaws, due to manufacturing errors.

In consideration of the present situation that no intelligent sampling has been developed for the surface topography measurement, a novel areal adaptive sampling method is developed in this thesis. Applying this method to the case of raster scanning profilometers, the measurement efficiency for structured surfaces is expected to be significantly improved. In the simulation results, the adaptive method has shown evidence of performance improvement (sampling accuracies, sampling duration) compared to uniform sampling methods, particularly for linear patterns and rectangular tessellations. Considering that the current areal measurement duration for a scanning system can often be hours, the proposed method is able to considerably increase measurement efficiency.

5.6 **Summary and conclusions**

A summary of the work of this chapter and the conclusions are given below.

1. Intelligent sampling could be a substitute of the currently prevailing uniform sampling. The expected measurement efficiency and accuracy illustrate the promise of intelligent sampling.
2. There are generally four categories of intelligent sampling in terms of the sampling principles. These are jittered uniform sampling, low-discrepancy pattern sampling, model-based sampling and adaptive sampling. Each of these methods has different advantages. For example, low-discrepancy patterns are optimal in statistical estimation. Model-based sampling methods and the adaptive sampling are optimal in geometric approximation. Specifically,

- a. Previous research has shown that the jittered uniform sampling presents a high accuracy results compared to uniform sampling and low-discrepancy sampling methods for flatness measurement.
 - b. The numerical evidence in this thesis does not show that low-discrepancy sampling patterns have a consistent advantage over uniform sampling in the measurement of flatness or average surface roughness. However, low discrepancy patterns present high stability in geometric measurement compared to uniform methods.
 - c. Model-based sampling is one of the most popular intelligent sampling methods in geometric measurements. Model-based sampling requires high accuracy positioning of the work-piece at the measurement stage. This restriction limits the popularity of this method on structured surface measurement because of the high precision requirements. However, if replacing the CAD model with a preliminary measurement, the obstacle can possibly be removed. There is still a long way from realising model-based sampling in practical measurements.
 - d. Adaptive sampling is another very popular sampling method at present. It is sensitive to the start position; however, it is a promising method because it does not need high accuracy pre-positioning.
3. For fixed sampling patterns, i.e. uniform sampling, jittered uniform sampling and low-discrepancy pattern sampling, a sampling pattern can be exactly determined by designating the sampling conditions, for example the sampling length, spacing or the sampling number. However, model-based sampling and adaptive sampling have other controllable sampling conditions, for example the tolerance thresholds. The predefined thresholds cannot directly determine the number of sampling points. These thresholds determine the number of adaptive iteration cycles or the allowed maximum sampling errors. Hence the reconstruction accuracy and the number of sampling points can be controlled.

4. The error evaluation criteria within the design of model-based sampling or adaptive sampling can be a critical influence on the sampling accuracy. The relationship between the error evaluation criteria and the reconstruction accuracy is still not clear at the moment.
5. Intelligent sampling may be promising if the non-uniform sampling theory in the shift-invariant spaces can be applied. Two problems need to be solved in terms of reconstruction algorithms and data storage. With a rational solution to these difficulties, intelligent sampling has real potential for the next generation of geometric information sampling. For example, intelligent sampling can be applied to a large size CCD/CMOS CSI, a raster scan-based stylus instruments or scanning probe microscopes (SPM).
6. Sequential profiling adaptive sampling method has been developed in this thesis. It is developed for raster scan-based stylus instruments or SPMs. The numerical case studies show that this proposed method works efficiently on time reduction and improvement of sampling accuracy, compared to uniform sampling. A comparison of the performances of these sampling methods needs to be carried out to validate the proposed sampling method.

6. ERROR EVALUATIONS

6.1 Reconstruction

6.1.1 Introduction

The current research on signal sampling concentrates on the following two questions [6]:

1. Given a class of signal functions $f \in V(\mathbb{R}^d)$ where V is a specific function space, what conditions of a sampling set $X = \{x_j, j \in J\}$, where J is a countable index set, can guarantee that f can be uniquely and stably reconstructed from the sampling set?
2. How can a function $f \in V(\mathbb{R}^d)$ be recovered from the sampling set $X = \{x_j, j \in J\}$ using an efficient and stable algorithm?

Question 1 considers what kind of a sampling set can give an exact reconstruction; Question 2 leads to numerical solutions for the reconstruction. Sampling and reconstruction constitute an inverse problem in signal processing. Each of them cannot stand alone without consideration of the other.

As discussed in Section 3.4, prior recent research on signal sampling has answered the two questions for many signal functions in shift-invariant spaces, such as the Paley-Wiener subspace, wavelet subspaces and spline-like subspaces [4-6, 92, 157, 167]. However, applications of these theories are still limited, for example in magnetic resonance imaging (MRI) [6]. In geometric metrology, shift-invariant space sampling theories are not popular. One of the most important reasons for this is that many current structured surfaces have regional interests, for example, geometric primitive edges and corners on a structured surface. The shift-invariant space sampling theory provides a jittered sampling which cannot solve the efficiency problem for such surfaces.

Many current geometric products belong to a wider function space than “integer” shift-invariant space. It is believed that these surfaces can be sampled in a far more efficient way than a “jittered” sampling (see the jittered sampling in a shift-invariant space in Section 0). However, no sampling theory except approximation theory supports this at the moment.

A variety of research in geometric metrology concentrates on sampling or reconstruction separately, for example [45, 112, 130, 164]. these researchers give up “exact reconstruction” in theory deduction, and try to closely approximate the original signal as an alternative from discrete modelling and approximations [10]. For example, a one-dimensional sampling set $X = \{x_j, j \in J\}$ can be approximated by an N degree polynomial spline (or B-spline) curve with a regular knot setting. For example, in Figure 6.1, a practical uniform sampled signal $f(x_j), j \in J$ within the support $[0, L], L \in \mathbb{Z}$ can be approximated by a third degree polynomial spline, i.e.

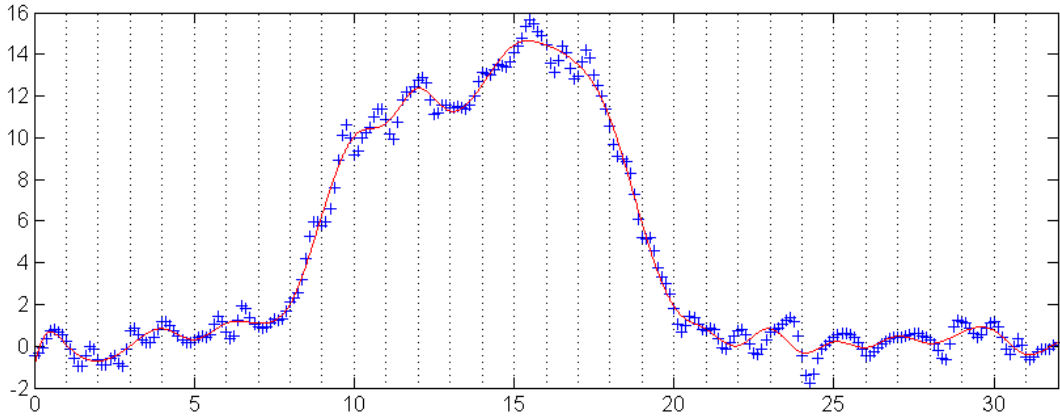
$$f(x) \approx p(x, a) + \sum_{k=1}^{L-1} c_k (x - k)_+^3 \quad (6.1)$$

where $p(x, a) = a_0 + a_1 x + a_2 x^2 + a_3 x^3$, $(x - k)_+ = x - k$ if $x > k$ and 0 otherwise, or can be approximated by a third degree B-spline curve, i.e.

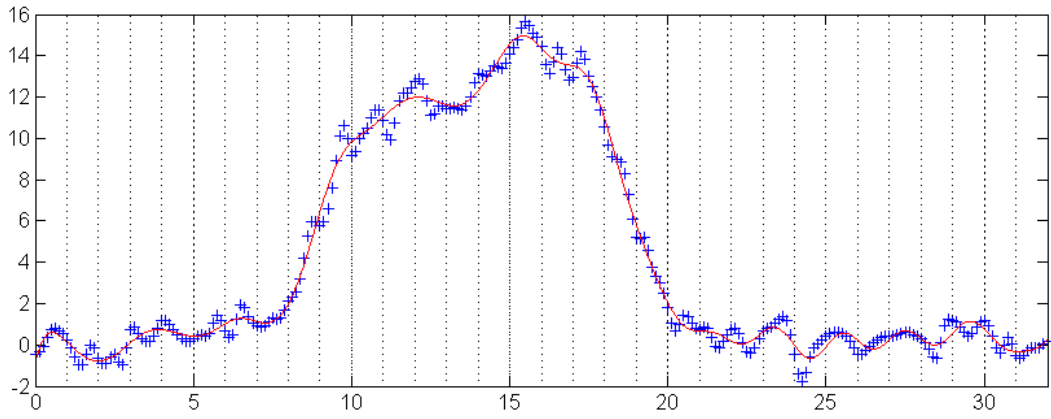
$$f(x) \approx \sum_{k=-1}^{L+1} c_k \beta_3(x - k) \quad (6.2)$$

where $\beta_3 = \chi[-\frac{1}{2}, \frac{1}{2}] * \chi[-\frac{1}{2}, \frac{1}{2}] * \chi[-\frac{1}{2}, \frac{1}{2}] * \chi[-\frac{1}{2}, \frac{1}{2}]^{\text{xiv}}$.

^{xiv} $\chi[a, b]$ is a characteristic function which has the value 1 within $[a, b]$ and 0 otherwise.



(a)



(b)

Figure 6.1. Approximation of a uniform sampling set using (a) a third degree polynomial spline curve and (b) a fourth order B-spline curve with integer position knots.

It is apparent that signal samples can be approximated using many different forms, thus the reconstruction results always vary. This arbitrariness induces a reconstruction uncertainty which tends to be rejected in geometric metrology. In areal surface measurement, many applicable reconstruction methods have been investigated in Zhang's thesis [179]. Among them, two reconstruction methods which have received enough attention here, are thought to be helpful in areal surface reconstruction from non-uniform samples: tensor product B-spline reconstruction and triangulation-based reconstruction.

Tensor product B-spline reconstruction works efficiently for regular (or near regular) lattice samples, or partially regular samples, but may not be efficient for scattered data (see example data in Figure 6.2). Triangulation-based reconstruction works well for the scattered samples. Detailed algorithms are given in the following.

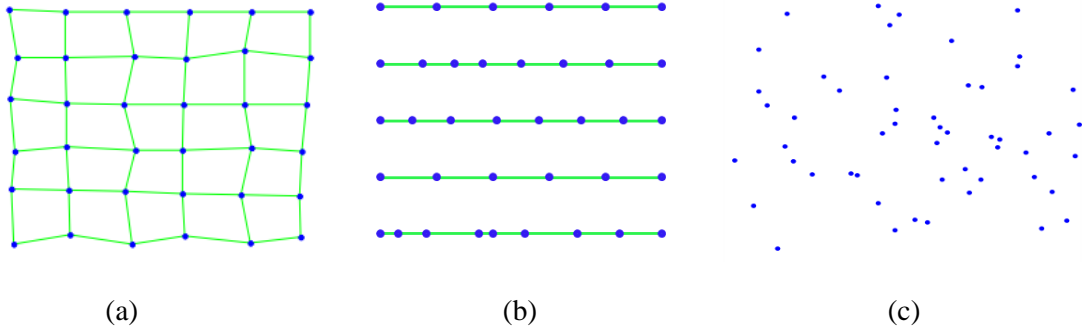


Figure 6.2. Three types of surface sample data with different point distributions. (a) A near-regular lattice sample data, (b) a partially regular lattice sample data which have regular sampling distances on y-direction, and (c) scattered data.

6.1.2 Tensor product reconstruction using B-splines

6.1.2.1 Tensor product reconstruction and basis functions

The tensor product method has been widely used for reconstruction of regular lattice data (for example, the uniform sampling result in Figure 6.2a or partially regular latticed data in Figure 6.2a). This wide use is due to the method's high numerical stability and computational efficiency. The tensor product method presents a surface as a tensor product of two bases, for example

$$\begin{cases} \phi(x, \mathbf{a}) = \sum_{k=1}^S a_k \phi_k(x) \\ \varphi(y, \mathbf{b}) = \sum_{l=1}^T b_l \varphi_l(y) \end{cases}, \quad (6.3)$$

in the x and y directions independently. Thus the surface can be expressed as

$$z = \phi(x, \mathbf{a}) \times \varphi(y, \mathbf{b}) = \sum_{k=1}^K \sum_{l=1}^L a_k b_l \phi_k(x) \varphi_l(y) = \sum_{k=1}^K \sum_{l=1}^L c_{k,l} \psi_{k,l}(x, y), \quad (6.4)$$

where $\{\phi_k\}$ and $\{\varphi_l\}$ are preset base functions and the coefficient vectors \mathbf{a} and \mathbf{b} should be calculated from the data. Chebyshev polynomials, polynomial splines and B-splines provide base functions for the tensor product surface reconstruction [10]. For example, two spline curve forms are given in equations (6.1) and (6.2). Using a uniform expression, any signal function can be approximated using

$$f(\cdot) \approx \sum_{k=0}^K c_k \varphi_k(\cdot). \quad (6.5)$$

Several general basis functions and approximation methods are as follows:

1. Polynomial curve approximation with the monomial basis

$$\phi_k(x) = x^k. \quad (6.6)$$

The polynomial function provides a very simple approximation to a surface signal f . However, if f becomes sophisticated, the required curve degree K grows simultaneously. Thus the values of the basis function grow unacceptably large (which makes them unstable) and an ill-conditioned matrix is generated which would cause computational instability.

To avoid this instability, scale normalisation is widely accepted in advance, for example using

$$z = \frac{x - (x_{\max} + x_{\min}) / 2}{(x_{\max} - x_{\min}) / 2}. \quad (6.7)$$

Hence, x is normalised within the interval $[-1, 1]$. The polynomial curve approximation then becomes

$$f(z) \approx \sum_{k=0}^K c_k \varphi_k(z). \quad (6.8)$$

2. Chebyshev polynomials approximation with the basis [2]

$$\phi_k(z) = \begin{cases} 1, & \text{if } k=0 \\ z, & \text{if } k=1 \\ 2x\phi_{k-1}(z) - \phi_{k-2}(z), & \text{if } k \geq 2 \end{cases}, \quad (6.9)$$

where z is the normalised x coordinates using equation (6.7).

The Chebyshev polynomials are orthogonal within the interval $[-1, 1]$ which overcomes the ill-conditioning problem in the simple polynomial approximation.

3. Spline approximation I – piecewise polynomial form.

It is known that Runge's phenomenon will arise when approximating using a high order polynomial. When a curve becomes complex, spline approximation is preferred which divides a curve/surface into several sections and approximating each of them piecewisely using a low order polynomial. A popular n degree spline approximation basis is [115]

$$\phi_k(x) = \begin{cases} p_n(x, a), & \text{if } k=0 \\ (x - \lambda_k)_+^n, & \text{if } 1 \leq k \leq K \end{cases}. \quad (6.10)$$

where $p_n(x, a) = a_0 + a_1x + \dots + a_nx^n$; $(x - \lambda_k)_+ = x - \lambda_k$ if $x > \lambda_k$ and 0 otherwise; K is the number of knots (or breakpoints) which divide the curve interval into sections and $x_{\min} < \lambda_1 < \lambda_2 < \dots < \lambda_K < x_{\max}$.

4. Spline approximation II – B-spline form.

The B-spline form provides another expression [10, 32] of the basis functions which have better numerical performance than the piecewise polynomial form, for example compact support (local support). This brings a computation efficiency due to a band matrix that is welcome in metrology [52, 54].

$$\phi_k(x) = N_{n,k}(x) = \begin{cases} \chi[\lambda_k, \lambda_{k+1}), & \text{if } n=0, k=1, 2, \dots, K \\ \chi[\lambda_k, \lambda_{k+1}], & \text{if } n=0, k=K+1 \\ \frac{(\lambda_k - x)N_{n-1,k}(x)}{\lambda_k - \lambda_{k-n}}, & \text{if } n \geq 1, k=1 \\ \frac{(x - \lambda_{k-n-1})N_{n-1,k-1}(x)}{\lambda_{k-1} - \lambda_{k-n-1}} + \frac{(\lambda_k - x)N_{n-1,k}(x)}{\lambda_k - \lambda_{k-n}}, & \text{if } n \geq 1, 1 < k \leq K+n \\ \frac{(x - \lambda_{k-n-1})N_{n-1,k-1}(x)}{\lambda_{k-1} - \lambda_{k-n-1}}, & \text{if } n \geq 1, k=K+n+1 \end{cases} \quad \text{xiv} \quad (6.11)$$

where n is the degree of the basis function, K is the number of knots and

$$x_{\min} = \lambda_{-\infty} = \lambda_{-1} = \lambda_0 < \lambda_1 < \lambda_2 < \dots < \lambda_K < \lambda_{K+1} = \lambda_{K+2} = \lambda_{+\infty} = x_{\max}. \quad (6.12)$$

The repeated knot settings at the ends induce a partition of unity (see Section 3.4) within a limited interval. Figure 4.4 presents such a B-spline basis function within $[0, 10]$ with the interior knot positions $[2, 5, 6, 9]$.

Sometimes, if the knots are uniformly distributed with the distance $d = \lambda_k - \lambda_{k-1}$, a uniform expression of the basis function is preferred [54]:

$$\phi_k(x) = \beta_n(x - \lambda_k). \quad (6.13)$$

where $\beta_n = \chi[-d/2, d/2) * \dots * \chi[-d/2, d/2)$ ^{xiv} with n times convolution. For example, a third degree B-spline basis is presented in Figure 6.3 which is commonly chosen in practice, as it gives enough smoothness in most metrology applications [10].

In this thesis, the B-spline form reconstruction is used because of its computation efficiency and stability.

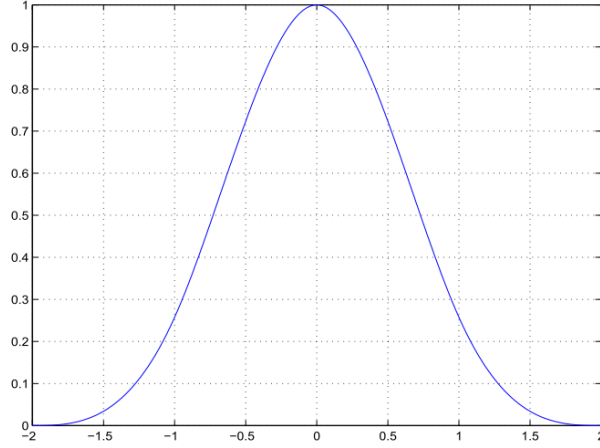


Figure 6.3. A third degree B-spline basis with the support $[-2, 2]$.

6.1.2.2 The reconstruction algorithm

In this section, the tensor product B-spline reconstruction algorithm is presented. Given a sampling set $X = \{x_j, j \in J\}$, with the sampling values $f|_X$, the original signal can be approximated using

$$\sum_{k=0}^{K+n+1} c_k N_{n,k}(x) = f(x_j) \quad (6.14)$$

with a proper knot setting $x_{\min} = \lambda_0 < \lambda_1 < \lambda_2 \cdots < \lambda_K < \lambda_{K+1} = x_{\max}$, where $N_{k,n}$ is the B-spline basis function in equation (6.11). Defining the matrix U with the entries $U_{j,k} = N_{n,k}(x_j)$, the following linear algebra equation can be written:

$$UC = f|_X. \quad (6.15)$$

In the one-dimensional case, the linear system in equation (6.15) has been solved in [52], i.e.

$$C = (U^T U)^{-1} U^T f|_X. \quad (6.16)$$

The band matrix $U^T U$ brings remarkable computation efficiency [52, 63]. In two-dimensional cases, the situation becomes complex and some variations can result.

(a) Scattered samples. In the two-dimensional case, given a sampling set with scattered samples $(x_i, y_i, z_i), i=1, 2, \dots, I$, with a proper knot setting in x and y directions for example in equation (6.12) and

$$y_{\min} = \gamma_{-\infty} = \gamma_{-1} = \gamma_0 < \gamma_1 < \gamma_2 \cdots < \gamma_L < \lambda_{L+1} = \lambda_{L+2} = \lambda_{+\infty} = y_{\max}, \quad (6.17)$$

and let Φ, Γ, Ψ, C, Z be defined with the entries as below

$$(\Phi)_{i,k} = N_{n,\lambda_k}(x_i), \quad i=1, 2, \dots, I, \quad k=1, 2, \dots, K+n+1, \quad (6.18)$$

$$(\Gamma)_{i,l} = N_{n,\gamma_l}(y_i), \quad i=1, 2, \dots, I, \quad l=1, 2, \dots, L+n+1, \quad (6.19)$$

$$(\Psi)_{i,kl} = N_{n,\lambda_k}(x_i)N_{n,\gamma_l}(y_i), \quad i=1, 2, \dots, I, \quad (6.20)$$

C be a $kl \times 1$ coefficient vector and $Z = [z_1, z_2, \dots, z_3]^T$, the following linear system can be constructed based on equation (6.4)

$$\Psi C = Z, \quad (6.21)$$

which has the same form as the one-dimensional case as in equation (6.15).

This general solution applies to any kind of sample shown in Figure 6.2 if the number of sample points is not large (for example less than thousands of points). In the case of a densely sampled data, this method shows inefficient computation. The computation efficiency can be significantly improved if the samples have a grid distribution.

(b) Grid samples. Consider a two-dimensional regular grid sample $(x_i, y_j, z_{i,j})$, $i=1, 2, \dots, I$, $j=1, 2, \dots, J$, with a proper knot setting in the x and y directions given in equations (6.12) and (6.17), let Φ, Ψ, C, Z be defined with the entries as below

$$(\Phi)_{i,k} = N_{n,\lambda_k}(x_i), \quad i=1, 2, \dots, I, \quad k=1, 2, \dots, K, \quad (6.22)$$

$$(\Psi)_{j,l} = N_{n,\gamma_l}(y_j), \quad j=1, 2, \dots, J, \quad l=1, 2, \dots, L, \quad (6.23)$$

$$(C)_{k,l} = c_{k,l}, \quad k=1,2,\dots,K, \quad l=1,2,\dots,L, \quad (6.24)$$

$$(Z)_{i,j} = z_{i,j}, \quad i=1,2,\dots,I, \quad j=1,2,\dots,J, \quad (6.25)$$

then the tensor product expression of the surface can be written as

$$\Phi C \Psi^T = Z. \quad (6.26)$$

In this two-dimensional case, the algebra system has been formulised in [10]. Firstly, solve the equation

$$(\Phi^T \Phi) C' = \Phi^T Z \quad (6.27)$$

with the output C' . Then the second solution follows with the final output C ,

$$C(\Psi^T \Psi) = C' \Psi. \quad (6.28)$$

Hence, the surface approximation can be substituted by two curve approximations.

(c) Partial lattice samples. For partially regular lattice sample data as in Figure 6.2b $(x_{i,j}, y_j, z_{i,j}), j=1,2,\dots,J, i=1,2,\dots,I(j)$, the solution for regular grid data above is not applicable. For example, if a partial lattice sample is given with a constant y sampling spacing (see Figure 6.2b), while in the x direction the samples are freely distributed at each y -position, construction of the x basis matrix Φ of equation (6.22) becomes infeasible because the number of $x_{i,j}$ differs at different y_j . However, a slight modification of the algorithm above can make the partial lattice sample reconstruction solvable.

With a proper knot setting, for example in equations (6.12) and (6.17), the following matrices are constructed at a specific y -position y_j ,

$$(\Phi_j)_{i,k} = N_{n,\gamma_k}(x_{i,j}), \quad i=1,2,\dots,I(j), \quad k=1,2,\dots,K. \quad (6.29)$$

$$\Psi_j = [N_{n,\gamma_1}(y_j), N_{n,\gamma_2}(y_j), \dots, N_{n,\gamma_L}(y_j)], \quad l=1,2,\dots,L, \quad (6.30)$$

$$(C)_{k,l} = c_{k,l}, \quad k=1,2,\dots,K, \quad l=1,2,\dots,L, \quad (6.31)$$

$$Z_j = [z_{1,j}, z_{2,j}, \dots, z_{I(j),j}]. \quad (6.32)$$

Then, the following equation applies according to equation (6.4) for all $j=1,2,\dots,J$

$$\Phi_j C \Psi_j^T = Z_j^T. \quad (6.33)$$

By substituting $C \Psi_j^T$ with $C'_{:,j}$, i.e.

$$C \Psi_j^T = C'_{:,j}, \quad (6.34)$$

$C'_{:,j}$ can be solved with the linear system

$$(\Phi_j^T \Phi_j) C'_{:,j} = \Phi_j^T Z_j^T. \quad (6.35)$$

Let

$$C' = [C'_{:,1}, C'_{:,2}, \dots, C'_{:,J}], \quad (6.36)$$

and

$$\Psi^T = [\Psi_1^T, \Psi_2^T, \dots, \Psi_J^T], \quad (6.37)$$

then the following linear system can be solved with C as the output

$$C \Psi^T = C', \quad (6.38)$$

based on equation (6.34).

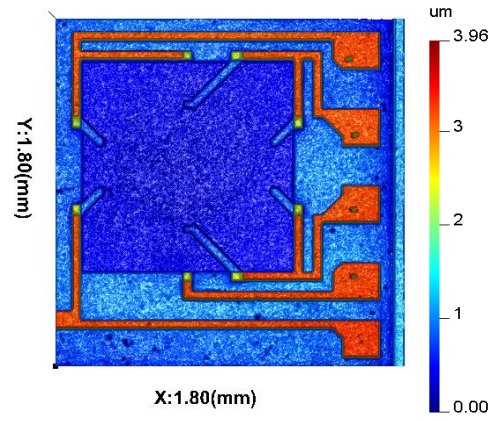
6.1.2.3 Selection of the knots

It is known that the selection of knots directly relates to the reconstruction results. Selecting more knots can improve the reconstruction accuracy but reduce the computation efficiency simultaneously. A proper selection of knots should make a balance between accuracy and efficiency, which has been discussed elsewhere in coordinate metrology [181].

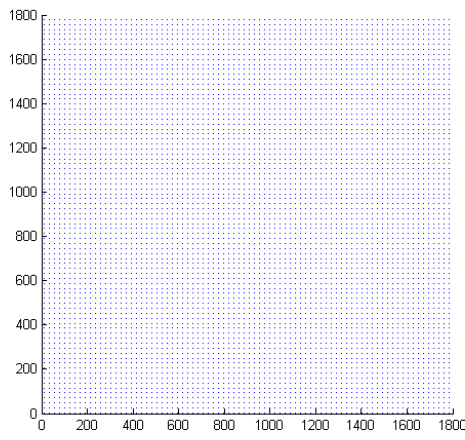
With measurement of structured surfaces, the investigated surfaces usually have small area of interest, and regional high-curvature features. A non-uniform knot setting is necessary which is supposed to adapt the surface geometry changes. Considering that many intelligent sampling methods provide an adaptive sample setting, and under the assumption that the sample values are accurate enough, interpolation is preferable to approximations.

In this thesis, when reconstructing using the first degree (order two) B-spline, the knots are selected to be the same as the sample positions of the sampling set $X = \{x_j, j=1,2,...,J\}$. Thus U in equation (6.15) becomes a $J \times J$ matrix, and $UC = f|_X$ has a unique solution for C . when reconstructing using the third degree (order four) B-spline, the knots are selected to be the same as positions of the sampling set. Combined with the two clamping conditions, for example $f'_{x_{\min}} = f'_{x_{\max}} = 0$, U in equation (6.15) becomes a $(J+2) \times (J+2)$ matrix, and $UC = f|_X$ has a unique solution for C .

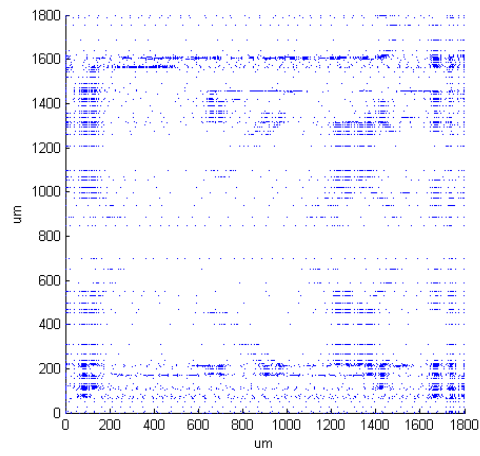
The reconstruction algorithm for the scattered samples is not used in this work because it is not an interpolation. The reconstruction algorithm for the grid data and the partial latticed data is used for uniform sampling and the proposed sequential profiling adaptive sampling results. In this way, an interpolation result can be provided for the uniform samples; while for the partial lattice samples, a near interpolation result can be obtained. The selection of knots for the partially latticed data needs particular care. The reconstruction accuracy usually is the priority of concern. Figure 6.4 shows an illustration of the utilisation of the tensor production reconstruction using B-splines. In this example, the reconstructions for a grid data and a partial lattice data are carried out. The stable performance of the two algorithms is presented.



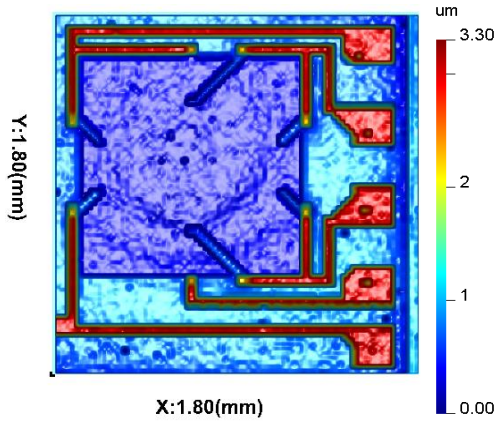
(a) The original surface (1024×1024)



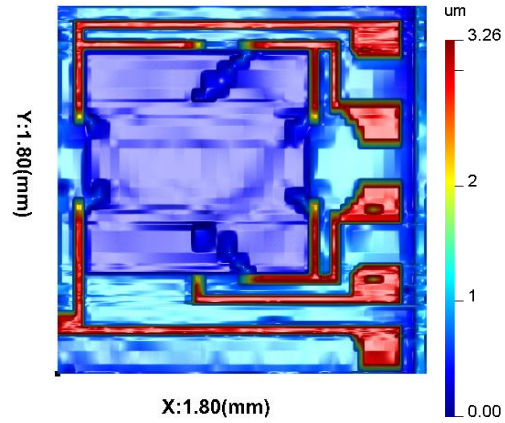
(b) A uniform sample (80×80)



(c) A partial lattice sample (6400)



(d) The grid data reconstruction result
(RMSE = $0.285 \mu\text{m}$)



(e) The partial lattice data reconstruction result
(RMSE = $0.156 \mu\text{m}$)

Figure 6.4. Illustration examples of the performances of the tensor product reconstruction with B-splines for the grid data and the partial lattice data.

6.1.3 Triangulation based reconstruction

Reconstruction of scattered sample data using the tensor product method lacks computational efficiency. Triangulation-based methods are a simple and stable substitution. For example, Delaunay triangulation [22, 36] establishes neighbourhood connections among the data points with the Delaunay triangulation algorithm, which neglects all the non-neighbouring points in the Voronoi diagram (see Figure 6.5) of the given points, and avoids poorly shaped triangles. Following this structuring process, regional reconstructions [22] (linear or cubic) within each triangle patch can be carried out. These methods are able to guarantee a reconstruction to arbitrary accuracy if the sample points are dense enough, which provides the theoretical foundation for developing new reconstruction techniques. MATLAB provides a simple command reconstruction [149] from scattered data based on Delaunay triangulation, which is used in this thesis.

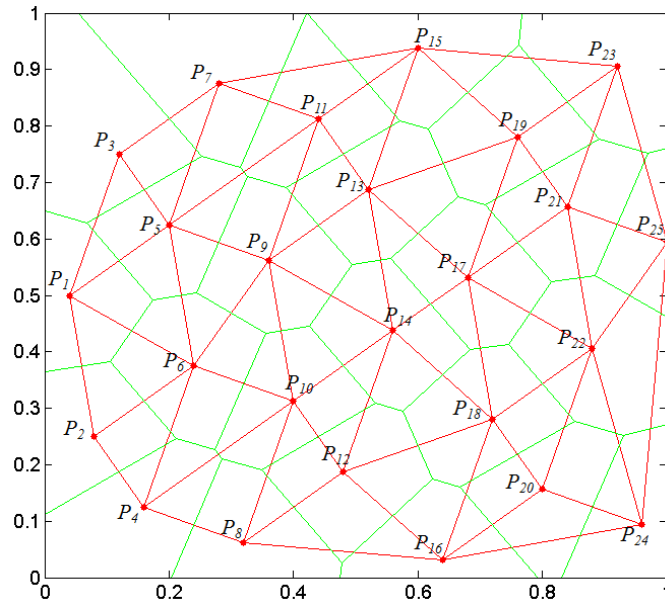


Figure 6.5. Delaunay triangulation (red) and Voronoi tessellation-diagram (green) of a planar space based on a twenty-five scattered samples.

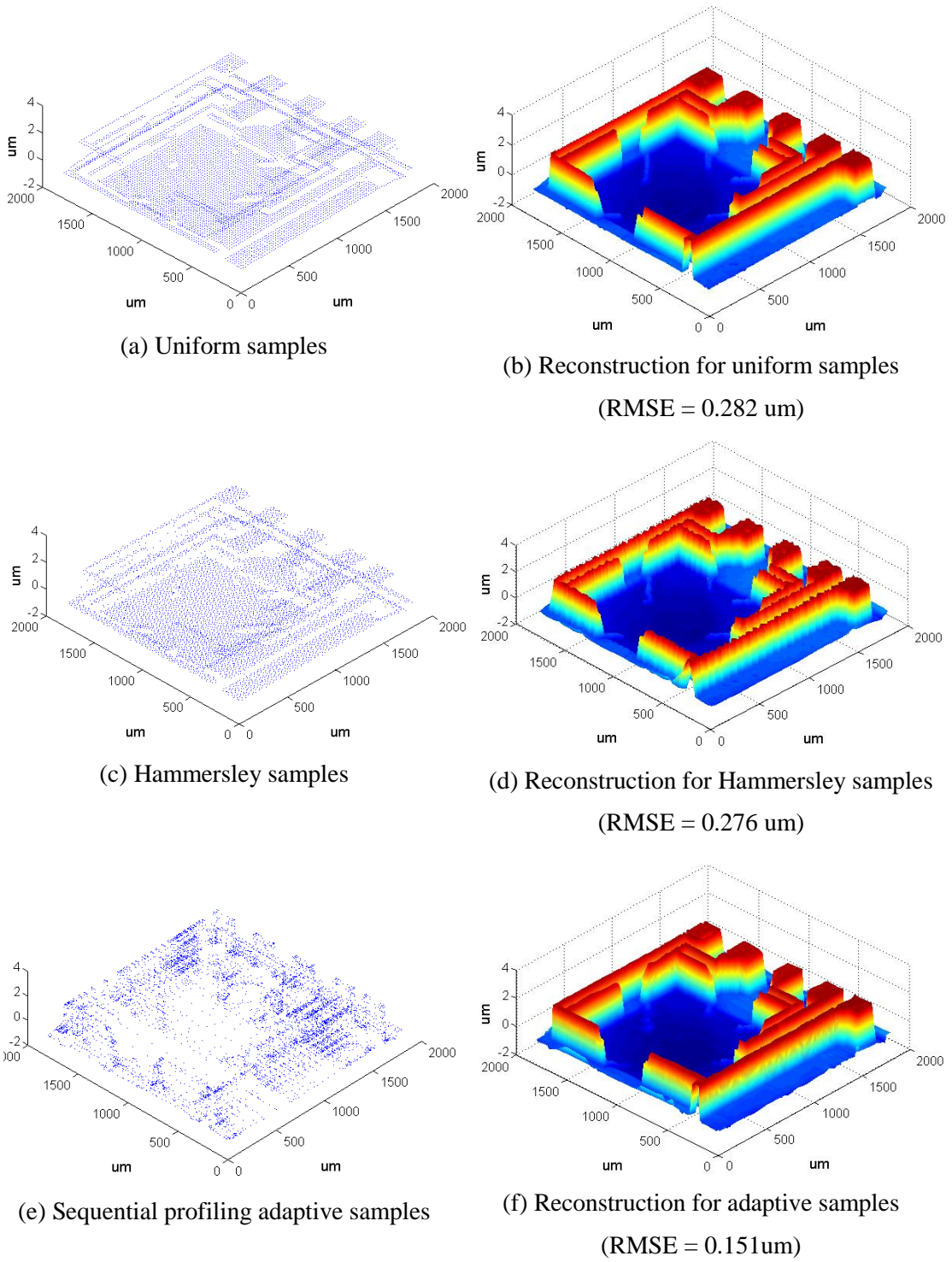


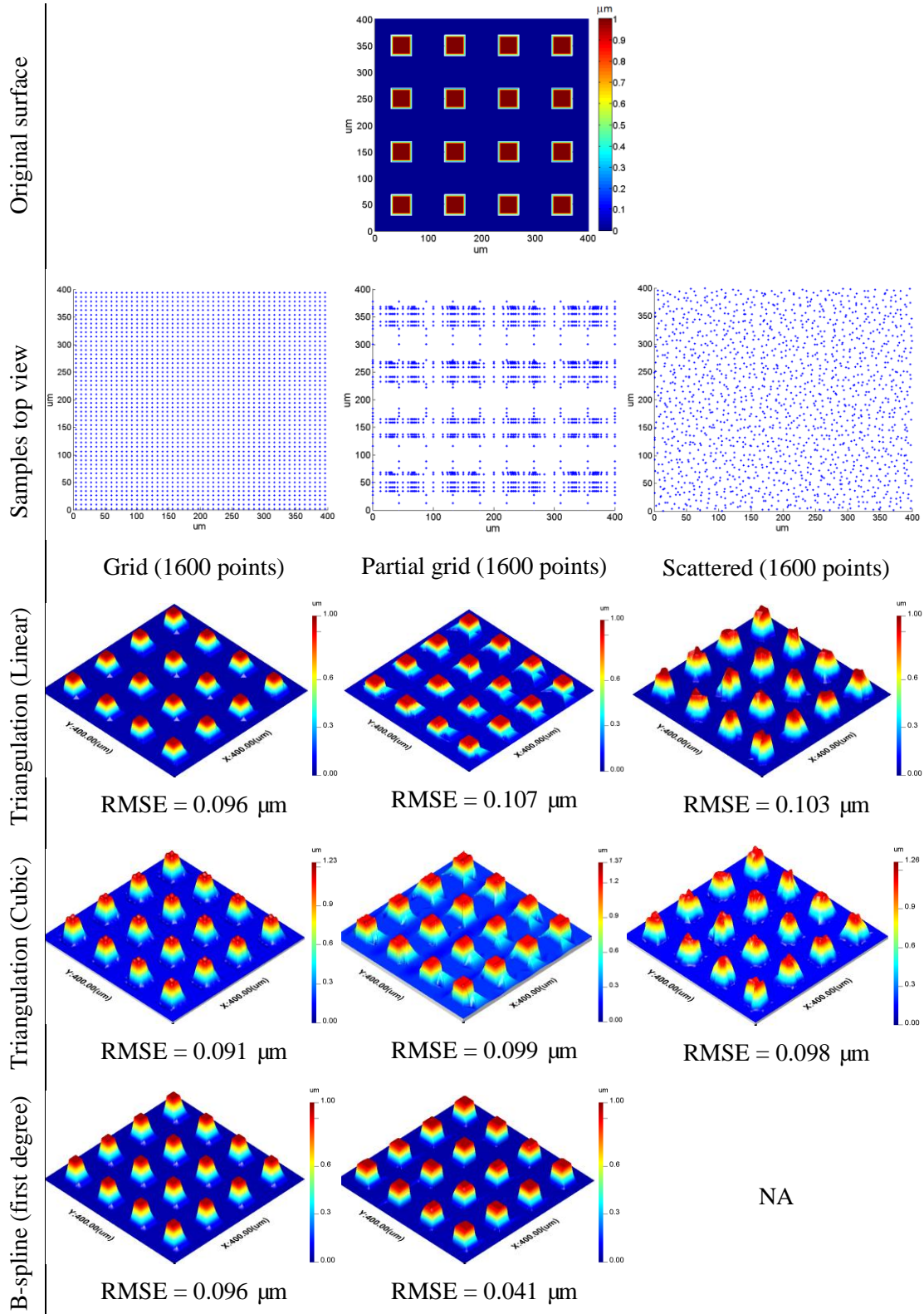
Figure 6.6. The performance of the Delaunay triangulation-based reconstruction for the uniform, Hammersley and Halton pattern sampling of a MEMS surface with 80×80 sampling points.

Delaunay triangulation-based reconstruction works stably for numerical computations. Figure 6.6 illustrates a Delaunay triangulation-based linear reconstruction of a MEMS surface with diverse sampling designs, like uniform sampling, low-discrepancy patterns and adaptive sampling (scattered and partially regular grid). This is a significant advantage that tensor product B-spline-based sampling cannot provide. Note that uniform sampling and Hammersley sampling provides similar performance in this case, though Hammersley sampling has zig-zag reconstructed boundaries which are obviously reluctant to accept for visualisation.

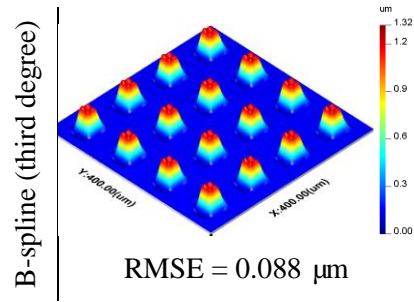
6.1.4 An example illustration of the reconstruction methods

The performance of two categories of reconstruction method is presented in this section. The sample results generated from the three different sample settings, i.e. uniform, partial lattice and non-uniform, are reconstructed in terms of the measurement of a tessellation surface (see Table 6.1). The reconstructed results and the RMS height deviations are presented as performance indicators.

The conclusions on which reconstruction method works stably or accurately cannot be obtained based on the single case. Different reconstruction methods have different performance on different sampling settings. For example, the tensor-product reconstruction methods are more applicable to grid or partial grid samples. In this work, the question on conclusion of reconstruction techniques is suspended due to time limitation. In the later sampling tests of this thesis work, all the reconstruction methods will be used and the best results are selected for analysis.



(Continued)



NA

NA

Table 6.1. Performance of different reconstruction methods for a tessellation surface.

6.2 A sampling toolbox

To test the sampling performance of different sampling methods, a simulation sampling toolbox has been developed using MATLAB 2012b. The sampling toolbox is for laboratory use, which provides diverse sampling methods and reconstruction methods for input of high density surface data. Through a sequential sampling simulation and reconstruction, the performance of different sampling methods can be examined.

Four step procedures are constructed as the modules of the sampling toolbox as shown in Figure 6.7. The user interface of this toolbox is presented in Figure 6.8. The clear and concise interface design shows the good operability of the toolbox.

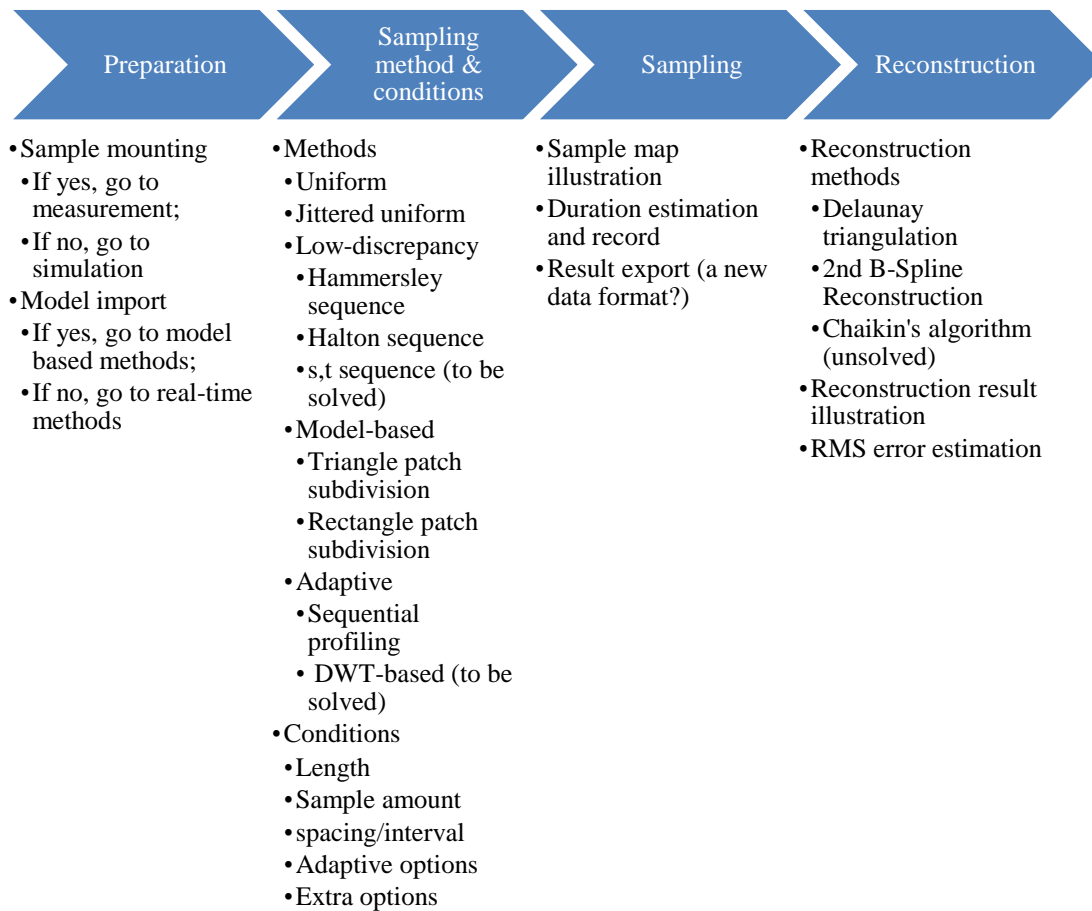


Figure 6.7. The module chart of the sampling toolbox.

1. Preparation. In this step, users are asked to select a surface model or high density sample data for sampling test.
2. Selection of sampling method and conditions. Users are asked to select a sampling method and the related sampling conditions, for example the number of sample points, the minimum sampling distance, or adaptive thresholds for adaptive sampling methods. The current methods available include uniform sampling, jittered uniform sampling, Hammersley pattern sampling, Halton pattern sampling, sequential profiling adaptive sampling, triangle patch model-based sampling and rectangle patch model-based sampling.
3. Sampling. In this step, the sampling process is simulated and the elapsed computation time is recorded. The sampling result is presented at the end and the

result can be exported (the current sampling result can be exported as a .MAT file that is supported by MATLAB).

4. Reconstruction. Surface reconstruction is carried out in this step. Users are required to select proper reconstruction methods. The available reconstruction methods at the moment include the tensor product B-spline reconstruction (the first and third degree) and Delaunay triangulation-based reconstruction (linear and cubic). The recovered data can be exported as a '.sdf' file which can be read by most of surface texture analysis software, for example Surfstand and Mountains.

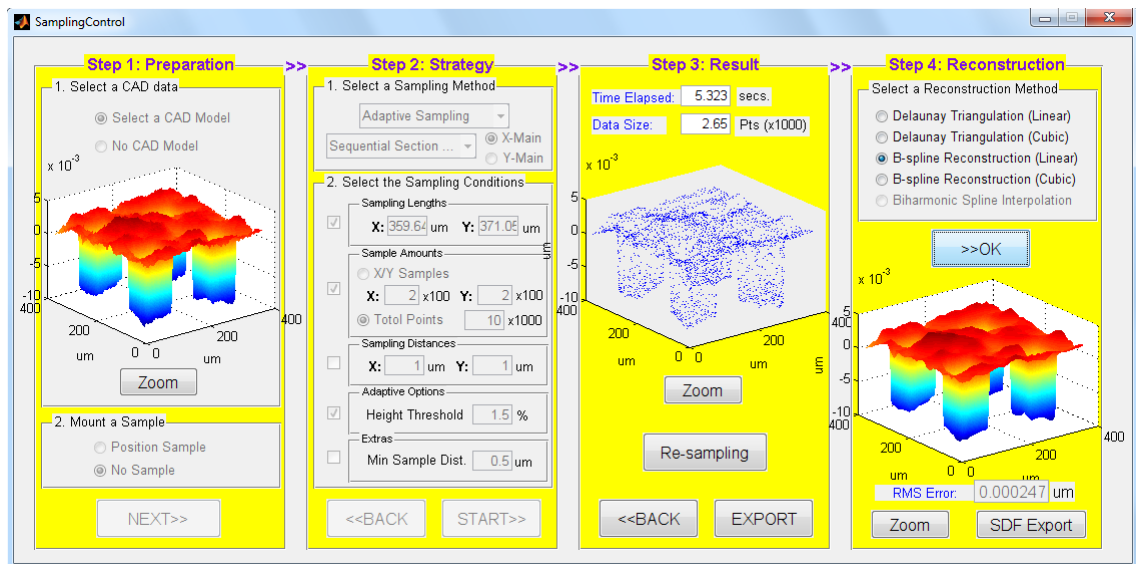


Figure 6.8. The user interface of the sampling toolbox.

6.3 Evaluation of sampling error

With the aid of the described reconstruction and the sampling toolbox, the performance of different sampling methods can be conveniently examined.

The most general error evaluation method is calculation of the RMS value of the height residuals, which are derived from the difference of a sampling-reconstructed surface from the model surface [9, 88]. In this work, the height residuals are analysed as the main sampling error, which is regarded as the RMS deviation because it reveals the height deviations on average.

Other characterisation parameter-based error evaluation methods also prevail. For example conventionally, surface geometry descriptors such as Sa , Sq or Ssk [86] are measured as the comparison criteria. Specifically, researchers tend to compare the Sa of different surface sample results to that of a high density sampled surface. A larger deviation of the Sa implies a worse sampling result. However, in terms of structured surfaces, these statistical parameters, for example the field parameters Sa , Sq , etc., are not meaningful for the characterisation [76].

In a new feature-based characterisation system [68, 127], surfaces, particularly structured surfaces, are treated as a composition of regional geometric features. Characterisation of each individually recognised feature and statistics of the relevant feature attributes have been developed and widely accepted [68]. Some feature-based characterisation parameters are employed as the judging criteria of sampling errors.

6.3.1 Root mean square height deviation

Estimations of the statistical values (for example, RMS value, maximum, etc.) of the height residuals are usually employed when measuring freeform surfaces. In this way, CAD model and the measured surface are compared based on height information and a height residual map can then be obtained (see Figure 6.9). Evaluation of the residuals map would seem to be appropriate for performance comparison of different sampling methods. This solution has been used in nearly all of the current research in metrology [27, 42, 44, 45, 130, 164].

In this study, the RMS height deviation is calculated as one of the main sampling errors using the following equation

$$e = \sqrt{\sum_{i=1}^N (z_i - z'_i)^2}, \quad (6.39)$$

where z_i is each value of the standard high-density sampled data matrix, z'_i is each value of the reconstructed surface data matrix, which has the same sample size as the standard data and N is the size of the high-density sampled data matrix.

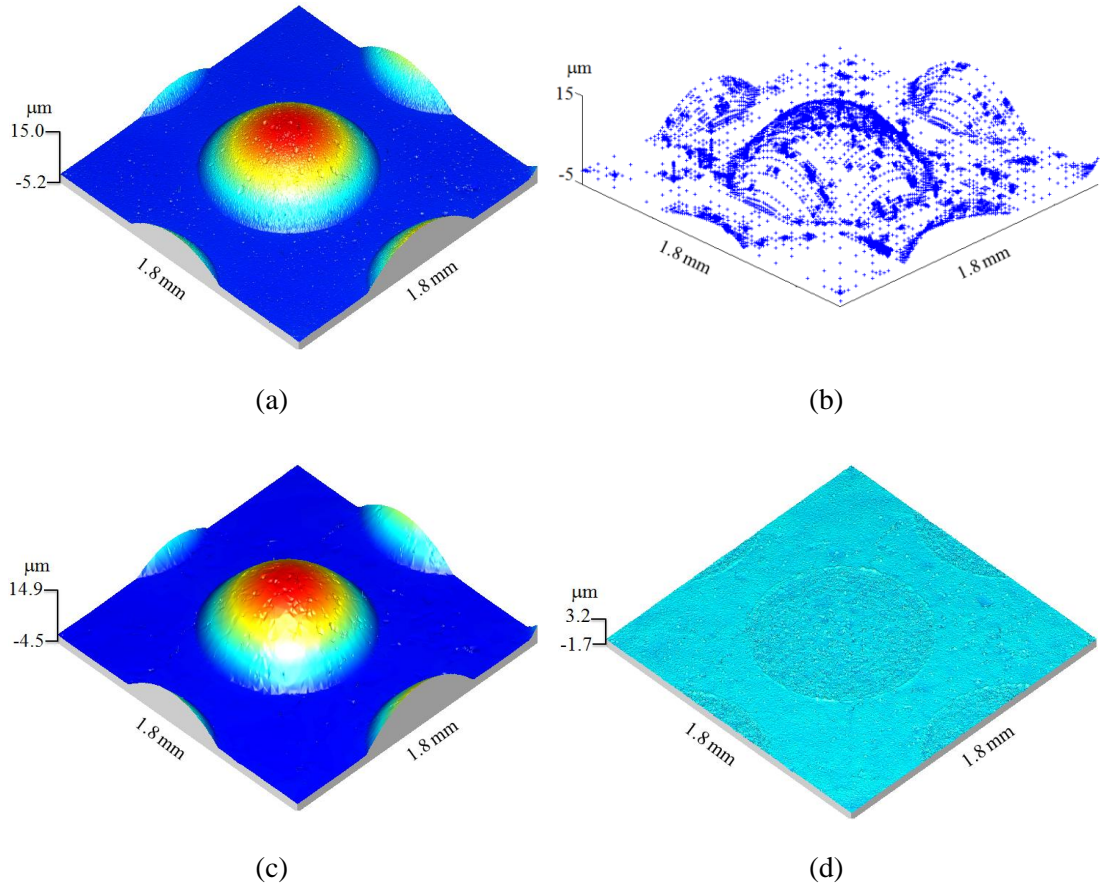


Figure 6.9. Illustration of a height residual map (d) of a sub-sampled surface (c) from the original high-density sample surface (a) using the adaptive samples (b).

6.3.2 Feature-based characterisation

Feature-based characterisation has been recognised as being of high importance in advanced metrology techniques [16], particularly for the characterisation of structured surfaces by extracting micro-scale dimensional parameters [75, 159]. For example, with the “five steps to a feature parameter” toolbox [127], some general feature related parameters can be characterised.

The feature-based parameters are then used for the performance comparison of different sampling methods. For example, the mean absolute deviations of evaluation parameters from that of the original high-density sampled results are investigated in this paper

$$e = \text{mean}(|p_0 - p_i|), \quad (6.40)$$

in which p_0 is an evaluation parameter (for example, step height, roundness) extracted from the original high-density sampled surface and p_i are the corresponding parameters extracted from a reconstructed surface that was sampled at a lower density. For example, Figure 6.10a shows a Fresnel lens surface (Table 6.5c) reconstructed from a 2500 Hammersley pattern sample. The areal segmentation (see Figure 6.10b) is carried out by extracting the feature edges (bold yellow curves). Evaluation parameters p_i such as radius and roundness of a circle feature can be consequently estimated (Figure 6.10c). If repeated tests are carried out, a mean value of the results from the same sampling setting is taken.

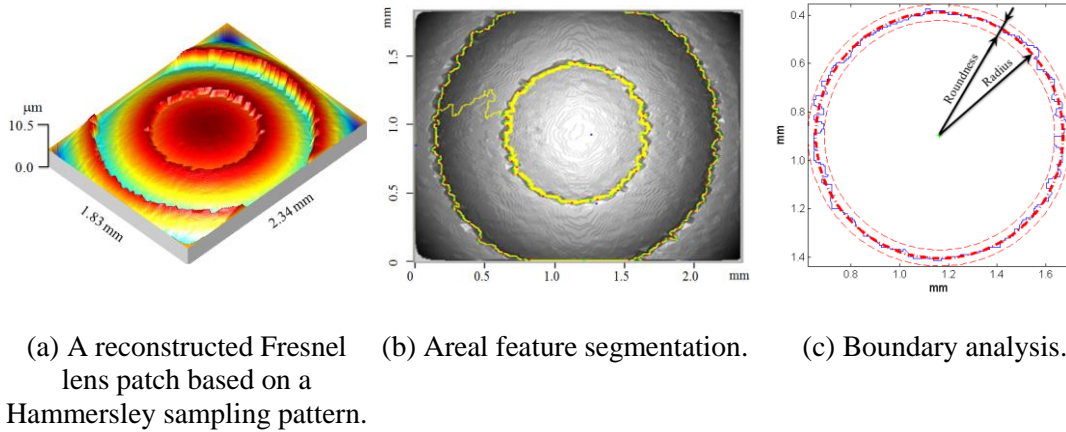


Figure 6.10. A feature-based characterisation of a circle edged feature.

In the following sections, the “five steps to a feature parameter” technique and a developed boundary characterisation algorithm are presented to show how a feature-based parameter is characterised.

6.3.2.1 Five steps to a feature parameter

In the ISO standard 25178 Part 2 [68], a feature characterisation approach is defined with a software toolbox called “five steps to a feature parameter”. The feature characterisation derives from the concept that surface topography is a collection of surface features (for example hills, valleys and saddles, or planar and steps and the

like [100, 159, 174]), and among these, significant features have the main influence on the surface functions. Based on this idea, surface topography can be segmented into a series of significant features and the features can be characterised individually or jointly.

The five steps include: (1) selection of the type of texture feature; (2) segmentation; (3) determining significant features; (4) selection of feature attributes; and (5) attribute statistics.

1) Type of texture feature

The three main ‘Maxwell’ types of texture features are areal features (hills and dales), line features (course and ridge lines) and point features (peaks, pits and saddle points). Other features include step planar and edges, etc.

2) Segmentation

Segmentation is used to determine the regions of the scale-limited surface that define the scale-limited features. For example in Figure 6.11 (middle), a human skin surface is segmented into a series of hill features.

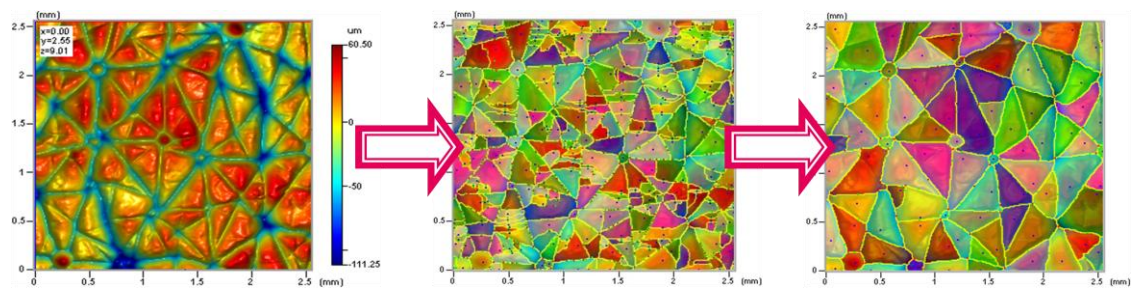


Figure 6.11. A ‘Maxwell’ feature characterisation of a human skin: (left) original surface topography, (middle) initial feature segmentation, (right) denoised result by Wolf prune at 5 %.

3) Determining significant features

A given “function” does not interact with all features in the same way; different features interact differently. Thus it is essential to determine those features that are

functionally significant from those that are not. Figure 6.11 (right) illustrates a denoising result in which the significant features are determined.

4) Selection of feature attributes

Once the set of significant features has been determined, it is necessary to determine suitable feature attributes for characterisation. Most attributes are a dimensional measurement of the feature, for example length, depth, area or volume of a feature (see Table 6.2).

Feature Class	Feature Attributes	Designated Symbol
Areal	Local peak/pit height	lpvh
	Volume of areal feature	VolS/VolE
	Area of areal feature	Area
	Circumference of areal feature	Circ
Line	Length of line	Leng
Point	Local peak/pit height	lpvh
	Local curvature at critical point	Curvature
Areal, Line, Point	Attribute takes value of one	Count

Table 6.2. Common feature attributes suggested by ISO 25178 Part 2 [68].

5) Attribute statistics

Feature attributes constitute calculation of a suitable statistic for the significant features, a feature parameter, or alternatively a histogram of attribute values. An example of feature attribute statistics is given in Table 6.3.

However, the feature attributes of functional surfaces are more wide-ranging than those suggested by ISO standards. More characterisation methods would be needed to extract all the attributes. In this thesis, a “four steps to a micro-scale dimensional parameter” characterisation toolbox is developed to address the dimensional parameters.

Attribute statistic	Designated symbol	Threshold
Arithmetic mean of attribute values	Mean	—
Maximum attribute value	Max	—
Minimum attribute value	Min	—
RMS attribute value	RMS	—
Percentage above a specified value	Perc	Value of threshold in units of attribute
Histogram	Hist	—
Sum of all the attribute values	Sum	—

Table 6.3. Attribute statistics suggested by ISO 25178 Part 2 [68].

6.3.2.2 Four steps to a micro-scale dimensional parameter

There are two major drawbacks of the current feature characterisation toolbox [68]. Firstly, most attributes of the surface features (see Table 6.2) are a measure of the size of simple geometries, whereas possible feature attributes of functional surfaces are far more comprehensive than those listed in [2]. For example, the micro-scale features of a structured surface usually have designed specifications such as size, geometrical tolerance and surface texture [37]. Also in ISO Technical Report ISO/TR 14638 [72], up to eighteen classes of characteristics of geometric features have been described. Secondly, characterisation of the feature boundaries has received little attention. However, the concept of boundary characterisation has been recognised as being of great importance in Verma's research [159].

A boundary analysis method is proposed here based on a tangent analysis algorithm. Dimensional parameters of interest can be easily extracted from a point cloud by sequentially employing the “areal feature segmentation” [126, 142], “boundary segmentation” [145, 159], “dimensional parameter selection” (such as the defined attributes in [68]) and “parameter calculation and statistics” [127]. Specifically, the four steps include:

1. Areal feature segmentation

Areal feature segmentation uses the current “hill and valley” [11] and “edge” [12] feature recognition techniques. A structured surface can be intelligently segmented into many small surface regions with different areal features.

2. Boundary analysis

Once the areal features with their boundaries are obtained, straight line and arc features are extracted from these boundaries. A boundary analysis algorithm is given below. Until this step, all the areal and line features are presented to the users.

3. Selection of the dimensional parameters

The parameters of interest and the reference features are selected in this step. Some of the dimensional parameters are listed in Table 6.4. For example, the size parameter can be an area or volume by selecting areal feature; the distance parameter can be defined as between a point and a straight line by selecting a point and a line feature.

Size (areal)	Distance (areal, line, point)
Area	Plane to plane
Volume	Line to plane
Circle diameter	Point to plane
Square side width	Line to line
Rectangle width/length	Point to line
	Point to point
Radius (line)	Angle (line)
Of a circle or arc	Absolute
	Relative

Table 6.4. Some commonly used dimensional parameters.

4. Parameter calculation and statistics

Using some standard algorithms such as least squares fitting, general geometric features such as straight lines, planes or circles can be evaluated,

and the dimensional parameters can be estimated. A subsequent statistic relating to the parameters of all the related features in other areal feature regions can be calculated, for example in Table 6.3.

6.3.2.3 A boundary analysis algorithm

There are many algorithms that can realize the boundary analysis in step 2 of section 6.3.2.2. A systematic introduction to the prevailing methodologies are given in [13, 145] in terms of image analysis. These methods have similar process methodologies that include an initial segmentation of features and a subsequent region merging process. In this thesis, another solution to characterise straight lines and circle features based on tangent analysis is developed. By applying flexible threshold settings, it is demonstrated by experiments that the proposed method works very well for characterising structured surfaces.

1) Boundary preparation

Surface topography measurement results are usually expressed as a point cloud. Aided by a feature characterisation toolbox [68], different areal features can be segmented by recognising their boundaries (see Figure 6.12a). Boundary data is usually expressed as a simple closed planar curve (see Figure 6.12b).

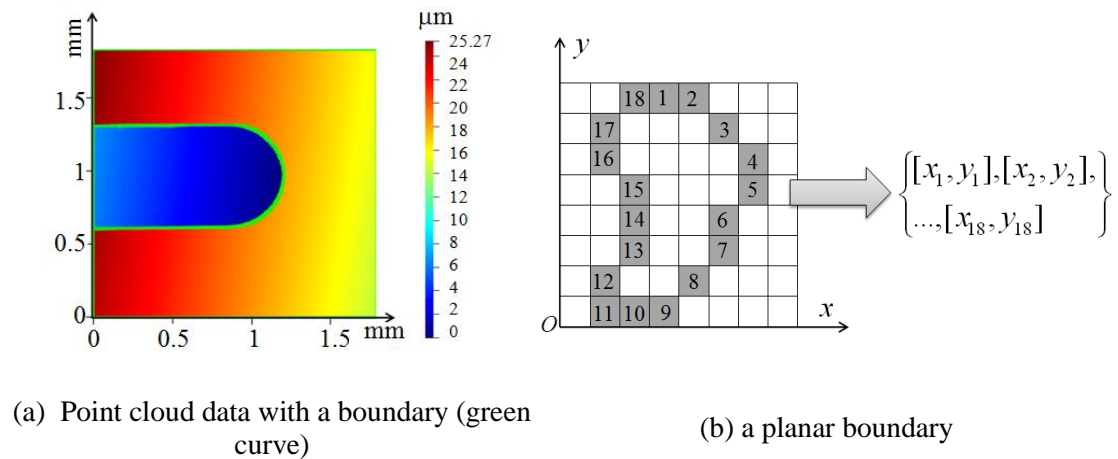


Figure 6.12. Illustration of a boundary data.

2) Initial recognition

This algorithm assumes that all simple closed curves are comprised of straight line and arc segments. This initial recognition is carried out by sequential computation of tangent angles, histogram projection and straight line extraction.

- i. From a starting point, each boundary point and its neighbouring points are successively fitted to a straight line (Figure 6.13a). Then the tangent angles, θ , are recorded according to their boundary point position (Figure 6.13b).
- ii. A histogram (Figure 6.13c) is generated by counting the frequency of occurrence of the tangent angles. In this way, straight lines on a boundary become discrete high peaks, while arcs become valleys which connect neighbouring peaks.

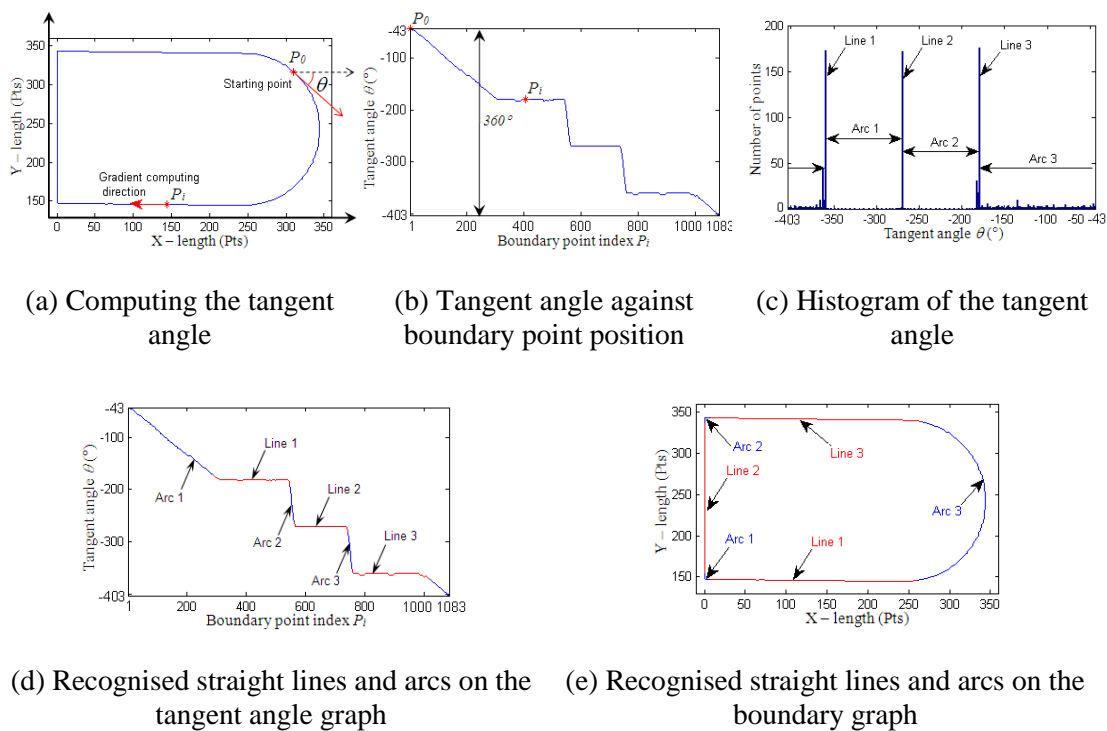


Figure 6.13. Illustration of tangent analysis for a simple boundary.

- iii. A peak-search algorithm is used to find the highest peaks in the histogram. To reduce the influence of noise, a peak height threshold and an angle threshold are pre-set to discriminate neighbouring peaks. From this, straight lines are identified, as shown in Figure 6.13d. The straight line and arc segments are

identified by mapping the boundary indices to the original boundary graph (see Figure 6.13e).

3) Merging of segments

In practical cases, noise would disturb a correct identification as shown in Figure 6.14. A final merging process is needed to prune the small segments. This process involves merging neighbouring straight line segments that are very close. The following criteria are considered for the merging of the segments in this work.

- i. If two neighbouring straight line segments are very close (their distance is less than twenty points), detect the difference between their average tangent angles. If it is less than an angle discrimination threshold (user defined), the connecting arc is considered as noise and they are combined into a new straight line.
- ii. If the length of the straight line segments is less than a preset straight line length threshold (user defined), remove it from the straight line list and combine it with its neighbouring arcs.

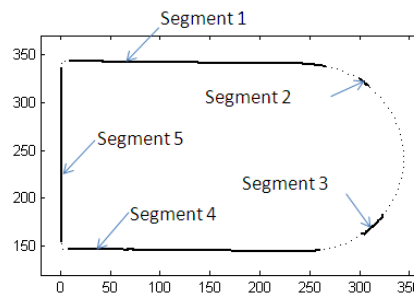


Figure 6.14. A noised segmentation.

6.3.2.4 A feature characterisation case

Type ACG crossed gratings [70] are one type of specimen used for calibrating the horizontal and vertical amplification coefficients and the x - y perpendicularity of an instrument [29]. They are comprised of four indicators as shown in Figure 6.15a: the average pitches in the x and y directions – L_x and L_y , the average angle θ between the

x and y axes and the average depth d . There are no standard algorithms for calibrating the type CG artefacts at present. This case study tries to specify the four indicators to show how feature characterisation works in the characterisation of structured surfaces.

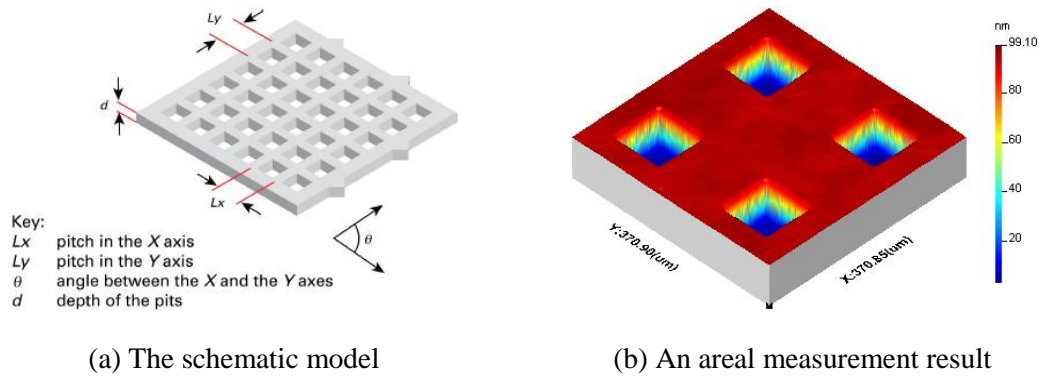


Figure 6.15. Type ACG crossed grating standard.

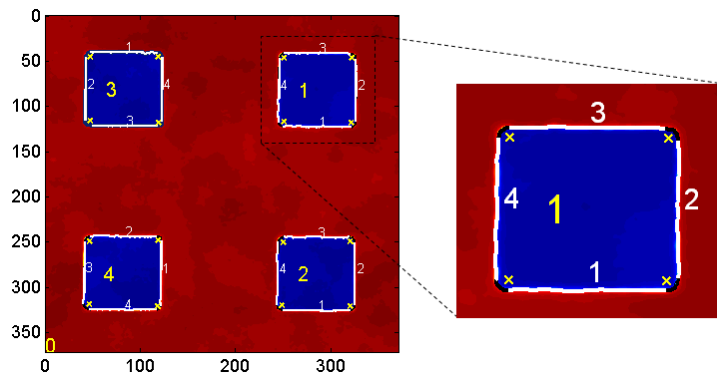


Figure 6.16. A segmentation result of the type ACG measurement result in Figure 6.15.
 (Black regions: arcs; white regions: straight lines; yellow crosses: fitted circle centres)

Firstly, a surface texture measurement data cloud of points (Figure 6.15b) is obtained using an instrument such as a CSI. Then the “four steps to a micro-dimensional parameter” command is applied. Using the edge detection method in [174] with a Wolf prune coefficient of 5 % in Step 1, an angle discrimination threshold of 10° and a length threshold of ten points in Step 2, the surface features such as square holes, straight line edges and their connected corners of 90° can be successfully extracted. As shown in Figure 6.16, the yellow coloured numbers are the indices of the

recognised areal features; their boundaries are split into straight line and arc segments which are coloured in white and black respectively.

After all the features are recognised, the key characterising indicators can be estimated using proper mathematical methods. For example, the average depth d can be computed using least squares plane fitting; the average pitch L_x , L_y and the included angle θ can be estimated using the least squares straight line fitting.

6.4 Numerical experiments

Based on the introduced reconstruction methods, the sampling toolbox and evaluation approaches described in earlier sections, performance tests of the diverse sampling methods are carried out in the following experiment.

6.4.1 Experimental settings

Three basic types of structured surfaces are employed as the testing surfaces, which include a linear pattern, a tessellation and a rotationally symmetric pattern (see Table 6.5). The multi-patterned type described in Chapter 2 is not discussed here because it can be seen as a composition of the other three basic types. Specifically, the three representative structured surfaces include a five parallel-grooves calibration artefact, a nine pits crossed-grating calibration artefact and a Fresnel lens central patch. They are measured at a high accuracy with the instrument-allowed sample densities (see Table 6.5a, b and c) which are used with reference data for the comparison of the sampling performance test. A performance evaluation procedure is described as follows.

1. Standard data preparation.

For a given real surface, obtain the standard measurement result (for example a 1024×1024 regular lattice of data) using the instrument-allowed high density sample setting. Standard feature related parameters (for example groove-width, step height, see Table 6.5, which are selected with consideration to the main functions of the structured surfaces) are characterised for later use.

2. Sampling.

Re-sample the standard surface data using different sampling methods and sample sizes. In this study, seven sampling methods and six different sample sizes (see Table 6.5) on each of the specimens are tested.

3. Reconstruction.

Employ potential reconstruction methods to reconstruct the “continuous” surface with the same sample design as the originals – the standard measurement result. The best reconstruction results with the lowest RMS height deviations are selected.

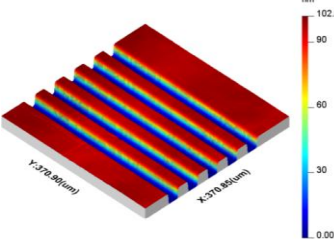
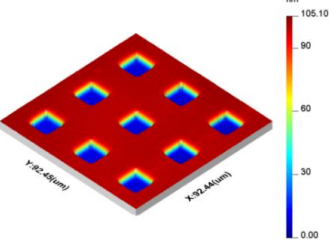
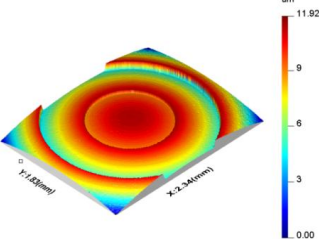
	Sample 1	Sample 2	Sample 3
Specimen names	Five-parallel-grooves calibration artefact	Nine-pits-crossed-grating calibration artefact	Fresnel lens central patch
Rendering of the high-density sampled results	 <p>(a) five-parallel-grooves (linear pattern) (1024 × 1024)</p>	 <p>(b) nine-pits-crossed-grating (tessellation) (256 × 256)</p>	 <p>(c) Fresnel lens (rotationally symmetric) (358 × 240)</p>
Evaluation parameters	<ol style="list-style-type: none"> 1. RMS height deviation 2. Mean groove width 3. Step height 	<ol style="list-style-type: none"> 1. RMS height deviation 2. Mean pitch distance 3. Step height 	<ol style="list-style-type: none"> 1. RMS height deviation 2. Radius of the central lens boundary 3. Roundness of the central lens edge
Tested sample sizes	Six sizes: 2.5k, 10k, 40k, 90k, 160k and 250k	Six sizes: 1.2k, 2.5k, 5k, 10k, 15.6k and 22.5k	Six sizes: 1.2k, 2.5k, 5k, 10k, 22.5k and 40k

Table 6.5. The three typical structured surface specimens and the experimental settings.

4. Performance evaluation.

Extract the RMS height deviations for each reconstructed data from the standard data; extract feature related parameters from each reconstructed surface and calculate the differences from the standard measurement results.

The smaller the height residual or a parameter difference, the better of performance the used sampling design has.

Note that the tested sample sizes are selected based on the following criteria: (1) the tested sample sizes are representatively selected which indicates they may be normally used in practical measurements; (2) the tested sample cannot be too small in which case excessive reconstruction distortion occurs; (3) the tested sample size cannot be too large in which case the reconstruction error causes minor fluctuations and the evaluation process may be time consuming.

6.4.2 Results and conclusions

The results in Table 6.6 show the sampling errors, i.e. the RMS height deviations and the discrepancies of each evaluation parameter between each sampling-reconstruction result, and the standard high-density sample result. These results indicates that the sampling error has a power function-like relationship against sample size

$$y = cx^b, \quad (6.41)$$

where y is sampling error, x denotes the sample sizes, and c and b need to be calculated to give a best fit function. Other researchers have shown similar results [81, 130, 164, 172]. A linear plot of the sampling errors against the sample sizes cannot render a clear performance comparison when sample size increases.

Since a linear relationship exists between $\ln y$ and $\ln x$ deduced from the above power function

$$\ln y = \ln c + b \ln x, \quad (6.42)$$

log-log plotting is employed in this thesis so that the sampling performance can be shown clearly. By plotting the sampling-reconstruction errors against the sample sizes and giving the best fitting power functions, the sampling errors of each evaluation parameters extracted from the numerical experimental results are presented in Table 6.6. To give a better understanding of the acceptable range of the sampling error, the

tolerance levels^{xv} for different measurement tasks are also given. The sampling design with lower sampling errors under tolerance levels are regarded as acceptable.

The three graphs in the first row of Table 6.6 show the RMS height deviations of the sampling-reconstructed surface from the ‘standard’ measurement results for the three specimens in Table 6.5. The second row of Table 6.6 show the evaluation errors of later key feature attributes for the three specimens, respectively groove width for linear pattern, pitch distance for tessellation, and radius for rotational symmetric pattern. The third row of Table 6.6 shows the evaluation errors of step heights for linear and tessellation patterns, and roundness for the central lens boundary of Sample 3.

In general, all the nine graphs show a consistent trend that different sampling errors decrease along the increase of used sample sizes, with the only exception in Table 6.6f the rectangle-patch adaptive sampling error fitting curve. The reason is that in the characterisation of the radius of the central Fresnel lens boundary (Table 6.6f), recognition of the feature boundaries fail for many cases with limited sampling points. In these tests, only three characterisation processes (blue crosses with dashed curves) succeed (also for Table 6.6j) which means the only three successful sample value-based fitting trend may be instable in a high probability. The consistent changing trend of the sampling error versus sample size is still widely expected.

Other anomalies can also be observed. For example the blue solid line in Figure 6.6e shows awful performance of uniform sampling when measuring mean pitch distances. This could be caused by the inherent aliasing of uniform sampling. Because the grid features in Sample 2 have boundaries along x - and y -directions. Loose uniform sampling positions tends to miss the real boundaries. This drawback can be

^{xv} For Sample 1 and Sample 2 which have similar scales, considering the instrumental limits and sample scales, the lateral acceptable measuring error is 360 nm which is the lateral resolution of the used interferometer; while the height tolerance level is 2.5 nm which is 2.5 % of the extreme height of the specimens (instrumental vertical resolution is 10 pm which is significant small and can be ignored). For Sample 3, the vertical acceptable measuring error is 0.25 μm which 2.5 % of the extreme height of this specimen and about eight times (instrumental vertical resolution is 80 nm which is smaller than this value); while the tolerances of lateral radius and roundness are 3.5 μm and 1.7 μm which are respectively the $\frac{1}{2}$ and $\frac{1}{4}$ of lateral resolution of the used profilometers.

complemented by jittered sampling and other methods. Table 6.6b also presents not good performance of uniform sampling for the evaluation of groove width of linear features because of aliasing in x -direction. It can be regarded as rational that when employing uniform sampling on tessellation patterns, the aliasing is further amplified because of double aliasing in both x - and y -directions.

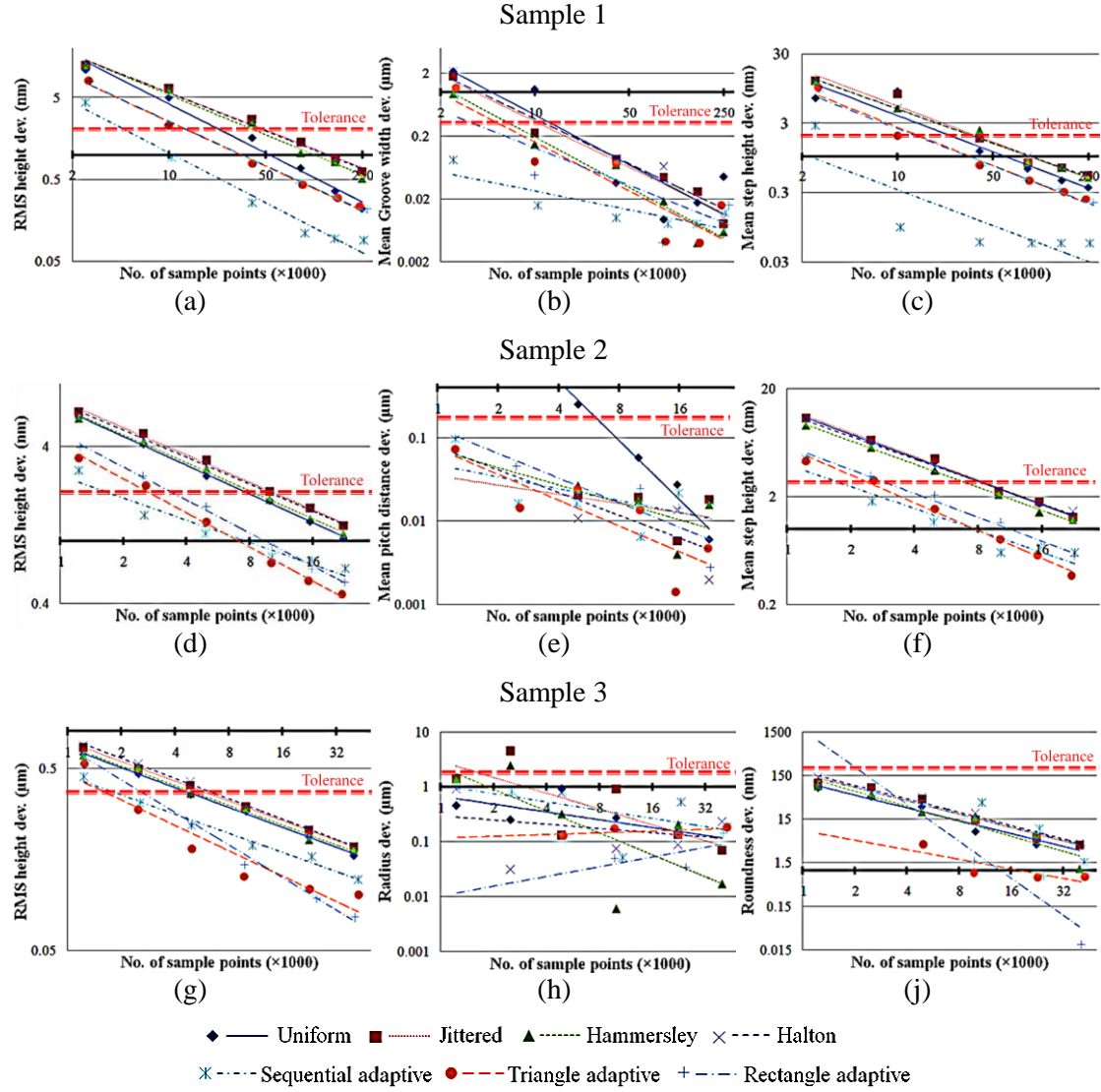


Table 6.6. Deviations of the evaluation parameters from the standard result for Sample 1, Sample 2 and Sample 3. (log-log plots)

The following conclusions can be drawn in sequence.

1. Adaptive sampling methods usually have prominent advantages over other methods in terms of minimising the sampling error (height deviations and feature parameters) for structured surfaces.
2. Uniform sampling, jittered uniform sampling, Hammersley pattern and Halton pattern sampling have similar capabilities in terms of retaining the measuring accuracies for measurement of structured surfaces. None of the methods show clear advantages over others.
3. For measuring linear patterns, sequential profiling adaptive sampling always has distinct advantages over other methods.
4. For measuring tessellations, the three adaptive methods show their advantages on measuring the height related parameters such as step height. They have similar capabilities as other fixed sampling patterns when measuring lateral parameters such as mean pitch distance.
5. For measuring rotationally symmetric patterns, triangle patch and rectangle patch adaptive subdivision samplings show significant advantages.

Low-discrepancy pattern sampling methods have similar performance to uniform or jittered uniform sampling. For the measurement of structured surfaces, the advantages of low-discrepancy pattern sampling methods are not apparent and sometimes these methods may not be an improvement over uniform methods. Sometimes, uniform sampling may be a better solution compared to other fixed patterns; evidence for this can be seen in Table 6.6a. This conclusion coincides with the experiments in Section 5.3.

The fundamental advantages of adaptive sampling are in evidence in this thesis. These methodologies allocate their sampling efforts according to their earlier sample results or models. In other words, they can adapt the sampling effort to key positions which have higher impact factors for enhancing the reconstruction accuracy than others. Although adaptive sampling approaches have no clear advantages for measuring the pitch distance of crossed-gratings (see Table 6.6e), they have been shown to be effective for other structured surfaces and other parameters of tessellated surfaces.

The challenges, however, of applying adaptive sampling to practical measurement still exist. Sequential profiling adaptive method may suffer from the mechanical constraints of stability (for example thermal drift) and accuracy in y-direction scanning. Most of the other efficient sampling methods are difficult to implement within the operation envelope of stylus instruments, with regard to complex scan route designs and redundant scan duration. In terms of interferometers, many of the reviewed sampling methods may be promising, with the aid of a high resolution CCD and pixel stratification process or lens auto-switch systems. However, considering the inevitable positioning errors and optical resolution constraints, a specialised research work on intelligent sampling for interferometers may be required. In addition, more theoretical work is necessary to further the research on intelligent sampling. For example, the data storage solutions need to be reconsidered as has been introduced at the beginning of this paper. The reverse problem of sampling and reconstruction needs to be fully investigated on the basis of geometric measurement. Also, determination of the sample size for an adaptive measurement is a challenging research topic which requires particular attention.

6.5 Summary and conclusions

A summary of the evaluation related issues is given below.

1. Reconstruction is the reverse process of sampling. Many reconstruction techniques have been developed to reconstruct discrete sampling data of surface topography to its continuous form. For intelligent sampling, the sampling data is normally used after an accurate reconstruction. Hence, non-uniform sample data can be processed using matrix computations.
2. At present, reconstruction techniques are usually investigated separately from the sampling methods in geometric measurements. The relationship between sampling and reconstruction has not been clearly understood within current researchers in surface measurement. The author recognises this point and hopes future research on surface sampling can be carried out to fully address this issue.

3. Two categories of reconstruction techniques are selected for use because of their popularity and computational stability. They are the tensor product reconstruction with B-splines and the Delaunay triangulation-based reconstructions. The preceding investigation results show that tensor product methods have computational convenience for the reconstruction of regular grid or partially regular grid samples. Triangulation-based reconstruction costs more in terms of computation but is flexible and robust for diverse sample patterns.
4. To conveniently test the performance of different sampling methods, a sampling toolbox has been developed. This toolbox embeds the introduced sampling methods and reconstruction algorithms. With this tool, sampling can be numerically simulated and the reconstructed continuous surface can be easily obtained.
5. There are different methods to evaluate sampling error. The most general method is regarded to be the RMS height deviation. This quantity has been widely used in the evaluation of freeform surfaces. The RMS height deviation evaluates the average height difference between the sampling-reconstructed surface and the original surface. Considering the specialty of structured surfaces, feature-based characterisation is employed for error evaluation. By designating some of the key feature parameters, the sampling-reconstructed surfaces and the original surface are all characterised. The error of the feature parameters between the original surface and the reconstructed surfaces are evaluated for reference.
6. With the theoretical preparations on reconstruction and error evaluation, the performance comparison test has been carried out on three representative structured surfaces. On the basis of the comparison results, no prominent advantages were found between the fixed sampling patterns, i.e. uniform sampling, jittered uniform sampling, Hammersley pattern and Halton pattern sampling. The model-based sampling and adaptive sampling methods show distinctive performances in most cases. In particular, the proposed sequential profiling adaptive sampling shows remarkable advantages for the measurement of linear patterned structured surfaces.

7. The difficulties of transferring intelligent sampling techniques to practical instruments are challenging. For example, the mechanical and optical limitations of stylus instruments or interferometers have not been considered at the moment; and the reverse problem of sampling and reconstruction has not been fully understood.

With successful solutions to these challenges, efficient samplings are a promise prospect for the next generation of measurement techniques, especially where large areas need to covered with high resolution.

7. CONCLUSIONS AND FUTURE WORK

7.1 The research conclusions

This thesis concerns the improvement of sampling techniques for the measurement of structured surfaces, which is regarded as a solution to the contradiction of the measurement accuracy and efficiency when measuring structured surfaces.

Global statistical sampling and local uniform sampling with diverse intelligent sampling methods have been investigated. All the current sampling techniques are developed for use in computer graphics and coordinate metrology. On account of this situation, a sequential profiling adaptive sampling has been developed for surface topography measurement, in particular the measurement of structured surfaces. A performance test has been carried out at the end of the thesis and the efficiency of the proposed sampling method is validated.

The three preset objectives of this thesis have been sequentially obtained. The contributions of this thesis are summarised in this section. The research conclusions generated from this work are also included.

1. An investigation of the background information on the measurement of structured surfaces was carried out. A practical sampling framework was proposed.
 - a. The state of the art in the measurement of structured surfaces was investigated. Specifically surface definitions, general applications, measurement tasks and the challenges of structured surfaces were summarised. Among the measurement challenges, the challenge to guarantee both high measurement efficiency and accuracy demands a revolution of sampling design.
 - b. A practical sampling framework was proposed for the general measurement of structured surfaces. This framework has been used in practical cases which include global sampling and sequential local sampling. Here the

sampling framework was firstly summarised and suggested to be considered in general measurement procedures.

- c. Global sampling is concerned with a selection of sampling units from a surface topography population. Hence an evaluation of the sample units can be taken to estimate some properties of the population. Global sampling procedures normally include determination of sampling units, selection of sampling methods and determination of sample sizes in sequence.
 - d. Local sampling is concerned with discretisation of a surface topography; after which the original surface can be recovered from the discrete samples. A general procedure for local sampling includes determination of sampling methods, selection of the sampling conditions and reconstruction methods. Specifically, the sampling conditions include sample size, spacing (interval) and sample lengths (areas).
 - e. Uniform sampling is the prevailing local sampling technique at present. However, the drawbacks of uniform sampling have been recognised nowadays along with the emergence of structured surfaces, for example spectral aliasing and the lack of measurement efficiency. Intelligent sampling has been recognised as an efficient solution to this problem. Intelligent sampling has been developed in the areas of statistics, computer graphics and coordinate metrology. However, the surface topography of structured surfaces requires new intelligent sampling methods that better fit the purpose in terms of enhancing measurement efficiency and accuracy.
2. Determination of the sampling conditions of uniform sampling is revisited and new conclusions are found.
- a. Selection of the sampling interval/spacing based on past research, for example spectral aliasing analysis and parameter variation, was investigated. The study in this thesis show that the past research outputs are not well adapted to the measurement of structured surfaces. Therefore, the practical limitations, for example tip size employed, and the feature characteristics,

become the selection considerations. ISO 25178 Part 3 [69] recommends that the maximum sampling spacing be set as $1/5$ of the S-filter nesting index (i.e. the wavelength of the smallest features of interest). A series of common values have been recommended for convenience of practical use.

- b. Selection of the sampling length/area has been rarely discussed in the past. This consideration directly relates to frequency sampling. In order to give an accurate spectral analysis, selection of sampling length needs to be carefully treated. The research conclusion shows that the sampling length should be an integer (or close to an integer, for example ten times) multiple of the feature period of a structured surface.
3. Potential intelligent sampling methods were investigated and a novel adaptive sampling was developed. Followed by an error evaluation test, the performance of adaptive sampling and other intelligent methods were validated.
- a. There are four categories of intelligent sampling methods generated from statistics, computer graphics and coordinate metrology. They are referred to as jittered uniform sampling, low-discrepancy pattern sampling, model-based sampling and adaptive sampling in this thesis. Past research shows that these intelligent sampling methods perform efficiently and accurately, compared to uniform sampling.
 - b. None of the present intelligent sampling methods were developed for the measurement of structured surfaces. On account of this situation, a sequential profiling adaptive sampling was developed which is designed for raster scan-based instruments. The sequential profiling sampling method is supposed to have prominent advantages for the measurement of tessellated and linear structured surfaces, compared to uniform methods. Numerical results have shown prominent advantages of this technique compared to current uniform sampling methods. Specifically
 - i. The sequential profiling adaptive sampling usually produces 20 % to 50 % lower RMS residual error than uniform sampling when using

the same sample size. This implies that at the same accuracy level, the sequential profiling adaptive sampling usually needs 40 % to 60 % less sample size than uniform sampling.

- ii. The sequential profiling adaptive sampling usually costs 20 % to 50 % less measuring time (proportional to the number of scanning profiles) than uniform sampling for the measurement of linear patterns and rectangular tessellation structured surfaces, when implementing the same sample size. This indicates to have the same measurement requirement regarding to sampling accuracy, the sequential profiling adaptive sampling is able to achieve a 50 % to 80 % improvement in reduction of measuring duration compared to uniform methods.
- c. Reconstruction techniques are investigated as the reverse process of sampling. The relationship between reconstruction and sampling has not been clearly understood in current geometric metrology. In this thesis, two kinds of the most popular reconstruction methods for non-uniform data were used.
- d. A sampling test toolbox was developed for the laboratorial use. The selected sampling methods and reconstruction algorithms were imbedded in this tool. Hence, the sampling-reconstruction process can be conveniently performed.
- e. The most widely used sampling error evaluation indicator is the root mean square height deviation. This error has been used in the sampling test for the measurement of freeform surfaces. For the measurement of structured surfaces, a feature-based characterisation technique based on a self-developed boundary segmentation algorithm was proposed. The dimensional parameters of micro/nano-scale surface features can be characterised and hence they can be easily compared.
- f. Finally a sampling test experiment was carried out. Selected seven representative sampling methods are tested. With proper reconstruction,

some selected characterisation indicators were measured. Hence, the sampling error was characterised for each sampling method. The experimental results show that model-based sampling and adaptive sampling methods have distinct performance over others in most of the cases for the measurement of structured surfaces. In particular, the proposed sequential profiling adaptive sampling shows remarkable advantages for the measurement of the linear patterned structured surfaces.

- g. As an innovative measurement technique, intelligent sampling presents many difficulties when transferring to practical instruments. Efficient samplings can be promising for the next generation of measurement techniques if the challenges can be successfully solved.

Of the contributions mentioned above, the most important have been summarised briefly at the beginning of the thesis, i.e. Section 1.5.

In brief, this thesis presents an initial research into sampling for the measurement of structured surfaces. Some of the conclusions can also be applied to the measurement of stochastic surfaces, for example the proposed general sampling framework and the conclusions obtained in the global sampling stage. Intelligent sampling is assumed to be the next generation of the sampling techniques. The numerical evidence in this thesis shows that intelligent sampling can guarantee the measurement efficiency and the accuracy. However, much research work still needs to be carried out, for example, theoretical solutions regarding the relationship between sampling and reconstruction, and the difficulties of instrumental design.

7.2 Future work

The research conclusions indicate that some future work is necessary before intelligent sampling can be made fully available for practical measurement. This future work can be divided into two separate parts which concentrate on the mathematics and instrumental design.

The first part is related to the theoretical improvement. There are many intelligent local signal sampling methods at present. However, reconstruction techniques are

rarely investigated in terms of a combined consideration with the novel sampling methods. Sampling and reconstruction have usually been treated separately. This situation seems to have created a bottleneck in the current sampling development. Various developments of sampling methods or reconstruction methods can bring improved efficiency to future measurements; however, intelligent sampling methods simultaneously produce complexities in the practical use. Robust research on the relationship between sampling and reconstruction is expected to be the next step. The research output can then be used to guide the sampling design for the measurement of surface topography.

Secondly, the practical challenges of applying intelligent sampling to practical measurements need to be resolved. For example, the determination of the sample size for an adaptive measurement is a very difficult question requiring particular attention. Sequential profiling adaptive method may suffer from the mechanical constraints of stability and accuracy in y-direction scanning. Other efficient sampling methods are still difficult to implement within the operation envelope of stylus instruments. Interferometers may require a high resolution CCD and pixel stratification process or lens auto-switch system to realize efficient sampling. The proposed sequential profiling adaptive sampling can only be used for raster scan-based instruments. In addition, considering the inevitable positioning errors and optical resolution constraints, research into non-model-based adaptive sampling for interferometers is in urgent demand. Data storage solutions also need to be reconsidered which was discussed at the beginning of this paper. The feasibility of applying intelligent sampling in current instruments needs to be investigated.

With developed supporting theory and practical improvement, efficient sampling methods are a promising proposition for the next generation of measurement techniques, especially where large areas need to be covered with high resolution.

REFERENCES

- [1] 3M Abrasive Systems Div. (1997) Trizact Abrasives. Product catalog 60-4400-3566-9 (273) BE.
- [2] Abramowitz M, Stegun IA (1964) Handbook of Mathematical Functions: With Formulas, Graphs, and Mathematical Tables. Dover Publications.
- [3] Aldroubi A, Cabrelli C, Heil C, Kornelson K, Molter U (2010) Invariance of a Shift-Invariant Space. *Journal of Fourier Analysis and Applications* 16(1):60-75.
- [4] Aldroubi A, Feichtinger H (1998) Exact Iterative Reconstruction Algorithm for Multivariate Irregularly Sampled Functions in Spline-Like Spaces: The L^p -Theory. *Proceedings of the American Mathematical Society* 126:2677-2686.
- [5] Aldroubi A, Gröchenig K (2000) Beurling-Landau-Type Theorems for Non-Uniform Sampling in Shift Invariant Spline Spaces. *Journal of Fourier Analysis and Applications* 6(1):93-103.
- [6] Aldroubi A, Gröchenig K (2001) Nonuniform Sampling and Reconstruction in Shift-Invariant Spaces. *SIAM Rev* 43(4):585-620.
- [7] Alting L, Kimura F, Hansen HN, Bissacco G (2003) Micro Engineering. *CIRP Annals - Manufacturing Technology* 52(2):635-657.
- [8] ASME B46.1 (2009) Surface Texture (Surface Roughness, Waviness, and Lay).1-98.
- [9] Barari A, ElMaraghy HA, Knopf GK (2007) Search-Guided Sampling to Reduce Uncertainty of Minimum Deviation Zone Estimation. *Journal of Computing and Information Science in Engineering* 7(4):360-371.
- [10] Barker RM, Cox MG, Forbes AB, Harris PM (2004) Best Practice Guide No. 4 Software Support for Metrology: Discrete Modelling and Experimental Data Analysis. Teddington, UK.
- [11] Barthlott W, Neinhuis C (1997) Purity of the Sacred Lotus, or Escape from Contamination in Biological Surfaces. *Planta* 202(1):1-8.
- [12] Benedetto J, Ferreira PJSG (2001) Modern Sampling Theory: Mathematics and Applications. Birkhäuser.
- [13] Besl PJ, Jain RC (1988) Segmentation through Variable-Order Surface Fitting. *IEEE Trans Pattern Anal Mach Intell* 10(2):167-192.
- [14] Bico J, Thiele U, Quéré D (2002) Wetting of Textured Surfaces. *Colloids and Surfaces A: Physicochemical and Engineering Aspects* 206(1-3):41-46.
- [15] Bissacco G (2004) Surface Generation and Optimization in Micromilling (PhD Thesis). Technical University of Denmark.
- [16] Blunt L, Jiang X (2003) Advanced Techniques for Assessment Surface Topography: Development of a Basis for 3D Surface Texture Standards "Surfstand". Kogan Page Science, London.
- [17] Blunt L, Xiao S (2010) The Use of Surface Segmentation Methods to Characterise Laser Zone Surface Structure on Hard Disc Drives. *Wear* 271(3-4):604-609.
- [18] Boden SA, Bagnall DM (2006) Bio-Mimetic Subwavelength Surface for near-Zero Reflection Sunrise to Sunset. See <http://eprints.ecs.soton.ac.uk/14404/>
- [19] Breitenbach A (1999) Against Spectral Leakage. *Measurement* 25(2):135-142.

- [20] Bruzzone AAG, Costa HL, Lonardo PM, Lucca DA (2008) Advances in Engineered Surfaces for Functional Performance. *CIRP Annals - Manufacturing Technology* 57(2):750-769.
- [21] Candès EJ (2006) Compressive Sampling. *Proceedings of the International Congress of Mathematicians, Madrid, Spain*, pp. 1433-1452.
- [22] Cazals F, Giesen J, Boissonnat J-D, Teillaud M (2006) Delaunay Triangulation Based Surface Reconstruction. in *Effective Computational Geometry for Curves and Surfaces*. Springer Berlin Heidelberg, pp. 231-276.
- [23] Chaikin GM (1974) An Algorithm for High-Speed Curve Generation. *Computer Graphics and Image Processing* 3(4):346-349.
- [24] Chambers RL, Skinner CJ (2003) *Analysis of Survey Data*. John Wiley and Sons.
- [25] Chatfield C (1996) *The Analysis of Time Series: An Introduction*, Fifth Edition. Chapman & Hall.
- [26] Cheung BCF, Lee WB, Kong LB, To S (2009) Development of a Surface Intrinsic Feature Based Method for Generic Form Characterization of Ultra-Precision Freeform Surfaces. *EUSPEN Special Group Meeting*, Edinburgh.
- [27] Cho MW, Kim K (1995) New Inspection Planning Strategy for Sculptured Surfaces Using Coordinate Measuring Machine. *International Journal of Production Research* 33(2):427-444.
- [28] Clabburn R (2004) *Stepped Surface Diffuser*. Microsharp Corporation Limited.
- [29] Claudiu LG, Richard KL, Frank H (2012) Calibration of the Scales of Areal Surface Topography Measuring Instruments: Part 2. Amplification, Linearity and Squareness. *Measurement Science and Technology* 23(6):065005.
- [30] Coleman B, Meehan P, Reidy J, Weeks P (1987) Coherent Sampling Helps When Specifying DSP A/D Converters. *EDN*.
- [31] Corbett J, McKeown PA, Peggs GN, Whatmore R (2000) *Nanotechnology: International Developments and Emerging Products*. *CIRP Annals - Manufacturing Technology* 49(2):523-545.
- [32] Cox MG (1972) The Numerical Evaluation of B-Splines. *IMA Journal of Applied Mathematics* 10(2):134-149.
- [33] Danzl R, Helml F, Scherer S (2009) Focus Variation - a New Technology for High Resolution Optical 3D Surface Metrology. *The 10th International Conference of the Slovenian Society for Non-Destructive Testing*, Ljubljana, Slovenia.
- [34] Davies MA, Evans CJ, Patterson SR, Vohra R, Bergner BC (2003) Application of Precision Diamond Machining to the Manufacture of Micro-Photonics Components. *Proceedings of the SPIE* 5183:94-108.
- [35] De Chiffre L, Kunzmann H, Peggs GN, Lucca DA (2003) Surfaces in Precision Engineering, Microengineering and Nanotechnology. *CIRP Annals - Manufacturing Technology* 52(2):561-577.
- [36] Delaunay (1934) Sur La Sphere Vide. *Izv Akad Nauk SSSR Otdelenie Matematicheskii i Estestvennyka Nauk* 7(7):793-800.
- [37] Denkena B, Käßner J, Wang B (2010) Advanced Microstructures and Its Production through Cutting and Grinding. *CIRP Annals - Manufacturing Technology* 59(1):67-72.
- [38] Dong WP, Mainsah E, Stoutt KJ (1996) Determination of Appropriate Sampling Conditions for Three-Dimensional Microtopography Measurement. *International Journal of Machine Tools and Manufacture* 36(12):1347-1362.

- [39] Donoho DL (2006) Compressed Sensing. *Information Theory, IEEE Transactions on* 52(4):1289-1306.
- [40] Duarte MF, Davenport MA, Takhar D, Laska JN, Ting S, Kelly KF, et al. (2008) Single-Pixel Imaging Via Compressive Sampling. *Signal Processing Magazine, IEEE* 25(2):83-91.
- [41] Duffin RJ, Schaeffer AC (1952) A Class of Nonharmonic Fourier Series. *Transactions of the American Mathematical Society* 72(2):341-366.
- [42] Edgeworth R, Wilhelm RG (1999) Adaptive Sampling for Coordinate Metrology. *Precision Engineering* 23(3):144-154.
- [43] El-Ali J, Sorger PK, Jensen KF (2006) Cells on Chips. *Nature* 442(7101):403-411.
- [44] Elkott DF, Elmaraghy HA, Elmaraghy WH (2002) Automatic Sampling for CMM Inspection Planning of Free-Form Surfaces. *International Journal of Production Research* 40(11):2653 - 2676.
- [45] Elkott DF, Veldhuis SC (2005) Isoparametric Line Sampling for the Inspection Planning of Sculptured Surfaces. *Computer-Aided Design* 37(2):189-200.
- [46] Evans CJ, Bryan JB (1999) "Structured", "Textured" or "Engineered" Surfaces. *CIRP Annals - Manufacturing Technology* 48(2):541-556.
- [47] Firby PA (1987) Controlling Interference in Graphics. *The Mathematical Gazette* 71(456):118-124.
- [48] Fujisawa N, Poole-Warren LA, Woodard JC, Bertram CD, Schindhelm K (1999) A Novel Textured Surface for Blood-Contact. *Biomaterials* 20(10):955-962.
- [49] Gad-el-Hak M (2002) *The Mems Handbook*. CRC Press.
- [50] G  hlin R, Ax  n N, Jacobson S (1998) The Influence of Tip Shape in Abrasion Studied by Controlled Multiasperity Surfaces. *Wear* 223(1-2):150-156.
- [51] G  hlin R, Jacobson S (1999) The Particle Size Effect in Abrasion Studied by Controlled Abrasive Surfaces. *Wear* 224(1):118-125.
- [52] Golub GH, Loan CFV (1996) *Matrix Computations* (3rd ed). Johns Hopkins University Press.
- [53] Gombert A, Glaubitt W, Rose K, Dreibholz J, Bl  si B, Heinzl A, et al. (2000) Antireflective Transparent Covers for Solar Devices. *Solar Energy* 68(4):357-360.
- [54] Grochenig K, Schwab H (2003) Fast Local Reconstruction Methods for Nonuniform Sampling in Shift-Invariant Spaces. *SIAM Journal on Matrix Analysis and Applications* 24(4):899-913.
- [55] Grunbaum B, Shephard GC (1986) *Tilings and Patterns: An Introduction*. W.H.Freeman & Co Ltd.
- [56] Hall DL, Llinas J (2001) *Handbook of Multisensor Data Fusion*. CRC Press.
- [57] Halton JH (1960) On the Efficiency of Certain Quasi-Random Sequences of Points in Evaluating Multi-Dimensional Integrals. *Numerische Mathematik* 2(1):84-90.
- [58] Hammersley JM (1960) Monte Carlo Methods for Solving Multivariable Problems. *Annals of the New York Academy of Sciences* 86(Numerical Properties of Functions of More Than One Independent Variable):844-874.
- [59] Hansen HN, Carneiro K, Haitjema H, De Chiffre L (2006) Dimensional Micro and Nano Metrology. *CIRP Annals - Manufacturing Technology* 55(2):721-743.
- [60] Harris FJ (1978) On the Use of Windows for Harmonic Analysis with the Discrete Fourier Transform. *Proceedings of the IEEE* 66(1):51-83.
- [61] Haykin SS, Veen BV (2003) *Signals and Systems*. Wiley.

- [62] Hu J, Li Y, Wang Y, Cai J (2004) Adaptive Sampling Method for Laser Measuring Free-Form Surface. *The International Journal of Advanced Manufacturing Technology* 24(11):886-890.
- [63] Hutchinson MF, de Hoog FR (1985) Smoothing Noisy Data with Spline Functions. *Numerische Mathematik* 47(1):99-106.
- [64] ISO 1101 (2004) Geometrical Product Specification (GPS) - Geometrical Tolerancing - Tolerances of Form, Orientation, Location and Run-Out.
- [65] ISO 3534-1 (2006) Statistics -- Vocabulary and Symbols -- Part 1: General Statistical Terms and Terms Used in Probability.
- [66] ISO 4287 (1997) Geometrical Product Specifications (GPS) -- Surface Texture: Profile Method -- Terms, Definitions and Surface Texture Parameters.
- [67] ISO 13565-2 (1996) Geometrical Product Specifications (GPS) -- Surface Texture: Profile Method; Surfaces Having Stratified Functional Properties -- Part 2: Height Characterization Using the Linear Material Ratio Curve.
- [68] ISO 25178-2 (2012) Geometrical Product Specification (GPS) - Surface Texture: Areal - Part 2: Terms, Definitions and Surface Texture Parameters.
- [69] ISO 25178-3 (2011) Geometrical Product Specification (GPS) - Surface Texture: Areal - Part 3: Specification Operators.
- [70] ISO 25178-701 (2010) Geometrical Product Specifications (GPS) -- Surface Texture: Areal -- Part 701: Calibration and Measurement Standards for Contact (Stylus) Instruments.
- [71] ISO/DIS 25178-71 (2010) Geometrical Product Specifications (GPS) -- Surface Texture: Areal -- Part 71: Software Measurement Standards.
- [72] ISO/TR 14638 (1995) Geometrical Product Specifications (GPS) — Masterplan.
- [73] ITRS Reports (2005) International Technology Roadmap for Semiconductors, Metrology.
- [74] Jiang X, Blunt L, Scott PJ (2009) Metrology of Structured Surfaces. EUSPEN Special Group Meeting, Edinburgh.
- [75] Jiang X, Scott P, Whitehouse D (2007) Freeform Surface Characterisation - a Fresh Strategy. *CIRP Annals - Manufacturing Technology* 56(1):553-556.
- [76] Jiang X, Scott PJ, Whitehouse DJ, Blunt L (2007) Paradigm Shifts in Surface Metrology. Part II. The Current Shift. *Proceedings of the Royal Society A* 463(2085):2071-2099.
- [77] Jiang XJ, Whitehouse DJ (2012) Technological Shifts in Surface Metrology. *CIRP Annals - Manufacturing Technology* 61(2):815-836.
- [78] Kawasegi N, Sugimori H, Morimoto H, Morita N, Hori I (2009) Development of Cutting Tools with Microscale and Nanoscale Textures to Improve Frictional Behavior. *Precision Engineering* 33(3):248-254.
- [79] Killmaier, T, Ramesh B, A (2003) Genetic Approach for Automatic Detection of Form Deviations of Geometrical Features for Effective Measurement Strategy. *Precision Engineering* 27(4):370-381.
- [80] Kim DE, Cha KH, Sung IH, Bryan J (2002) Design of Surface Micro-Structures for Friction Control in Micro-Systems Applications. *CIRP Annals - Manufacturing Technology* 51(1):495-498.
- [81] Kim W-S, Raman S (2000) On the Selection of Flatness Measurement Points in Coordinate Measuring Machine Inspection. *International Journal of Machine Tools and Manufacture* 40(3):427-443.

- [82] Kish L (1995) Survey Sampling. Wiley-Blackwell.
- [83] Kocis L, Whiten WJ (1997) Computational Investigations of Low-Discrepancy Sequences. *ACM Transactions on Mathematical Software (TOMS)* 23(2):266-294.
- [84] Ladislav K, William JW (1997) Computational Investigations of Low-Discrepancy Sequences. *ACM Trans Math Softw* 23(2):266-294.
- [85] Leach R (2001) Measurement Good Practice Guide No. 37 the Measurement of Surface Texture Using Stylus Instruments. Teddington, UK.
- [86] Leach R (2009) Fundamental Principles of Engineering Nanometrology. Elsevier Science Ltd.
- [87] Leach R, Brown L, Jiang X, Blunt R, Conroy M, Mauger D (2008) Measurement Good Practice Guide No. 108 Guide to the Measurement of Smooth Surface Topography Using Coherence Scanning Interferometry. Teddington, UK.
- [88] Lee G, Mou J, Shen Y (1997) Sampling Strategy Design for Dimensional Measurement of Geometric Features Using Coordinate Measuring Machine. *International Journal of Machine Tools and Manufacture* 37(7):917-934.
- [89] Li SZ (1995) Adaptive Sampling and Mesh Generation. *Computer Aided Design* 27(3):235-240.
- [90] Lin TY (1993) Characterisation, Sampling and Measurement Variation of Surface Topography: A Viewpoint from Standardisation (PhD thesis). University of Birmingham, Birmingham, UK.
- [91] Lin TY, Blunt L, Stout KJ (1993) Determination of Proper Frequency Bandwidth for 3D Topography Measurement Using Spectral Analysis. Part I: Isotropic Surfaces. *Wear* 166(2):221-232.
- [92] Liu YM, Walter GG (1995) Irregular Sampling in Wavelet Subspaces. *Journal of Fourier Analysis and Applications* 2(2):181-189.
- [93] Lonardo PM, De Chiffre L, Bruzzone AAG (2004) Characterisation of Functional Surfaces. *Proceedings of 2nd International Conference on Tribology in Manufacturing Processes*, Nyborg, Denmark, pp. 39-62.
- [94] Lonardo PM, Lucca DA, De Chiffre L (2002) Emerging Trends in Surface Metrology. *CIRP Annals - Manufacturing Technology* 51(2):701-723.
- [95] Lustig M, Donoho DL, Santos JM, Pauly JM (2008) Compressed Sensing Mri. *Signal Processing Magazine, IEEE* 25(2):72-82.
- [96] Machleidt T, Sparrer E, Dorozhovets N, Manske E, Franke K-H, Kapusi D (2009) Navigation in a Large Measurement Volume by Using AFM Technology as a Sensor System in the Npmm. *tm - Technisches Messen* 76(5):274-277.
- [97] Mainsah E (1994) Investigation of Pre-Characterisation Aspects of Three-Dimensional Micro-Topography (PhD thesis). University of Birmingham, Birmingham, UK.
- [98] Man HC, Zhang XM, Yue TM, Lau WS (1997) Excimer Laser Surface Modification of Engineering Ceramics for Adhesive Bonding. *Journal of Materials Processing Technology* 66(1-3):123-129.
- [99] Martin D (1995) A Fire-Resistant, Retroreflective Structure. United States Patent 5888618.
- [100] Maxwell JC (1859) On Hills and Dales. *The London, Edinburgh and Dublin Philosophical Magazine and Journal of Science* 40(269):421425-421425.

- [101] McGeough JA, Leu MC, Rajurkar KP, De Silva AKM, Liu Q (2001) Electroforming Process and Application to Micro/Macro Manufacturing. *CIRP Annals - Manufacturing Technology* 50(2):499-514.
- [102] Montgomery DC, Runger GC (2003) *Applied Statistics and Probability for Engineers* (3rd ed). John Wiley & Sons, Inc., New York.
- [103] Muijderland EA (1965) Spiral Groove Bearings. *Industrial Lubrication and Tribology* 17(1):12-17.
- [104] Nguyen AT, Butler DL (2005) Correlation-Length-Based Sampling Conditions for Various Engineering Surfaces. *Measurement Science and Technology* 16(9):1813-1822.
- [105] Nimkar ND, Bhavnani SH, Jaeger RC (2006) Effect of Nucleation Site Spacing on the Pool Boiling Characteristics of a Structured Surface. *International Journal of Heat and Mass Transfer* 49(17-18):2829-2839.
- [106] Nuttall A (1981) Some Windows with Very Good Sidelobe Behavior. *Acoustics, Speech and Signal Processing, IEEE Transactions on* 29(1):84-91.
- [107] Ohlsson R, Wihlborg A, Westberg H (2001) The Accuracy of Fast 3D Topography Measurements. *International Journal of Machine Tools and Manufacture* 41(13-14):1899-1907.
- [108] Parker JA, Kenyon RV, Troxel DE (1983) Comparison of Interpolating Methods for Image Resampling. *IEEE Trans Med Imaging* 2(1):31-39.
- [109] Pawlus, P, Chetwynd, D G (1996) Efficient Characterization of Surface Topography in Cylinder Bores. *Precision Engineering* 19(2-3):164-174.
- [110] Pawlus P (2007) Digitisation of Surface Topography Measurement Results. *Measurement* 40(6):672-686.
- [111] Petkovski M, Bogdanova S, Bogdanov M (2006) A Simple Adaptive Sampling Algorithm. Serbia, Belgrade, pp. 329-332.
- [112] Petkovski M, Bogdanova S, Bogdanov M (2007) An Example of Adaptive Sampling and Reconstruction of Signals: Application of Chaikin's Algorithm. *Systems, Signals and Image Processing, 14th International Workshop on*, pp. 49-52.
- [113] Pettersson U, Jacobson S (2003) Influence of Surface Texture on Boundary Lubricated Sliding Contacts. *Tribology International* 36(11):857-864.
- [114] Pharr M, Humphreys G, D GH (2004) *Physically Based Rendering: From Theory to Implementation*. Morgan Kaufmann.
- [115] Piegl LA, Tiller W (1997) *The Nurbs Book* (2 ed). Springer.
- [116] Poon CY, Bhushan B (1995) Comparison of Surface Roughness Measurements by Stylus Profiler, AFM and Non-Contact Optical Profiler. *Wear* 190(1):76-88.
- [117] Proakis JG, Manolakis DK (1995) *Digital Signal Processing: Principles, Algorithms and Applications*. Prentice Hall.
- [118] Rangelow IW, Ivanov T, Ivanova K, Volland BE, Grabiec P, Sarov Y, et al. (2007) Piezoresistive and Self-Actuated 128-Cantilever Arrays for Nanotechnology Applications. *Microelectronic Engineering* 84(5-8):1260-1264.
- [119] Ratzel JN (1980) *The Discrete Representation of Spatially Continuous Images*. Massachusetts Institute of Technology.
- [120] Remondino F (2003) From Point Cloud to Surface: The Modeling and Visualization Problem, In: *International Archives of the Photogrammetry, Remote Sensing and Spatial Information Sciences, XXXIV-5/W10*. Tarasp, Switzerland.

- [121] Roadmap I (2009) International Technology Roadmap for Semiconductors, 2005 Edition. Executive Summary Semiconductor Industry Association.
- [122] Rosen B-G (2008) Towards Optimized Sampling of Surface Roughness. Proceedings of the XII International Colloquium on surfaces, pp. 110-119.
- [123] Ros  n BG, Garnier J (2010) Uncertainties and Optimized Sampling in Surface Roughness Characterization. Wear 271(3-4):610-615.
- [124] Roth RM, Seroussi G (1954) On Irregularities of Distribution. Mathematika 1:73-79.
- [125] Sarikaya M (1999) Biomimetics: Materials Fabrication through Biology. Proceedings of the National Academy of Sciences 96(25):14183-14185.
- [126] Scott PJ (2004) Pattern Analysis and Metrology: The Extraction of Stable Features from Observable Measurements. Proceedings of the Royal Society A 460:2845-2864.
- [127] Scott PJ (2009) Feature Parameters. Wear 266(5-6):548-551.
- [128] Senturia SD (2005) Microsystem Design. Springer.
- [129] Shannon CE (1949) Communication in the Presence of Noise. Proc IRE 37:10-21.
- [130] Shih CS, Gerhardt LA, Chu WC-C, Lin C, Chang C-H, Wan C-H, et al. (2008) Non-Uniform Surface Sampling Techniques for Three-Dimensional Object Inspection. Optical Engineering 47(5):053606-053615.
- [131] Shimizu M, Fujita Y (1998) Fresnel Lens Manufacturing Apparatus. United States Patent 5840352.
- [132] Silk EA, Kim J, Kiger K (2006) Spray Cooling of Enhanced Surfaces: Impact of Structured Surface Geometry and Spray Axis Inclination. International Journal of Heat and Mass Transfer 49(25-26):4910-4920.
- [133] Slepian D (1976) On Bandwidth. Proceedings of the IEEE 64(3):292-300.
- [134] Stout K, Sullivan PJ, Dong WP, Mainsah E, Luo N, Mathia T, et al. (1993) Development of Methods for the Characterisation of Roughness in Three Dimensions. University of Birmingham.
- [135] Stout KJ (1998) Engineering Surfaces - a Philosophy of Manufacture (a Proposal for Good Manufacturing Practice). Proceedings of the Institution of Mechanical Engineers, Part B: Journal of Engineering Manufacture 212(3):169-174.
- [136] Stout KJ, Blunt L (2001) A Contribution to the Debate on Surface Classifications—Random, Systematic, Unstructured, Structured and Engineered. International Journal of Machine Tools and Manufacture 41(13-14):2039-2044.
- [137] Stout KJ, Blunt L, Mainsah E, Luo N, Dong WP, Mathia T, et al. (2000) Development of Methods for the Characterisation of Roughness in Three Dimensions. Penton Press.
- [138] Stout KJ, Sullivan PJ, Dong WP, Mainsah E, Luo N, Mathia T, et al. (1993) Development of Methods for the Characterisation of Roughness in Three Dimensions. Office for official publications of the European Communities, Luxembourg.
- [139] Su F, Chakrabarty K, Fair RB (2006) Microfluidics-Based Biochips: Technology Issues, Implementation Platforms, and Design-Automation Challenges. Computer-Aided Design of Integrated Circuits and Systems, IEEE Transactions on 25(2):211-223.
- [140] Suh NP, Saka N (1987) Surface Engineering. CIRP Annals - Manufacturing Technology 36(1):403-408.

- [141] Szczech TJ (1992) Retroreflective Material with Improved Angularity. United States Patent 5138488.
- [142] Takahashi S, Ikeda T, Shinagawa Y, Kunii TL, Ueda M (1995) Algorithms for Extracting Correct Critical Points and Constructing Topological Graphs from Discrete Geographical Elevation Data. *Computer Graphics Forum* 14(3):181-192.
- [143] Takeuchi Y, Maeda S, Kawai T, Sawada K (2002) Manufacture of Multiple-Focus Micro Fresnel Lenses by Means of Nonrotational Diamond Grooving. *CIRP Annals - Manufacturing Technology* 51(1):343-346.
- [144] Tanaka HT (1995) Accuracy-Based Sampling and Reconstruction with Adaptive Meshes for Parallel Hierarchical Triangulation. *Comput Vis Image Underst* 61(3):335-350.
- [145] Taubin G (1991) Estimation of Planar Curves, Surfaces, and Nonplanar Space Curves Defined by Implicit Equations with Applications to Edge and Range Image Segmentation. *IEEE Trans Pattern Anal Mach Intell* 13(11):1115-1138.
- [146] Taylor W (1905) An Improvement in Golf Balls, British Patent No 18 688. British Patent Office.
- [147] Terzopoulos D, Vasilescu M (1991) Sampling and Reconstruction with Adaptive Meshes. *Computer Vision and Pattern Recognition, 1991 Proceedings CVPR '91, IEEE Computer Society Conference on*, pp. 70-75.
- [148] The MathWorks (2011) Matlab R2011b Documentation: Functions - Surf. See <http://www.mathworks.co.uk/help/techdoc/ref/surf.html>.
- [149] The MathWorks (2012) Matlab R2012a Documentation: Functions - Griddata. See <http://www.mathworks.co.uk/help/techdoc/ref/griddata.html>.
- [150] Thomas TR, Charlton G (1981) Variation of Roughness Parameters on Some Typical Manufactured Surfaces. *Precision Engineering* 3(2):91-96.
- [151] Thompson SK (1992) Sampling. Wiley-Interscience.
- [152] Thompson SK, Seber GAF, Okogbaa OG (1996) Adaptive Sampling. Wiley New York.
- [153] Tian Y, Wang J, Peng Z, Jiang X (2011) Numerical Analysis of Cartilage Surfaces for Osteoarthritis Diagnosis Using Field and Feature Parameters. *Wear* 271(9-10):2370-2378.
- [154] Tian Y, Wang J, Peng Z, Jiang X (2012) A New Approach to Numerical Characterisation of Wear Particle Surfaces in Three-Dimensions for Wear Study. *Wear* 282-283(0):59-68.
- [155] Tsukada T, Sasajima K (1982) An Optimum Sampling Interval for Digitizing Surface Asperity Profiles. *Wear* 83(1):119-128.
- [156] TWI Ltd. (2008) Surfi-Sculpt®: Reshaping the Future. See <http://www.twi.co.uk/>.
- [157] Unser M (2000) Sampling—50 Years after Shannon. *Proceedings of the IEEE*:569--587.
- [158] Van der Corput JG (1935) Verteilungsfunktionen I. *Akad Wetensch* 38:813-821.
- [159] Verma R (2010) Characterisation of Engineered Surfaces (PhD Thesis). The University of North Carolina at Charlotte, Charlotte, USA.
- [160] Vorburger TV, Raja J (1990) Surface Finish Metrology Tutorial. National Inst. of Standards and Technology.
- [161] Vukusic P, Sambles JR (2003) Photonic Structures in Biology. *Nature* 424(6950):852-855.

- [162] Wakuda M, Yamauchi Y, Kanzaki S, Yasuda Y (2003) Effect of Surface Texturing on Friction Reduction between Ceramic and Steel Materials under Lubricated Sliding Contact. *Wear* 254(3-4):356-363.
- [163] Walter GG (1992) A Sampling Theorem for Wavelet Subspaces. *Information Theory, IEEE Transactions on* 38(2):881-884.
- [164] Wang J, Jiang X, Blunt LA, Leach RK, Scott PJ (2011) Efficiency of Adaptive Sampling in Surface Texture Measurement for Structured Surfaces. *Proceedings of the 13th International Conference on Metrology and Properties of Engineering Surfaces*:214-218.
- [165] Wang J, Jiang X, Blunt LA, Leach RK, Scott PJ (2012) A Boundary Segmentation Algorithm for Extracting Micro-Scale Dimensional Parameters in the Measurement of Structured Surfaces. *Proceedings of the 12th international conference of the EUSPEN, Stockholm, Sweden*, pp. 113-116.
- [166] Wang J, Jiang X, Gurdak E, Scott P, Leach R, Tomlins P, et al. (2011) Numerical Characterisation of Biomedical Titanium Surface Texture Using Novel Feature Parameters. *Wear* 271(7-8):1059-1065.
- [167] Wen C, Itoh S, Shiki J (1998) Irregular Sampling Theorems for Wavelet Subspaces. *Information Theory, IEEE Transactions on* 44(3):1131-1142.
- [168] Whitehouse DJ (2002) *Surfaces and Their Measurement*. Taylor & Francis.
- [169] Whitehouse DJ, Archard JF (1970) The Properties of Random Surfaces of Significance in Their Contact. *Proceedings of the Royal Society of London A Mathematical and Physical Sciences* 316(1524):97-121.
- [170] Whittaker JM (1928) The "Fourier" Theory of the Cardinal Function. *Proceedings of the Edinburgh Mathematical Society (Series 2)* 1:169-176.
- [171] Wieczorowski M (2001) Spiral Sampling as a Fast Way of Data Acquisition in Surface Topography. *International Journal of Machine Tools and Manufacture* 41(13-14):2017-2022.
- [172] Woo TC, Liang R, Hsieh CC, Lee NK (1995) Efficient Sampling for Surface Measurements. *Journal of Manufacturing Systems* 14(5):345-354.
- [173] Wu J-J (1999) Spectral Analysis for the Effect of Stylus Tip Curvature on Measuring Rough Profiles. *Wear* 230(2):194-200.
- [174] Xiao S, Xie F, Blunt L, Scott P, Jiang X (2006) Feature Extraction for Structured Surface Based on Surface Networks and Edge Detection. *Materials Science in Semiconductor Processing* 9(1-3):210-214.
- [175] Yanagi K, Kobayashi N, Kasahara K (1995) The Allowable Spacing for Lattice Data Sampling by a Round Stylus Tip and an Assessment of the Envelope Surface. *International Journal of Machine Tools and Manufacture* 35(2):183-186.
- [176] Yao K (1967) Applications of Reproducing Kernel Hilbert Spaces - Bandlimited Signal Models. *Information and Control* 11(4):429-444.
- [177] Yim DY, Kim SW (1991) Optimum Sampling Interval for Ra Roughness Measurement. *Proceedings of the Institution of Mechanical Engineers Part A, Journal of power and energy* 205(C2):139-142.
- [178] Zahouani H (1998) Spectral and 3D Motifs Identification of Anisotropic Topographical Components. *Analysis and Filtering of Anisotropic Patterns by Morphological Rose Approach*. *International Journal of Machine Tools and Manufacture* 38(5-6):615-623.
- [179] Zhang X (2009) *Free-Form Surface Fitting for Precision Coordinate Metrology (PhD Thesis)*. University of Huddersfield, Huddersfield, UK.

- [180] Zhou X, Sun W (1999) On the Sampling Theorem for Wavelet Subspaces. *Journal of Fourier Analysis and Applications* 5(4):347-354.
- [181] Zhu X (1981) *Lecture Notes on the Principles and Applications of B-Spline Curves and Surfaces*. University of Minnesota, Dept. of Mechanical Engineering.